Simulation of a Novel Restraint Safety Concept for Motorcycles

Von der Fakultät Konstruktions-, Produktions- und Fahrzeugtechnik
der Universität Stuttgart
zur Erlangung der Würde eines Doktor-Ingenieurs (Dr.-Ing.)
genehmigte Abhandlung

von
Steffen Georg Maier
aus Bad Friedrichshall

Hauptberichter: apl. Prof. Dr.-Ing. Jörg Fehr
Mitberichter: Prof. Alessandro Scattina, PhD

Tag der mündlichen Prüfung: 7. Juli 2023

Institut für Technische und Numerische Mechanik
der Universität Stuttgart

2023

Vorwort

Das Thema dieser Arbeit entstand aus einer Idee des Erfinders Laurent Doléac, der sich das große Ziel gesetzt hat, die passive Sicherheit von Motorradaufsassen zu revolutionieren. Durch seine Initiative fand sich ein Konsortium aus industriellen und akademischen Partnern unter Förderung des Wirtschaftsministeriums Baden-Württembergs. Gemeinsam mit den Unternehmen Doléac Models, SAS-TEC GmbH, DYNAmore GmbH und ZF Friedrichshafen AG hat das Institut für Technische und Numerische Mechanik (ITM) an dieser neuen Sicherheitsidee geforscht. Ich danke allen am Projekt Beteiligten für die fruchtbaren Diskussionen und die Zusammenarbeit. Ganz besonders wünsche ich Laurent Doléac weiterhin den Pioniergeist, das Durchsetzungsvermögen und die Leidenschaft sein Vorhaben zu verfolgen. Ich hatte großes Glück, dass seine Idee und die daraus entstandene ingenieurwissenschaftliche Aufgabe, das Sicherheitskonzept zu entwerfen und zu untersuchen, mich gefunden hat.

Die Möglichkeit am ITM und mit diesem Thema zu promovieren zu können verdanke ich maßgeblich der Teilnahme an einem Auslandsstudienprogramm am Georgia Institute of Technology in Atlanta in den USA. Das Stipendium, das vom ITM organisiert wurde, hat meinen Forschungsdrang geweckt und mir letztendlich die Möglichkeit eröffnet, diesen anschließend als wissenschaftlicher Mitarbeiter und Doktorand in Stuttgart weiter auszuleben.

Die letzten fünf Jahre waren für mich sehr prägend und bereichernd, nicht nur wegen des fachlichen Diskurses mit meinen tollen Kollegen und anderen Forschern, sondern auch besonders wegen der engen Betreuung durch Prof. Jörg Fehr. Ich möchte mich bei ihm bedanken, dass er mich stets motiviert und fokussiert hat, für unsere unzähligen aufschlussreichen Diskussionen über viele Themen und für die vielen Gelegenheiten, meine Arbeit zu präsentieren. Seine ansteckende Energie und Motivation, Dinge anzupacken, und immer positiv an Herausforderungen heranzugehen werden mich noch lange prägen. Des Weiteren danke ich auch Prof. Peter Eberhard, Prof. Michael Hanss und Dr. Pascal Ziegler für die von Vertrauen und gegenseitigem Respekt geprägte Arbeitsatmosphäre am Institut, bei der auch der Spaß nicht zu kurz kam. Ich habe die Freiheit, die ich bei meiner Forschung hatte, stets genossen und ich werde nicht nur die humorvollen Kaffeepausen sehr vermissen. Ich durfte während meiner Zeit am ITM viele studentische Arbeiten betreuen, die zu meiner Forschung viel beigetragen haben. Außerdem möchte ich meinem Mitberichter Prof. Alessandro Scattina dafür danken, dass er sich bereit erklärt hat, diese Arbeit zu lesen und zu begutachten.

Nicht zuletzt möchte ich meiner Familie und all den Menschen, die meinen Lebensweg positiv beeinflusst haben, für ihre beständige Unterstützung danken. Insbesondere gilt der Dank meinen Eltern, die mich mein ganzes Leben lang bestmöglich und bedingungslos unterstützen und meiner Frau Franziska, die jederzeit hinter mir steht.

Stuttgart, im August 2023   Steffen Maier

Contents

VIII

Zusammenfassung

Unfälle mit motorisierten Zweirädern sind komplexe Ereignisse, deren Ausgang von vielen Faktoren abhängt. Ein gewaltsamer Abwurf der Fahrerin oder des Fahrers vom Motorrad ist ein sehr wahrscheinlicher Unfallhergang. Durch einen Aufprall gegen einen anderen Verkehrsteilnehmer, die Straße oder Straßenbegrenzungsobjekte erleidet der Aufsasse dabei oft mehrere schwere Verletzungen an allen Körperregionen, die zu bleibenden Schäden oder sogar zum Tod führen können. Ein neuartiges Rückhaltekonzept will dieses Problem der unzureichenden passiven Sicherheit von Motorradfahrern und -fahrerinnen lösen, ohne dabei die Vorteile eines motorisierten Zweirads als kompaktes Verkehrsmittel, wie z.B. die gute Rundumsicht und Wendigkeit, zu beeinträchtigen und ohne das einzigartige Fahrverhalten zu verlieren. Die innovative Idee sieht vor, dass der Aufsasse im Falle eines Unfallaufpralls durch Oberschenkelgurte, mehrere Airbags und Beinanprallprotektoren am Motorrad zurückgehalten wird.

Das Ziel dieser Arbeit ist, das vorgeschlagene Sicherheitskonzept rechnerisch zu modellieren, zu simulieren und zu untersuchen. Die wichtigsten Forschungsfragen sind: *Ist es sicherer, auf einem Motorrad zurückgehalten zu werden, als der intrinsischen Unvorhersehbarkeit eines konventionellen Motorradunfalls ausgesetzt zu sein? Welche virtuellen Modelle und numerischen Methoden erlauben es uns, dies zu beantworten?*

Zur Beantwortung dieser Fragen fasst die Arbeit die wichtigsten Aspekte des Unfallverhaltens von Motorrädern und ihren Aufsassen zusammen und analysiert den Stand der Technik der passiven Sicherheit von Motorrädern. Die Arbeit skizziert Modelle und Simulationen einer rechnergestützten Strategie für eine zeit- und kosteneffiziente Auslegung und Untersuchung des Rückhaltekonzepts für Motorräder. Die Modellierungs- und Simulationsstrategie kombiniert mehrere einzelne Entwicklungsaufgaben in einer Methodik, die aus drei aufeinanderfolgenden virtuellen Entwicklungsstufen mit kontinuierlich steigendem Detaillierungsgrad und erwarteter Wiedergabetreue in Mehrkörper- und Finite-Elemente-Simulationsumgebungen besteht. Für ein robustes Design werden verfügbare numerische Modelle von Crashtest-Dummys und moderne Menschmodelle verwendet, die den Bewegungsapparat, das Nervensystem und die inneren Organe eines Menschen detailliert abbilden. Die Fahrzeug- und Aufsassenersatzmodelle werden in empfohlenen repräsentativen Unfallszenarien simuliert und in kinematischen, kinetischen und energiebasierten Analysen sowie hinsichtlich einer breiten Auswahl biomechanischer Verletzungskriterien für den gesamten Körper bewertet.

Die Ergebnisse zeigen, was mit einer vollständig virtuellen Konzeptstudie möglich ist. Es ist eine effiziente und effektive Simulationsstrategie, die die individuellen Vorteile der verschiedenen Simulationsmodelle ausnutzt um das Unfallverhalten des Motorrads, seiner passiven Sicherheitssysteme und verschiedener Aufsassen vorherzusagen. Die Simulationen zeigen eine geführte und kontrollierte Trajektorie und Verzögerung des Motorradaufsassen,

was zu weniger kritischen biomechanischen Belastungen im Vergleich zu einem Aufprall mit einem herkömmlichen Motorrad führt. Die Ergebnisse sind eine aussagekräftige Beschreibung der Funktionsprinzipien und der kausalen Zusammenhänge des Rückhaltesystems und eine quantifizierte Leistungsbewertung des Konzepts. Die Kombination mehrerer passiver Sicherheitssysteme zeigt sich sehr vielversprechend, um das Unfallverhalten positiv zu beeinflussen und die Unfallfolgen zu mindern. Eine Limitierung dieser Studie besteht darin, dass nur die primäre Unfallphase untersucht wurde – die unmittelbare Zeitspanne nach dem ersten Kontakt zwischen den gegnerischen Fahrzeugen, bei Kollisionskonfigurationen mit einem Pkw nach einer anerkannter Norm. Die Studie ist der erste Schritt zu einer ganzheitlichen Bewertung der innovativen Idee aber ihre Modellierung muss noch durch Laborexperimente verifiziert werden, und ihre Untersuchung muss letztendlich viel mehr mögliche Unfalltypen umfassen, um schädliche Auswirkungen in auslegungsüberschreitenden Szenarien auszuschließen.

Abstract

Accidents of powered two-wheelers are complex events whose outcome depends on many factors. Violent ejection of a rider from the motorcycle is a very likely accident pathway. The rider, striking objects in its path and the ground, often suffers multiple serious injuries at all body regions, resulting in permanent harm or even death. A novel restraint concept wants to solve this problem of insufficient passive safety of motorcycle riders without compromising a powered two-wheeler's advantages as a compact means of transport, such as great all-around visibility and maneuverability, and without losing its unique driving behavior. The innovative idea envisages that in case of an accident impact, the rider is restrained by thigh belts, multiple airbags, and leg impact protectors to the motorcycle.

This work aims to model, simulate, and investigate the proposed safety concept computationally. The main research questions are: *Is it safer to be restrained to a motorcycle than to be exposed to the intrinsic unpredictability of a conventional motorcycle accident? What virtual models and numerical methods allow us to answer this?*

To answer these questions, the work summarizes the most important aspects of the accident behavior of motorcycles and their riders and analyses the state-of-the-art in motorcycle passive safety. The work delineates models and simulations of a computational strategy for a time and cost-efficient design and investigation of the restraint concept for motorcycles. The modeling and simulation strategy combines multiple individual development tasks in a methodology that consists of three successive virtual development stages with a continuously increasing level of detail and expected fidelity in multibody and finite element simulation environments. Aiming for a robust design, it uses available numerical models of anthropomorphic test devices, better known as crash test dummies, and multiple state-of-the-art human body models that detail the musculoskeletal system, the nervous system, and the internal organs of a human. The vehicle and rider surrogate models are simulated in recommended representative accident scenarios and evaluated in kinematic, kinetic, and energy-based analyses as well as regarding a broad range of biomechanical injury criteria for the whole body.

The results show what is possible with an entirely virtual concept study. It is an efficient and effective simulation strategy that exploits individual advantages of the different simulation models to predict the accident behavior of the motorcycle, its passive safety systems, and diverse riders. The simulations show a guided and controlled trajectory and deceleration of the motorcycle rider, resulting in fewer critical biomechanical loads compared to an impact with a conventional motorcycle. The results are a meaningful description of the functional principles and causal relationships of the restraint and a quantified performance evaluation of the concept. The combination of several passive safety systems shows much promise in positively influencing accident behavior and mitigating consequences. A limitation of this study is that only the primary impact phase was investigated – the immediate period

after the first contact between the opposing vehicles in collision configurations with a passenger car according to a recognized standard. The study is the first step towards a holistic assessment of the innovative idea, but its modeling still needs to be verified by laboratory experiments, and its investigation must ultimately include many more possible accident types to exclude detrimental effects in off-design scenarios.

Chapter 1

Introduction

The United Nations estimate that by 2045 66.4 % of the worldwide population will live in cities [UN19]. It is predicted that by that time, the number of passenger cars will rise by more than 950 million from 2019 to almost 2.1 billion vehicles [OPEC20]. Most existing urban infrastructure cannot support such an increase in vehicles and the impact on global resources and the climate are not yet determined. Powered two-wheelers (PTWs), more commonly called *motorcycles*, as small mobility solutions will play a vital role in dealing with this development. At present and globally, they already attract vast and varied users. They are popular as compact means of individual transportation in increasingly congested urban traffic and tight parking conditions. Due to their low weight and compactness, they have a good power-to-weight ratio and are very agile. Due to the lower resource consumption in production with an associated lower price, lower energy consumption, and lower maintenance costs compared to passenger cars, they are popular as a cheap form of individual mobility that saves resources. Due to their unique handling and the sensation of freedom when riding, for many users, a PTW is more than just a means of transportation in everyday life, but riding is also a leisure or exciting sports activity. However, besides exaltation, they pose an excessive risk of dire consequences.

> "Another bend: and I have the honour of one of England' straightest and fastest roads. The burble of my exhaust unwound like a long cord behind me. [...] I pull the throttle right open, on the top of the slope, and we swoop flying across the dip, and up-down up-down the switchback beyond: the weighty machine launching itself like a projectile with a whirr of wheels into the air at the take-off of each rise, [...] A skittish motor-bike with a touch of blood in it is better than all the riding animals on earth, because of its logical extension of our faculties, and the hint, the provocation, to excess conferred by its honeyed untiring smoothness."

> — E.T. Lawrence, better known as Lawrence of Arabia, who died 1935 at the age of 46 as a result of a motorcycle accident, in *The Road* [Lawrence55].

In 2022, an estimated 49.9 million PTWs were sold worldwide [Statista23], only slightly less than the 65.4 million cars sold in that same period [Gu22]. The most recent global report on road safety [WHO18] of the World Health Organization (WHO) provides data on registered cars and motorized two- and three-wheelers of worldwide countries. Compiling these numbers versus the respective population of the countries results in a telling illustration, shown in Figure 1.1. It portrays the global share of cars and motorized two- and three-wheelers, which varies significantly by region. In many Western countries, the number of motorized two- and three-wheelers are high, but their share is much lower compared to cars. In North America, for example, they are very often used as recreational vehicles for touring. In Europe, this is more mixed, as they are also commonly used for commuting in increasingly dense urban traffic. Whether explicitly permitted or not, PTWs slip between slow and stationary traffic and use tight parking areas. In many Asian and South American countries, PTWs outnumber cars as they are often the only affordable form of motorized transportation and have a primarily utilitarian function [Haworth12, Van ElslandeEtAl16, Perlot21].

As an efficient mode of transportation from societal, economic, and environmental perspectives, there are good reasons to promote the use of PTWs. Due to the high traffic volume and restrictions on constructing more traffic routes, many cities have reached their capacity
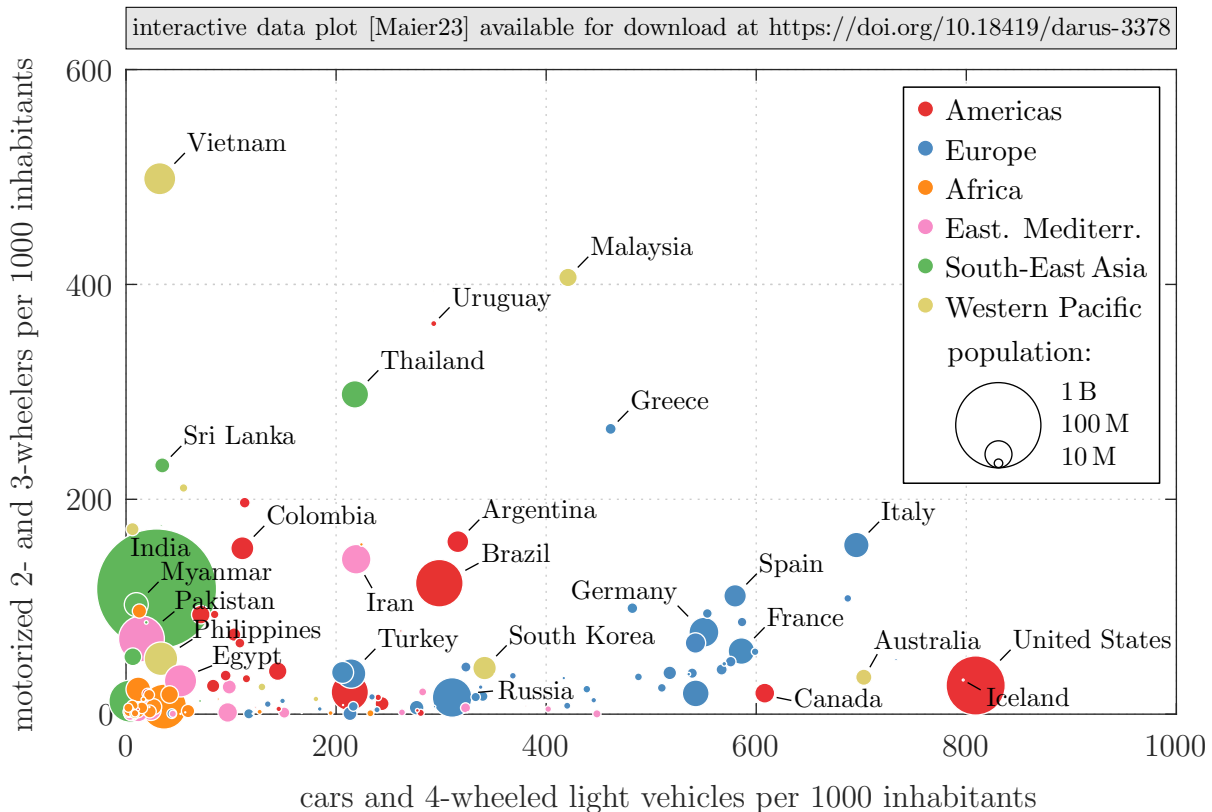

Figure 1.1: Registered cars and motorized two- and three-wheelers in worldwide countries in WHO classified regions based on the data set from [WHO18]. Note: No data available for some countries, e.g., for China.

limits at peak traffic times. Traffic jams cause enormous direct and indirect costs and burden the quality of life. Increasing the shift to smaller vehicles that occupy less physical space on the road can provide much-needed relief. A case study of the Leuven-Brussels motorway journey [Yperman11] examines the impact of a modal shift in which 10 % of cars are replaced by motorcycles. The traffic flow model simulation states that traffic loss hours decrease by 63 % from 1925 hours in a reference scenario to only 706 hours lost. Regardless of the type of drive, PTWs consume fewer resources in production and have a lower energy consumption than less compact cars. Considering the average occupancy in an evaluation of different transportation modes for urban areas [BrunnerEtAl18], electric scooters perform among the best. They are more efficient than other electric vehicles, buses, and the tram; only bicycles and e-bicycles are more efficient. Of course, they do not provide the same comfort and functionality as cars, with no weather protection and carrying no more than two people and no significant cargo. However, there are many single-occupant trips, especially in commuting, as the average occupancy of cars is only 1.7 in Europe [FiorelloEtAl16] and 1.67 in the US [BTS21]. PTWs are seen as a sustainable element in urban mobility [DorockiWantuch-Matla21]. Especially combined with electric drives, they have an enormous potential to reduce the consumption of resources and land, thus protecting the environment while meeting people's desire for individual mobility. However, the poor passive safety is their decisive disadvantage at considerable social costs.

1.1   The Excessive Risk of Motorcycling

Road traffic fatalities remain a leading cause of death. The WHO provides worldwide data on causes of death in [WHO20]. Each death is assigned to one of in total 116 causes. Ranking the causes by frequency for multiple age groups leads to the three leading causes of death for each age group illustrated in Figure 1.2. The full ranking is provided in Appendix A.2. It shows that road traffic injuries are the leading cause of death in the 15-29 year age group. It is also the second most frequent cause in the 5-14 year age group and the third most frequent cause in the 30-49 year age group. In absolute numbers, about 1.35 million people are currently killed in road traffic accidents worldwide each year, which are 2.5 % of all deaths (ranking eighth overall).

Motorcyclists are particularly at risk. A worldwide examination [WHO18] in Figure 1.3 shows the large share of riders and pillions (their passengers) of motorized two- and three-wheelers of all road traffic fatalities. The high numbers of road traffic fatalities in South-East Asia and the Western Pacifics and to some extent in the Americas combined with a large share of killed riders and pillions of motorized two- and three-wheelers in those regions contribute to a worldwide share of 28 %. These are close to 380,000 people killed every year. This is just one percent less than the deaths of drivers and passengers of four-wheeled vehicles. Vulnerable road users – pedestrians, cyclists, and riders and passengers of motorized two- and three-wheelers – account for more than half of all fatalities.
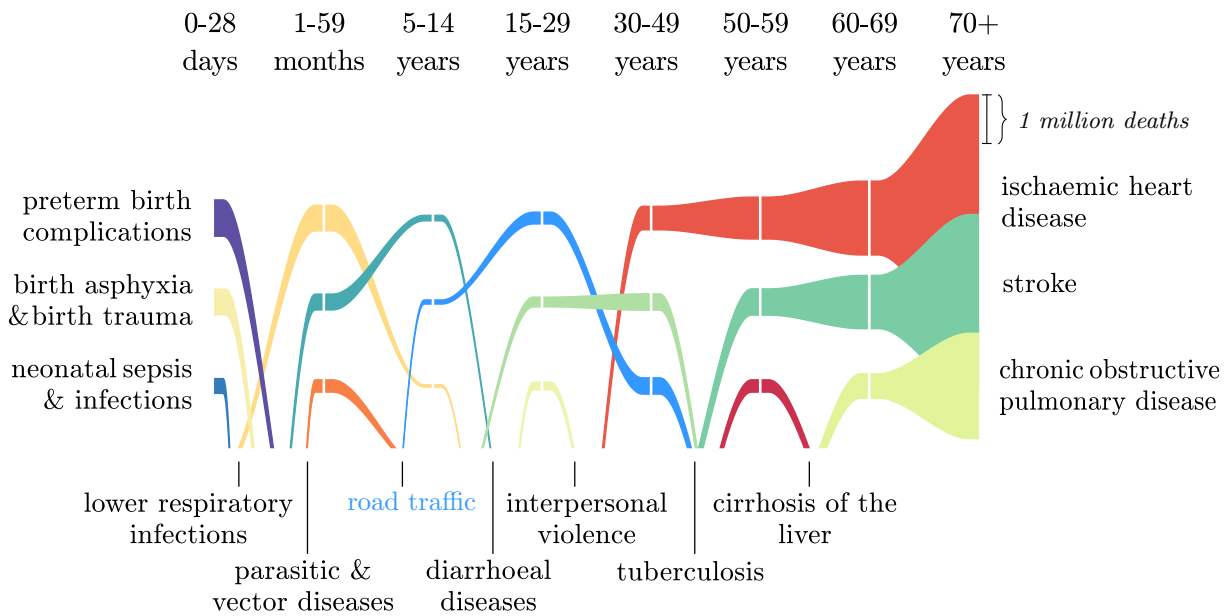
Figure 1.2: Leading causes of worldwide deaths by age group from the data set and classification according to [WHO20] for 2019. The widths of the profiles at the tick marks represent the number of deaths. The full ranking is given in Appendix A.2.
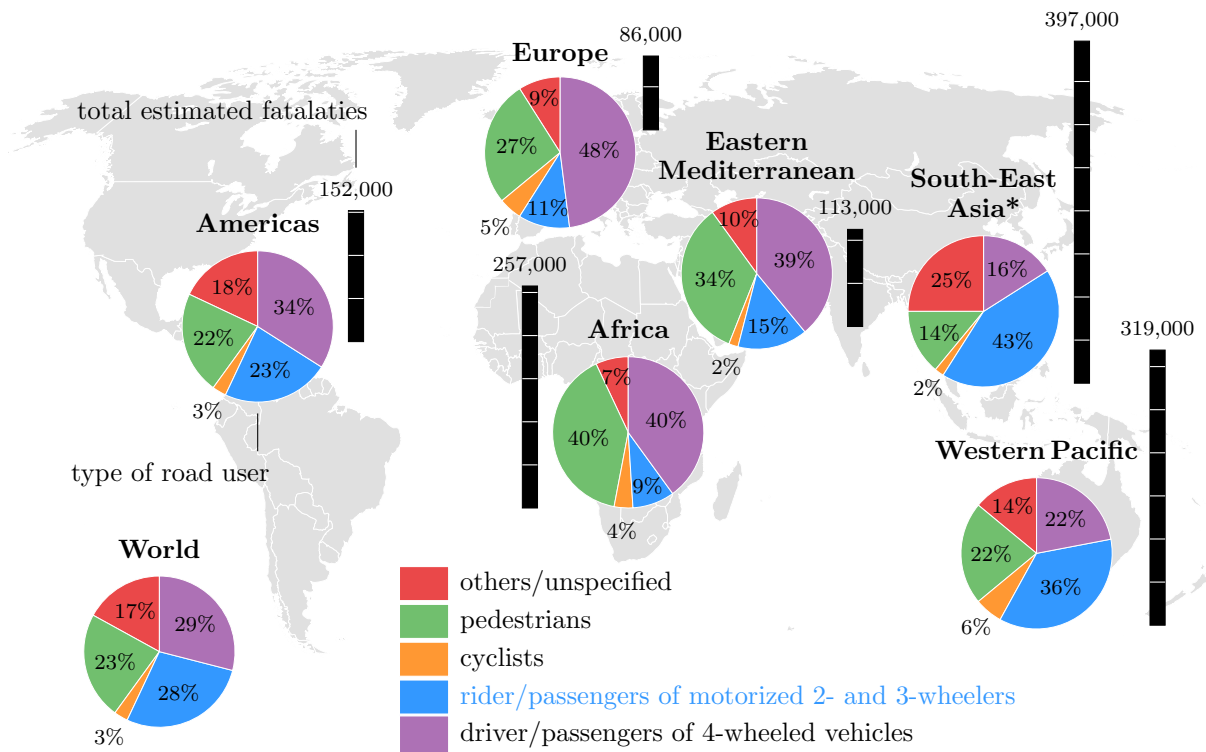
Figure 1.3: Estimated road traffic fatalities with the type of road user per WHO region, compiled from the data set of [WHO18] for 2016. *No available data for some countries, e.g., China, contribute to a large share of 'other/unspecified'.

Long-term and in-depth data from national databases and reports for Germany show that the risk of a fatal accident is many times higher than for other modes of transport. In 2019[1], 9.9 billion kilometers were traveled on motorcycles in Germany, excluding light PTWs (L1 vehicles, see Figure 2.1) [Destatis21b, BASt23]. This mileage corresponds to only about 1.5 % of the almost 644.8 billion kilometers traveled by users of passenger cars in that same period. However, motorcycles accounted for over 17.7 % of all road traffic fatalities in that year. Here, passenger cars are most frequently involved in fatal accidents involving motorcycle occupants. In collisions of this type, 94 % of the fatally injured accident victims were motorcyclists or their pillions, although 68 % of these accidents were caused by the car drivers [Destatis21a]. Figure 1.4 clearly displays these extraordinary risks for motorcyclists. For the same mileage, being killed on a motorcycle is 26 times more likely than being killed while driving a car. Figure 1.5 shows that although the risk of serious injury or death has decreased considerably in the past decades, the positive development lags well behind the progress that has been made for users of passenger cars.

The reason for these alarming figures is the current insufficient passive protection of motorcyclists. A motorcycle accident is a very complex event, the outcome of which depends on many factors. The vehicle itself does not provide protection to the rider in the event of a collision with an accident opponent or a roadside structure or in a solo accident.
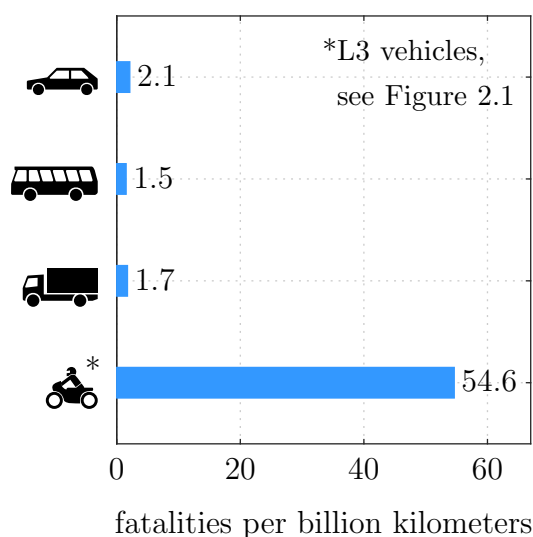
Figure 1.4: Road-traffic fatalities of drivers and passengers of cars, buses, trucks and motorcycles per traveled billion kilometers in Germany in 2019 [Destatis21b, BASt23].
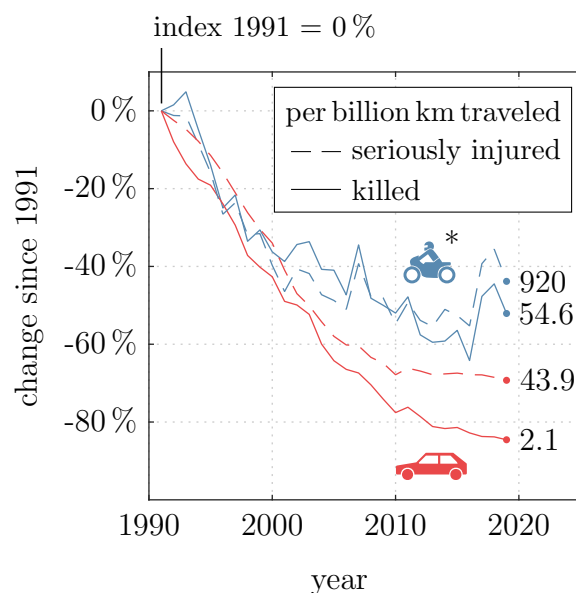
Figure 1.5: Killed and seriously injured users of passenger cars and motorcycles per billion traveled kilometers in Germany since 1991 [Destatis21b].

---

[1]While figures are also available for 2020 and 2021, the Federal Highway Research Institute of Germany states that due to the corona pandemic, the mileage for 2020 and 2021 is subject to great uncertainty and may not be final [BASt23].

Motorcycles do not have the safety features that many car occupants take for granted. They do not have seat belts, airbags, or a safety cell providing a survival space, nor the stability of four wheels. Instead, violent ejection of the rider from the motorcycle is a likely accident pathway when the vehicle suddenly comes to a standstill due to an impact. The rider, striking objects in its path and the ground, thereby often suffers multiple serious injuries in all body regions resulting in permanent harm or, very often, death, as shown in the statistics above. The inherent problem of low passive protection of powered two-wheelers has not yet been solved. Because of the complex accident behavior and due to the exposed position of the riders on a two-wheeler, it is very difficult to find truly safe passive safety solutions that are effective in the many possible accident configurations and that at least have neutral or non-detrimental effects on the accident consequences in off-design accident scenarios.

1.2 Restraint Safety Concept of the *Safe Motorcycle*

Laurent Doléac has set himself the goal of solving the problem of the insufficient protection of motorcycle riders and devised a radical and completely new safety concept for motorcycles. He calls it the *Safe Motorcycle* – an oxymoron[2] that illustrates the great challenge. It aims to improve passive rider safety in accidents significantly. The proposed concept consists of a newly designed motorcycle frame and body, seat belts, multiple airbags, foam leg impact protectors, and a side impact structure; see initial renderings of the vehicle concept in Figure 1.6 and initial animations of the safety idea in Figure 1.7.

© Doléac Models

Figure 1.6: Renderings of the vehicle concept of the Safe Motorcycle.

---

[2]"A rhetorical figure by which contradictory or incongruous terms are conjoined so as to give point to the statement or expression; an expression, in its superficial or literal meaning self-contradictory or absurd, but involving a point." [Oxford89], for example, a *deafening silence*.

© Doléac Models
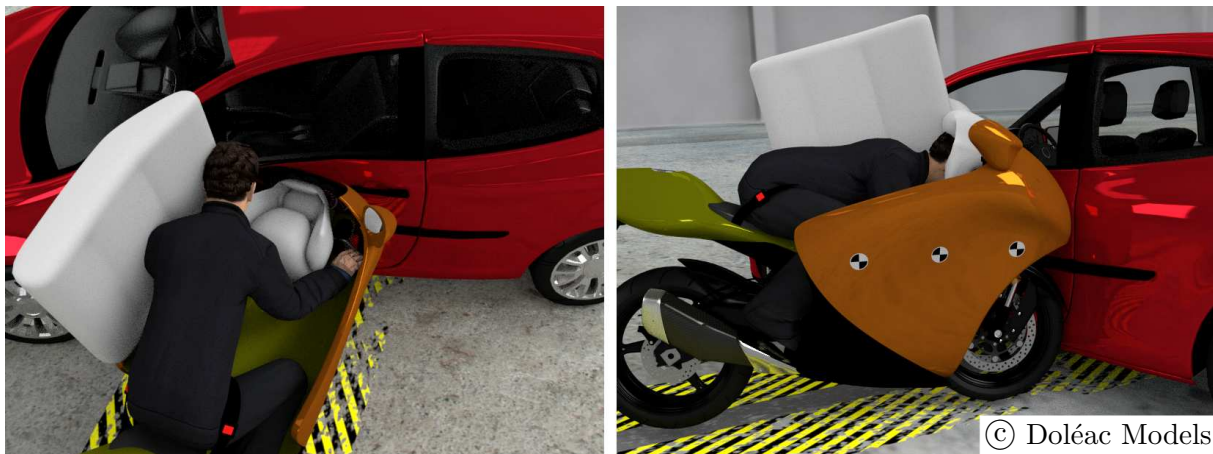
Figure 1.7: Animations of the safety concept. A video project presentation is provided at [Maier20].

He envisages that in the event of an accident impact, the two belts around the thighs restrain the rider to the motorcycle. The restraint causes the rider's upper body to rotate around the belt fastening. The surrounding airbags then decelerate the upper body rotation in a controlled manner and protect the rider from hard contact with an opposing vehicle, the road, or road-side structures. The foam impact protectors absorb the impact of the legs on the motorcycle cockpit. The side impact structure protects the lower extremities laterally. The fairing is shaped so that comfortable mounting, riding, and balancing the vehicle while being stationary should still be possible. The envisioned unique selling point of the safety concept is the preservation of an open design and, thus, the "DNA" of a motorcycle without any rollover structure, which is very important to many motorcyclists. The open design preserves the better all-round visibility and maneuverability of a two-wheeler, for example in traffic jams, compared to heavier closed vehicles. The goal of Laurent Doléac is to supersede a motorcycle rider's safety clothing and helmet entirely in the future and, therefore, significantly increase the suitability of motorcycles as commuter vehicles and/or shared mobility solutions.

The project was pursued by a small group of industrial and academic partners. Laurent Doléac from Doléac Models is the ideator and inventor of the safety concept. He holds a patent on the idea and has prepared a CAD model. The SAS-TEC GmbH is a manufacturer of body armor and an expert for energy-absorbing soft and hard foams. They supply the foam material for the leg impact protectors and carried out tests on the company's test stand. The simulation service company DYNAmore GmbH provides support with the software package LS-DYNA and expertise in computer-aided occupant and crash simulation. They also conducted tests in the company's materials laboratory to characterize the foam material. The ZF Friedrichshafen AG is a leading international company for occupant protection systems. Within the project, they participated in discussions on the design of the safety systems providing insight into occupant protection. The Institute of Engineering

and Computational Mechanics (ITM) of the University of Stuttgart is responsible for
the numerical modeling and simulation of the accident behavior of the motorcycle safety
concept. The author's work in the project at the ITM is the basis for this thesis.

1.3 Virtual Methods in Crashworthiness Design

In today's automotive crashworthiness design, computer-aided tools, methods, and pro-
cesses are a means of fast and cost-effective development dealing with a complex network
of stakeholders, many variants, and ever-increasing safety requirements and competition.
At the beginning of the development process, mainly virtual investigations pre-emptively
simulate system behavior; later, physical tests of prototypes complement the simulation
models. The final certification and rating of the performance are currently done mainly
by testing the complete vehicle as illustrated in Figure 1.8 following a similar depiction
in [FranzEtAl13].

The ability to reproduce the response of a complex system, such as the crash behavior of
an automobile and its safety equipment, can be depicted as a building block approach from
virtual and physical testing as shown in Figure 1.9. This concept is known as *Rouchon's*
testing pyramid [Rouchon90], which is often referred to in the aerospace industry. The
aim is to gradually build up knowledge from individual constituents such as models and
experiments of small material samples (coupons) at a fundamental level to elements,
subsystem assemblies, and finally to the entire vehicle structure and systems of a product.
In the process, the modeling is continuously aligned and verified at each of the individual
levels. Physical full-scale test crash tests of an entire system are extremely expensive. The
dashed lines show the trend to increase virtual testing at all levels and physical testing at
lower levels, especially for generic parts, as similary pointed out by [ZuardyHerrmann11].
This aims to avoid costly physical testing at higher levels. It is enabled by more powerful,
efficient, and theoretically sound simulation tools, as well as by the rapid increase in the
speed of computers.
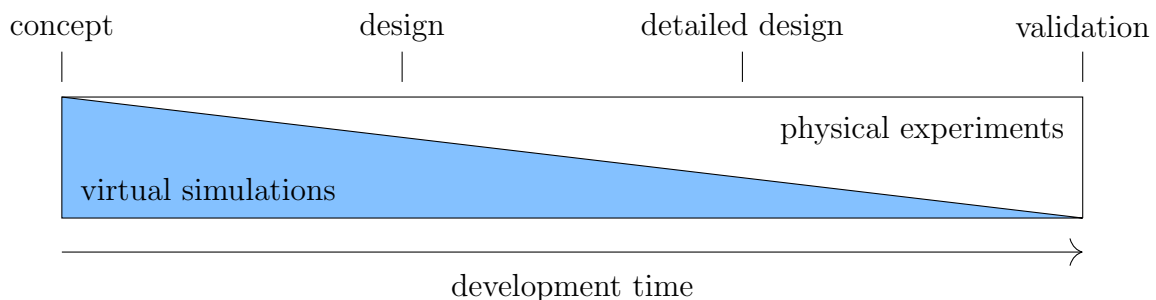
Figure 1.8: Use of tools in the development process of automotive passive safety.
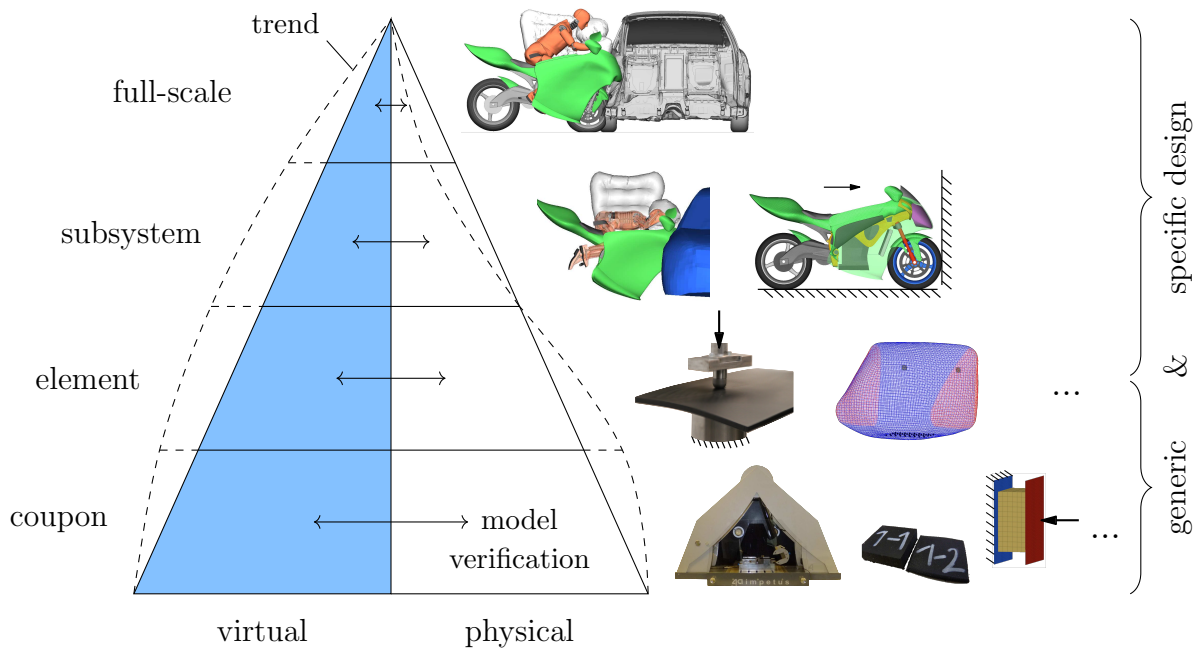
Figure 1.9: Testing pyramid with examples for the proposed safety concept from this work.

1.4   Objectives and Outline of the Thesis

Accidents involving motorcycles are very diverse. A safety system that effectively protects diverse riders must function robustly in many possible accident constellations. This results in many design iterations and cannot be achieved with costly experimental methods alone. Therefore, virtual methods must be applied. This includes procedures that allow for a systematic modeling approach for the design and the parameter setting of the passive safety systems of the proposed novel concept and the investigation of its performance in representative accident scenarios. To test many solutions efficiently, models with varying levels of detail, complexity, and computing effort that capture different aspects of the accident behavior are necessary.

This research aims to computationally model the proposed novel restraint safety concept to predict and describe its performance through virtual simulations of the accident behavior. Available virtual methods and tools, as well as numerical capabilities from occupant protection research and development of passenger cars, are well advanced. Generic models and existing knowledge used in occupant passive safety are the starting point for the thesis. The building block approach is the basis for predicting the system behavior of the safety concept. According to the step-by-step approach of the testing pyramid, the virtual modeling at higher levels must be chosen so that the verification with physical elements and subsystems can be done individually. This follows the trend of a virtual approach to finding functional optimums with minimal financial and human resources. To achieve this, this work develops a simulation strategy and incidental methods to study the passive

safety of motorcycles for a methodological description of the safety principles. In summary, the **objectives** (O) of this work thus are,

(O1) an efficient and effective simulation strategy with a systematic and modular modeling approach for optimizing and assessing different aspects of system design and accident behavior,

(O2) a realistic and reliable reproduction of the accident behavior of the motorcycle with passive safety systems and diverse riders for frequent accident scenarios,

(O3) a meaningful description of the functional and causal principles of the rider restraint and its influence on the accident outcome,

(O4) and a quantified performance evaluation of the concept.

To enhance the scientific understanding and the computational modeling of motorcycle passive safety, the main **research questions** (RQ) are:

(RQ1) Is it safer to be restrained to a motorcycle than to be exposed to the randomness and the unpredictability of an accident with a conventional motorcycle?

(RQ2) What virtual models and numerical methods allow us to answer this - at best, very efficiently and effectively?

Structure

Chapter 2 establishes the vast circumstances of a new safety concept for motorcyclists. It summarizes the most important aspects of the accident behavior of motorcycles and their riders for a compact overview. The state-of-the-art of motorcycle passive safety and previous attempts to improve it are analyzed. It selects and discusses a set of impact configurations representing the most frequent accidents involving PTWs and compiles a set of injury criteria to correlate accident consequences. Both are fundamental for the latter performance quantification of the novel safety concept.

Chapter 3 outlines the available computational methods and models for vehicle crashworthiness by classifying and categorizing them. It identifies and substantiates the chosen modeling approaches used in the pursued modeling and simulation strategy. It culminates in an overview of multibody systems and the finite element method, focusing on the essential aspects of computerized methods of today's very capable software packages.

Chapter 4 describes the modeling of the vehicle interaction of a motorcycle and an opposing vehicle, the passive safety systems of the motorcycle, and various rider surrogates. The novelty of this work is a virtual procedure from low to high fidelity to achieve different levels of computational effort and model complexity. This involves demonstrating an effective

method to characterize a numeric material model through an optimization of a polynomial representation of experimental test data incorporating material card requirements and material property knowledge. For the given problem, in total, three model environments with successively increasing complexity and expected fidelity – an MB model, an FE model, and a hybrid model approach in between – are developed and linked to each other. They provide a whole range of simulation models with which problems can be investigated efficiently, i.e., in a short time, and in detail, i.e., with high fidelity.

Chapter 5 shows the results of the simulations, subdivided into the different stages of the modeling and simulation strategy. The evaluation of the results far exceeds a mere evaluation and assessment of biomechanical loading and injury criteria values. The operating principles are described and quantified using kinematic, kinetic, and energy-based analyses. Graphical representations provide a meaningful description of the functional and causal principles of a PTW rider restraint and the accident outcome, as well as a quantified performance assessment of the concept.

Chapter 6 recapitulates and discusses the thesis aim based on the set objectives including the limitations of this study.

Chapter 7 concludes the research questions and gives an outlook.

Chapter 2

Accident Behavior of Motorcycles and Motorcyclists

Now that the significance of consequences of traffic accidents involving motorized two-wheelers for their users have been illustrated, as well as the objectives of this thesis have been established, fundamental aspects of motorcycles and their accident behavior will be summarized.

First, this chapter briefly introduces current motorcycles and their most frequent accident scenarios involving PTWs. A representative set of accident configurations is discussed and selected for the investigations in this work. It then describes the typical accident behavior of common motorcycles and their riders, as well as the available or rather not available protective design and passive safety equipment. This includes the description of the state-of-the-art safety measures of conventional motorcycles as well as more advanced safety principles that are, however, much less common. Lastly, the effectiveness of currently used protection is shown based on the consequences of accidents for motorcyclists from real-world accident data, and methods for quantifying and correlating biomechanical loads with rider injuries are compiled.

2.1   Types of Powered Two-Wheelers

A powered two-wheeler (synonymous to motorized two-wheeler) can be mostly defined as a single-track motor vehicle with two wheels and one or two seats. It allows for a very minimalistic form of motorized locomotion in which the motorcycle rider is typically, except for personally worn protective clothing, directly exposed to the elements of the environment. Compared to cars, motorcycles are very light and have more or less the same range of driving performance as passenger cars, although their acceleration capabilities

are often much better due to their low weight and often weight-related high engine power output.

Types of PTWs are manifold. Their classification by national and international authorities is commonly based on engine size or power and maximum design speeds. Their informal classification into types and subtypes by their users is most often established by a rider's seating position, the vehicle driving characteristics, or purpose. Figure 2.1 provides an incomplete overview of motorcycle types and their classification according to the European Union's current classification of two-wheeled motor vehicles [EuropeanParliamentandCouncil13]. Categories for light vehicles beyond (L2 and L4-L7) apply to two-wheelers with sidecars, three-wheeled tricycles, and small four-wheeled vehicles such as quads with varying wheel arrangements and mass and power classes. An often used classification [UNECE17] from the United Nations Economic Commission for Europe (UNECE) defines mofas, mopeds, and electric bikes with an engine capacity smaller than $50\,cm^3$ or maximum design speed less than $50\,km/h$ as category L1 vehicles; PTWs above as L3 vehicles. Such a classification determines the vehicle's national registrations and the conditions for the national issue of the driver's license. Powered cycles are classified as conventional bicycles in Europe and do not require a driver's license, registration and license plate, or insurance. Light two-wheel powered vehicles and low-performance motorcycles are also subject to less stringent licensing in most European countries. Thus, driver's licenses can often be obtained at a younger age and with rather minimal lessons of practice or are part of driver's licenses for cars. However, a separate driving license must be obtained to use motorcycles of the medium and higher power classes.

Depending on the different motorcycle types and geometries, there are specific seating positions for motorcyclists. Figure 2.2 provides profiles of such characteristic rider postures sorted by the torso angle. On a chopper or cruiser, shown on the very left, the rider sits slightly inclined to the back on a low seat, and the lower legs are vertical or even stretched forward. On the other side of the range, on a sport bike, the rider leans forward into the wind with his lower legs angled backward. The middle two seating positions are often referred to as the standard neutral position. Especially on sporty vehicles, the body postures are not static. A rider crouches down for good aerodynamics or leans inside of a turn for better cornering. There are numerous publications that describe and evaluate the posture of motorcyclists. In [ArunachalamEtAl19], a recent overview of the wide range of surveys and studies on motorcycle riding postures, primarily aimed at comfort and discomfort analysis, can be found. For the work presented here, rider postures from [Kolling97] are considered, as further described for the rider surrogate modeling in Section 4.4.

powered cycles: electric power $\leq 1\,\text{kW}$ and assisted speed $\leq 25\,\text{km/h}$

pedelec

light two-wheel powered vehicles: engine capacity $\leq 50\,\text{cm}^3$, electric power $\leq 4\,\text{kW}$, and maximum design vehicle speed $\leq 45\,\text{km/h}$

mofa   moped

L1*
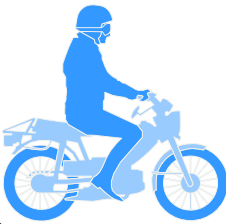
low-performance: engine capacity $\leq 125\,\text{cm}^3$ and power $\leq 11\,\text{kW}$ and **medium-performance motorcycles:** power $\leq 35\,\text{kW}$

scooter

high-performance motorcycles: power $\geq 35\,\text{kW}$
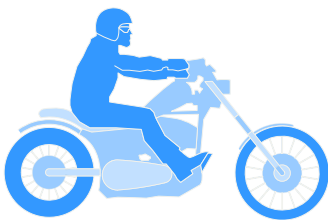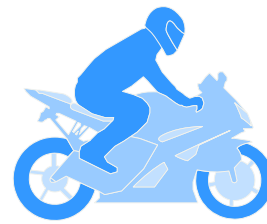
chopper   tourer   sport bike

enduro and trial motorcycles

enduro   trial

L3*

Figure 2.1: Typical types of powered two-wheelers (PTWs) with classification (**bold**) according to [EuropeanParliamentandCouncil13] and vehicle categories* from [UNECE17].

(a) chopper   (b) tourer   (c) enduro   (d) sport bike
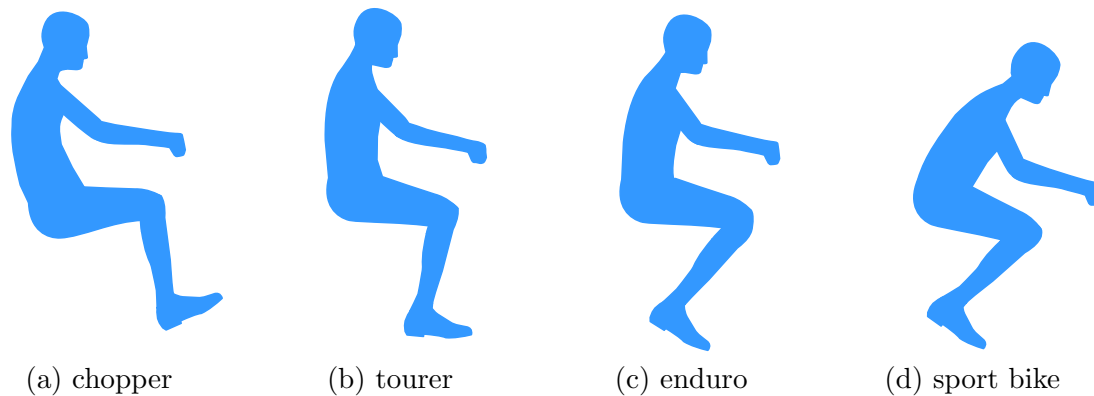
Figure 2.2: Rider postures for different types of motorcycles, according to [Kolling97].

2.2 Traffic Accident Scenarios of Powered Two-Wheelers

The events that cause accidents of motorized two-wheelers are very diverse. There are countless national and international surveys with real-world motorcycle accident statistics. Due to the variety of their spatial layout, temporal sequence, and types of motorcycles involved on different types of roads, it is difficult to make valid generalizations and representative summaries that are then also applicable across regions. Nevertheless, the following sections attempt to illustrate the most important patterns from the findings of a recent, in-depth accident investigation and introduce a widely used set of representative accident configurations for a well-informed quantification of the safety performance (O4).

2.2.1 Accident Scenario Statistics

Frequent Accidents According to the MAIDS In Depth Study

The MAIDS (Motorcycle Accidents In Depth Study) report [ACEM09a, ACEM09b] is the most recent large-scale study of motorcycle accidents. In total 921 accidents in the European countries France, Germany, Italy, Netherlands, and Spain in the years 1999-2000 were reconstructed in detail [ACEM03]. One of the study's main objectives was to identify the causes and consequences of accidents of PTWs and their riders in a well-defined sampling area. In the following, the most important findings of the analysed 523 L3 and 398 L1 vehicle accidents of the MAIDS in-depth study for a description of the most common accident scenarios are summarized. The given data of L1 and L3 vehicles are added as totals for PTWs.

In general, an accident of a PTW can first be divided into two types of accidents: Accidents that involve other road users and solo accidents of the PTW. The MAIDS analysis shows
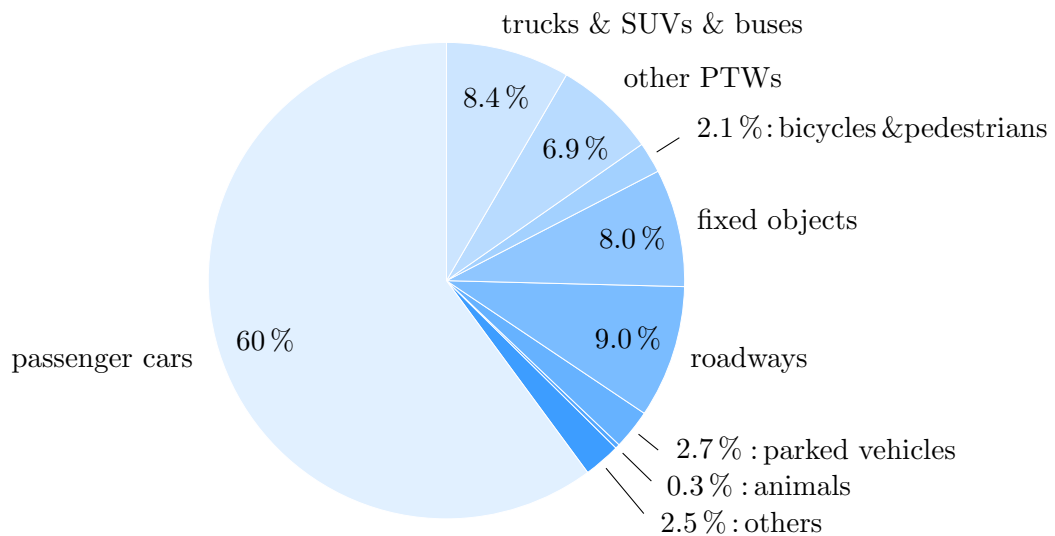
Figure 2.3: Frequency of collision partners of PTWs from [ACEM09a].

that the majority of the accidents with 80.2 % are collisions of the PTW with another vehicle and other road users. Only 15.5 % are solo accidents of a PTW. However, solo accidents are likely to be underreported in the first place [Haworth03]. Figure 2.3 gives the frequency of types of collision partners. By far, passenger cars and similar vehicles are the most frequent accident opponents. Less frequent are collisions with other two-wheelers and pedestrians. Here, solo accidents are represented by collisions with fixed objects and roadways. This diagram does not strictly identify the causes of the accidents but only represents the object with which the PTW ultimately collided. Thus, even initial solo accidents such as falls may also eventually result in collisions with other road users and roadside objects.

For collisions of a PTW with another vehicle, the frequency of the line of sights, both of the PTW and the opposing vehicle, are given in Figure 2.4. It shows that PTWs have mainly frontal collision contacts (89.6 %), while the frequency of collision contact points of the opposing vehicles is much more evenly distributed. Here, the difference between the frequency of a frontal collision for L3 (92 %) is very similar to those of L1 vehicles (87 %). The evaluation of the collision vehicle speeds, shown in Table 2.1, shows that speeds above 50 km/h are significantly less frequent than speeds below 50 km/h but with some variation for the types of PTW. Not surprisingly, the distribution for L3 PTWs shows generally higher impact speeds with 62 % crashes occurring at speeds below 50 km/h and 95 % than for L1 PTWs. The majority of the riders (68.1 %) had not lost control at the time of the collision.

As expected, the traveling speeds of PTWs in solo accidents were found to be faster. Less than 10 % are slower than 40 km/h. The other speeds are fairly evenly distributed between 40 to 80 km/h. As many as 21 % are traveling at speeds of more than 100 kilometers per hour.
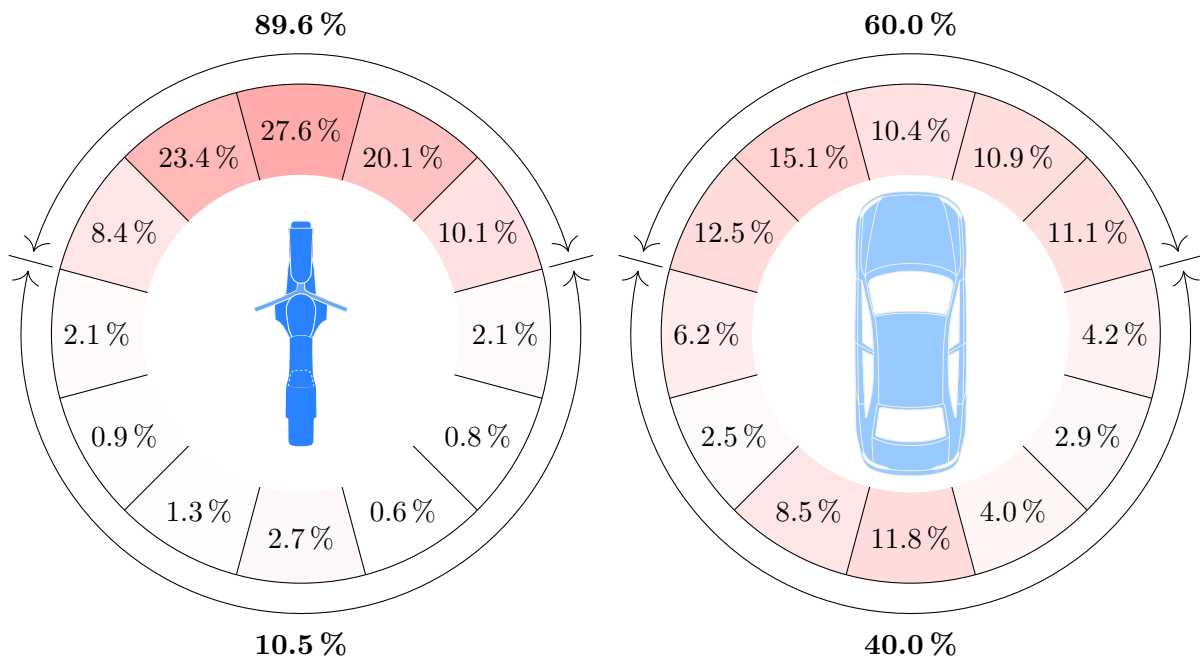
Figure 2.4: Frequency of the line of sight of the PTW (left) and the accident opponent vehicle (right) to the respective opposing vehicle in collisions from [ACEM09a].

Table 2.1: Frequency of the impact velocity of PTW and accident opponent vehicles in collisions from [ACEM09a], where *represents over 75 % cases respectively.

impact speed	PTW (solo accidents excluded)		other vehicle	
0 km/h		1.7 %		13.0 %
10 km/h		5.4 %		22.0 %
20 km/h		15.0 %	*	28.6 %
30 km/h		21.2 %		12.6 %
40 km/h	*	22.1 %		6.7 %
50 km/h		12.9 %		5.8 %
50 km/h		6.8 %		2.6 %
60 km/h		4.6 %		2.2 %
70 km/h		4.1 %		1.8 %
90 km/h		2.1 %		1.2 %
100 km/h or higher		4.1 %		1.8 %
unknown		0 %		1.7 %

The MAIDS study concludes that accidents of PTWs have a wide diversity of accident characteristics. The provided data state that passenger cars are the most frequent collision partners with a large accumulation of frontal collisions of the PTWs. Most PTW impact speeds are below 50 km/h. As a limitation, it should be noted that the given study considers a large proportion of category L1 vehicles, which tend to be used more in urban traffic and at lower speeds. However, within the scope of this work, a category L3 motorcycle is examined. This limitation does not directly impact the work presented here, though, as the study does not recommend representative accident scenarios.

2.2.2   Representative Accident Configurations

Accident Configurations According to ISO 13232

Several years earlier, as part of the international standard ISO 13232 [ISO13232:2005], which was first published in 1996, accident data were analyzed to identify common accidents involving L3 motorcycles. The standard was conceived as a standardized framework for performing analyses on protective devices fitted to motorcycles and was last updated in 2005. It defines representative impact scenarios, specifies methods and variables to be measured in crash tests, and describes injury indices and risk/benefit analyses. To this day, it still remains the only standardized framework that recommends test and evaluation methods for evaluating research on rider protection devices on motorcycles and is widely accepted and used.

Using accident data from a selection of 501 real-world crashes between motorcycles and cars in Los Angeles (USA) from 1976 to 1977 and Hannover (Germany) from 1980 to 1985, the most frequent impact configurations and involved vehicles were identified [Van Driessche94]. Each impact configuration is described with nomenclature $X_1X_2X_3$-Y/Z consisting of a numerical code $X_1X_2X_3$, indicating the relative geometric positions of the motorcycle and the opposing vehicle at impact, followed by the speeds at impact in meters per second of the opponent vehicle Y and motorcycle Z. The generation of the three-digit numerical code $X_1X_2X_3$ is described in Figure 2.5. The first digit indicates the contact point at the passenger car, the second digit the contact point at the motorcycle, and the third digit the relative heading angle between the longitudinal axes of the vehicles at impact. Ultimately, the standard isolates seven representative impact scenario configurations ① to ⑦, shown in Figure 2.6, and requires them for test procedures. The scenarios include collisions between a motorcycle and a passenger car, with the motorcycle and car either stationary or moving forward up to a speed of ≈ 48 km/h (13.4 m/s). The contact points on the motorcycle and car are at the front and side, respectively. There are no rear contact collisions included. The standard defines the opposing vehicle as a four-door saloon with a mass of 1,238-1.450 kg and an overall height of 137-147 cm. The set does not include scenarios with roadside barriers.

Limitations of the ISO 13232 Configurations

Since its introduction to this date, the set has been quickly adapted and widely used, such as in experimental tests [ChinnEtAl96, KalliskeAlbus98, KuroeNamikiIijima05] and computer simulations [ChawlaEtAl05, BarbaniBaldanziniPierini14, BońkowskiHynčíkLv20] to list only a few. However, the selection of configurations has been discussed for years. Shortly after the introduction, [BergBürkleSchmidts98] already pointed out that the selected configurations do not correspond to the most frequent accidents from a German database. They also recommend distinguishing between motorcycles and light motorcycles, such as scooters, for impact speeds. The discussion continues to this day, as recently [GrassiEtAl18a] and [PuthanEtAl21] conducted detailed studies on the representativeness of ISO 13232 configurations by comparing them to the above shown MAIDS report results and accident databases from Germany, India, and China. Both studies conclude that further impact configurations should be added and further opposing vehicle types should be considered, but [PuthanEtAl21] also admit that regional differences in accident characteristics are broad and it will be challenging to find a global compromise.

The discussion about the representation of the ISO 13232 configuration did not conclude yet so that an alternative has become generally accepted. Therefore, it is decided to apply the ISO 13232 standard set of accident configurations in this thesis here, as developers and researchers did in previous years and continue to do so. Ultimately, communication and the comparable exchange of results within the community are chosen important enough not to apply a less accepted set. Using the ISO 13232 configurations also ensures that the scenarios can be tested in full-scale crash experiments. Ultimately, testability was also a factor in the original selection for the ISO 13232 standard.

X_1: car contact point X_2: motorcycle contact point X_3: relative heading angle
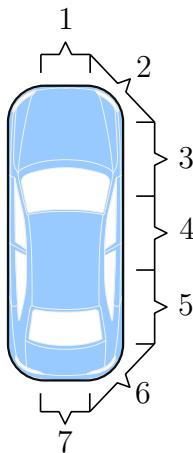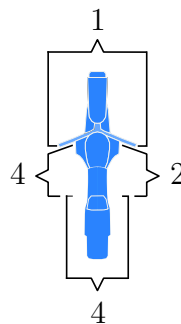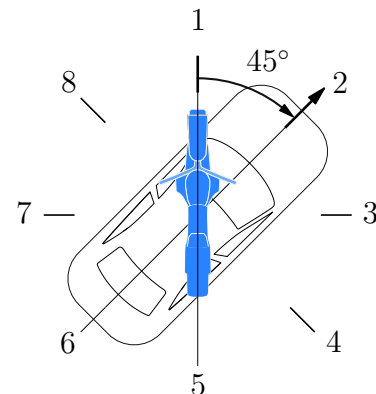
Figure 2.5: Denomination of relative positions of motorcycle and car at the impact from [ISO13232:2005].
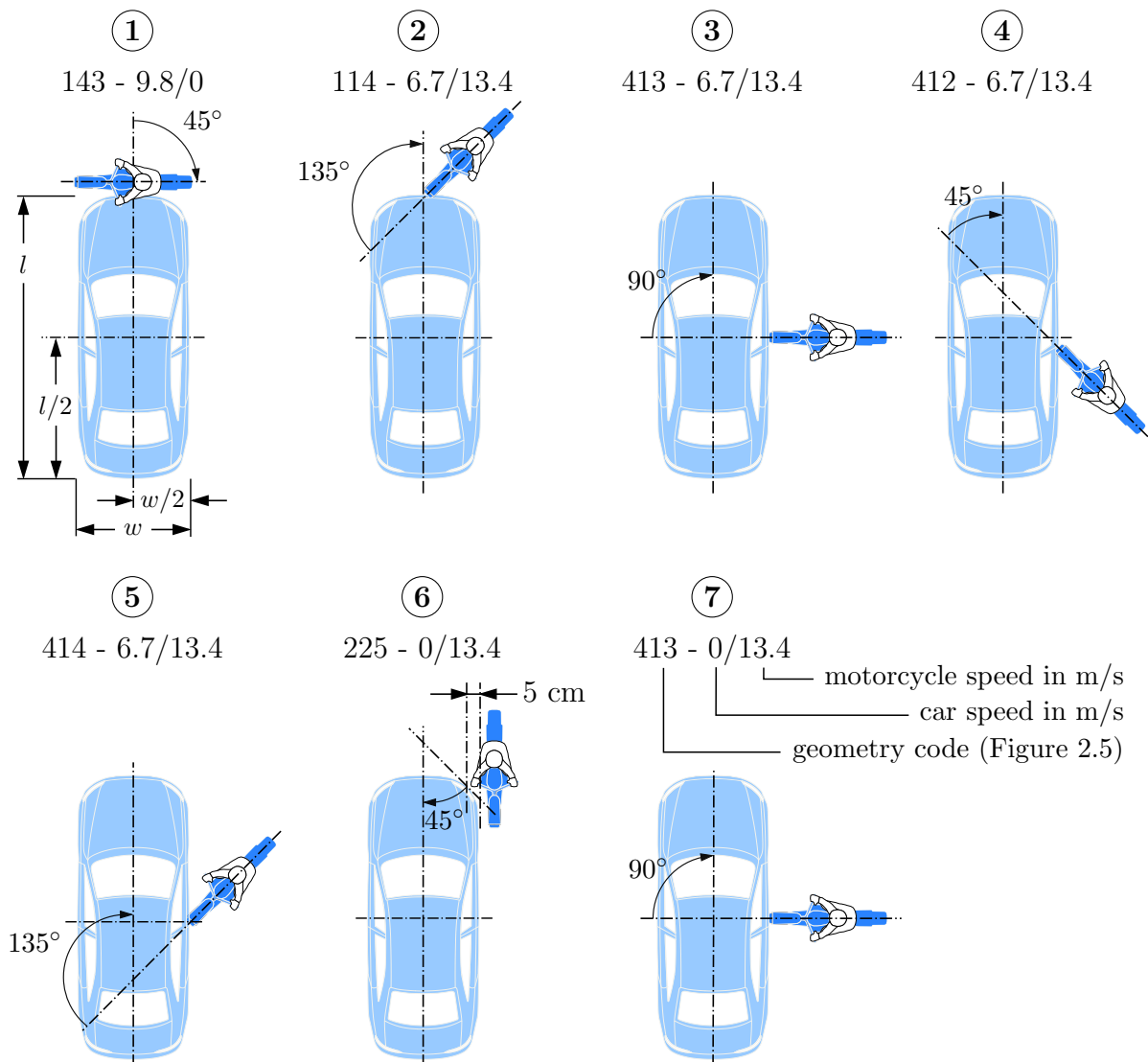
Figure 2.6: Representative set of impact configurations according to [ISO13232:2005].

2.3 Passive Safety Equipment for Motorcyclists

Motorcycles do not provide anywhere near the same level of crashworthiness and rider protection as automobiles do for their occupants. A car is much more stable and easier to see. In the event of an accident, a car has the advantage of significantly more weight and volume. It fully encloses the occupants in a safety cell and provides passive safety features such as seat belts and airbags. In contrast, the safety equipment of most motorcyclists is currently limited to personally worn protective equipment. The current safety strategy of conventional motorcycles does not go beyond the intention or, even more so, hope that the vehicle user will be able to get as little as possible entangled with the motorcycle and will be thrown off quickly instead, as will be discussed below.

Besides obvious technical challenges to making such small and open vehicles safe, there are many other reasons why the passive safety of two-wheeled vehicles has not reached the same

status and, thus, the same level of technology as the passive safety of vehicle occupants of automobiles. The passive safety of automobiles and its continuous improvement receives much more attention. This is reflected in the fact that in the development of automobiles, national approval authorities now set transnational standards and regulations for the performance and evaluation as well as for the target criteria of crash tests. Furthermore, consumer protection organizations and automobile clubs that carry out their own crash tests and safety assessments are helping to ensure that the passive safety of passenger cars receives much more attention from the general public and has become a significant factor in vehicle purchases. In contrast, the passive safety equipment of motorcycles and its performance in accidents does not receive a similar public interest. Because of the lack of legal regulations or independent evaluations for consumer information, two-wheeler manufacturers currently need more incentives to fundamentally improve the rider's safety.

Nonetheless, there have been many efforts to improve the passive safety of PTWs. The following section describes the typical accident behavior of PTWs and summarizes the technical solutions to improve the passive safety of motorcyclists. This summary excludes improvements beyond the technical equipment of vehicle and rider, i.e., improved traffic route planning, road construction, and driver education. The research and development activities and the current usage of passive safety equipment to date make clear how difficult it is to find truly safe solutions that are effective in all accident scenarios or at least have neutral and non-detrimental effects in some scenarios or off-design scenarios. The advantages and disadvantages of existing solutions are a significant aspect of understanding and evaluating new solutions (O3) and are therefore described in detail.

2.3.1 Motorcycle Accident Behavior

As shown above, the MAIDS report and underlying studies for the ISO 13232 standard identifies a collision with a passenger car as by far the most frequent accident scenario for PTWs. Several types of rider kinematics have been identified for these collisions in crash tests with conventional motorcycles [LindenmannGrandelBerg86, BergBürkleSchmidts98] and in experiments including a pillon [GrandelSchapter87]. The observed patterns can be divided, as shown by [AppelOtteWüstemann86], into one of the types illustrated in Figure 2.7: (a) a direct impact, (b) a rollover, or (c) a flyover of the rider. At the impact, the type depends on the points of contact of the collision opponents; during the collision phase, it depends on the vehicles' geometries and structural properties. In a direct impact, the rider is decelerated the most; hence the resulting immediate energy input into the rider is the highest. The energy input is lower for a rollover and for a flyover even lower. In the case of a rollover or flyover, the rider is assumed to detach from the motorcycle, which remains the decisive safety principle of today's motorized two-wheelers. This principle expects that injuries in the subsequent so-called secondary accident phase will be less than in a direct car impact. The chances of being injured less severely are promising only if

(a) direct impact with
    high energy transfer
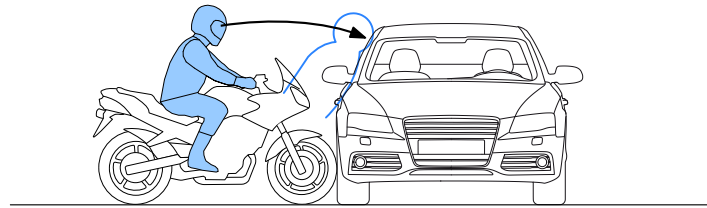
(b) rollover with
    medium energy transfer
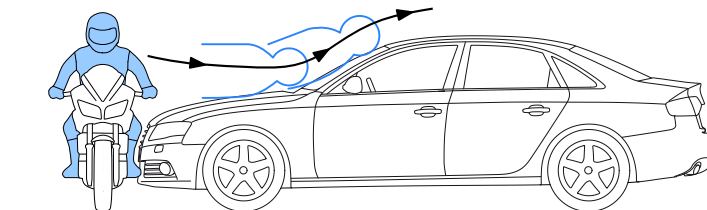
(c) flyover with
    low energy transfer
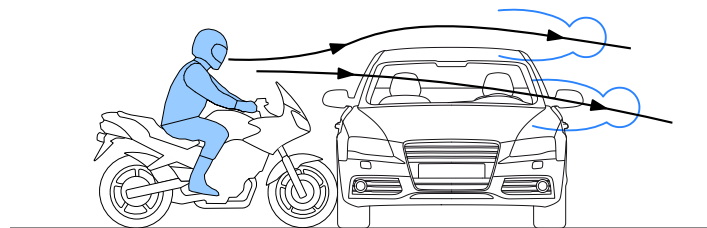
Figure 2.7: Types of collisions of a conventional motorcycle and motorcyclist against an opposing vehicle as classified by [AppelOtteWüstemann86].

the rider is wearing effective personal protective equipment and slides freely to the final position after impact without coming into contact with other vehicles or fixed objects.

As described by [Lechner86] in his review of 300 accident descriptions, the causes and kinematics of solo accident initiation are manifold. He divided these into falls on the roadway and run-offs from the roadway. Figure 2.8 shows, as examples for falls, (a) slipping of the front wheel and (b) the rear wheel, which in turn leads to instant centers of rotations at the rear and front wheel contact points, and the typical, very likely resulting accident event of motorcycle and rider. In (a), when the front wheel slips or the motorcycle turns around parts that contact the road behind the motorcycle's center of gravity, the crash kinematics are often adverse to the rider because it leads to a negative spin of the vehicle. When sliding, the rider is in front of the two-wheeler and might be jammed between the two-wheeler and the ground. In a collision, the rider may be trapped between the two-wheeler and a hazard. In (b), the rear wheel slides or motorcycle parts in front of the motorcycle's center of gravity contact the roadway. This leads to positive vehicle spin. Separation of rider and vehicle is favored and the rider likely slides behind the two-wheeler. Both (a) and (b) are referred to as *lowside* accidents, where the rider falls to the low side of the lean in a turn. Other types are *highside* accidents where the rider falls to the opposite side of a turn while trying to correct, causing the motorcycle to flip over, and *topside* accidents where the motorcyclist flips over the handlebars because the motorcycle suddenly decelerates, as shown in an overview in [PetitEtAl20].

center of gravity

instant center
of rotation (ICR)

negative
spin

ICR

positive
spin

(a) front wheel slide   (b) rear wheel slide
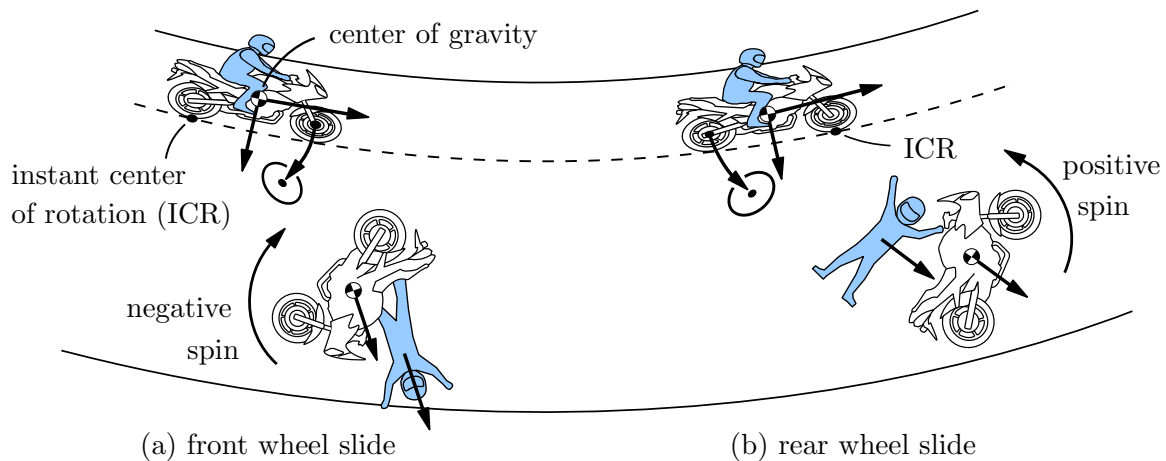
Figure 2.8: Exemplary types of solo accident behavior of conventional motorcycles and motorcyclists after a loss of control as described by [AppelOtteWüstemann86] and [Lechner86].

Secondary accident phases and solo accidents often involve collisions with roadside obstacles, such as several types of road traffic barriers. The interaction of PTW riders and such structures are very complex and lead to many possible rider trajectories, specified in [DanielloCristinoGabler13]. The accident behavior has been studied in experimental and simulation research. For a comprehensive overview of the impact behavior of motorcyclists against roadside barriers and the improvement of these for the specific protection of motorcyclists, see [BürkleBerg01, GärtnerRückerBerg06, Peldschus09].

2.3.2 Motorcycle Safety Design

There are two main approaches to passive safety in motorcycle literature, see Figure 2.9. In the first principle, the rider is restrained to the motorcycle. In a collision, kinetic energy from the motorcycle is converted into deformation work. The rider restraints, like belts or airbags, aim to prevent direct contact between the motorcyclist and an accident opponent up to a certain collision speed. In the second principle, the rider must be separated from the motorcycle as soon as possible and a direct impact must be avoided. Here, it is important that the rider does not get tangled up in parts of the motorcycle. In the best case, a flyover of the motorcyclist over the accident opponent, i.e., a car, is initiated. Here, in theory, the injuries of a flyover should be less than those of a direct impact.

Figure 2.9: Principles of motorcycle passive safety, according to [LangwiederSpornerPolauke87].

passive safety

rider restraint

optimization of
rider trajectory
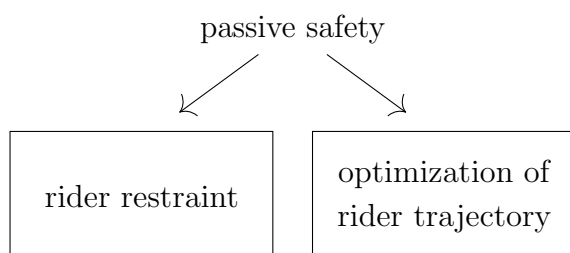
The accident behavior of today's conventional PTWs based on the latter safety principle has been intensively studied in the past, see [Sporner82, BergBürkleSchmidts98], with an excellent overview by [BergEtAl04]. In these works, vehicle analyses, real-world accident data evaluations, full-scale crash tests, and accident simulations were carried out to determine the positive and negative influences of the design on the rider's accident behavior. In [BergEtAl04], experiments were performed with common motorcycle types at that time. The influence of motorcycle types and the design of seats, tanks, footrests, fairings, and handlebars were investigated by evaluating real-world accident data and in full-scale crash tests with ATDs as rider surrogates in accident scenarios, according to ISO-13232. The evaluation of design features from a total of 91 motorcycle types resulted in recommendations such as tank ramp angles and the design of bodywork and handlebar. Motorcycle types with a high and upright riding position and thus high head height performed best. Advantageous designs of the seat, tank, and fairing, as well as the upright riding position, help to separate the rider from the motorcycle. This favors an upward-forward trajectory of the rider and thus prevents the head from hitting the other vehicle's roof edge in a frontal collision of a motorcycle into the side of a passenger car (configuration ISO 13232-⑦). Motorcycles with low seating positions, like choppers and sport bikes, performed concept related significantly worse.

The conventional motorcycles investigated in [BergEtAl04] still represent the state-of-the-art of motorcycles currently operated worldwide. All of them follow the second passive safety principle of an optimized rider trajectory in accidents if passive safety design was even considered during development. The following section summarizes past and current research and development efforts of PTW safety systems that go beyond this principle. These are systems that support the rider or influence the vehicle driving behavior in order to actively avoid and mitigate the effects of an accident, i.e., active safety systems, and these are systems that follow the first principle and restrain the rider to the vehicle. Motorcycle types that are equipped with a first-principle safety system and actually made it to the motorcycle market are described in Addenda 1 and 2.

Active Safety Systems

Active safety systems aim to prevent accidents and reduce their frequency. In addition to good brakes and tires, such current systems for PTWs are anti-lock braking systems (ABS), stability control for braking while cornering, blind spot detection systems, etc. [SavinoEtAl20]. A recent study on active safety systems for motorcycles [SavinoPieriniFitzharris19] summarizes current and possible future systems and discusses the relevance of five available systems: (i) ABS, (ii) autonomous emergency braking, (iii) collision warning, (iv) curve warning, and (v) curve assistance. Based on a large accident data set, they quantify the proportion of accidents the systems can potentially influence. ABS is most significant with being relevant for 40.6 % of the surveyed accidents.

A combination of all five systems in 57 %. Another way to protect motorcyclists through active systems is to prevent collisions between cars and motorcyclists by having other road users avoid accidents. A recent analysis on the safety benefits of motorcycle-detecting automatic emergency braking integrated into passenger vehicles [DeanEtAl21] predicts that with almost full market penetration of such systems, it would be possible to reduce the number of motorcycle crashes by 28 % in 2065.

This summary shows that while some improvements have taken place, such as the introduction of standard ABS for new PTWs over $125\,\text{cm}^3$ and the development and the full market deployment of other systems planned, there are currently no fully effective active safety systems for motorcycles or the road users around them. A large proportion of accidents still cannot be avoided even with an optimal driver response and technical assistance in accident prediction and avoidance. Therefore, comprehensive safety for motorcycles cannot be achieved by active safety systems alone but must be complemented by effective passive safety measures, as is the case for passenger cars.

Vehicle Safety Structures

The essential difference between an occupant of a car and a rider of a two-wheeler is that the rider sits exposed on top of his vehicle rather than in an enclosed space that isolates and protects him. On some motorcycles that are currently available, widely protruding components of the drivetrain and fairing, as well as attachments such as luggage bags, form minimal lateral safety spaces for the legs, see Figure 2.10. Some motorcycles have crash bars, which are tubular structures that stick out past the motorcycle to shield the vehicle itself and the rider. These potentially protect the rider's legs in the event of side collisions or sideswipe collisions [MohaymanyEghbalian07]. There have been considerable research efforts in the past to minimize motorcyclists' injuries occurring during collisions with dedicated leg protection. These efforts involved many ideas, such as crash bars, reinforced fairings, and energy-absorbing components at the rider's leg, as extensively summarized by [Sakamoto90]. Concepts aimed at restraining the legs resulted in negative effects such as torso pitch after impact, which increases the risk of upper body injuries, and were
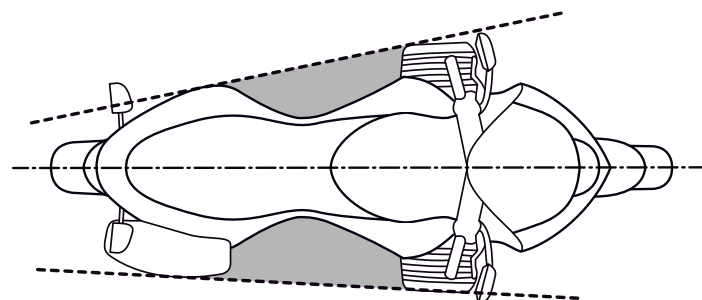
Figure 2.10: Lateral leg protection spaces (grey) through protruding motorcycle parts.

therefore considered impractical. A concept that is somewhat similar to the side impact structure presented in this thesis here is the "UKDS" (UK Draft Specification) motorcycle leg protector device. It is a side-mounted, very robust fairing that follows the contour of the legs and prevents frontal and lateral displacement of the legs by incorporating energy-absorbing components. It aims to maintain space for the legs to prevent them from getting trapped between the motorcycle and opposing vehicle, retain the legs within space provided by the protectors, and absorb impact energy. Results from ISO 13232 experiments and simulations [RogersZellner98] showed that while beneficial in some scenarios, the robust restraint of the knee, resulting in an alteration of impact kinematics because of forward and/or lateral pitch, leads to increased head injury severity. Ultimately, because of the proven harmful effect, it was recommended that the concept not be pursued further. A very recent idea is an airbag-based device for riders' lower limb protection in side impacts [PallacciEtAl19]. Two airbags per vehicle side, one in front and one behind the leg, are proposed. The preliminary effectiveness assessment with FE simulations showed potential for lower limb protection, but adverse effects in body loads are also noted. None of the above-proposed concepts come close to the structural protection of a rider's whole body. They are aimed at local protection of the legs, while retention evidently does not work to improve rider impact kinematics. A survival space in the form of a kind of passenger cell for the entire body of the rider, which is substantially motivated to increase passive safety, offers only the C1 scooter from BMW, see Addendum 1. A concept that is, or rather was, unique in the world of two-wheeled transportation.

Addendum 1: Enclosed Scooter BMW C1 – Produced from 1999 ot 2002

The BMW C1 was a new concept of a city scooter, conceived in the early 1990s, designed for urban traffic [Leek12]. The PTW, shown in Figure 2.11, has a curved roof with a glass windshield designed to repel wind and weather. The aluminum rollover structure has a front crumple zone and provides space for the rider (Figure 2.12). The rider is restrained to the vehicle in an upright position with a lap belt and two diagonal belts across the chest. Sidebars to the left and right of the shoulders prevent the rider's upper body from leaving the safety cell and the intrusion of opposing structures. A non-restrained pillion is less protected and takes a seat outside behind. The overall idea behind the vehicle is good weather protection with significantly improved passive safety where the rider does not need to wear a helmet or protective clothing – ideal for daily commuting.

Component and full-scale crash tests and vehicle crash simulations of the concept are given in [KalliskeAlbusFaerber98, KalliskeAlbus98]. Two of the seven ISO 13232 configurations and six more self-defined full-scale laboratory crash tests, including solo accidents, were performed. In [KalliskeAlbus98], it is "expected that the [concept] guarantees the rider a very high degree of passive safety." A comparison to

a conventional scooter for frontal impact ISO 13232 ⑦ with helmeted crash test dummies as rider surrogates resulted in significantly lower head accelerations and reduced neck loads. Slightly larger accelerations were measured for the chest and pelvis but which correlate to those of a belted automobile occupant. Similar results were measured for ①. In [OsendorferRauscher01], two severe real-world impacts against passenger cars are described. These resulted in only minor AIS1 (Abbreviated Injury Scale; see Addendum 3 on page 36) injuries to the unhelmeted rider in both cases. Based on the recommendation of Germany's Federal Highway Research Institute (BASt) in [KalliskeAlbusFaerber98], the legal helmet requirement in Germany was waived. Many European countries followed this recommendation, although abrasions can occur even with this concept and sturdy clothing is still recommended [OsendorferRauscher01].

The vehicle polarized and struggled to appeal to a sufficient number of buyers. In addition to quality problems and high costs, the safety concept related sensitivity to wind were perceived as serious disadvantages [Riedel00, Schmidt03]. Despite the benefits of additional weather protection and increased passive safety, sales were disappointing. The C1 was eventually discontinued in 2002 with only 26,300 vehicles produced [Leek12].

© BMW AG[3]

Figure 2.11: BMW C1.

© BMW AG[3]

Figure 2.12: BMW C1 space frame.

[3]BMW PressClub: BMW C1 – Mit Freude in die Stadt. https://www.press.bmwgroup.com/deutschland/article/detail/T0005918DE/bmw-c1-mit-freude-in-die-stadt, 2000.

Vehicle-Mounted Airbags

The concept of an airbag dates back to the 1940s. While the majority of automotive patents for automobiles were issued during the 60s, they were first introduced in the 70s and are now standard equipment on the vast majority of passenger vehicles [NayakEtAl13]. Equipping PTWs with a frontal airbag seems an obvious technical measure to also improve

the passive safety of a motorcycle. This measure has been proposed and studied regularly for decades now, see e.g. [BothwellKnightPeterson73, SpornerLangwiederPolauke87, ChinnEtAl96, KuroeNamikiIijima05, Bhosale13, Autoliv22], to name just some, spanning the last 50 years. Here, the basic idea is to use the airbag in case of a frontal impact of the PTW against an accident opponent. The airbag is supported either by parts of the motorcycle itself, like in [KanbeDeguchiHannya07], or by opposing structures, like in [AikyoEtAl15]. The intended effect is composed of one or more of the following ideas: dissipate as much energy as possible on impact to reduce the rider's velocity, avoid contact with the roof rail or other hard surfaces of a car, and/or act as a ramp that guides the rider over the roof of a car.

It has shown that motorcycle-mounted airbags are beneficial in reducing the impact velocity of the rider in frontal collisions. With the Honda Gold Wing, there is finally a model with a centrally placed airbag for the rider, albeit only optional; see Addendum 2. However, there are multiple reasons why the solution has not yet found a wider application. Single frontal airbag show limited effectiveness in frontal collisions with a moving opponent or oblique collisions, where the rider is susceptible to missing the airbag. They do not provide any additional protection in the event of a lateral impact. Furthermore, depending on the type of motorcycle, see Section 2.1, a motorcyclist sometimes sits more, sometimes less upright on his vehicle. It must be ruled that a forward-leaning driver is hit by the airbag when being in a frequent rider position.

> **Addendum 2: Heavy Touring Motorcycle Honda Gold Wing GL 1800 - Available with an Optional Frontal Airbag Since 2007**
>
> The Gold Wing GL 1800 is a heavy touring motorcycle that has been in production since 2006 as a continuous evolution from previous model lines. In addition to the weight of up to 400 kg, the motorization with a 6-cylinder combustion engine with 1800 ccm and up to 125 horsepower is enormous. Due to the extensive additional equipment, such as an audio and alarm system, cruise control, and seat heating, the vehicle takes a pioneering and exceptional position in two-wheeler engineering. Thus it is often called the "car on two wheels" [SzymezakRybiczka08]. After a development period of 15 years, the Honda Gold Wing has been available with a frontal airbag for passive safety since 2007. The system consists of multiple acceleration sensors in the front fork, a control unit, and a large 150 liter V-shaped airbag, see Figure 2.13. The inflated airbag is supported by the voluminous motorcycle cockpit and two outside straps. The airbag is designed to be effective in frontal crashes, as shown in Figure 2.14, as a frontal impact of a motorcycle against a collision partner is identified to be the most common in Figure 2.3. The airbag volume is that large because it aims to absorb the energy of the entire body of the occupant with no additional restraint available.

In [KuroeNamikiIijima05], an evaluation of full-scale impact tests of all of the seven ISO 13232 configurations with an airbag-equipped motorcycle and a motorcycle without an airbag was conducted. The airbag sensors did not detect an impact in configurations ① and ⑤. The positive effect of the airbag is mainly a reduction in the risk of head injury in ② and ④. Surprisingly, the rider surrogate loading for the frontal impacts ③ and ⑦ could not be reduced since relatively low loads were already measured for the comparative motorcycle.

The Gold Wing is an exotic vehicle. Not all of these vehicles sold are equipped with an airbag; it is only an optional accessory. The transferability of this concept to other motorcycle types is limited. The large airbag requires the rider always to be in an upright position (see Figure 2.2), and few motorcycles have a similarly large cockpit that can support the airbag.

© Honda Motor Europe Ltd.[4]

© Honda Motor Europe Ltd.[5]

Figure 2.13: Honda Gold Wing GL 1800 with inflated front airbag.

Figure 2.14: Crash test of Honda Gold Wing.

Honda European News Room: [4]Gold Wing with Airbag Rear 3/4. https://hondanews.eu/eu/en/cars/media/photos/10234/gold-wing-with-airbag-rear-34, 2007. [5]Gold Wing ADAC Crashtest Side. https://hondanews.eu/eu/en/cars/media/photos/10235/gold-wing-adac-crashtest-side, 2007.

Safety Belts

There have been few efforts to secure the passenger of a PTW to the vehicle with belts. In [GrassiEtAl18b], a safety jacket for the passenger is investigated, which is connected to the rear of a motorcycle with a single belt at the back. Numeric modeling and simulations of the concept resulted in a reduction of head and neck loads in a collision between a motorcycle and a moving car (configuration ③) by preventing the head from hitting the car. In [Murri07], a similar harness consisting of shoulder, lap, and crotch straps is experimentally tested in sled tests and full-scale crash tests. Comparisons with motorcycles for collisions into the side of a stationary passenger car (⑦) without harness show that

the system can prevent severe collisions of the head with the roof rail of the car. This design idea has not been pursued further. To date, the BMW C1 scooter remains the only sold PTW to feature seat belts for the rider; see Addendum 1.

2.3.3 Personal Protective Equipment

Since current PTWs do not provide sufficient protection for the rider, passive safety systems are dominated by personal protective equipment. This equipment includes helmets, safety clothing and protectors, and, more recently, wearable airbag systems.

Helmets

Helmets are the most widely used and essential safety devices for motorcycle riders and pillions. They can be divided into three major types: full-face helmets, modular or flip-up helmets, and open-face or half helmets without chin guards. Typically, they have a hard outer shell that distributes the force of an impact to protect the skull from fractures and prevent objects from penetrating the skull. A deformable inner shell with an energy-absorbing material limits the forces of the impact by absorbing some of the energy that would otherwise be absorbed by the head and brain, reducing the induced accelerations. In addition, they have comfort functions for motorcyclists. They isolate the rider's face from the wind, resulting noise, weather, and flying particles from insects up to airborne gravel. A comprehensive review of state-of-the-art helmet design and testing can be found in [FernandesAlves de Sousa13].

That helmets are effective in their safety function can be shown in simulations and experiments and is verified by specifications of regulations such as ECE regulation R 22 [UNECE21] of the United Nations Economic Commission for Europe (UN/ECE) or the Federal Motor Vehicle Safety Standard FMVSS 218 [NHTSA20]. According to a review of many existing studies from [LiuEtAl08], motorcycle helmets are estimated to reduce the risk of death by 42 % and the risk of injury by 69 %. Data from the US, where in 2019 still 29.8 % of riders chose not to wear a helmet, suggests that motorcycle helmets are 37 % effective in preventing fatalities to riders and 41 % to pillions [NHTSA21]. In contrast, there is no clear statistical evidence on whether helmets lead to more neck injuries and how effective the different types of helmets are; see the scoping works [LiuEtAl08, TabaryEtAl21].

A very recent development is the airbag helmet for bicycle riders from the Swedish company Hövding. It is worn as a collar around the neck. Acceleration sensors detect a fall and inflate an airbag helmet. Studies [StigsonEtAl17, AbayazidEtAl21] show that it can outperform conventional bicyclist helmets, which are practically limited in the size of their padding. In the case of an airbag system, the protective cover remains tightly packed until use. However, so far, it is not aimed at motorcycle use.

Safety Clothing

Besides comfort functions such as keeping the rider dry and warm, various types of clothing worn all over the body aim to mitigate injuries. Jackets, pants, or full-body suits protect riders against lacerations and abrasion injuries when they slide on the road surface after falling off. They also prevent the contamination of open wounds and fractures by road dirt. Their outer surfaces are usually made of some durable synthetic material or leather. Non-slip gloves allow a firm grip around the controls. Heavy footwear is designed to protect the lower parts of the legs against abrasion or crushing. Protectors – also referred to as armor – worn on the limb joints, as well as on the back and tailbone, are protective elements adapted to the shape of the body, which are made of strong and shock-absorbing materials and aim to mitigate hard impacts. These can be worn individually or are often integrated into the clothing. Materials used for motorcycle armor are hard plastics, silicones, and different types of foams [NatarajanRajan22]. Their protective effect, the reduction of peak loads submitted onto the human body, aims to prevent or reduce the severity of contusions, fractures, and joint damages. Their working principle can be divided into

- internal dissipation of impact energy within the protector,

- delayed transfer of impact energy over a longer period of time,

- and distributed transfer of impact energy over a larger area.

Quantitatively, the reduction of force and energy transmission to the bony structures is demonstrated in the experimental study [SchwarzeHurschlerWelke19] by cadaver tests of a protected knee compared to an unprotected condition. Body-worn protectors are tested and certified, for example, by the European standards EN1621-1 [EN1621-1:2012] for protectors worn at the shoulders, elbows, forearm, knees, shins, and hips or EN1621-2 [EN1621-2:2014] for back protectors. In EN1621-1, their performance is quantified and certified with a drop tower test (depicted in Figure 4.28) in which a 5 kg impactor is dropped on the protector from a height of 1 m, which corresponds to an impact energy of 50 J. The protector rests on a heavy steel anvil with a force sensor at its base. An average transmitted peak force of less than 35 kN corresponds to protection level 1; an average force of less than 20 kN corresponds to the higher rated protection level 2. Such tests are performed in this thesis to evaluate the proposed leg impact protection of the proposed safety concept, provided in Section 4.3.4.

An observational study of injury data from 7148 motorcyclists involved in crashes examines the effectiveness of motorcycle jackets, pants, gloves, knee-high or ankle-high boots, and back protectors [WuEtAl19]. Wearing protective clothing is associated with a lower risk of soft tissue injuries such as abrasions and lacerations. However, no significant protective effect against more severe injuries such as fractures, dislocations, or sprains is found,

except for knee-high or ankle-high boots, which reduce the risk of foot and ankle fractures. Correspondingly, [de RomeEtAl11] show that wearing a motorcycle jacket makes it less likely to be hospitalized, especially if fitted with body armor. However, an association between the use of body armor and the risk of fractures is not found. Likewise, a review of the vast number of available studies on the influence of back protectors by [EkmejianEtAl16] concludes that there is a lack of evidence for the effectiveness of back protectors in preventing severe injuries of motorcyclists. According to [AlbaneseEtAl17], the energy attenuation performance of impact protectors rated by EN1621-1 and the specified levels might be insufficient to prevent injuries effectively. However, it is questionable whether the fulfillment of higher limits can be technically solved while, at the same time, the clothing does not become too heavy and leaves enough freedom of movement.

Since very recently, companies begin to incorporate airbags into protective clothing, such as jackets. However, airbag systems make the jacket considerably heavier and more uncomfortable to wear, and a testing study of existing systems on the market [SerreEtAl19] shows limited protective effect in the chest area which is confined to lower impact speeds below a threshold speed of around 30 to 40 km/h.

2.3.4 Current Usage of Passive Safety Equipment

In Table 2.2 the current usage of the above-described passive safety equipment is summarized. The MAIDS study data show that most riders wore personal protective equipment when the accident occurred. In all the sampling regions, helmets were mandatory for the riders, and over 90 % wore a helmet. Out of these, at least 85.6 % are full-face, open-face, and half-type helmets, which are regarded as providing a high standard of protection or at least it is not statistically clear which helmet type is superior to the others (see Section 2.3.3). The MAIDS report is a high-quality study that provides an equally large exposure data set as a control group. It can be used, for example, to compare the helmet-wearing rate of riders who have not crashed. Because the rates are very similar (90.4 % vs. 92.3 %), it can be deduced that wearing a helmet is not associated with a greater or lesser risk of having an accident. According to the study, there are substantial differences in the robustness of other clothing items. It ranges from *heavy* (material: i.e., leather, kevlar, imitation leather; shoe: i.e., heavy/work boot, PTW boot) to *medium* (material: i.e., denim, nylon; shoes: i.e., medium street shoe, loafer) to only *light* (material: i.e., thin cotton; shoe: i.e., sandals). The share of vehicle passive safety systems of motorcycles itself is currently negligible.

Table 2.2: Usage shares of the described passive safety equipment.

protective equipment	share of equipment types	total used share
personal[a] — clothing		
helmets	full-face · open-face · half-type · other & unknown · none	90.4 %
jackets	heavy · medium · light	100 %
pants		100 %
gloves		66.4 %
shoes		99.9 %
vehicle		
safety structures	BMW C1[b] Honda Gold Wing[c]	< 0.01 %
airbags		< 0.01 %
safety belts	0 % 50 % 100 %	< 0.01 %
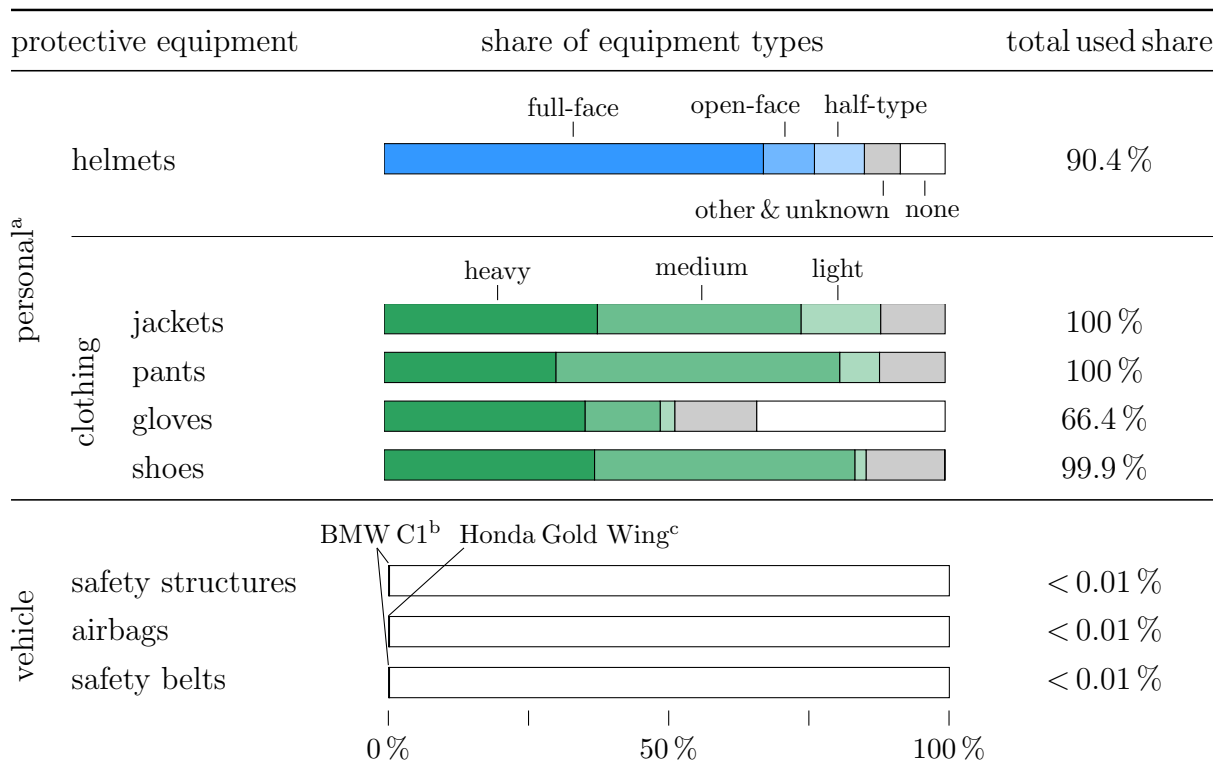
[a]for motorcycles riders, excluding pillions [ACEM09a]   [b][Leek12]   [c]estimated

2.4   Traffic Accident Consequences for Motorcyclists

In summary, Section 2.3 describes typical motorcycle accident behavior and current approaches to motorcycle safety, surveys the safety equipment available on the market, and shows its current application – all necessary for a well-informed and meaningful discussion of objective (O3). What remains to evaluate the status of road safety of PTW riders is an assessment of the resulting consequences of current accident scenarios and the given level of protection for O4. Is there room for improvement? If so, what are the injury patterns that need to be prevented? A final section then seeks to establish the methods used in the technological development of passive safety systems to correlate mechanical loads to the risks of such injury.

2.4.1   Injury Statistics

Injury Data from MAIDS In Depth Study

The MAIDS in-depth accident study recorded 3417 injuries of 921 PTW riders and 227 injuries of 79 PTW passengers in the 921 accidents shown in Section 2.2.1, while only riders are considered below. The data leads to a distribution of rider trauma status shown in Table 2.3. It quantifies that about 10.9 % of those accidents were lethal.

In Figure 2.15 (a) a summary of the recorded injuries greater than AIS 1 (Abbreviated Injury Scale; see Addendum 3) across eight different body regions, as well as the rider's whole body, is given. It illustrates that riders sustained injuries at all body parts. Most injuries were to the upper and lower extremities, closely followed by the head. The spine, including the neck, sustains about as many injuries as the neck and the combination of the abdomen and pelvis. To analyze the severity of the injuries, first, the respective

Table 2.3: Trauma status of 921 PTW riders involved in accidents in [ACEM09a].

no trauma	3	0.3 %	
first aid only	22	2.4 %	
disabled	4	0.4 %	
hospital treatment up to 8 days	522	56.8 %	
hospital treatment more than 8 days	121	13.1 %	
hospital treatment, unknown number of days	142	15.4 %	
fatal	100	10.9 %	
unknown	7	0.8 %	
total	n = 921	100 %	

maximum injury per body region is identified. The severity of this injury is then rated by the Maximum AIS (MAIS) and classified from minor (MAIS 1) to maximal (MAIS 6), as given in Figure 2.15 (b). Here, as stated in Table 2.4, maximal injuries are usually, but not inevitably, fatal. The distribution shows that the majority of injuries are minor or moderate. Severe, critical, and maximum injuries occur to the head, neck, spine, chest, and abdomen. What the data do not show is that the severe consequences of PTW accidents can be attributed to a particularly vulnerable body region with the current level of protection. Instead, it seems that the whole body of a motorcycle rider needs better protection.

Addendum 3: Injury Classification According to the Abbreviated Injury Scale

The abbreviated injury scale (AIS) is a widely used standardized rating scale system for single-injury severity. The scale is used to quantify the severity of a particular injury by assigning a numerical score to traumatic injuries, targeting their survivability. The classification ranges from 0 (non-injured) to 6 (maximal) as summarized in Table 2.4. The severity of the injury is always evaluated concerning the whole body, assuming that it has only this one injury. First published in the 1970s, it was initially designed for motor vehicle accidents and has since been revised several times to include many types of injury trauma [LoftisPriceGillich18].

Table 2.4: Abbreviated injury scale (AIS) classification with AIS codebook injury examples [Gennarelli08] and mean survival probability of an individual injury according to [GennarelliWodzin06].

AIS code	injury classification	injury examples	probability of survival
0	non-injured		
1	minor	skin abrasion or hematoma, muscle strain, headache	99.33 %
2	moderate	hip joint dislocation, achilles tendon tear, tibia fracture, muscle tear	99.25 %
3	serious	femur fracture, skin avulsion, bladder rupture, amputation below knee	96.5 %
4	severe	iliac artery or vein rupture, amputation at hip, open chest wound, liver rupture	85.4 %
5	critical	spine cord laceration, aorta transection	60.4 %
6	maximal	massive destruction of skull & brain, complete cord syndrome at C3 or above, liver seperation	21.0 %

18.4 % (n=628)	head	17.7 % (n=395)
1.1 % (n=38)	neck	1.7 % (n=38)
5.0 % (n=171)	spine	5.6 % (n=124)
7.4 % (n=254)	thorax	8.8 % (n=196)
24.3 % (n=830)	upper extremeties	23.1 % (n=515)
4.1 % (n=140)	abdomen	4.8 % (n=108)
2.2 % (n=75)	pelvis	3.1 % (n=69)
31.8 % (n=1086)	lower extremeties	30.6 % (n=681)
5.7 % (n=195)	whole body	5.7 % (n=127)

MAIS classification

minor moderate severe
serious critical maximal
unknown
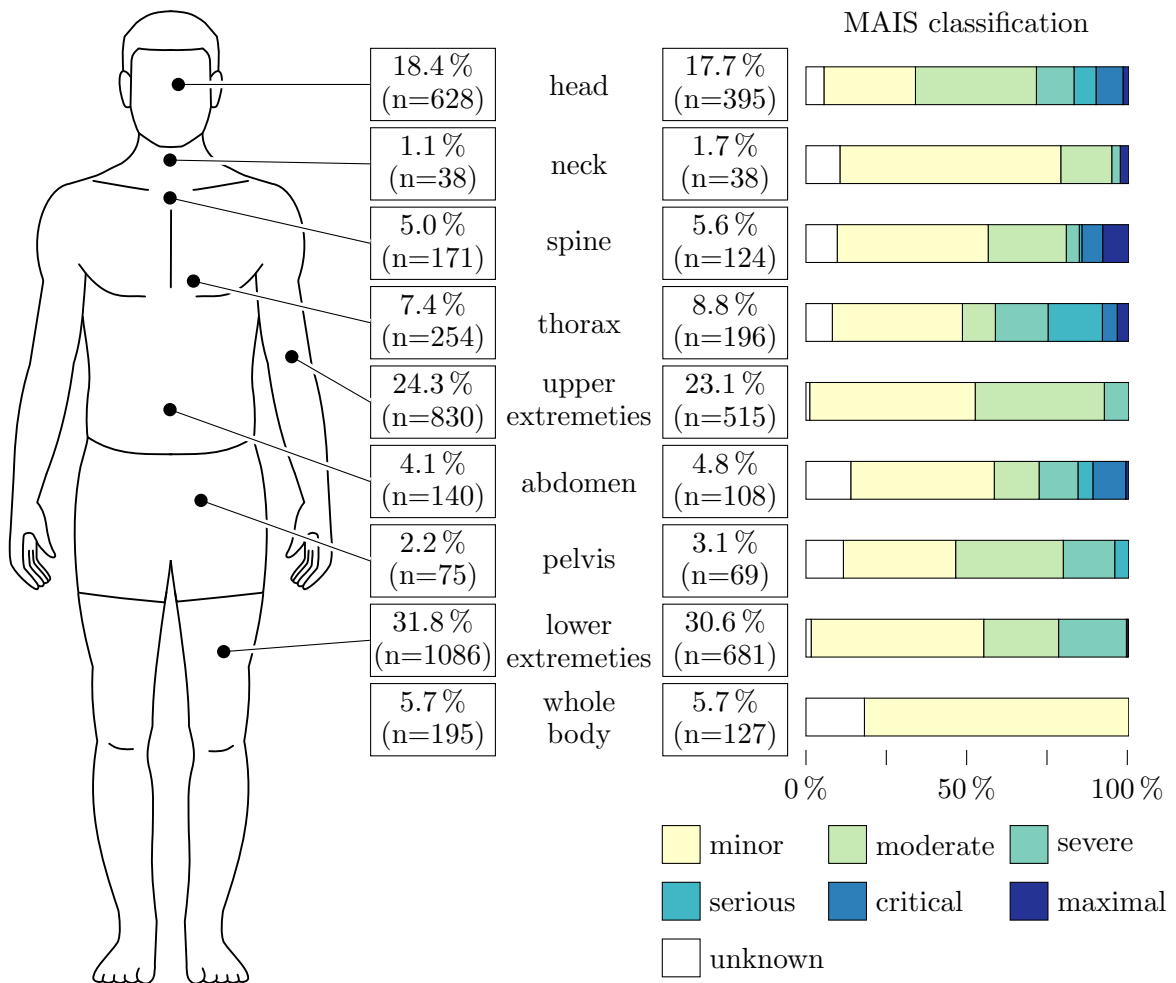
(a) Injuries greater than AIS 1, where n is the number of injuries (total: n=3417). Multiple injuries per body regions are possible.

(b) Maximum AIS (MAIS) per body region, where n is the number of the most severe injuries per body region (total: n=2227).

Figure 2.15: Distribution of PTW rider injuries per body region conglomerated from [ACEM09a]. Neck injuries exclude spine injuries.

2.4.2 Correlation with Injury Criteria

To replicate and study human accident behavior in crash tests, mechanical surrogates of humans are used nowadays. Figure 2.16 shows such an anthropometric test device (ATD). Better known as crash test dummies, they are designed to match their human counterparts in shape, size, mass, stiffness, and articulation and reproduce their energy absorption and dissipation under high external loading based on experiments with post-mortem human subjects. Various types of such devices exist – mainly to depict car occupants – and they are classified by size, age, sex, and impact direction, e.g., a frontal, side, or rear impact. They are instrumented with sensors that measure time histories such as accelerations, forces, moments, and deformations at multiple body locations. In addition to
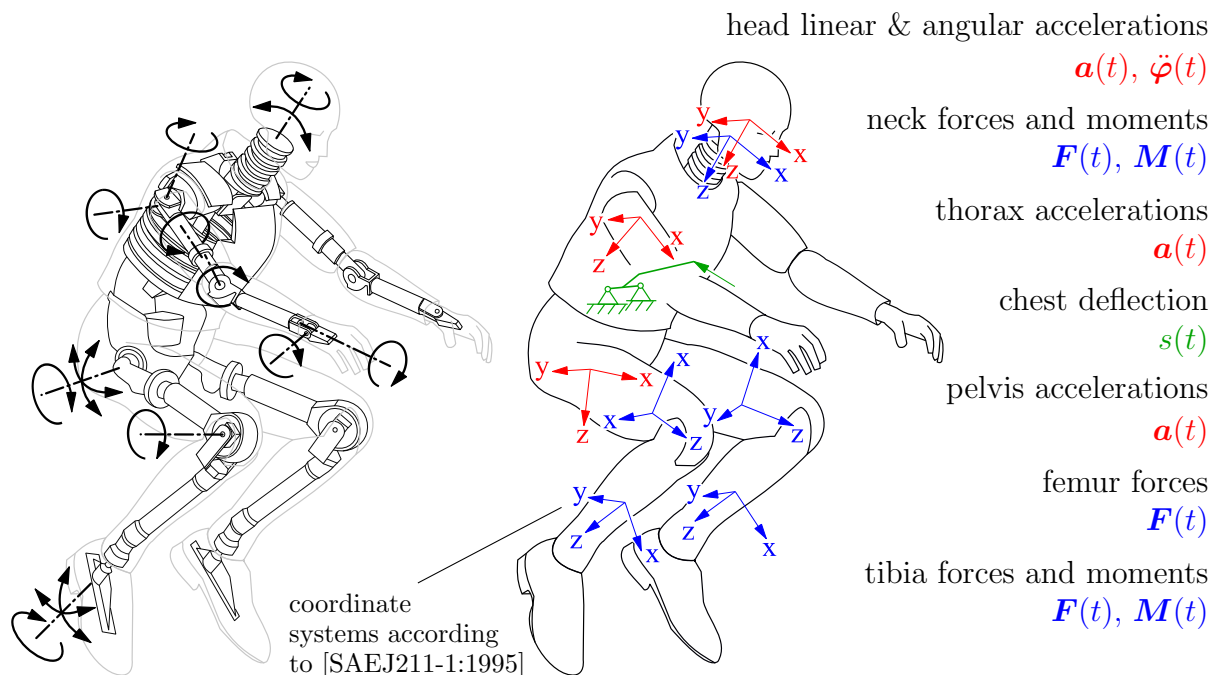
head linear & angular accelerations
$\boldsymbol{a}(t), \ddot{\boldsymbol{\varphi}}(t)$

neck forces and moments
$\boldsymbol{F}(t), \boldsymbol{M}(t)$

thorax accelerations
$\boldsymbol{a}(t)$

chest deflection
$s(t)$

pelvis accelerations
$\boldsymbol{a}(t)$

femur forces
$\boldsymbol{F}(t)$

tibia forces and moments
$\boldsymbol{F}(t), \boldsymbol{M}(t)$

coordinate systems according to [SAEJ211-1:1995]

Figure 2.16: Joint degrees of freedom (left) and sensor variables, from top to bottom, with locations and orientations (right) of the Hybrid III 50$^{\text{th}}$ anthropometric test device (ATD).

virtual models of these ATDs for computational accident investigations, there are now very complex virtual-only human body models (HBMs) available. A description and discussion of available and eventually used models of ATDs and HBMs in this computational work are provided in the rider surrogate modeling description in Section 4.4.

To evaluate the loading, injury criteria correlate sensor loads with probabilities of certain injuries for specific body regions. Since the severity of an injury cannot always be correlated with the maxima of the load, derived quantities, such as, for example, the head injury criterion (HIC), described in [KleinbergerEtAl98], have been developed. The HIC is a normalized integral of the resultant of the acceleration $a_{\text{res}}(t) = \|\boldsymbol{a}(t)\|_2$ measured at the head's center of gravity, see Figure 2.16. It rates the loading by its value and duration by

$$\text{HIC}(t_2 - t_1) = \max_{t_1, t_2} \left\{ (t_2 - t_1) \left[\frac{1}{t_2 - t_1} \int_{t_1}^{t_2} a_{\text{res}}(t) dt \right]^{2.5} \right\}, \tag{2.1}$$

where $a_{\text{res}}(t)$ is expressed in the standard gravitational acceleration g $= 9.81 \, \text{m/s}^2$ and t in s. Injury risk curves, such as those in [NHTSA95], shown in Figure 2.17, then correlate injury probabilities P for AIS levels to the value of the criterion. Here, these estimate that for a value of 350 for HIC(36) (which means that the maximum integral interval is not longer than 36 ms) the risk for an AIS3+ injury is 6.5 %. Based on these injury probabilities, threshold values as biomechanical limits are set so that for a certain load case, a certain injury risk is not exceeded. Thus, according to FMVSS 208 [NHTSA11]
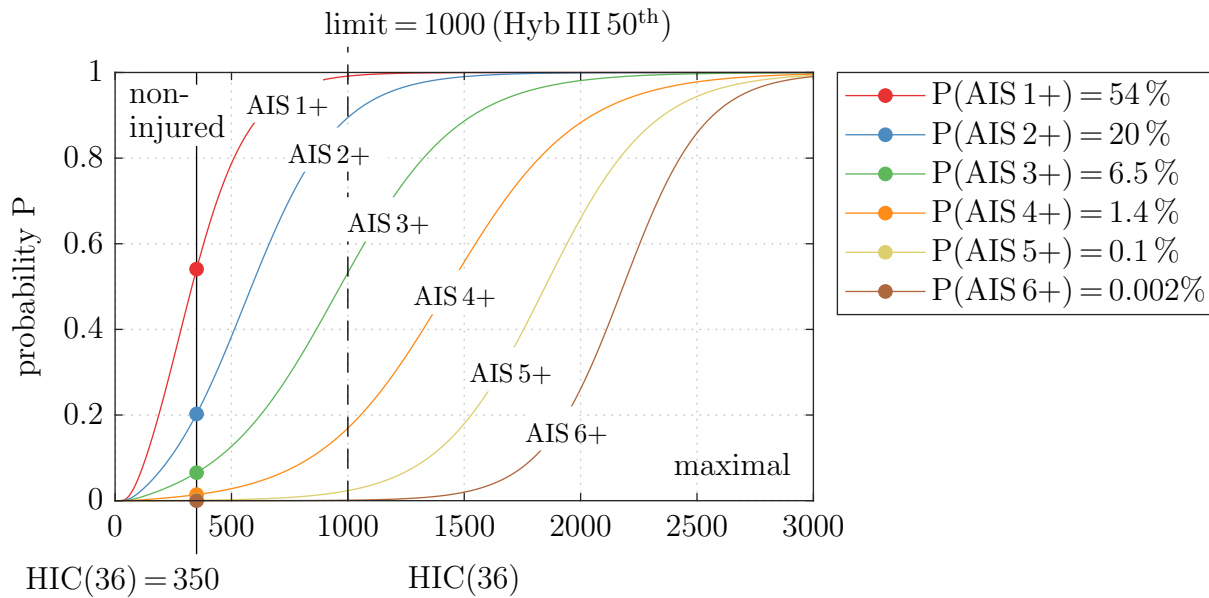
Figure 2.17: AIS injury risk curves for Head Injury Criterio HIC(36) and exemplary AIS probabilities for a HIC(36) of 350.

for a frontal impact of a passenger car against a rigid barrier with 30 mph ($\approx$ 48 km/h), the HIC(36) shall not exceed 1000.

For a comprehensive overview and discussion of injury mechanisms and available injury criteria for injury risk correlation, see e.g. [YoganandanNahumMelvin14] or [SchmittEtAl19]. For passenger vehicle occupant protection, there are national and international regulations, such as the ECE regulations by (UN/ECE) or FMVSS for the US, that specify injury criteria and respective maximal values for specific load cases. Also, consumer ratings such as the New Car Assessment Programs for the United States (US NCAP) and the European Union (Euro NCAP) provide constantly updated biomechanical criteria from the latest scientific findings of occupant protection. To the best of the authors' knowledge, for the passive safety of motorcyclists, such governmental regulations or consumer ratings currently do not exist. The most recent version of ISO 13232 recommends only a very limited set of criteria. Motivated by the assessment of injury accidents in Section 2.4.1, the work presented here aims to assess many potential injury mechanisms in the whole body. The selection of injury criteria considered, here for a 50th percentile Hybrid III ATD, is summarized in Table 2.5. It is based on a comprehensive set of injury criteria and corresponding biomechanical limits for motorcyclists from an extensive literature review by [BergEtAl04]. In the course of working on the subject, this selection is extended to include the GAMBIT, which is recommended in the international standard [ISO13232:2005], as well as the BrIC and the Nij criterium. For femur criteria, stricter thresholds from ECE-R 94 are used. For an exemplary determination of the injury criteria from the sensor history signals and the applied filter classes, see Appendix A.1.

Head Injuries

Head loading is measured via linear and angular accelerations at the head's center of gravity. In addition to the HIC described above, the resultant linear acceleration is evaluated with the a_{3ms}-criterion, which refers to the maximal acceleration lasting for 3 ms consecutively. The shown limits correspond, i.a., to ECE-R 94 [UNECE12] for a frontal impact of passenger cars with 56 km/h against a deformable barrier with an 40 % overlap, where the HIC (here called HPC for head performance criterion) shall not exceed 1000 and the a_{3ms} shall not exceed 80 g for 3 ms. The head is no independent body part. Since the head is connected to the neck and torso, it will eventually rotate. To also rate injuries resulting from head rotation, the generalized acceleration model for brain injury threshold (GAMBIT) from [Newman86] and the brain injury criterion (BrIC) from [TakhountsEtAl13] are calculated. The GAMBIT accounts for both translational and rotational acceleration by weighing the maximum linear and angular accelerations $a_{\text{res}}(t)$ and $\ddot{\varphi}_{\text{res}}(t)$ against critical linear and angular accelerations a_{C} and $\ddot{\varphi}_{\text{C}}$. As the most recent approach, the BrIC compares the x, y, and z-components of the maximal angular velocity $\boldsymbol{\omega}(t)$, integrated from the angular acceleration to respective critical angular velocities ω_{xC}, ω_{yC}, and ω_{zC}. The BrIC provides critical values for a cumulative strain damage measure (CSDM) and maximum principal strain (MPS). Here, the CSDM is used, where the critical value represents a 50 % probability of AIS4+ brain injuries. As illustrated in Figure A.2 (Appendix A.1), for the determination of the BrIC the maximum values of the components are used regardless of the instance of their occurrence.

Neck Injuries

Cervical spine injuries are evaluated individually by tensile force $F_{\text{z,tens}}$, compression force $F_{\text{z,compr}}$, shear force F_{xy} as well as forward moment $M_{\text{y,fwd}}$ from flexion bending and rearward moment $M_{\text{y,rwd}}$ from extension bending. It is measured at the upper neck with the convention from Figure 2.16. The moments are assessed by their maxima, the components of the forces for durations of 1 ms and 45 ms with thresholds according to [Melvin85]. These originate from experiments with a volunteer [MertzPatrick71] and represent the pain thresholds of an individual person. These limits are also used in part in ECE-R 94 and FMVSS 208. Additionally, the neck injury criterion (Nij) from [KleinbergerEtAl98, EppingerEtAl99] considers load collectives. It is a linear combination of tensile and compression forces $F_{\text{z,C/T}}$ with moments from flexion and extension $M_{\text{y,F/E}}$ against ATD-specific tolerances $F_{\text{int,C/T}}$ and $M_{\text{int,C/T}}$, shown in Figure 2.18. The Nij_{max} is the maximal value of the four possible combinations, designated as NTE, NTF, NCE, and NCF. The tolerances were originally developed to evaluate neck injuries in frontal impacts with individual tolerances for the Hybrid III ATD family and have since become part of FMVSS 208. The chosen set of neck injury criteria thus allows an individual evaluation

Figure 2.18: Tolerances of the neck injury criterion (Nij) according to FMVSS 208 for a Hybrid III 50th.
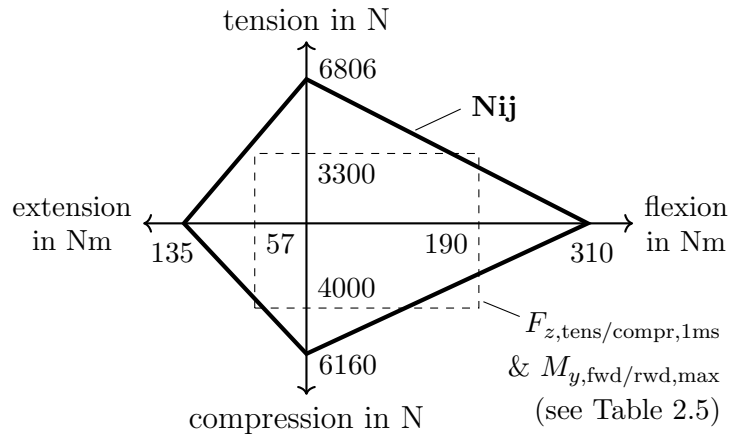
of load types and directions for different load durations and for the evaluation of combined loads' collectives.

Thoracic Injuries

Corresponding to FMVSS 208, the resulting thorax acceleration for a duration of more than 3 ms should be less than 60 g. As defined in ECE-R 94, the thorax compression criterium (ThCC), which is the compressive deflection of the sternum relative to the spine, shall not exceed 50 mm. In the physical ATD, it is measured via a potentiometer as a rotary sensor of a lever connected to the sternum, see Figure 2.16. The deflection results from the angular rotation multiplied with an ATD-specific linearizing factor. To assess dynamic thorax deformation, the viscous criterion (VC) of [LauViano86] as defined in ECE-R 94 is used. It is the product of the deformation velocity $V(t) = \frac{\mathrm{d}}{\mathrm{d}t}D(t)$ from deformation $D(t)$ and the instantaneous compression $C(t) = \frac{D(t)}{\text{initial torso thickness}}$, which is dimensionless. The critical value of $\mathrm{VC}_{\max} = 1\,\mathrm{m/s}$ corresponds experimentally to a 25 % probability of severe (AIS4+) thoracic injury [LauViano86].

Injuries of the Pelvis and the Lower Extremities

Regulations FMVSS 208 and ECE-R 94 do not provide injury criteria for the pelvis or abdomen. The set from [BergEtAl04] suggests a maximal acceleration of $a_{3\mathrm{ms}} = 60\,\mathrm{g}$. It is not stated where the criterion originated, but a discussion of this criterion and the respective limit is found in [Kramer90]. For the thighs, FMVSS 208 defines a maximum axial load of 10 kN for which ECE-R 94 in turn specifies only 9.07 kN. Therefore, the lower limits from ECE-R 94 are used. For the tibiae, ECE-R 94 defines a tibia index (TI) of less than 1.3. The tibia index, developed by [Mertz93], compares the axial force and internal bending moment in the tibia against an ATD-specific critical axial force $(F_\mathrm{C})_\mathrm{z}$ and moment $(M_\mathrm{C})_\mathrm{res}$ that represent structural tolerances.

Table 2.5: Selected injury criteria with biomechanical limits for the Hybrid III 50$^{\text{th}}$ ATD.

body region	injury criterion		limit
head	resultant acceleration	$a_{t_{\text{int}}} = \max\limits_{t_1} \left(\min\limits_{t_1 \leq t \leq t_1 + t_{\text{int}}} a_{\text{res}}(t) \right)$	80 g for $t_{\text{int}} = 3$ ms
	head injury criterion	$\text{HIC}(t_2 - t_1) =$ $\max\limits_{t_1, t_2} \left\{ (t_2 - t_1) \left[\dfrac{1}{t_2 - t_1} \int_{t_1}^{t_2} a_{\text{res}}(t)dt \right]^{2.5} \right\}$ with $a_{\text{res}}(t)$ in g and t in s	1000 for $t_2 - t_1 \leq 36$ ms
	generalized acceleration model for brain injury threshold	$\text{GAMBIT} = \left[\left(\dfrac{a_{\text{res}}(t)}{a_C} \right)^{2.5} + \left(\dfrac{\ddot{\varphi}_{\text{res}}(t)}{\ddot{\varphi}_C} \right)^{2.5} \right]^{\frac{1}{2.5}}$ with $a_C = 250$ g and $\ddot{\varphi}_C = 25$ krad/s^2	1
	brain injury criterion	$\text{BrIC(CSDM)} =$ $\sqrt{\left(\dfrac{\max |\omega_x(t)|}{\omega_{xC}} \right)^2 + \left(\dfrac{\max |\omega_y(t)|}{\omega_{yC}} \right)^2 + \left(\dfrac{\max |\omega_z(t)|}{\omega_{zC}} \right)^2}$ with $\omega_{xC} = 66.2, \omega_{yC} = 59.1, \omega_{zC} = 44.25$ rad/s	1
neck	tensile force	$F_{z,\text{tens},t_{\text{int}}} = \max\limits_{t_1} \left(\min\limits_{t_1 \leq t \leq t_1 + t_{\text{int}}} F_z(t) \right)$	3.3 kN for $t_{\text{int}} = 1$ ms 1.1 kN for $t_{\text{int}} = 45$ ms
	compression force	$F_{z,\text{compr},t_{\text{int}}} = \min\limits_{t_1} \left(\min\limits_{t_1 \leq t \leq t_1 + t_{\text{int}}} F_z(t) \right)$	4 kN for $t_{\text{int}} = 1$ ms 1.1 kN for $t_{\text{int}} = 45$ ms
	shear force	$F_{xy,t_{\text{int}}} = \max\limits_{t_1} \left(\min\limits_{t_1 \leq t \leq t_1 + t_{\text{int}}} \sqrt{F_x(t)^2 + F_y(t)^2} \right)$	3.1 kN for $t_{\text{int}} = 1$ ms 1.1 kN for $t_{\text{int}} = 45$ ms
	forward moment	$M_{y,\text{fwd},\max} = \min M_y(t)$	190 Nm
	rearward moment	$M_{y,\text{rwd},\max} = \max M_y(t)$	57 Nm
	neck injury criterion	$\text{Nij}_{\max} = \max \left(\left| \dfrac{F_z(t)}{F_{\text{int}}} \right| + \left| \dfrac{M_y(t)}{M_{\text{int}}} \right| \right)$ with $F_{\text{int,C/T}} = 6160/6806$ N, $M_{\text{int,F/E}} = 310/135$ Nm	1
thorax	resultant acceleration	$a_{t_{\text{int}}} = \max\limits_{t_1} \left(\min\limits_{t_1 \leq t \leq t_1 + t_{\text{int}}} a_{\text{res}}(t) \right)$	60 g for $t_{\text{int}} = 3$ ms
	thorax compression	$\text{ThCC} = \max s(t)$	50 mm
	viscous criterion	$\text{VC}_{\max} = \max \left(V(t) \cdot C(t) \right)$	1 m/s
pelvis	resultant acceleration	$a_{t_{\text{int}}} = \max\limits_{t_1} \left(\min\limits_{t_1 \leq t \leq t_1 + t_{\text{int}}} a_{\text{res}}(t) \right)$	60 g for $t_{\text{int}} = 3$ ms
femur	axial force	$|F_z|_{\max} = \max |F_z(t)|$	9.07 kN
tibia	tibia index	$\text{TI}_{\max} = \max \left(\left| \dfrac{\sqrt{M_x(t)^2 + M_y(t)^2}}{(M_C)_{\text{res}}} \right| + \left| \dfrac{F_z(t)}{(F_C)_z} \right| \right)$ with $(M_C)_{\text{res}} = 225$ Nm and $(F_C)_z = 35.9$ kN	1.3

Chapter 3

Computational Models for Crashworthiness

The actual simulation is preceded by its modeling. Connecting experiment and theory, it translates reality into a, to some extent, abstracted and therefore simplified mathematical representation with varying degrees of fidelity desired and model complexity required. This chapter provides the necessary background of computational modeling in crashworthiness, identifying and substantiating the choice of the modeling and simulation strategy of this thesis.

First, it is determined which modeling categories and methods are suitable to achieve the set objectives. For the sake of an overview, a categorization attempts to capture existing methods of modeling a vehicle structure's ability to protect its occupants in an impact, called *crashworthiness* [Du BoisEtAl04]. As part of that matter, appropriate methods are discussed and selected. This leads to a brief overview of the two fundamental methods used in this thesis – the multibody systems (MBS) method and the finite element method (FEM). In the context of the presented work, it focuses on the most important aspects of modeling with computerized procedures of today's sophisticated and very capable software packages.

3.1 Models for Vehicle Crashworthiness

3.1.1 General Model Classification

Before diving directly into modeling, one should recognize the types of methods available. There are many classifications of models, distinguished by multiple criteria, as overviewed in [Velten09]. For this thesis, a classification as Figure 3.1 is proposed. It states mechanistic vs. empirical and deterministic vs. stochastic approaches as the main complementary categories, depicted as combinatory fields in a common plane. In mechanistic modeling,

Figure 3.1: A model classification.
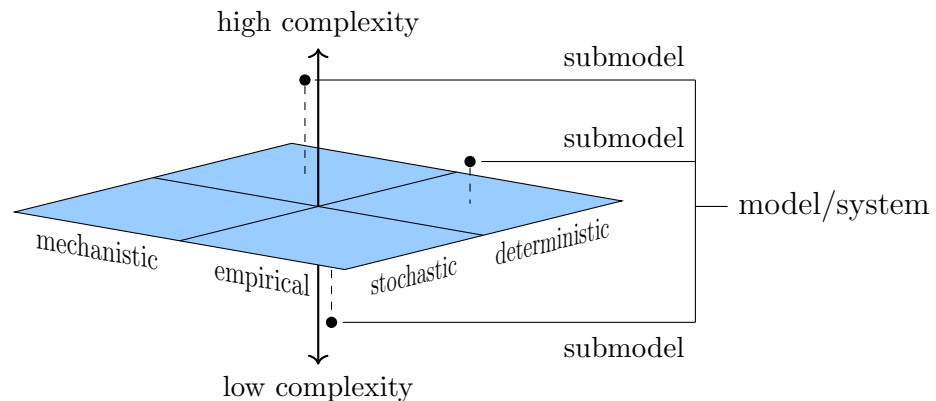
models are derived from fundamental laws of natural sciences, such as the laws of physics. They provide some level of explanation and, thus, understanding of the modeled phenomena. Empirical models are developed by emulating a behavior from observations and correlating it with various purely mathematical, e.g., statistical methods, which is referred to as system identification. The obtained parameters that describe the system response typically do not correlate with physical process parameters, providing meaningful knowledge of its internal workings. The denotation of mechanistic as white-box and empirical methods as black-box modeling is an allegory for targeting or omitting causal relationships between quantities and mechanisms of the system as their fundamental descriptive. Deterministic models make definite quantitative predictions; stochastic models involve random effects so that the prediction has a distribution. Moreover, models have different computational complexity, here represented by a vertical axis. A more complex model is characterized by a higher number of model parameters and degrees of freedom and often by more complicated, mostly non-linear model equations, which in turn leads to an increased computational effort for calculation and storage. An increase in complexity does not necessarily lead to better results but perhaps mainly to an increase in the number of parameters, which are increasingly challenging to assign appropriately. However, oversimplification can lead to the suppression of essential properties, which in turn weakens the validity of the result. A measure that represents this accuracy of the model results compared to the real world is referred to as model fidelity. A combination of several submodels leads to further models or model systems.

3.1.2 Model Categories for Investigating Crashworthiness

Current virtual design methods in automotive crashworthiness involve a vast range of computer-based numerical models of occupants and vehicle structures. The techniques used are manifold and difficult to overview. In literature, there are some reviews on the methods and models used [Belytschko92, DuddeckWehrle15, NoorsumarEtAl21]. As shown in Figure 3.2, most of the models can be classified into the three types of methods
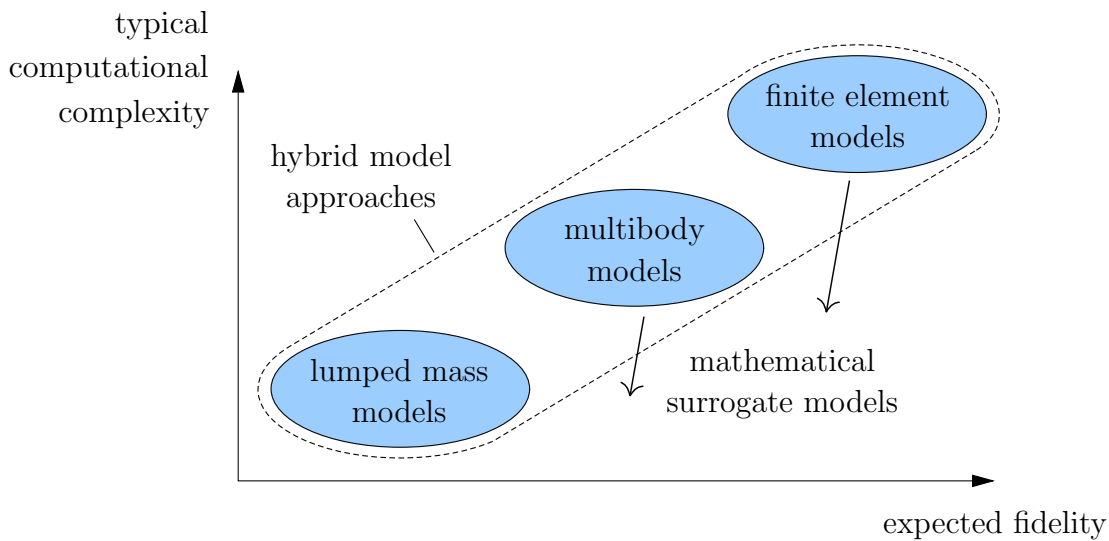
Figure 3.2: A categorisation of models for investigating crashworthiness.

leading to *lumped mass models*, *multibody models*, and *finite element models*, located qualitatively according to their typical model complexity and associated expected fidelity. Detailed FE models potentially have high model fidelity, but the associated high model complexity hinders a large number of evaluations. To optimize a system design or to attest its robustness, often many simulation runs are necessary. This motivates the combination of methods in *hybrid modeling approaches* or the reduction through *mathematical surrogate models*.

To discuss the model categories of Figure 3.2, examples in Figure 3.3 to 3.5 each shows a passenger car model of a frontal impact.

Lumped mass models, also referred to as lumped parameter models, replicate vehicle impacts with discrete mass elements in interaction through simple mechanical elements such as springs and dampers. They aim to capture the fundamental impact kinematics, often for unidirectional response with very few degrees of freedom. These slim and fast models are very well-suited for optimizations. However, it might be difficult to find lumped parameters to fit an actual structural design, or the few degrees of freedom might not sufficiently represent complex interactions.
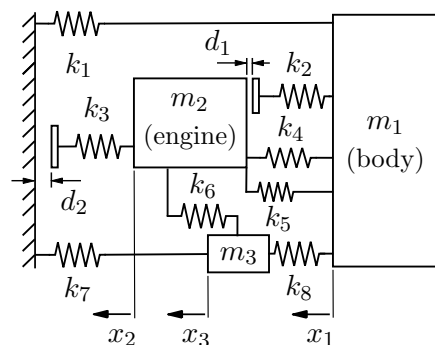

Figure 3.3: Lumped mass-spring vehicle model in [Kamal70] with coordinates x, masses m, spring coefficients k, and initial distances d.

Multibody models in crashworthiness are usually more complex systems of rigid bodies, constrained by idealized joints and loaded by internal and external force elements. In addition, contact interactions of the bodies are often implemented via nonlinear contact characteristics, also representing the deformation of the rigid bodies. A three-dimensional system of p rigid bodies with r holonomic, rheonomic constraints has a number of degrees of freedom of $f = 6p - r$ [SchiehlenEberhard14]. MB models are particularly suitable for systems of large displacements and rotations. In an impact evaluation, they can be used for kinematic and kinetic analysis, including injury criteria prediction of rider surrogates.

Figure 3.4: Simulation of the generic MB vehicle model from [SousaEtAl08] at a collision speed of 56 km/h after 40 ms.

Finite element models deal with geometry, material, constraint, and contact nonlinearities, making solving such models more difficult and computationally costly. Depending on the element formulation, each node has typically between three and six degrees of freedom. The models are used to accurately represent complex geometries and incorporate diverse material models in the detailed representation of vehicles and human surrogates. Analysis of FE models focuses on deformations and stresses. In impact analysis, they're applied to capture a vehicle's structural behavior and localized effects, such as, detailed injury mechanisms in HBMs. Driven by increased computational performance and high-performance computing, FEM developed as the state-of-the-art in the crashworthiness development process.

Figure 3.5: Simulation of the detailed FE vehicle model from [MarzouguiEtAl12, NHTSA12] at a collision speed of 56 km/h after 40 ms.

Models, referred to as **hybrid model approaches**, aim to gain an advantage by combining several methods, e.g., to take advantage of the faster MB models and the more detailed FE models. These are, substructure modeling approaches, hybrid FE-rigid body approaches, hybrid FE-elastic FE approaches, hybrid fine-rough FE mesh approaches, and space-mapping techniques as listed and described in [DuddeckWehrle15]. It also includes subsystem model approaches such as MB and FE crash pulse models where a vehicle impact response is substituted by a deterministic pulse, a simpler model, or from experiments such as full-vehicle simulations as described in [ReichertEtAl14]. Equivalent to laboratory sled tests, such deceleration pulses are then applied as prescribed motions to subsystem models of a vehicle interior.
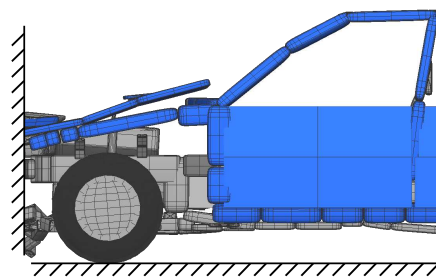
Mathematical surrogate models are simplifications of complex models using mathematical methods. These models aim to replace the more complex models with simpler ones that still capture the essential behavior introducing an acceptable error but with minimized computational effort. These methods are manifold and include linear and nonlinear model order reduction [Fehr11, FehrEtAl18] (e.g., combined trough clustering [GrunertFehr16]), machine learning approaches [HayFehrSchories20, KneiflGrunertFehr21, Hay22], and combinations or metamodels of the before mentioned [KneiflHayFehr22] to reference only a few techniques. More additional techniques and examples are listed in [DuddeckWehrle15].

Although not remotely comparable to safety investigations of passenger car occupants, there have been efforts to model motorcycle crashworthiness. A rare lumped mass model of a motorcycle is in [Happian-SmithMacaulayChinn87]. There are several MB models of PTWs to model car impacts [CanapleEtAl02, SudyoddeeEtAl19, LvHynčíkBońkowski19], solo accidents [Lechner86], and road-side barrier impacts [IbitoyeEtAl09, MoradiLankarani11, PtakEtAl19]. There are also published works on detailed FE models of various types of PTWs, such as sports and sport touring motorcycles [SchulzDobrovolnyHurlebaus16, MongiardiniEtAl17], a large touring motorcycle [NamikiNakamuraIijima05], or a tilting three-wheeled scooter [BarbaniBaldanziniPierini14]. However, there is a lack of models to efficiently investigate individual aspects of motorcycle crash behavior – such as the structural collision interaction of motorcycle crash structures – or a motorcyclist's accident response – such as the isolated examination of the rider trajectory of different rider surrogate models – in subsystem model approaches. Also, there is a lack of combinations of two or more models, such as different levels of detailing and complexity, into a connected workflow. This has long been state-of-the-art in the accident simulation of cars.

3.1.3 Methods and Models in This Work

The appropriate modeling technique is selected based on the objectives of the work in Section 1.4. The requirement for a systematic and modular approach (O1), as shown in the testing pyramid in Figure 1.9 requires a submodel approach. To achieve a meaningful description of the operating principles (O3) with a quantified performance evaluation (O4), which should allow future optimization based on the technical design and the associated design parameters, deterministic mechanistic approaches are preferred. Balancing fast computational models and simultaneously a realistic and reliable reproduction of the accident behavior (O2) multiple models for different purposes from low to high fidelity are used.

As the overview above shows, there are several methods to choose from. With lumped mass models, it is very difficult to model a complex accident behavior of a motorcycle and/or a motorcycle passenger. It has also hardly been done so far. This narrows the choice to the two fundamental methods of MBS and FEM. Because of its idealized modeling, MB models are well suited to represent the macrostructure of the vehicle, to begin with. FEM

requires more detailed information about the structure of a system. It requires geometry, the connection of parts, and the materials used, which makes the method less generic. It is therefore used at a more advanced stage of the investigations. As shown in the modeling strategy in Chaper 4 a hybrid modeling approach is used to efficiently combine methods to decrease the computational expense.

3.2 Multibody Systems

The term multibody system (MBS) refers to the constrained motion of rigid bodies loaded by external, internal, and inertial forces. In a classical MB approach, an engineering system is approximated with rigid bodies that have a fixed geometry with a fixed center of gravity (COG) and moment of inertia. These bodies are connected to each other and to the environment by ideal constraints and massless couplings and are loaded with discretized force elements and force fields, as shown in Figure 3.6 for an exemplary generic MBS. Typically, MBS, as well as their extension with elastic bodies, are used for systems that perform large displacements and rotations and small deformations.

3.2.1 Fundamentals

The procedure usually starts with a kinematic description of the system. Systems differ in terms of their typology. There are *open* trees or partially or entirely *closed* loop structures. When described in absolute coordinates, an unconstrained rigid body has six degrees of freedom, described by six differential equations. Each body constraint leads to additional algebraic equations. When using relative coordinates, the bodies are described relative to the previous body. In the case of an open MBS, the relative coordinates are minimal, and also it remains a minimal number of equations. For loops, there are additional constraint equations. A comprehensive overview of the mathematical and numerical principles of MBS is given in [SchiehlenEberhard14], a compact summary in [EberhardSchiehlen06].

The kinetics can be derived using Newton-Euler equations and d'Alembert's principle. For a holonomic tree structure – such as the macrostructure of a human body – with degree of freedom f, the equations of motion in minimal coordinates $\boldsymbol{y} \in \mathbb{R}^{f x 1}$ to

$$\boldsymbol{M}(\boldsymbol{y},t)\ddot{\boldsymbol{y}} + \boldsymbol{k}(\boldsymbol{y},\dot{\boldsymbol{y}},t) = \boldsymbol{q}(\boldsymbol{y},\dot{\boldsymbol{y}},t), \tag{3.1}$$

where $\boldsymbol{M} \in \mathbb{R}^{f x f}$ is the global mass matrix, $\boldsymbol{k} \in \mathbb{R}^{f x 1}$ the vector of generalized Coriolis and centrifugal and gyroscopic forces, and $\boldsymbol{q} \in \mathbb{R}^{f x 1}$ the vector of generalized constraint forces [SchiehlenEberhard14]. This relation is a second-order ordinary differential equation that can be solved numerically with explicit schemes. For crash impacts as highly dynamic events, they require a small time step for stability. However, compared to many applications of MBS, the time domain in crash simulations is relatively short.

To additionally represent elasticities in bodies, there is the approach of elastic multibody systems (EMBS), described in detail in [Shabana97]. It consists of a continuum formulation, a discretization of the geometry, and the choice of reference frame [FehrEberhard11]. There are methods for small elastic deformations (RNCF: relative nodal coordinate formulation) and larger deformations (ANCF: absolute nodal coordinate formulation). This approach still allows the efficient approximation of large motions of the respective reference frame.

3.2.2 Procedure for Computational Multibody Systems

To investigate complex systems nowadays, system generation, the automatic formulation of the equations of motion, and their numerical integration are performed with sophisticated software packages targeted at specific engineering applications, as shown for multiple examples in [EberhardSchiehlen06]. These include capable interactive and user-optimized pre- and post-processors that interact with the actual solver to provide an integrated workflow. Figure 3.6 illustrates the definition of a typical input structure of an EMBS and exemplifies a simplified lower MBS structure of the MADYMO active HBM [SISS20a].
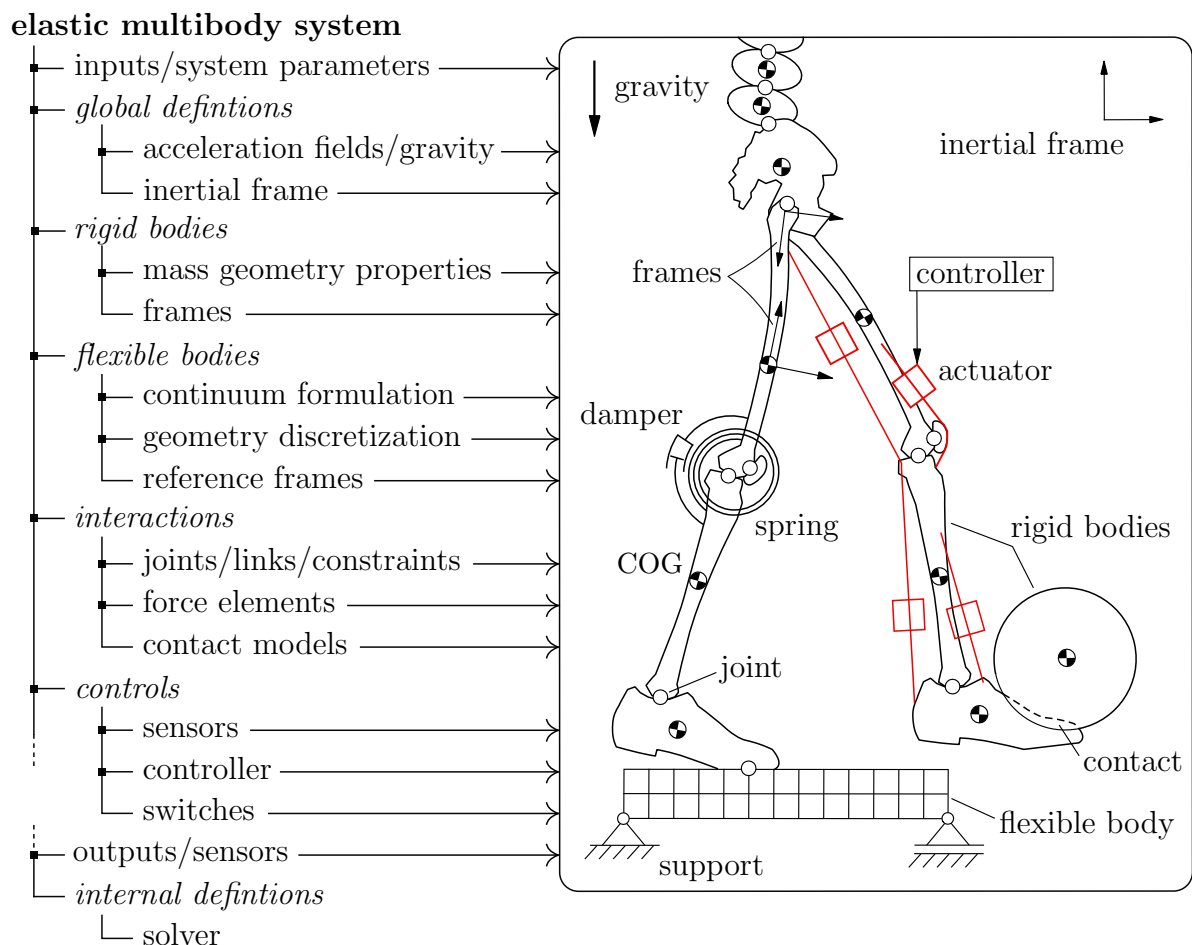

Figure 3.6: Typical EMBS definition structure and an artistic active HBM kicking a ball while standing on a balancing beam as an examplary system.

In this work, the commercial software package MADYMO[6] is used. It is a multiphysics solver that combines flexible MB capabilities and FE techniques. It is specifically designed to simulate the dynamic behavior of vehicle collision interaction and automotive occupant restrain systems and perform human injury assessment [SISS20b]. It bundles various modeling and analysis methodologies and provides a database of validated models of ATDs and HBMs.

Contact Interaction

In a crash simulation, deformations are significant. In addition to the formulation of elastic bodies, the deformation can also be modeled via extended contact algorithms between rigid bodies with a variety of interaction models [FloresLankarani16]. Figure 3.7 shows the determination of the force $F_e(\lambda)$ as a function of the penetration depth λ of contact between elliptic bodies in MADYMO [SISS20b] as one possible implementation. For the penetration depth, the tangent planes l_1 and l_2 at points P_1 (ellipsoid 1) and P_2 (ellipsoid 2) are iteratively determined. The distance between l_1 and l_2 is the penetration λ of the ellipsoids. The force model is initially determined by the loading curve $F_{e,\text{loading}}(\lambda)$. Above the elastic limit λ_e, the energy dissipation is described by hysteresis along the hysteretic slope and then along the unloading curve $F_{e,\text{loading}}(\lambda)$. MADYMO offers several formulations that differ, i.e., in the behavior when the load direction is reversed during unloading. The so-called elastic force F_e is perpendicular to the tangential planes. In addition, functions for damping and friction forces can be specified.

Figure 3.7: MADYMO ellipsoid to ellipsoid contact interaction with qualitative hysteretic force-penetration characteristic.
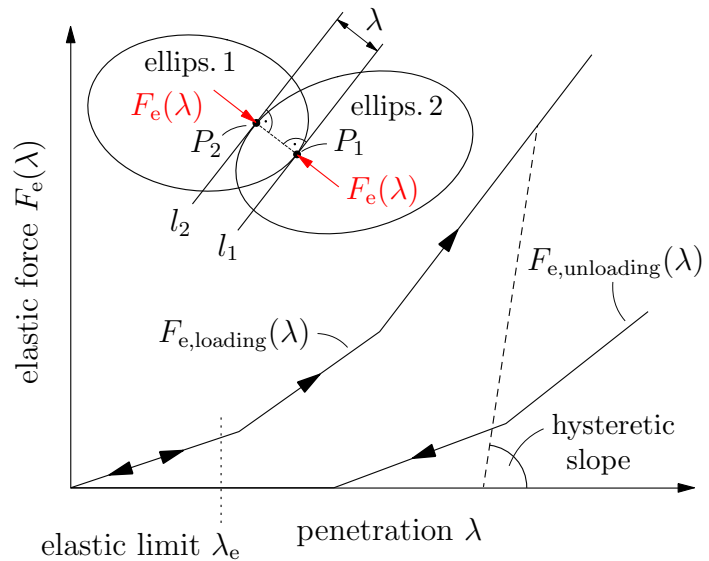
3.3   Finite Element Method

In MBS, the kinematics and kinetics of large displacements and large rotations are of interest, while the deformations of the individual bodies are small in comparison. In modeling with FEM, this is usually inverted. Here, the deformations and stresses of the bodies are of great interest, but they usually do not perform large rigid-body motions.

3.3.1   Fundamentals

The FEM comprises techniques to solve partial differential equations numerically for complex shapes. The basic idea is the spatial discretization of bodies by dividing them into an equivalent system of a finite number of smaller bodies (elements) interconnected at common points (nodes) to represent complex geometries. Various formulations exist for the local approximation of the elements, such as the *displacement* or *stiffness method*, where the displacements of the nodes are the unknowns of the problem. The method approximates the partial differential equations locally for transient problems with a set of ordinary differential equations with symmetric system matrices. These single functions are assembled into a global system of equations. For nonlinear dynamic problems this results in the governing equation for the nodal accelerations $\ddot{\boldsymbol{q}} \in \mathbb{R}^{n \times 1}$

$$\boldsymbol{M} \ddot{\boldsymbol{q}}_{\mathrm{el}} = \boldsymbol{f}^{\mathrm{int}} + \boldsymbol{f}^{\mathrm{ext}} \tag{3.2}$$

where $\boldsymbol{M} \in \mathbb{R}^{n \times n}$ is the mass matrix, the internal forces $\boldsymbol{f}^{\mathrm{int}} \in \mathbb{R}^{n \times 1}$, representing element stresses, and external forces $\boldsymbol{f}^{\mathrm{ext}} \in \mathbb{R}^{n \times 1}$ from boundary conditions, such as acceleration fields, constraints, or contacts [BelytschkoLiuMoran00]. The main advantage of FEM over other methods is its large generality [Bathe96]. An introduction to the proper use and understanding FEM, which is a huge field, is given in [Bathe96, BelytschkoLiuMoran00], a shorter summary focusing on its application in crashworthiness in [KhalilDu Bois04].

3.3.2   Procedure for Computational Finite Element Models

For FE modeling in this thesis, the commercial software package LS-DYNA[7] with its explicit solver is used. It is a general-purpose explicit and implicit solver extensively used for simulating automotive crashworthiness and other nonlinear and highly dynamic problems. Figure 3.8 gives a condensed overview of FE modeling. It shows a selection of the most important definitions with their essential principles of FE modeling in LS-DYNA [Hallquist06, LSTC18] and an example of a complex LS-DYNA model, the state-of-the-art VIVA+ HBM [JohnEtAl22, OpenVT22] of the Virtual Consortium.

---

[7]LS-DYNA, version R9.3.1 MPP, ANSYS, Inc., https://www.ansys.com/products/structures/ansys-ls-dyna.

(a) discretization with finite elements with various shapes,

0D: 1D: 2D: triangle   3D: tetrahedron

discrete   line   quadrilateral   triangular prism
element   hexahedron   ...
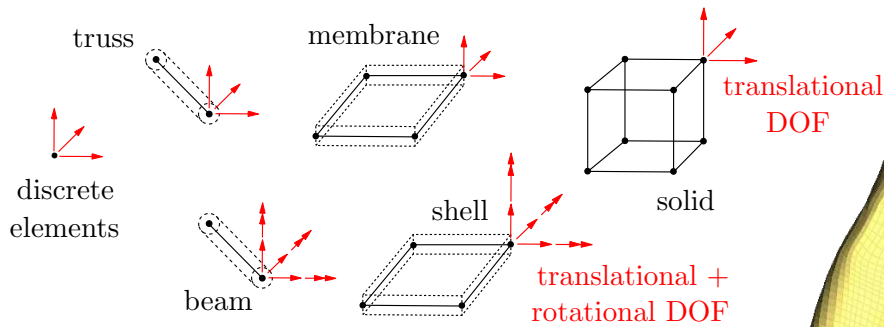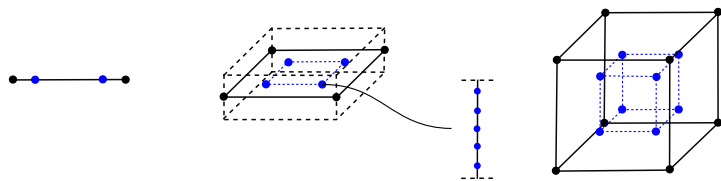
nodal degrees of freedom (DOF),

truss   membrane

                                                                translational DOF
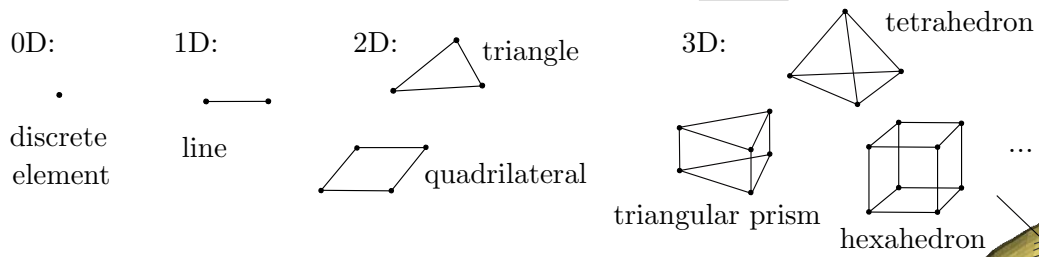
discrete   shell   solid
elements
                                                         translational +
beam   rotational DOF

and numbers and locations of integration points

Integration points: Approximation functions interpolate the nodal results
onto the interior of an element, such as the stress distribution within a solid.
Depending on the integration scheme, the location of integration points varies.
Accuracy and calculation time increase with the number of integration points.

(b) constraints

   • nodal ridig bodies   • kinematic joints   • single node constraints   • ...

(c) boundary conditions

   • prescribed motion   • prescribed force   • symmetry   • ...

(d) loads

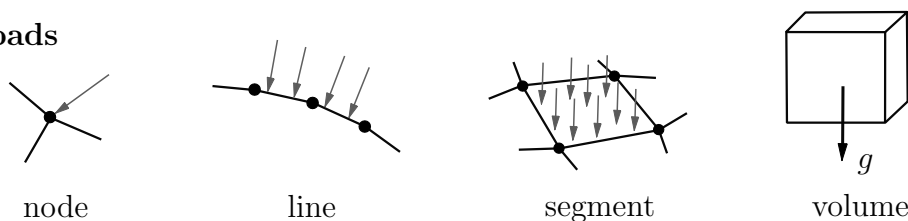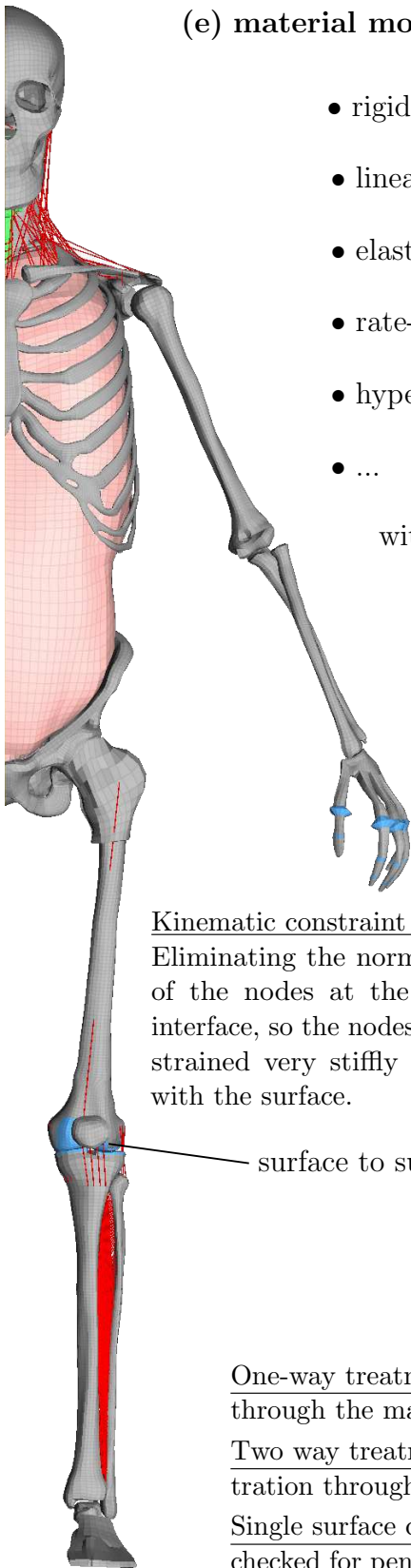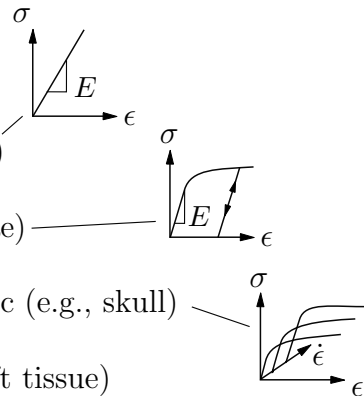   node   line   segment   volume

Figure 3.8: Some FE modeling aspects with the VIVA+ HBM [OpenVT22] as an example.
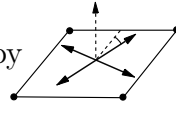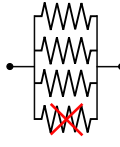
(e) material models, e.g.,

- rigid (e.g., teeth)

- linear elastic (e.g., ligament)

- elastic-plastic (e.g., vertebrae)

- rate-dependent elastic-plastic (e.g., skull)

- hyperelastic rubber (e.g. soft tissue)

- ...

with many material model-dependent options such as

- anisotropy
- damage

- failure   ...

(f) contact algorithms

Kinematic constraint method: Eliminating the normal DOF of the nodes at the contact interface, so the nodes are constrained very stiffly to move with the surface.

Penalty method: Nodes are checked for penetration through the contact interface. Placement of normal springs between the penetrating nodes and the contact interface, where the magnitude of a resulting force on the node is a function of the penetration.

...

surface to surface contact

slave

mesh contact surfaces
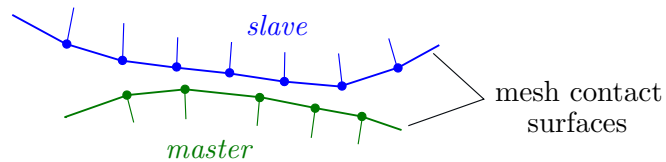
master

One-way treatment: Only slaves nodes are checked for penetration through the master surface.

Two way treatment: Both slave and master nodes are checked for penetration through the respective opposite surface.

Single surface contact: Only a slave surface is defined. Slave nodes are checked for penetrations through the slave surfaces, including self-contact.

The essential steps in the computational FE modeling workflow consist of:

(1) If nessesary simplify and de-feature the actual geometry for an idealized geometry.

(2) Disretize the geometry into finite elements.

(3) Choose an approximation for the variables within the elements to reduce the problem to a finite number of unknowns.

(4) Assign material models.

(5) Define the specific problem with constraints, boundary conditions, contacts algorithms, initial conditions etc.

} pre-processing

(6) Derive the system of equations for the unknowns.

(7) Solve the system of equations.

} solving

(8) Analyse the results and animations. – post-processing

Many of these steps are highly automated, such as meshing algorithms for discretizing. Other steps are no longer visible when using FE software. The choice of the approximation functions happens by the selection of the element type (shape and nodal degrees of freedom) and further specification (such as the number and location of integration points). The choice of the appropriate integration method for a numerical approximation depends on the type of partial differential equation, the smoothness of the data, and the response of interest. For crash simulations, explicit methods are preferred since the impact contact algorithms introduce noise [BelytschkoLiuMoran00]. Here the time step size is very small and important, particularly for the numerical stability of the solution. It depends on the highest natural frequency of the system and is largely determined automatically by the software [HallquistEtAl06].

Chapter 4

Modeling

After introducing the circumstance of this work, we now begin modeling the proposed safety concept. The modeling establishes a physical relationship between the motorcyclist, motorcycle, and environment, as illustrated in Figure 4.1. Although divided into individual Chapters 4 and 5, modeling is not just a process that precedes simulation; instead, modeling, simulation, and validation is an iterative process.

The conceived modeling strategy and its stages are based on the selected modeling methods in Chapter 3. The following delineates the vehicle modeling of the motorcycle and an accident opponent for the different stages. Subsequently, the modeling of the passive safety systems and their activation is set out. Following the building block approach introduced in Section 1.3, existing generic element models and simulation experience from occupant passive safety are used to model the seat belt and airbag systems. For modeling the leg impact protectors, an energy-absorbing foam is numerically characterized. It involves a regression model developed to represent rate-dependent loading and unloading. Lastly, the choice of rider surrogate models is discussed and substantiated, and the models ultimately used – virtual models of mechanical ATDs and HBMs – are introduced.

Figure 4.1: Modeling dependencies.
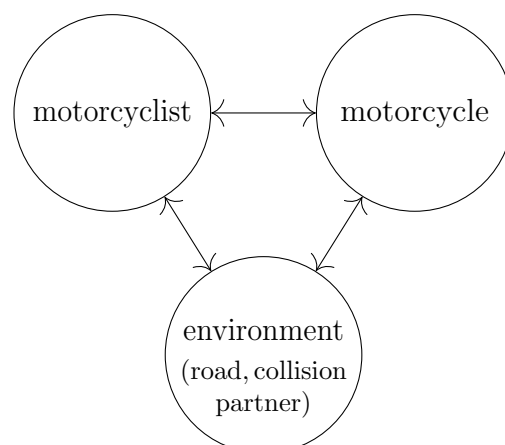
4.1   Modeling and Simulation Strategy

Standard methods and strategies used in the vehicle development process for occupant protection break down the accident event into multiple problems. Thus, in experiments, the performance of the components, the interaction of the vehicle structure with the opposing structure, and the occupants' behavior in the vehicle interior are often considered separately. Components or subassemblies are subjected to multiple component tests to assess the functionality of the various systems, the structural capacity of substructures, and the vehicle body individually. The interaction of the restraint systems with ATDs as vehicle occupants are optimized in sled tests. In these experiments, reinforced partial vehicle bodies represent the relevant vehicle cabin with interior components to investigate the effect of the passive safety systems without destroying an entire vehicle. Complex and costly full-vehicle laboratory crash tests of new products are rarely carried out during the design process but rather at the end of the development to prove the occupant protection for vehicle approval or evaluate occupant safety for consumer ratings. Similarly, in the virtual vehicle development process, multiple mathematical model representations are used for individual design aspects; see Section 3.1.2. Corresponding to the experimental procedure, the depth of reproduction in occupant safety studies is often reduced not to simulate the entire system. Thus, only the vehicle structures are considered for reconstructing the vehicle interaction and the dimensioning of the deformation and contact structures. Occupant restraint interaction and biomechanical loading is simulated using crash pulses and vehicle interior models.

Such a breakdown, both for experiments and simulations, is usually not possible when investigating the accident behavior of conventional motorcycles, e.g., in collisions with passenger cars. In this case, the rider interacts with the motorcycle, opposing vehicle structures, the road surface, and roadside structures. A safety concept that restrains the rider to the motorcycle and isolates it from the accident environment not only has the advantage of potentially improving passive safety – which must be demonstrated – but also allows to apply of similar modeling and simulation strategies for a more systematic investigation. Such a design strategy is shown in Figure 4.2. It consists of three subsequent development stages with a continuously increasing level of fidelity.

Stage I: The motorcycle and rider surrogate are approximated in a combined MB and FE modeling approach in the MADYMO software environment. The opposing vehicles are MB systems with joint restraint and contact characteristics based on simulation models of full-scale crash tests of conventional motorcycles, fitted to the experience from the full FE representations (see stage III). The airbags and the thigh belts are modeled using the 1D and 2D FE elements using the FE capabilities of the MADYMO software environment.

Stage II: The rider interaction surfaces of the motorcycle cockpit are modeled further detailed with FE elements in the LS-DYNA software environment. The modeling and

parameterization of the airbag inflation and thigh belt pretensioning and load-limiting are equivalent to the MB simulations. The FE rider interaction model represents deformable cockpit surfaces that include foam impact protectors. To replicate crash kinematics and vehicle intrusion, the motorcycle and car are (offline-)coupled to a crash pulse. Prescribed motions represent the multiaxial rigid body motions from the MB simulations, where the car geometry acts as reaction surfaces for the airbags.

Stage III: The motorcycle, the already before tuned passive safety systems equivalent to stage I and II, the rider surrogate, and an accident opponent are modeled as full FE representations in LS-DYNA. The structurally relevant components of the motorcycle that determine the crash behavior are deformable. The front and rear suspension, rotating wheels, and front fork steering are modeled with kinematic joints.

This procedure divides into *modeling* and *simulation* in between design iterations are carried out. Linking design updates for the motorcycle structure and passive safety systems back to the lower stages results in design loops through stages I and II. The sequence
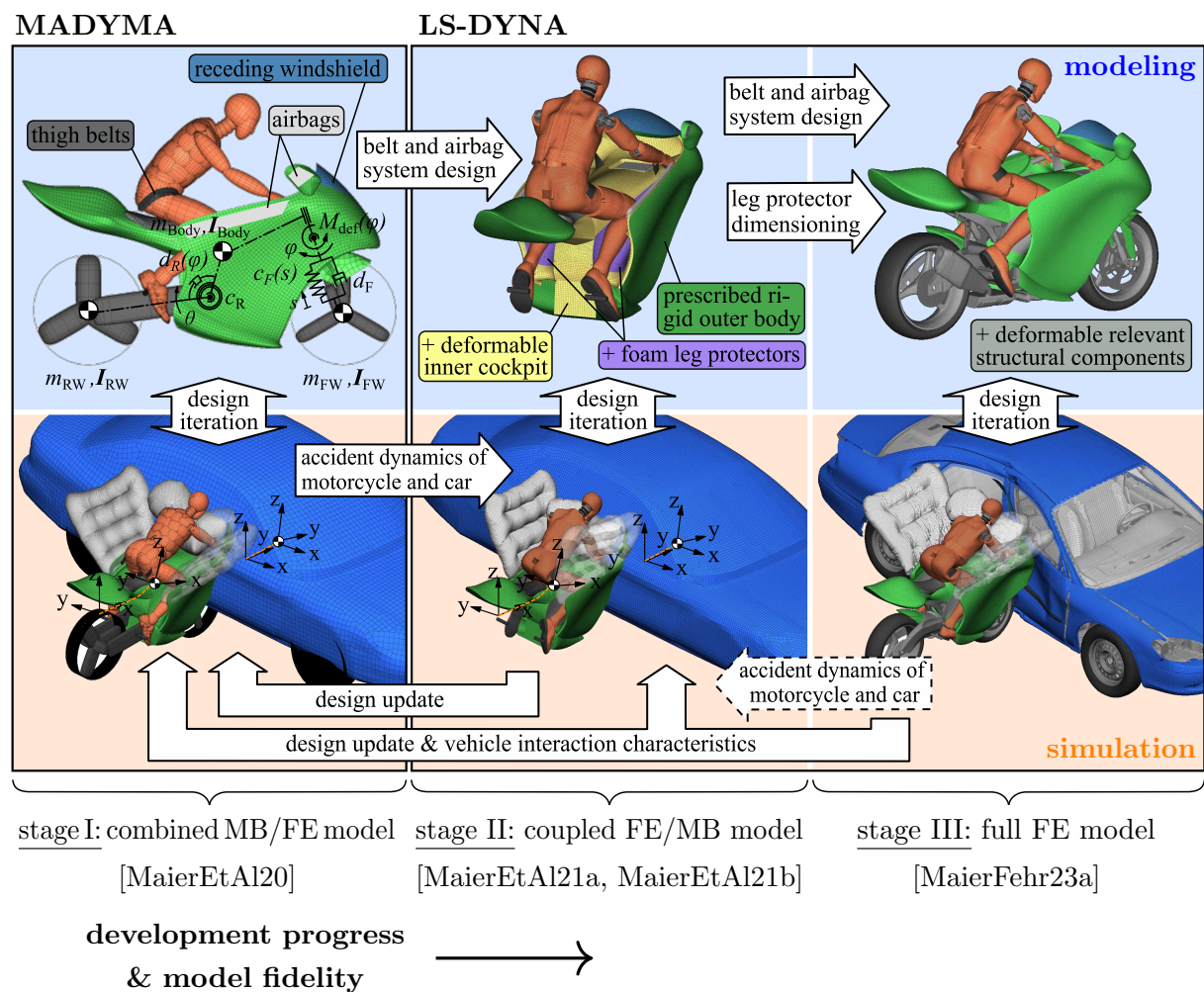
Figure 4.2: Modeling and simulation strategy.

could just as well be modified. Thus, vehicle accident trajectories of stage III can also be used in stage II.

The overall strategy was first described by the author in [MaierFehr21, MaierFehr23b]. The author first introduced the approach of stage I in [MaierEtAl20], the stage II approach in [MaierEtAl21a, MaierEtAl21b], and the stage III approach in [MaierFehr23a]. As the most laborious and time-consuming tasks, the positioning of the HBMs was initially layed out in the supervised student thesis [Kronwitter21] and the stage III full FE model was partially completed within the supervised student theses [Beckmann20, Liu20]. This chapter summarizes the author's works from [MaierEtAl20, MaierEtAl21a, MaierEtAl21b, MaierEtAl22, MaierFehr23a, MaierFehr23b].

4.2 Motorcycle and Opposing Vehicles

4.2.1 Multibody Model

To replicate the impact dynamics, the significant parts of the motorcycle are modeled as three rigid bodies: the body of the motorcycle, the front and rear wheel, specified by their geometry with ellipsoid and facet surfaces, and their mass m and inertia $\boldsymbol{I}$. These bodies are connected with kinematic joints as schematically shown in Figure 4.3 with restraint characteristics as in Figure 4.4. The main features are the couplings of (i) rotating wheels, (ii) front and rear suspension, (iii) front fork steering, and (iv) front fork impact deformation with kinematic joints constraining the relative motion of the parts. The coupling of front and rear suspension involves nonlinear spring restraints $c_{\mathrm{FW}}(s)$, $c_{\mathrm{RW}}(\theta)$,
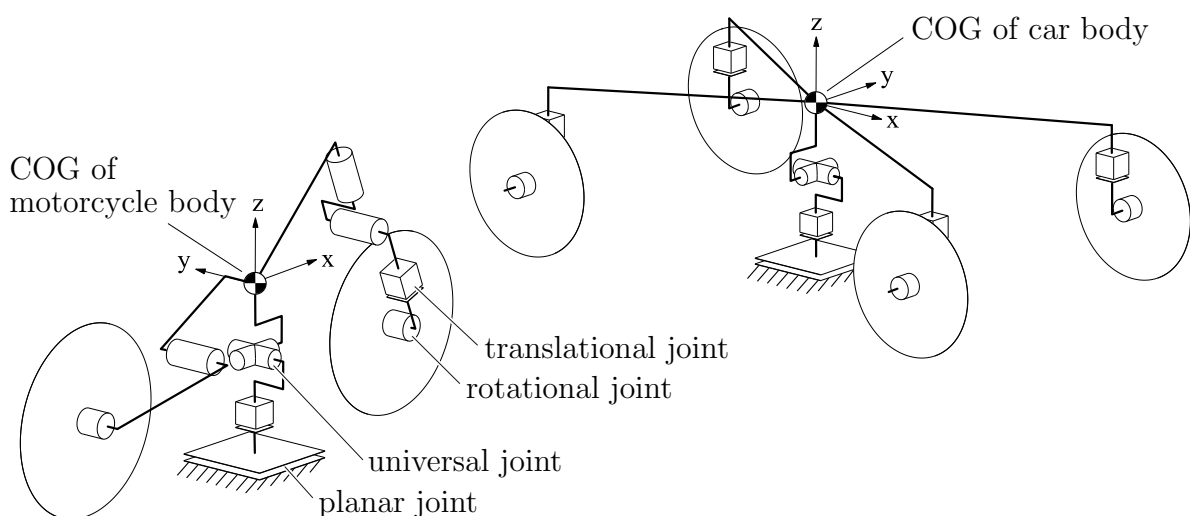
Figure 4.3: Kinematic structure of the MB models of the motorcycle (left) and the accident opponent (right).
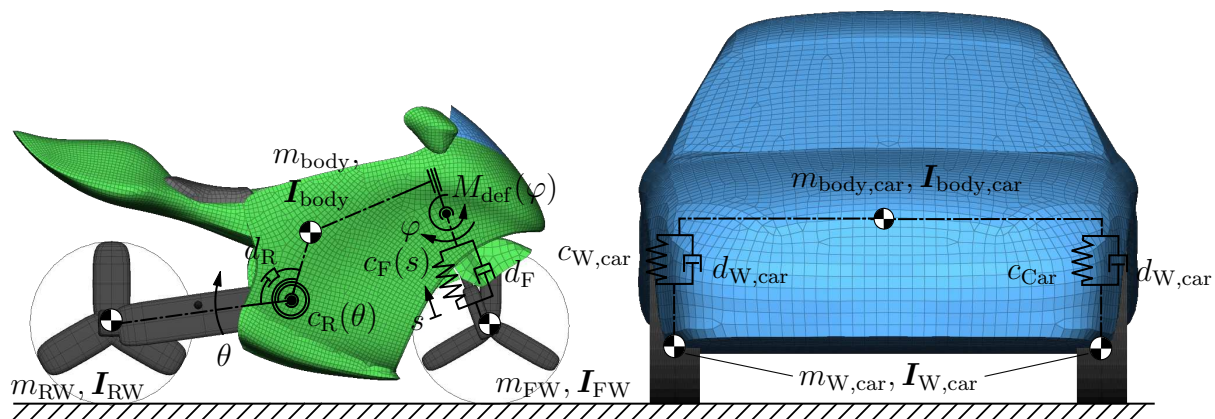
Figure 4.4: MB models of motorcycle and the accident opponent.

dependent on front suspension deflection s and rear suspension deflection angle θ, and constant dampening restraints d_{FW} and d_{RW}.

The front fork impact deflection φ given in Figure 4.5 is approximated with a linear elastic response up to the elastic limit φ_{e} (ⓐ). For higher impact deflection φ, the implemented loading characteristics represent at first failure with plastic deformation of the front fork and then collision of the front wheel with the motorcycle body along $M_{\mathrm{def,loading}}(\varphi)$ (ⓑ) with unloading characteristics parallel to the hysteresis slope (ⓒ) and along $M_{\mathrm{def,loading}}(\varphi)$(ⓓ). Reloading while unloading follows this path in reverse until $M_{\mathrm{def,loading}}(\varphi)$ is reached. The contact interaction characteristics between the opposing vehicle bodies are similar hysteretic models, summarized in Figure 3.7.

A similar MBS of a motorcycle with an equivalent kinematic structure is given in [CanapleEtAl02]. [PortalDias06] also describe a similar model without modeling front fork deformation.

Figure 4.5: Loading and unloading characteristics of the front fork impact deformation $M_{\mathrm{def}}(\varphi)$ in Figure 4.4.
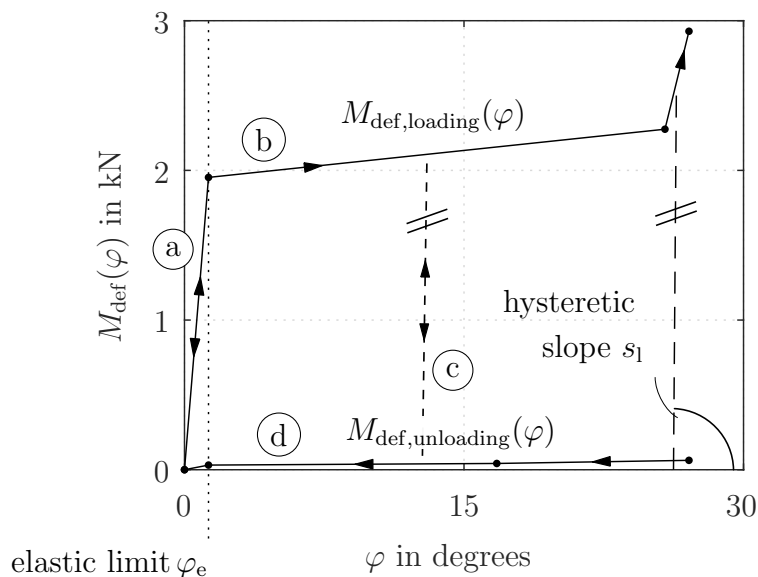
The opposing vehicle, which MB structure is also given in Figures 4.3 and 4.4, is a 2001 Ford Taurus, a four-door saloon with a mass of 1477 kg, an overall height of 147 cm, and vehicle parameters from a similar vehicle, a Ford Scorpio, from [Hiemer05]. The vehicle model aims to match the used FE model of stage III, see Section 4.2.3.

Conventional Motorcycles in Full Scale Crash Tests

The shown front fork restraint characteristics and the parameters of the implemented contact interaction characteristics are based on fitted simulations of full-scale crash tests of conventional motorcycles shown in Figures 4.6 and 4.7. The impacts according to [ISO13232:2005] with a helmeted Hybrid III 50th ATD are part of the investigations of [BergEtAl04], to which data we have access. The laboratory tests are documented with a test protocol and high-speed video footage, a 15-channel sensor data set of the ATD, and accelerometers at multiple points on the motorcycle. To quantitatively eval-
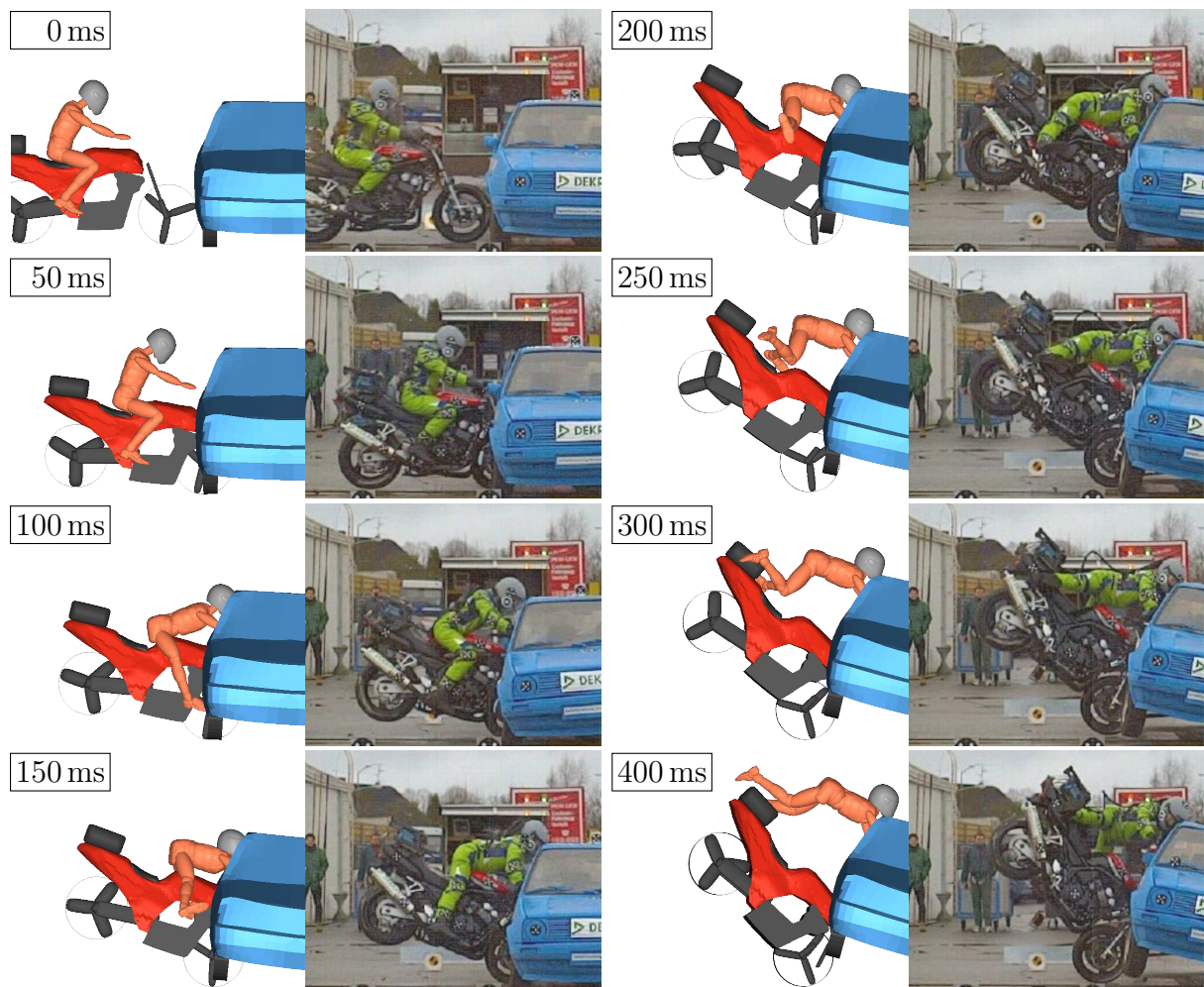
Figure 4.6: Simulation of crash test SH01.01 [BergEtAl04] of a conventional motorcycle Yamaha FZS 600 Fazer and a helmeted Hybrid III 50th against a VW Golf II in scenario ⑦.
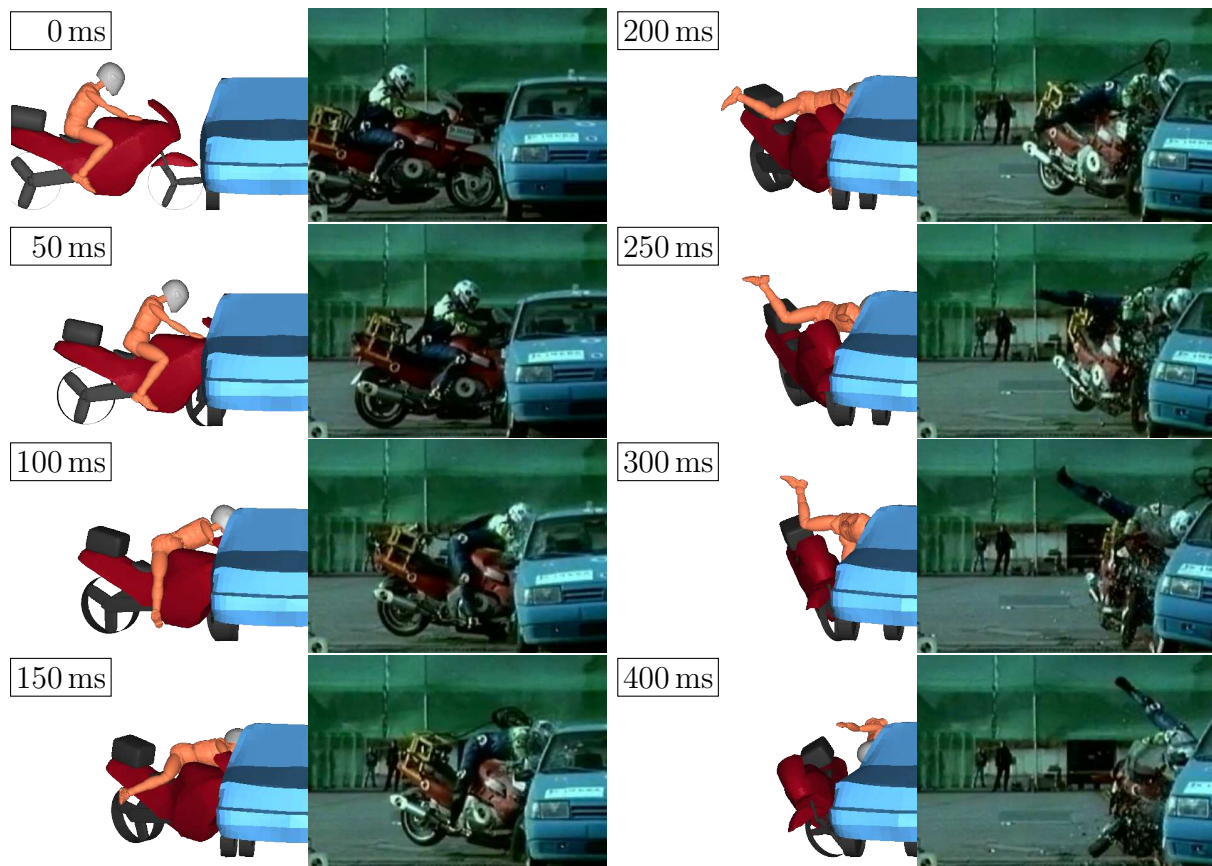
Figure 4.7: Simulation of crash test SH99.27 [BergEtAl04] of conventional motorcycle Yamaha GTS 1000 and helmeted Hybrid III 50th against a Fiat Tipo 1400 in scenario ③.

uate the dynamics in the experiment with the simulation results, the objective CORA evaluation (CORelation and Analysis, summarised in Addendum 4) is used. For this, the resulting motorcycle accelerations are compared, shown in Figures 4.8 and 4.9, each filtered with a CFC filter (CFC for channel frequency class, summarised in Addendum 5) with filter class 60.

In test SH01.01, the Yamaha FZS 600 Fazer impacts at 48.5 km/h at a right angle into the side of the stationary car. The motorcycle and car trajectories and accelerations conform well. Merely initial immersion of the suspension of the impacted side and, as a result, a similar helmet impact location at the car could not be achieved with the MBS approach. In test SH99.27, the Yamaha GTS 1000 impacts at 47.8 km/h at a right angle into the side of the car traveling at 23.9 km/h. The comparison shows similar motions for the motorcycle and car and conforming peak accelerations. This results in CORA ratings for the primary impact up to 300 ms of overall at least *fair*; for SH01.01 in the upper range of *fair*, very near *good*. The manual fitting procedure involves scaling a generic contact characteristic consisting of loading and unloading functions and a linear damping factor. Considering the simple model, the match according to CORA is acceptable. However, high-frequency components are not replicated.

The difference in motorcycle motion illustrates that the pitching of the motorcycle around its transverse axis depends on whether the motorcycle has sufficient deformation structure in front of the stiff forkhead and, therefore, a high contact point. In test SH99.27, the Yamaha GTS 1000 has a very unusual forkless front suspension with a single-sided swing arm, which appears weak in a frontal collision.

The contact characteristics between the front wheel and the road or vehicle are taken from the simulations shown above. For the deformation characteristics of the front fork and the contact characteristics between the motorcycle body and the car, characteristics similar to the Yamaha GTS 1000 from SH99.27 are used. This is to ensure that the motorcycle does not roll over in the event of a frontal impact.

Addendum 4: CORA Rating of Simulation vs. Experimental Data with ISO/TS 18671 Standardized Minimum Scores

The CORA (CORelation and Analysis) rating tool (version CORAplus Release 4.0.4) [Thunert17, GehreGadesWernicke09] offers a widely used objective metric of the correlation of two time history signals by combining two independent rating methods: a corridor rating and a cross-correlation rating. The tool determines how closely a time history signal matches a reference signal by evaluating corridors of the reference signal and by finding similarities in their phase, magnitude, and slope. The individual ratings are weighed by the rating factors W, as shown in Figure 4.10. The resulting total rating scores the conformance with a value between 0 for no correlation and 1 for a perfect match into four graded sections according to ISO/TS 18671:2014 [ISO/TS18571:2014] ≤ 0.58), *fair* (> 0.58), *good* (> 0.8) and *excellent* (> 0.94). Within this thesis the default CORA metric weights $W_{\mathrm{Z/P/M/S}}$, corridor widths a_0/b_0, and rating exponents $K_{\mathrm{Z/P/M/S}}$ for the ISO/TS 18671 method are used.
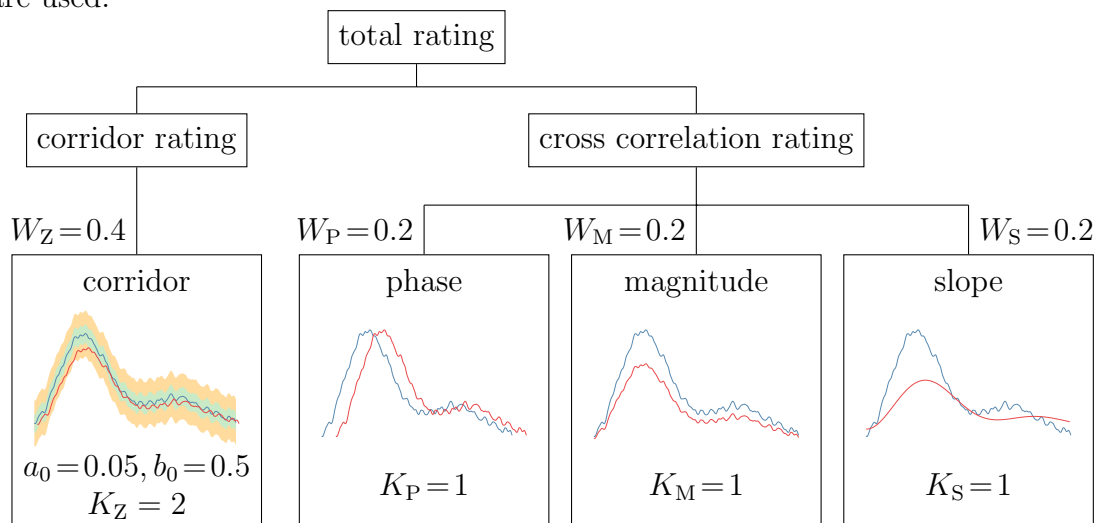
Figure 4.10: CORAplus rating scheme for the ISO/TS 18671 method with used parameters, summarized from [Thunert17].
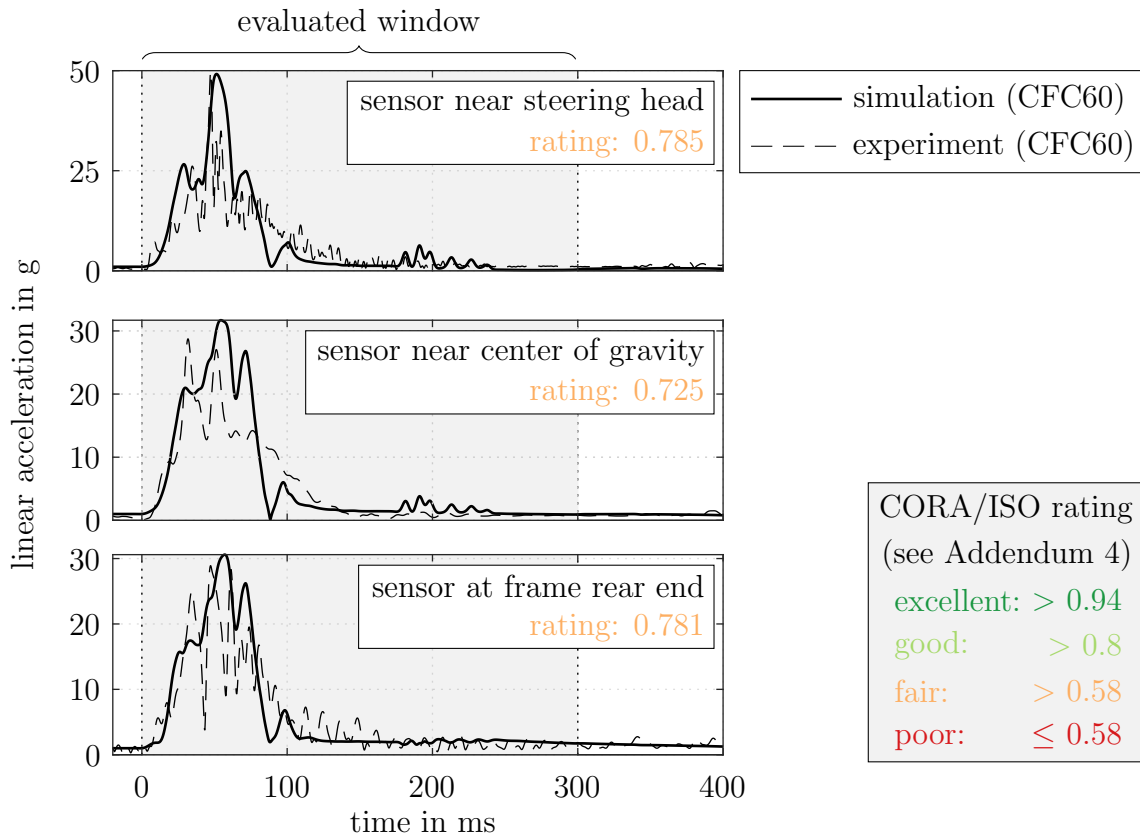
Figure 4.8: Resultant conventional motorcycle accelerations in MB simulations of full-scale crash test SH01.01, shown in Figure 4.6, compared to experimental sensor data.
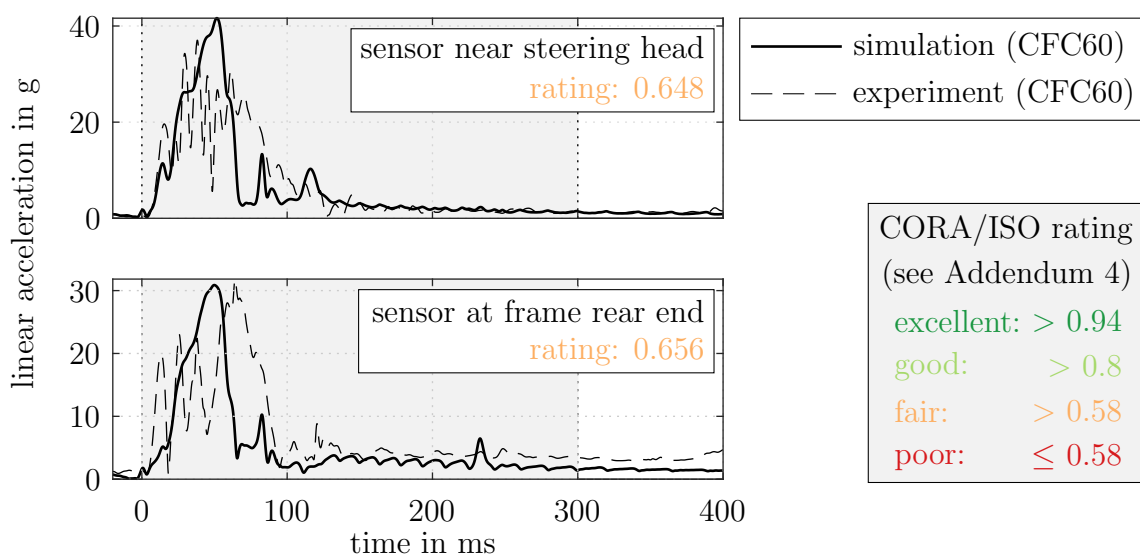
Figure 4.9: Resultant conventional motorcycle accelerations in MB simulations of full-scale crash test SH99.27, shown in Figure 4.7, compared to experimental sensor data.

Addendum 5: CFC Filtering According to SAE J211

The technical standard [SAEJ211-1:1995] provides guidelines and recommendations for acquiring and processing techniques of measurements of vehicle impacts tests, including subassemblies and occupant surrogates. It specifies four Channel Frequency Classes (CFC) of low-pass filters: CFC60, CFC180, CFC600, and CFC1000. It defines accuracy corridors dependent on the characteristic frequencies F_L, F_N, and F_H for each individual class as shown in Figure 4.11 for CFC600.

Figure 4.11: Corridor of required dynamic accuracy of CFC600 filter class according to [SAEJ211-1:1995].
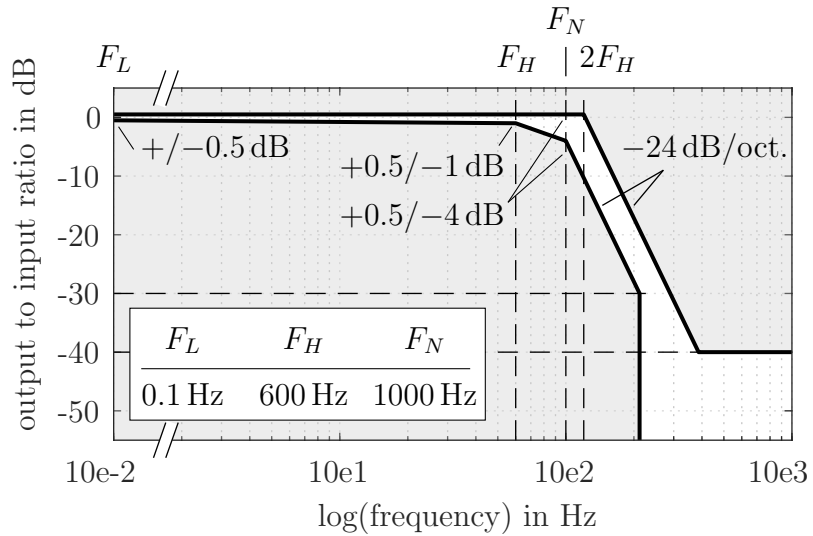
The recommended filtering procedure to achieve these requirements is a second-order Butterworth digital filter of an input signal $x(t)$ for an output $y(t)$ by the difference equation

$$y(t) = a_0 x(t) + a_1 x(t-1) + a_2 x(t-2) + b_1 x(t-1) + b_2 x(t-2)$$

with coefficients $a_0 = \dfrac{\omega_a^2}{1 + \sqrt{2}\omega_a + \omega_a^2}$, $a_1 = 2a_0$, $a_2 = a_0$, $b_1 = \dfrac{-2(\omega_a^2 - 1)}{1 + \sqrt{2}\omega_a + \omega_a^2}$, and $b_2 = \dfrac{-1 + \sqrt{2}\omega_a - \omega_a^2}{1 + \sqrt{2}\omega_a + \omega_a^2}$, where $\omega_d = 1.25 \cdot 2\pi \dfrac{\text{CFC}}{0.6}$ and $\omega_a = \tan\left(\dfrac{\omega_d T}{2}\right)$.

For phaseless filtering, the data is passed through this identical filter twice by reversing the time direction of the second filtering to compensate for the phase shift. The minimum sampling frequency for CFC filters is ten times the CFC number in Hertz. The individual choice of filter class must be made with technical expertise, but SAE J211-1 provides standard guidelines for vehicle and crash test dummy instrumentations as summarized in Tab. 4.1, which are applied accordingly in this thesis.

Table 4.1: CFC filter class recommendations for vehicle safety testing applications by [SAEJ211-1:1995].

dummy instrumentation		CFC
head	lin. & ang. accelerations	1000
neck	forces	1000
	moments	600
thorax	sternum accelerations	600
	deflections	180
pelvis	accelerations	1000
femur & tibia	forces	600

structural instrumentation		CFC
accelerations	total vehicle comparison	60
	sled tests	60
	component analysis	600
	for vel. & disp. integration	180
load cells	barrier forces	60
	belt restraint loads	60

4.2.2 Coupled Finite Element Rider Interaction Model

In the simplified FE approach, the motorcycle is reduced to the rider contact interaction surfaces, similar to a vehicle interior model in occupant protection investigations. It consists of a prescribed rigid body and deformable inner cockpit surfaces that include the proposed leg impact protectors. To prescribe the motion, the 3D multiaxial rigid-body trajectories from the linear and angular motion of the MB simulations are used, see Figure 4.12. For translational motion, the initial linear velocities and the time histories of the linear acceleration are used; for angular motion, the rotational velocities. The safety concept envisages that when deployed, the side airbags interact with the opposing vehicle structures or the ground. Therefore, the prescribed outer surface of the accident opponent act as the reaction surface for the airbags.

Figure 4.12: FE rider interaction model coupled to MB rigid body trajectories.
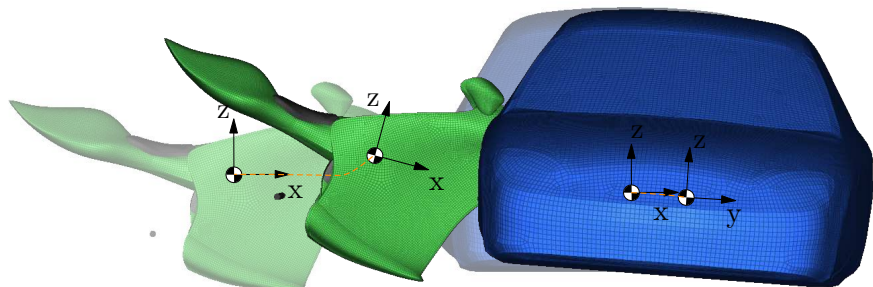
4.2.3   Full Finite Element Model

A full FE representation of the motorcycle provides in this work the highest degree of detail. From the ideator and inventor of the safety system, a CAD model is provided that represent the main structural features of the motorcycle geometrically. It comprises standard – "off the shelf" – components for motorcycles from various model libraries and many custom parts. So far, the geometry model has been used to illustrate the concept for renderings and animations. Figure 4.13 sketches the steps from initial geometry from CAD to coupled discretized mesh for FE analysis (Figure 4.14) using the telescopic front fork as an example. These consist of simplifying and de-featuring the CAD geometry due to the initially relatively low model quality, discretization, and connection of the components, as shown for revolute and translational joint couplings in the section cuts below.

To investigate crashworthiness, the model aims to represent the interaction with the crash opponent, structural loading and deformation, and energy absorption of the motorcycle. As a result, the focus of the model is on representing the crash-relevant structural components,

initial geometry $\longrightarrow$ **idealization** $\longrightarrow$ **discretization** $\longrightarrow$ **coupling/interfacing**
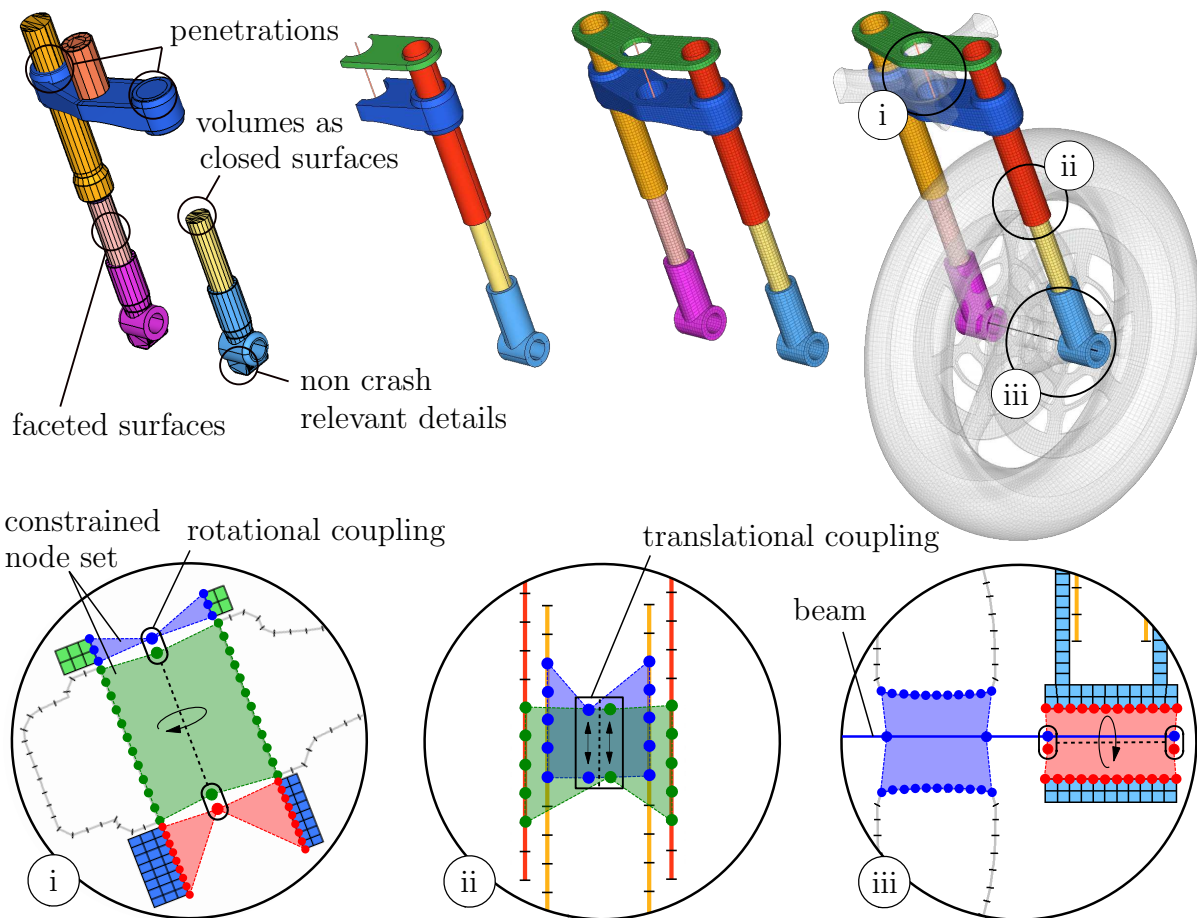
Figure 4.13: Finite element modeling/pre-processing workflow.

81 parts
323K nodes
60 beam elements
243K shell elements
135K solid elements

12 joint connections
25 extra node set connections
67 nodal rigid body connections
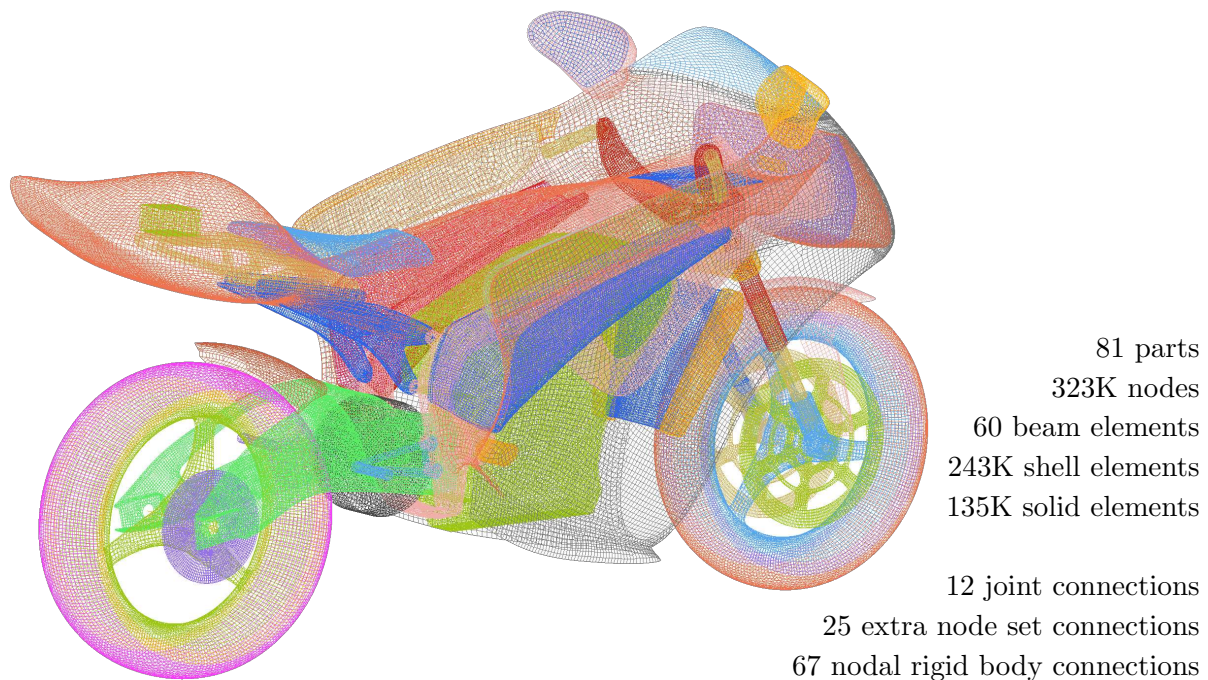
Figure 4.14: Discretization of the FE motorcycle model, shown as wireframe elements, with model characteristics.

which are the front wheel and tire, and the front suspension assembly. Components such as the drivetrain components are modeled as rigid parts because they are assumed not to deform as they are very stiff or outside of the significant crash deformation. As a unique feature of the proposed motorcycle structure, the foam crash box in the cockpit nose aims to control the energy transfer. It is intended to prevent pitching of the motorcycle or even rolling over in a frontal impact. The elevated side impact structures protect the lower extremities laterally. In total the model consists of 81 parts from 378,000 elements with 323,000 nodes. The suspension is modeled with eight kinematic joints; front wheel rotation (2), telescopic front fork suspension (2), rear-wheel rotation (2), front fork steering, and rear swing arm rotation. The other kinematic joints are for the hinged lids of the compartments behind which the airbags are located. To model tire pressure, airbag models are used. The modeling is recorded in the student theses [Beckmann20, Liu20].

Other detailed FE models of PTWs for crashworthiness are [NamikiNakamuraIijima05] (a large tourer), [MongiardiniEtAl17] (a sport tourer) [SchulzDobrovolnyHurlebaus16] (a sport bike), and [BarbaniBaldanziniPierini14] (a three-wheeled scooter).

As the accident opponent, a LS-DYNA model of a 2001 Ford Taurus[8] is used. With an overall height of 147 cm and a mass of 1477 kg the unoccupied four-door passenger sedan complies with [ISO13232:2005] requirements for height (137-147 cm) but slightly exceeds vehicle mass specifications (1238-1450 kg) for the opposing vehicle.

---

[8]2001 Ford Taurus model [MarzouguiEtAl12], version 4d (retrieved from [NHTSA12]), National Crash Analysis Center (NCAC).

4.3   Passive Safety Systems

The occupant protection in an automobile crash is determined by the vehicle crashworthiness and the occupants' restraint system [KentForman14]. Crashworthiness is the structural ability of a vehicle cell to deform by design and dissipate the kinetic energy of the impact while maintaining a sufficient survival space. The occupant restraint system controls and dissipates the remaining kinetic energy through the application of forces. Anything that applies these forces, such as the airbags, safety belts, and interior surfaces, can be considered to be a part of the restraint system. The combination a lap and shoulder belt as a three-point belt and multiple airbags surrounding the occupant has proven to be the most important passive safety systems for car occupants to this day.

The Safe Motorcycle follows a comparable concept using similar safety components. Therefore, existing models of these components as well as methods and expertise for simulating them can be used and benefitted from. This section deals with the modeling of the passive safety systems of the proposed safety concept while describing their function and operation principle from the system response.

4.3.1   Collision Detection

Some of these restraint systems require activation or *firing* at an appropriate time after the initial contact. For cars, these are usually acceleration sensors at the vehicle front and rear and pressure sensors in the doors connected to a decision logic [Leschke20]. For motorcycles, an accident detection is very rarely used.

Basic considerations on sensor concepts for accident detection and airbag deployment of a PTW and a range of possible sensors are proposed in [Engel92]. Such possible sensors measure deceleration, deformation, wheel, suspension motion, steering angle, tire pressure, and approximation to an obstacle. Currently, the Honda Gold Wing (introduced in Section 2.3.2) is the only produced motorcycle that detects an impact to activate passive safety systems. Here, front fork deceleration detected by multiple sensors is used [KobayashiMakabe13]. It has a decision time of $\approx 12\,\text{ms}$ for a frontal impact [KuroeNamikiIijima05]. However, detection of side or rear impacts is not possible. The supervised student thesis [Daub21] examines the virtual realization of the proposed sensors of [Engel92] in simulations of the motorcycle model for the ISO 13232 scenarios in the MB approach. It demonstrates the viability of detection for complete airbag inflation but also that many different sensors are needed to detect accidents in many impact configurations without unwanted false decisions, even under bumpy operational driving conditions. This, in turn, requires a complex decision logic. Therefore, in supervised student thesis [Rodegast22], machine learning algorithms are used for decision-making based on the MB simulation model for even more impact configurations. As a simplification this thesis here assumes an inerrant crash detection with an ideal time period of $12\,\text{ms}$ for all accident scenarios after an initial contact to activate the passive safety systems.

4.3.2   Thigh Belts

Modern seat belts in cars are sophisticated technical solutions. Besides the actual belt and buckle, they consist of a retractor, combining pretensioning and load limiting capabilities [Håland06]. After activation, the belt is tightened firmly against the occupant. When applying force on the body, the force is limited to avoid injuries caused by an otherwise too rigid restraint. This operating principle is also pursued here.

The structure of the model of the proposed belt system is schematically illustrated in Figure 4.15. It consists of two hybrid belt sections modeled with four-node 2D shells and two-node 1D truss elements. The shell nodes have translational and rotational degrees of freedom, transmitting forces and moments. The truss nodes have translational nodal degrees of freedom, carrying only in-line loads. In this abstracted form, belt buckles are not incorporated. The belt ends are connected to attachment points at the motorcycle body (anchors). At the outer anchors, retractors with nonlinear pretensioning and load limiting are implemented. For the MB simulations, the belts are routed with a dedicated belt fitting tool using the MADYMO pre-processor. In the coupled FE/MB and full FE models in LS-DYNA the belts are routed in a simulation-based approach, described in the positioning procedure in Section 4.4 below.

Pretensioning and Load Limiting

Pretensioning and load limiting aim to control the belt force $f(t)$ by manipulating the belt length $l(t)$ through belt pay-in and pay-out. Before activation, the retractor removes
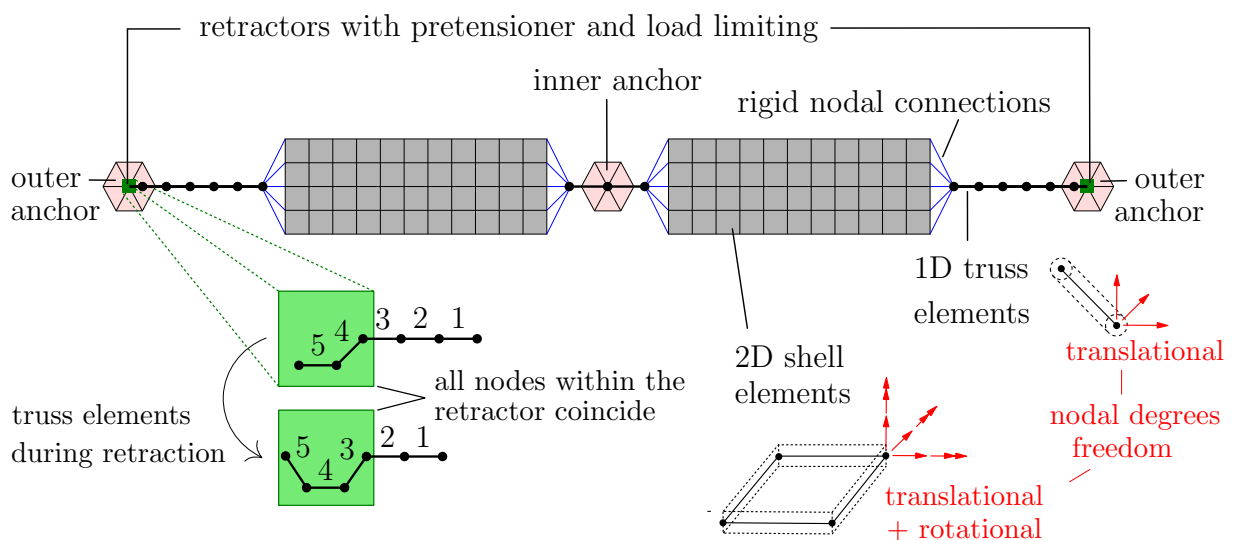
Figure 4.15: Structure of 1D truss and 2D membrane hybrid mesh belt model with retractors.

any pretension or slack in the belt by supplying or retracting belt length, applying a very small pay-in force. After firing, a pretensioning regime is determined by a function of belt pay-in vs. time

$$
L_{\text{pay}-\text{in}}(t) = \begin{cases} 0, & \text{if } t < t_{\text{fire}} \\ -\frac{100}{15}\frac{\text{mm}}{\text{ms}}(t - t_{\text{fire}}), & \text{if } t_{\text{fire}} \leq t \leq t_{\text{fire}} + 15 \text{ ms} \\ -100 \text{ mm}, & \text{if } t > t_{\text{fire}} + 15 \text{ ms} \end{cases} \tag{4.1}
$$

This states that after firing at t_{fire} each of the two outer belt ends are drawn by 100 mm within 15 ms into the respective retrator. Simultaneously, the force level at the outer belt ends is limited by the load limiter to $F_{\text{load}-\text{limit}} = 2$ kN in the particularly adjacent truss element by giving out belt material.

Figure 4.16 shows the resulting forces at each of the four belt ends of the two thigh belts for a frontal impact (scenario ⑦). At the outer ends, the force increases earlier due to the pretensioning and is then restricted to a constant load level by the load limiting. The force limit is not transferred very effectively to the inner ends due to the friction between the belt and the rider. Figure 4.17 gives the belt end force and length for one outer belt end. It illustrates the initial belt shortening and the accompanying quick increase in force and subsequent slackening of the belt for a controlled constant belt force. The regime can be divided into three consecutive phases: (i) pretensioning, (ii) load limiting, and (iii) a rigid restraint without any belt in or output. Here, pretensioning reduces the frontal displacement of the rider through early intervention of the belt restraint and provides a constant force level, thus reducing peak forces and peak deceleration of the rider. Apart from initial belt routing, the design variables are the belts' geometry, such as the width and the positions of the attachment points, the activation time, the belt pay-in function $L_{\text{pay}-\text{in}}(t)$, and the belt load limit $F_{\text{load}-\text{limit}}$.

Figure 4.16: Forces at the thigh belt ends (inner and outer belt end each) in a frontal impact. All curves are filtered with a CFC 1000 filter.

(a) belt end force and belt length   (b) belt end force vs. belt length
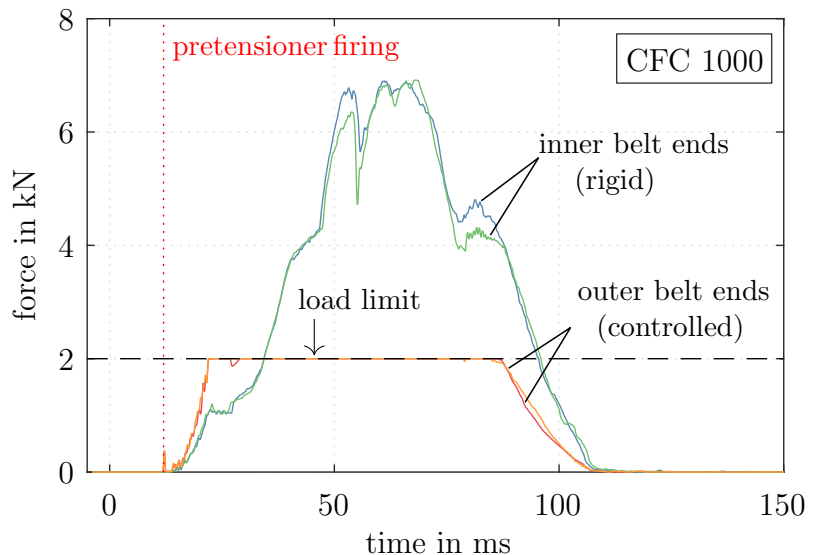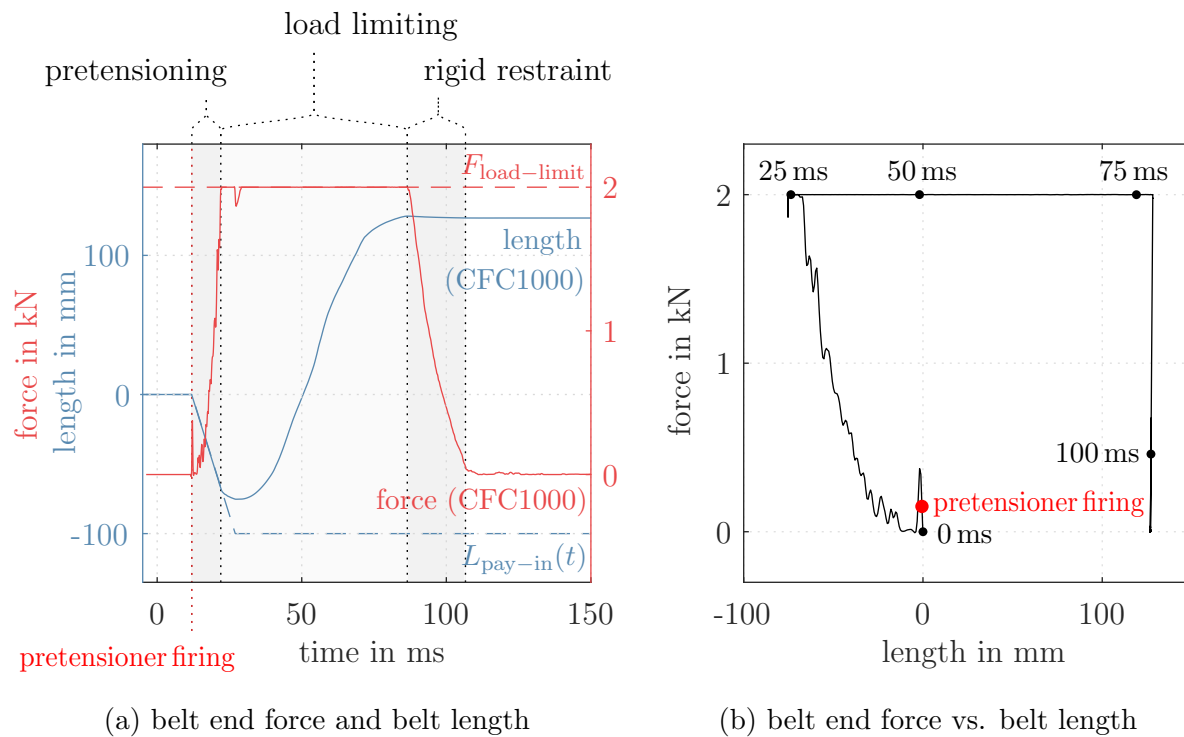
Figure 4.17: Belt pretensioning and force limiting in a frontal impact at an outer belt end.

4.3.3   Airbags

Airbags in automobiles are inflatable fabric bags concealed in the steering wheel, dashboard, and behind other interior panels. These are designed to tear open when the propellant gas rapidly fills the expanding bag. Small vent holes let the gas escape in a controlled manner when the passenger hits the airbag to influence the deceleration for minimal occupant loading. This operating principle is also pursued here with five airbags surrounding the rider frontal and laterally, as shown in Figure 4.18.
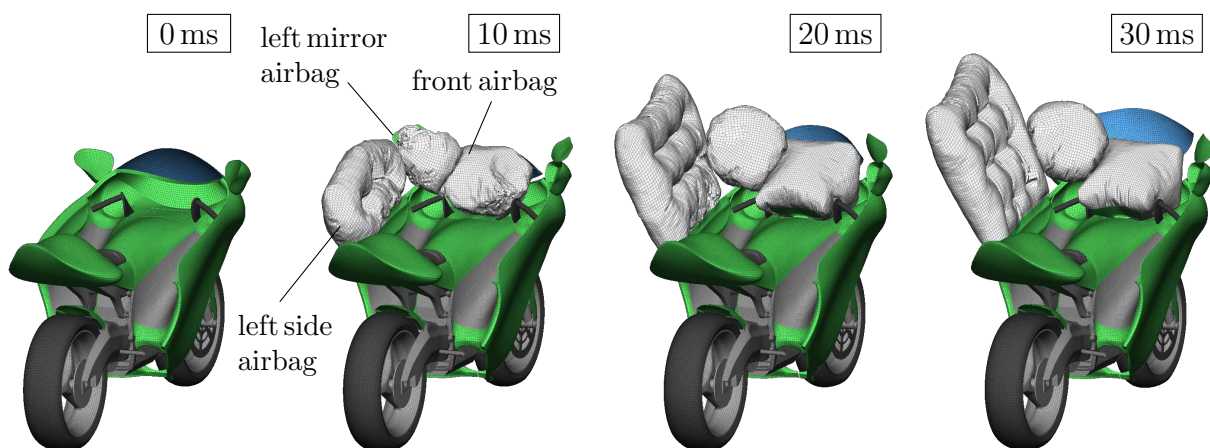
Figure 4.18: Airbag deployment of left and center airbags in full FE model.

The three types of airbags of the safety concept are single chamber 2D and 3D designs with and without internal structure and with and without exhaust openings, isolated in Figure 4.19. The front airbag is a 3D design, meaning that its geometry in its undistorted reference or design configuration encloses a volume, compared to the flat 2D design of the mirror airbag and the side airbag. The frontal airbag has a wedge shape with ≈ 38 liter, no internal structures, and two vents to regulate the airbag pressure and, consequentially,

front airbag: 3D design from three fabric pieces
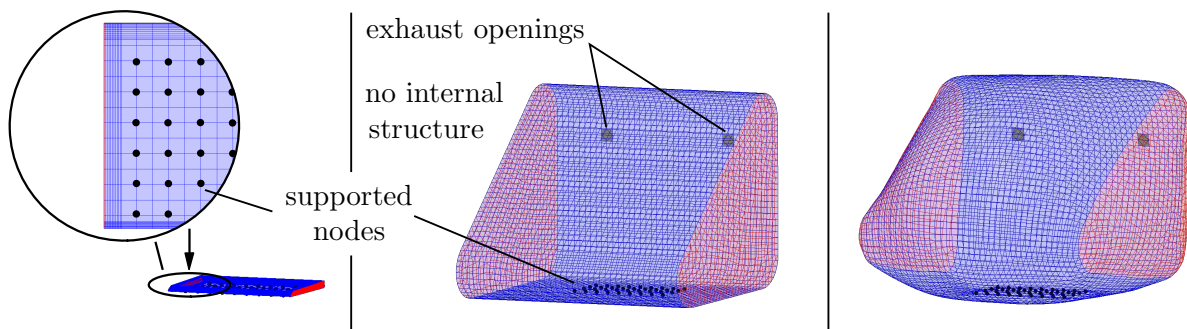
mirror airbags: 2D design from two fabric pieces
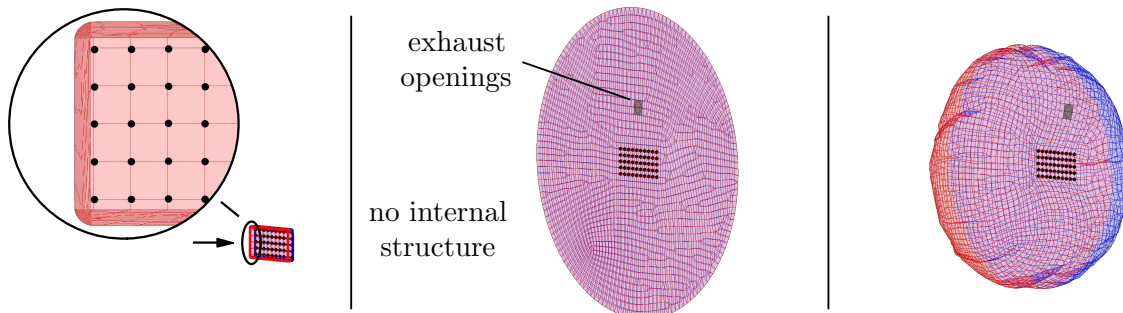
side airbags: 2D design from two outside fabric pieces and nine internal tethers

(a) initial mesh   (b) reference/design mesh   (c) expanded mesh
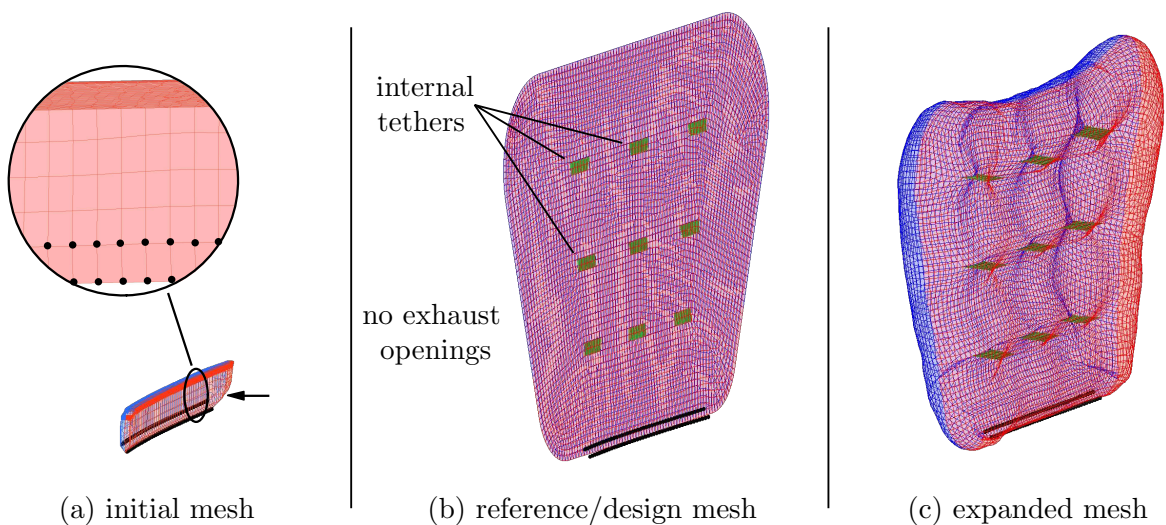
Figure 4.19: Airbag mesh discretizations and support constraints.

the rider's deceleration when impacting into the bag. The windshield is designed to fail under contact pressure from the expanding front airbag structurally. The mirror airbags (≈ 23 liter) have no internal structure and one vent each. They are placed inside the rear-view mirror housing behind hinged lids, which serve as a support surface when opened. The side airbags (≈ 78 liter) are closed bags with internal tethers to obtain a flat shape when inflated and sustain inflation.

- Uniform pressure method (UPM): The volume within the airbag chamber is not discretized. The states are scalar values from a thermodynamic model and uniform for the control volume. An equal resulting force is assumed to act normally onto the segments of the fabric FE mesh to compute the shape in the next step [WangNefske88].

- Arbitrary-Lagrangian-Eulerian (ALE) approach/corpuscular method: The gas flow in the airbag chamber and surrounding the airbag is three-dimensionally discretized. The ALE approach is a moving mesh-based method [FokinLokhandeFredriksson03]. The denomination stems from a combined description with an Eulerian formulation (observer focuses on specific locations in space; commonly used in pure flow problems) with a Lagrangian formulation (observer moves along with the moving body; widely used in structural problems). The corpuscular method constitutes techniques where the gas is modeled as a set of individual particles, where a particle represents many molecules [LinCheng18].

Methods to generate an initial tightly packed mesh geometry can be divided into:

- Flattening or folding: Flattened or folded bag meshes are constructed from CAD geometries or by using simulation-based techniques to move and deform the airbag mesh through a series of folding steps in a transient analysis [ChawlaBhosaleMukherjee05, RuffJostEichberger07]. The difficulty is to attain a well-behaved geometric mesh of a tightly packed folded airbag without penetrating elements. Here, user-friendliness depends on sophisticated preprocessors.

- Scaling: The above-described task is time-consuming. To avoid it, an undeformed reference or design mesh is mapped to a highly distorted scaled-down initial mesh. A special material model and algorithms allow the bag to relax into its original undeformed shape [TanavdeEtAl95].

By considering the gas flow and modelling a folded airbag, the beginning of the expansion of the airbag can be reproduced more accurately. These are therefore particularly important for more fundamental investigations of out-of-position postures of occupants [HirthHaufeOlovsson07, ChristBüttner12]. For this work, *UPM* and *scaling* are well suited and used, not least because both MADYMO and LS-DYNA offer a very similar implementation.

Uniform Pressure Method

As schematically illustrated in Figure 4.20, the airbags are discretized with triangle and quadrilateral elements in membrane formulation since bending stiffness is often assumed negligible for simulating thin airbag fabrics. The expansion is determined by gas mass flow $\dot{m}$ entering through the gas generator (inflator) and exiting through exhausts (vents), and leakage through airbag seams and through the fabric due to porosity. The mass balance complies for each time step i, such as

$$
\begin{aligned}
\dot{m}_{i,\text{tot}} &= \dot{m}_{i,\text{in}} + \dot{m}_{i,\text{out}} \\
&= \dot{m}_{i,12} + \dot{m}_{i,23,\text{exhaust}} + \dot{m}_{i,23,\text{leakage}}.
\end{aligned}
\tag{4.2}
$$

The internal airbag chamber variables are calculated from scalar thermodynamic equations. At each time step, the volume of the expanding chamber V is determined. Assuming an adiabatic airbag chamber and an ideal gas at an uniform pressure p and a temperature T, the pressure is expressed as

$$
p_i = (\gamma - 1)\, \rho_i \, e_i.
\tag{4.3}
$$

γ is the isentropic coefficient c_p/c_v, ρ is the density, and e is the specific internal energy. The dependency for two neighboring time steps is

$$
\frac{e_i}{e_{i-1}} = \left(\frac{V_{i-1}}{V_i}\right)^\gamma + \left(\frac{\rho_i}{\rho_{i-1}}\right)^\gamma.
\tag{4.4}
$$

From the volumes V_{i-1}, V_i, and the specific internal energy e_{i-1} of the previous and current steps, the current specific internal energy e_i is computed. From Eq. (4.3), this leads to the pressure and ultimately to the normal force acting on the airbag fabric nodes [HirthHaufeOlovsson07].
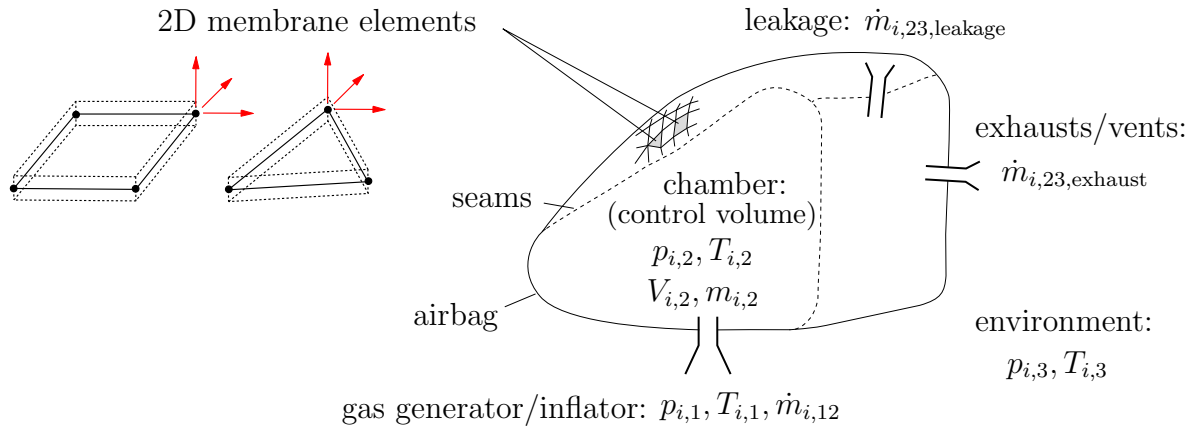
Figure 4.20: Structure of the airbag model with the uniform pressure method.

Figure 4.21: Scaling of initial mesh of frontal airbag.

directional scaling planes

(a) reference/design mesh   (b) scaled initial mesh
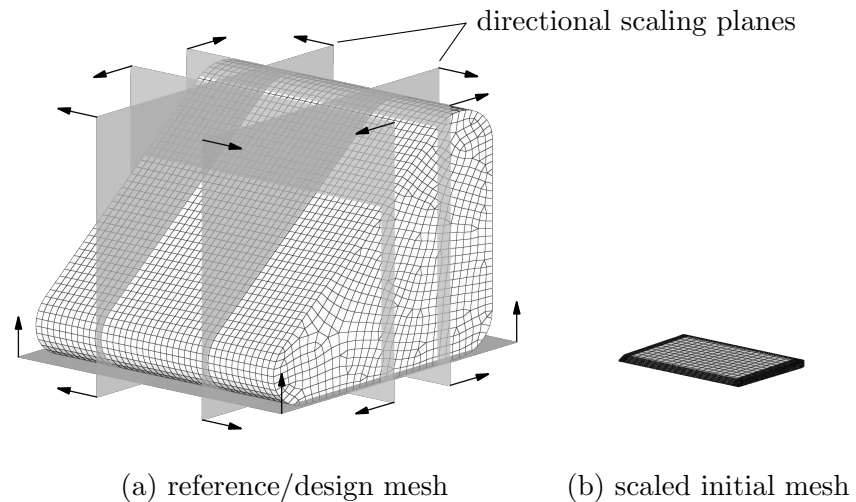
Initial Metric Method

The IMM uses two meshes, an *initial* mesh and an undeformed *reference* or design mesh, for the individual airbag chambers, overviewed in Figure 4.19. The reference meshes are shrunk normally to multiple directional scaling planes, illustrated in Figure 4.21. Due to scaling, the initial mesh has highly distorted elements. An algorithm maps the strains and stresses with respect to the undeformed reference mesh based on the geometric differences. to the initial scaled mesh. During inflation it allows the elements to relax to their reference shape [SISS20b]. It circumvents considerably more complex folding procedures, which is usually laborious and time-consuming, especially for complex geometries and/or tight packaging. For constitutive models of the bag, woven and coated fabric material models from the automotive industry are adopted.

Using these methods, the design variables, apart from the implemented fabric material model, include the external and internal geometry of the airbag, the mass inflow function with constant inflow temperature, and the exhaust hole area. Exemplary time histories of the resulting states of the frontal airbag are given in Figure 4.22. It consists of multiple consecutive phases: after firing (i) rapid inflation through the gas generator, followed by (ii) retention of chamber pressure and volume until (iii) deflation for a controlled rider deceleration, where the gas exits through the exhausts.

Figure 4.23 shows the relative position of the occupant to the three types of airbags. A frequently discussed problem of airbags on motorcycles is the threat of an out-of-position deployment [RametEtAl94, ChawlaMukherjee07]. In this case, the rider would be hit by the airbag while expanding. This impact can be serious as the airbag inflates within 30 to 40 ms and the speed of the airbag material coming out of the airbag module reaches 125 km/h. In the relative position shown here, the rider still has some available space to lean forward without risk of being hit, as the airbag is very small compared to,

say, the Honda Gold Wing's bag (38 vs. 150 liters). The volume here can be chosen much smaller, as the restraint task is shared with the belt.

4.3.4 Leg Impact Protectors

One of the ideas of the safety concept is to transfer protective elements of the motorcyclist's clothing, such body armor, onto the vehicle. The properties and features are – at best – large but very lightweight impact protection surfaces with excellent impact energy absorption and tight packaging with a minimal cross-section. These requirements result in a design of soft areas of a relatively thin layer of energy-absorbing foam around the rider's knees and thighs.

The chosen material, a polyurethane foam, is supplied by SAS-TEC. It can be produced in various densities (200 to 425 g/l) and has an impact-rate-dependent material behavior aimed at good energy absorption. The foam has a mixed open and closed cell structure, which gives it its rate-dependent mechanical properties. Under loading, the air in open foam bubbles is forced out through small openings. When the load is removed, the air flows back in. These material properties cause it to act very firmly during fast impacts while remaining soft during slower loading, similar to a non-Newtonian fluid. Currently, it is commercially available in shoulder, knee, elbow, and back protectors that are worn by riders of PTWs, bicycles, or horses, where it can achieve the highest protection levels of EN1621-1 and 2 (explained in Section 2.3.3). By using vegetable oils for the polyol portion, the foam is about 60 % made from renewable resources.

The protectors are 15 mm thick and flush with the adjacent cockpit surfaces. They're modeled using eight-node (hexahedron) and six-node (prism) 3D solid elements (ELFORM=-2; fully integrated elective reduced solids), shown in Figure 4.24. To model the material behavior in LS-DYNA dynamic pendulum impact, drop tower, and quasi-statics tests were conducted together with industrial partners. LS-DYNA provides a variety of material models (see Figure 3.8). To capture rate-dependent loading and hysteretic unloading of foams, the LS-DYNA material model `*MAT_FU_CHANG_FOAM` [LSTC18] is well suited. It is frequently used for a wide variety of foam materials (see e.g. [CroopLobo09]) and can be mapped with near-test data. The material characterization consists of three steps, shown in detail below: (i) the loading behavior of the material is derived from fitting pendulum impactor test data, (ii) the unloading behavior is approximated by a parameterized damage formulation, and (iii) the quality of the models is tested in a drop tower test setup that also quantifies protection levels according to EN1621-1. The novelty of the demonstrated procedure is the formulation of an optimization problem for the polynomial representation of experimental test data incorporating material map requirements and material behavior knowledge to characterize the `*MAT_FU_CHANG_FOAM` material input cards. The procedure was first introduced as part of [MaierEtAl21a, MaierEtAl21b].
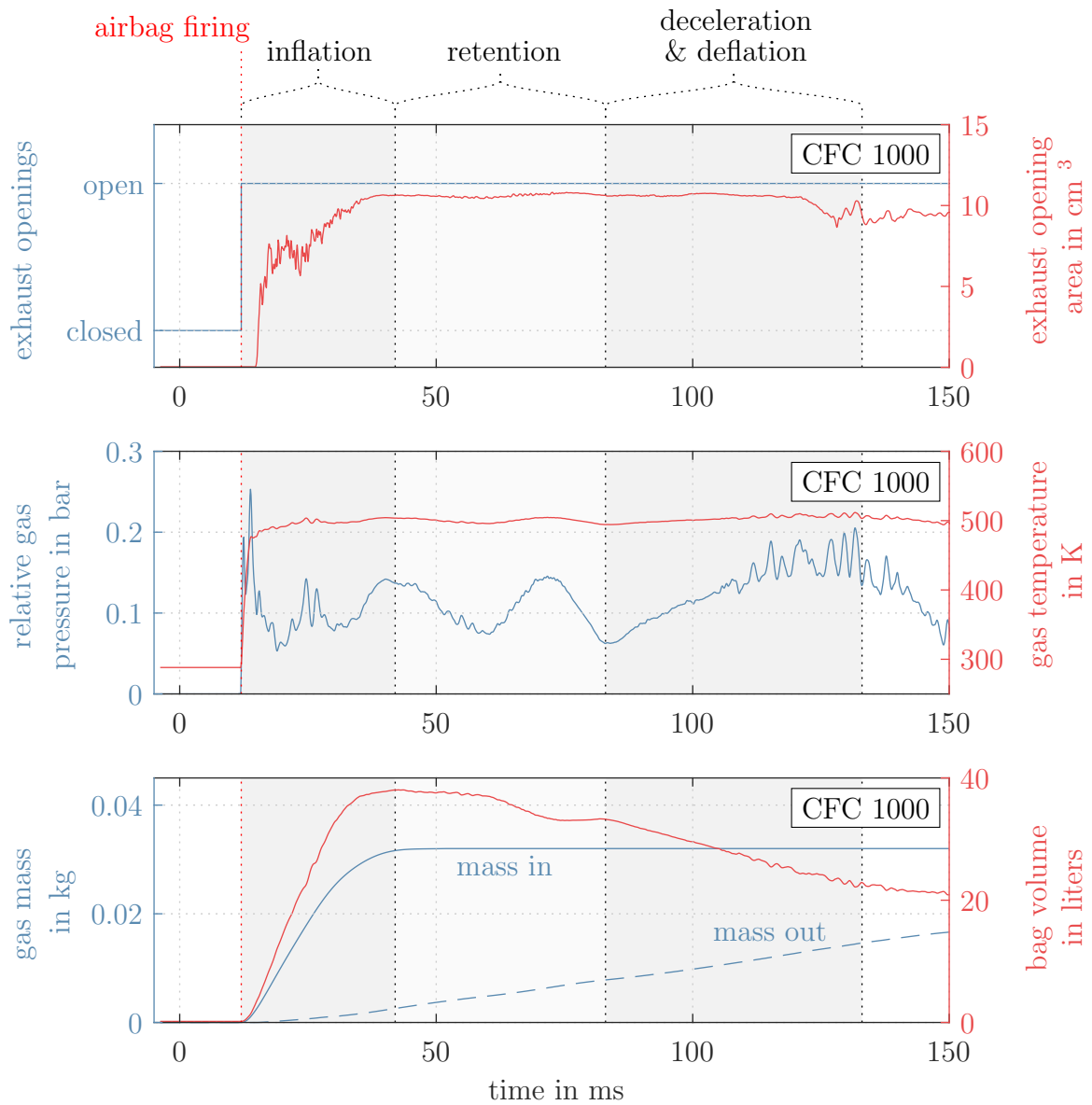
Figure 4.22: Airbag chamber variables for front airbag in a frontal impact.
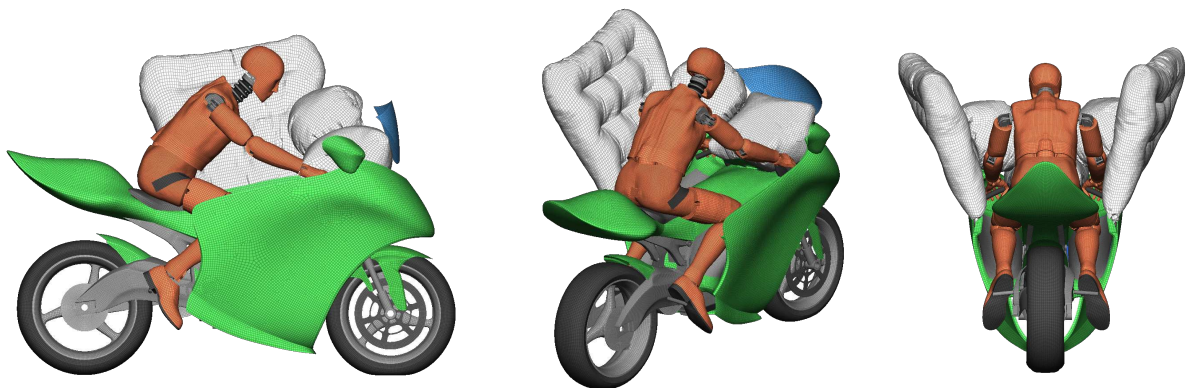
Figure 4.23: Rider position in respect to deployed airbags.

Characterisation of the Loading Behavior

The definition of the `*MAT_FU_CHANG_FOAM` material card requires engineering stress vs. engineering strain as a function of multiple constant strain rates. Figure 4.25 shows the dynamic test setup of the tests conducted by DYNAmore where a pendulum impactor drops from an initial height h_0 with force measurement via the impactor's mass and its acceleration and the displacement via the rotary angle ψ of the impactor arm. DYNAmore also conducted quasi-static tests with a universal testing machine. The foam specimens are conditioned at 23°C and 50 % relative humidity for at least 24 hours. Figure 4.26 gives the stress vs. strain vs. strain rate derived from the three dynamic strain rates with impact velocities of $v_1 = 0.5$, 1.5, and 4 m/s and one very slow constant loading and unloading velocity of $v_{\text{const.}} = 1$ mm/s, each measured five times. The quasi-static measurements ($v_{\text{const.}}$) do not form a closed loop but cut off during unloading because

raw foam sheets
of varying thickness

15 mm

3D solid elements
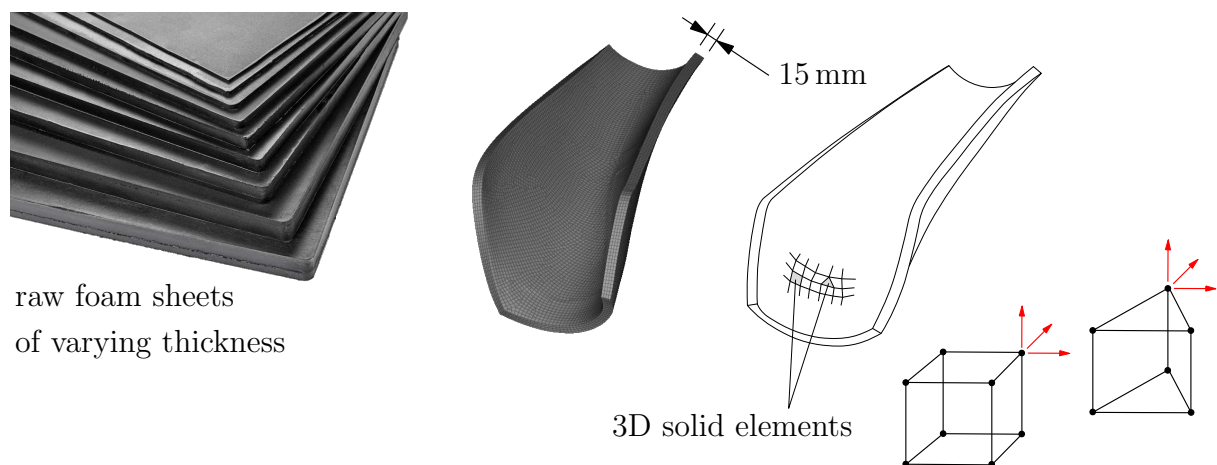
Figure 4.24: Raw foam sheets from SAS-TEC and leg impact protector mesh discretization.

foam specimen
20 mm×20 mm×10 mm

ψ

g

impactor with
$m = 2021$ g

h_0

anvil
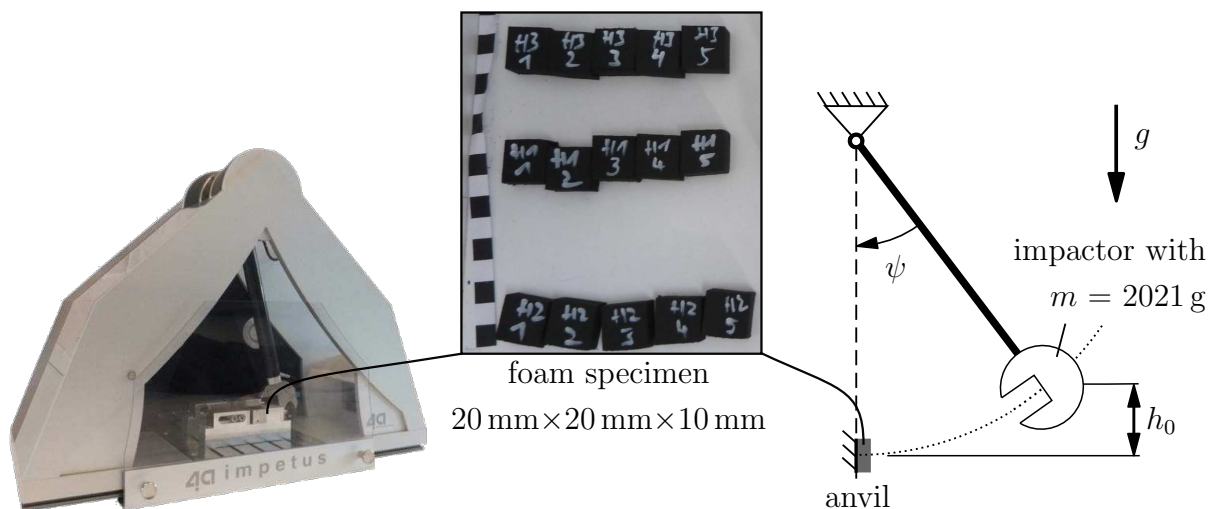
Figure 4.25: Experimental setup of dynamic pendulum impactor test at DYNAmore.

Figure 4.26: Dynamic and quasi-static experimental test data for the $425\,\mathrm{g/l}$ foam provided by DY-NAmore.
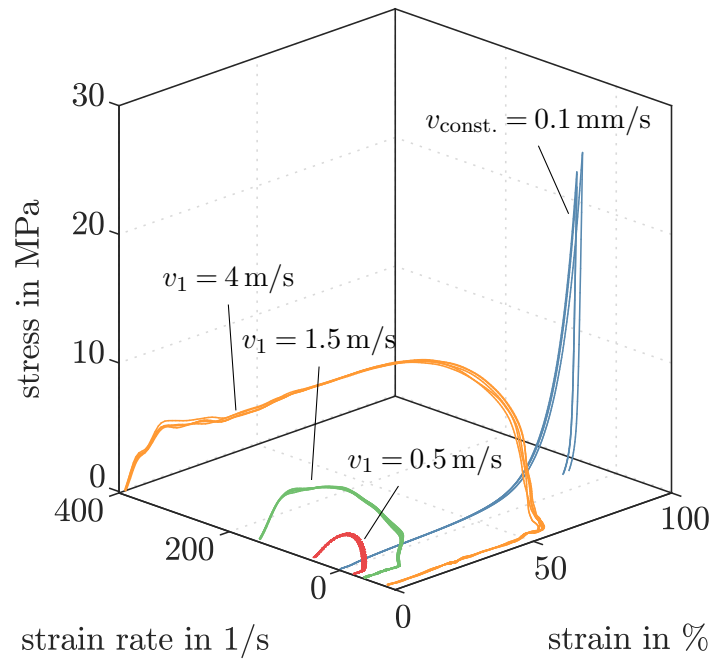
the impactor detaches from the foam samples due to the very slow unloading of the foam samples.

To derive stress vs. strain curves for the required constant strain rates, the dynamic and quasi-static measurement data is fitted using bipolynomial and polynomial surface and curve fits. For the 3D surface fit of the dynamic measurement data, the stress data points z are fitted on a non-uniformly spaced rectilinear 2D grid for strain (x) and strain rate (y). With polynomial coefficients $\boldsymbol{a}$ and $\boldsymbol{b}$ and with degrees n in x-direction and m in y- direction, it results in

$$z = F(x, y) = \left(\sum_{k=0}^{n} a_k x^k \right) \cdot \left(\sum_{l=0}^{m} b_l y^l \right) \text{ with } m, n \geq 0. \tag{4.5}$$

Depending on the order of these polynomials, this leads e.g., for $n = 2$ and $m = 3$ to

$$z = (a_0 + a_1 x + a_2 x^2) \cdot (b_0 + b_1 y + b_2 y^2 + b_3 y^3). \tag{4.6}$$

By computing, reordering, and renaming the coefficients this corresponds to

$$z = c_0 + c_1 x + c_2 y + c_3 xy + c_4 y^2 + c_5 xy^2. \tag{4.7}$$

where the polynomial coefficients $\boldsymbol{c}$ approximate the k stress measurement data points.

$$
\underbrace{\begin{bmatrix} z_1 \\ z_2 \\ \vdots \\ z_k \end{bmatrix}}_{\boldsymbol{z}} = \underbrace{\begin{bmatrix} 1 & x_1 & y_1 & x_1 y_1 & y_1^2 & x_1 y_1^2 \\ 1 & x_2 & y_2 & x_2 y_2 & y_2^2 & x_2 y_2^2 \\ \vdots & \vdots & \vdots & \vdots & \vdots & \vdots \\ 1 & x_k & y_k & x_k y_k & y_k^2 & x_k y_k^2 \end{bmatrix}}_{\boldsymbol{A}} \cdot \underbrace{\begin{bmatrix} c_0 \\ c_1 \\ c_2 \\ c_3 \\ c_4 \\ c_5 \end{bmatrix}}_{\boldsymbol{c}} \tag{4.8}
$$

The coefficients $\boldsymbol{c}$ are determined through the minimization of a quadratic objective function. Linear equality and inequality constraints incorporate LS-DYNA material card requirements and knowledge about surface topology to sustain a physically valid shape in surface regions with sparse or no data, see Equation (4.9).

$$
\min_{\boldsymbol{c}} \| \boldsymbol{z} - \boldsymbol{A} \cdot \boldsymbol{c} \|_2 \ \ \text{s.t.} \begin{cases} F(0, y) = 0 & \text{(4.9a)} \\[2mm] \dfrac{\partial}{\partial x} F(x) > 0 & \text{(4.9b)} \\[2mm] \dfrac{\partial}{\partial y} F(y) > 0 & \text{(4.9c)} \\[2mm] \dfrac{\partial}{\partial y} F(0, y) \leq p_1 & \text{(4.9d)} \\[2mm] \dfrac{\partial^2}{\partial x^2} F(x) > \ \text{ for } x > p_2 \cdot x_{\max} \text{ with } p_2 \in [0, 1] & \text{(4.9e)} \end{cases}
$$

The constraints consider `*MAT_FU_CHANG_FOAM` and `*DEFINE_TABLE` input card requirements such that

(4.9a) the surface intersects the strain rate axis,

(4.9b) the strain vs. strain rate curves do not intersect each other,

(4.9c) and each of the strain vs. strain rate curves is monotonically increasing.

Furthermore, the constraints incorporate knowledge about surface topology to get a valid surface fit, also in areas with sparse or no data by introducing additional parameters p_1 and p_2 such that

(4.9d) the slope is limited to p_1 in strain direction,

(4.9e) and a positive curvature is obtained in an upper portion p_2 up to the maximal strain $x_{\max}$ in strain direction.

One more paramter p_3 describes the logarithmic order of the grid in strain direction. The parameter reduces the required polynomial order for an adequate fit by shifting the discretization to where the matched surface curvature is higher; see the optimization results for the chosen $425\,\text{g/l}$ foam in Figure 4.27a and 4.27b. The quasi-static loading data in Figure 4.27b is fitted with the same procedure but with $m = 0$.

(a) dynamic loading data fit

(b) quasi-static loading data fit
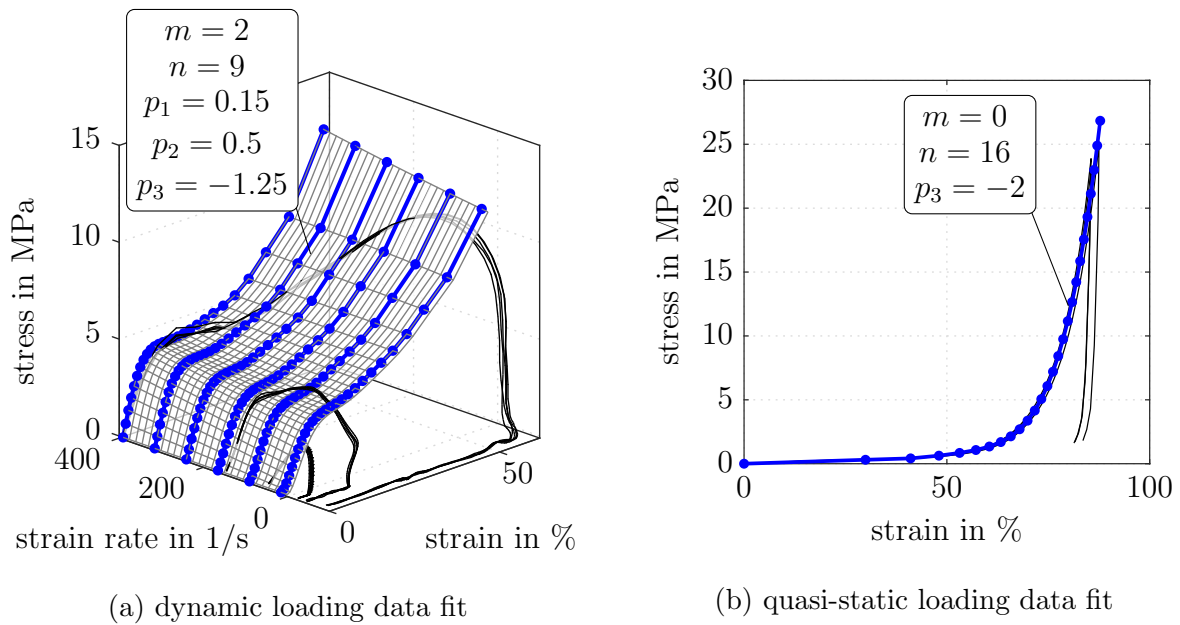
Figure 4.27: Material card curves (blue) fitted to dynamic and quasi-static experimental loading data with respective parameter choice of surface and curve fit for the 425 g/l foam.

Characterisation of the Unloading Behavior

For unloading `*MAT_FU_CHANG_FOAM` provides multiple methods, such as a method where the unloading response is given by a parameterized damage formulation d for the principal stresses σ_i. The damage formulation is based on the current and maximal values of the hyperelastic energy W with

$$\sigma_i = (1 - d)\,\sigma_i \quad \text{with} \quad d = (1 - \text{HU}) \left[1 - \left(\frac{W_{\text{current}}}{W_{\text{maximal}}} \right)^{\text{SHAPE}} \right]^{\text{EXPON}}. \qquad (4.10)$$

he parameter HU $\in$ [0,1] is a hysteretic unloading factor, and the parameters SHAPE and EXPON are a shape factor and an exponent for unloading. Figure 4.28 gives the fit for variations of these parameters in simulation runs to the experimental data. The simulation model approximates the anvil, the foam sample, and the pendulum impactor by two rigid plates and a 3D-element foam rectangle, shown at the very top. The plate on the left (anvil) is constrained, the plate on the right (pendulum head) impacts at v_1. For loading, the simulation agrees reasonably well except for initial loading, where the measurements show some oscillation, and for peak stress, where the measurement peaks are less sharp than the simulation stress response. For unloading, the parameters HU = 0.01, SHAPE = 7.5, and EXPON = 0.5 allow a good approximation of the measurement with the highest load spectrum. At the same time, it is not possible to match the unloading paths of all pendulum impact velocities simultaneously.
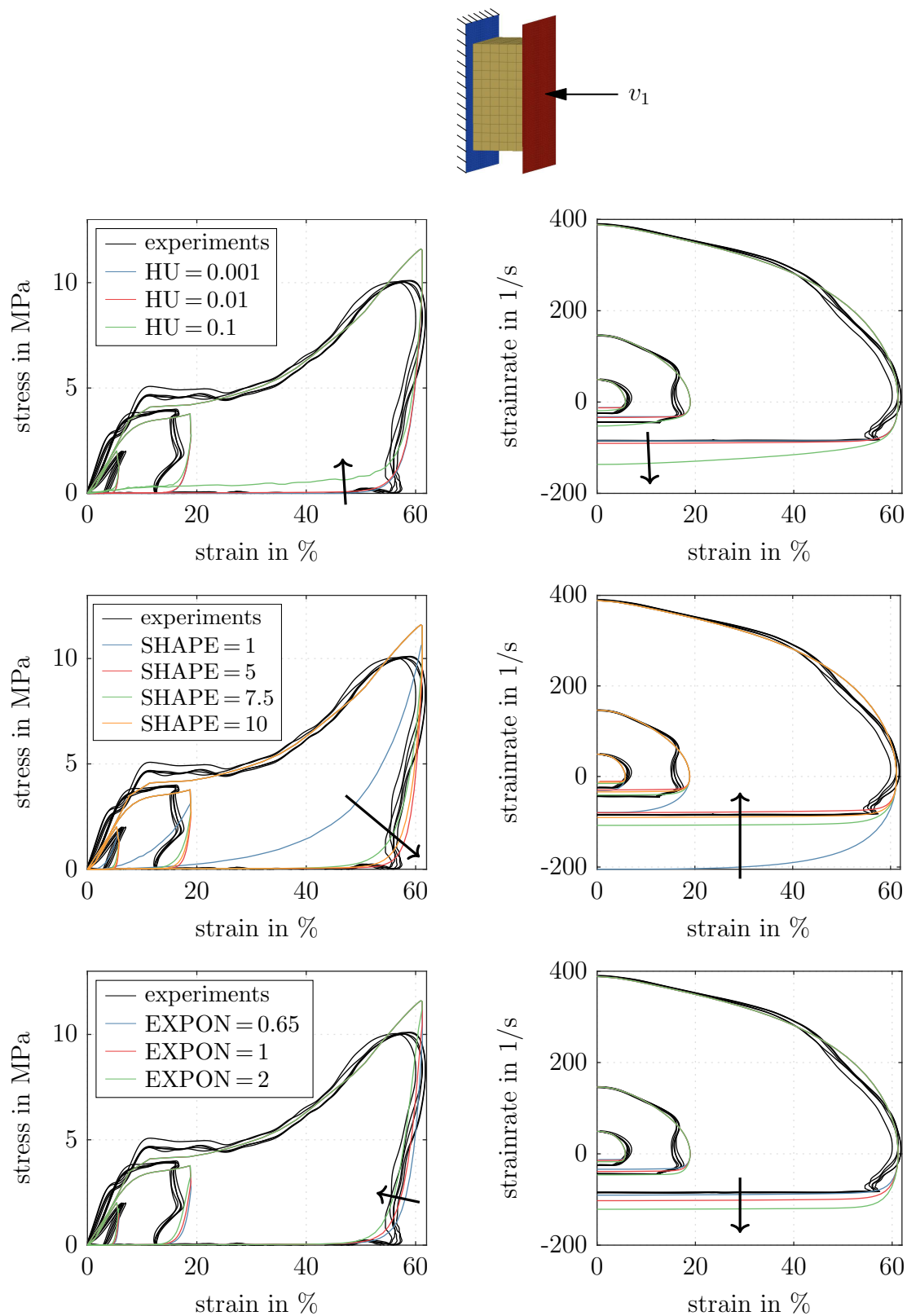
Figure 4.28: Simulation of unloading response with baseline parameters HU = 0.01, SHAPE = 7.5, and EXPON = 0.65 against experiments with the 425 g/l foam. The arrows indicate the trend of the series of the curves for increasing parameter values.
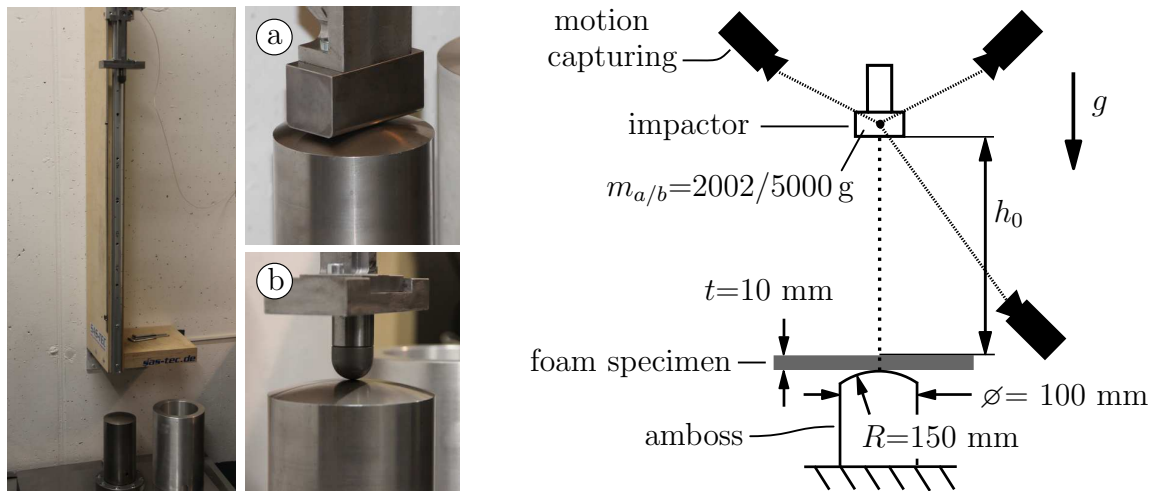
Figure 4.29: Experimental setup of drop tower impactor test at SAS-TEC.

Conformity with Drop Tower Tests

To evaluate the quality of the derived material models, experiments with drop tower setup shown in Figure 4.29 were conducted at SAS-TEC. The setup is typically used to quantify the protective performance of limb joint impact protectors worn at shoulders, elbows, forearms, knees, shins, and hips according to EN 1621-1 and back protectors according to EN 1621-2. The tests were conducted with two different steel impactors (ⓐ: $m_a = 5031$ g, width $= 80$ mm, depth $= 40$ mm, long edge corner radius $= 3.5$ mm; ⓑ: $m_b = 2404$ g, radius $= 12.5$ mm), dropped from an initial height h_0 with force sensing in the heavy steel anvil and displacement measurement with a motion capture camera system. The foam specimens were non-conditioned, and the test was repeated three times each.

For ⓐ, the force response of the simulation conforms very well to the experiment, both in magnitude and in shape (Figure 4.30; top). The height of the first rebound fits very well, while the subsequent rebounds are overestimated by the simulation significantly. Video recordings of the experiments and the unloading behavior in the quasi-static tests show that the material does not immediately adopt the initial geometry after an initial impact but remains temporally compressed. The viscoelastic foam needs some time to recover its original shape. This behavior is not reproduced in the simulations and could explain the difference as the impactor in the experiments hits the still-compressed foam in the following impacts.

For ⓑ, the force agrees qualitatively reasonably well to the experiment (Figure 4.30; bottom). While the initial rebound height of the experiment with a drop height of 0.5 m is quite similar and the subsequent rebounds are as expected overestimated, all the rebound heights at a drop height of 1 m deviate significantly. Here, the maximum achieved strain is $x_{max} = 90$ % is outside the generated material card data. To conclude: the comparison indicates that within the strain range of the material card ($x_{max} < 62$), the foam force response, as well as rebound behavior, can be accurately predicted for the initial impacts.
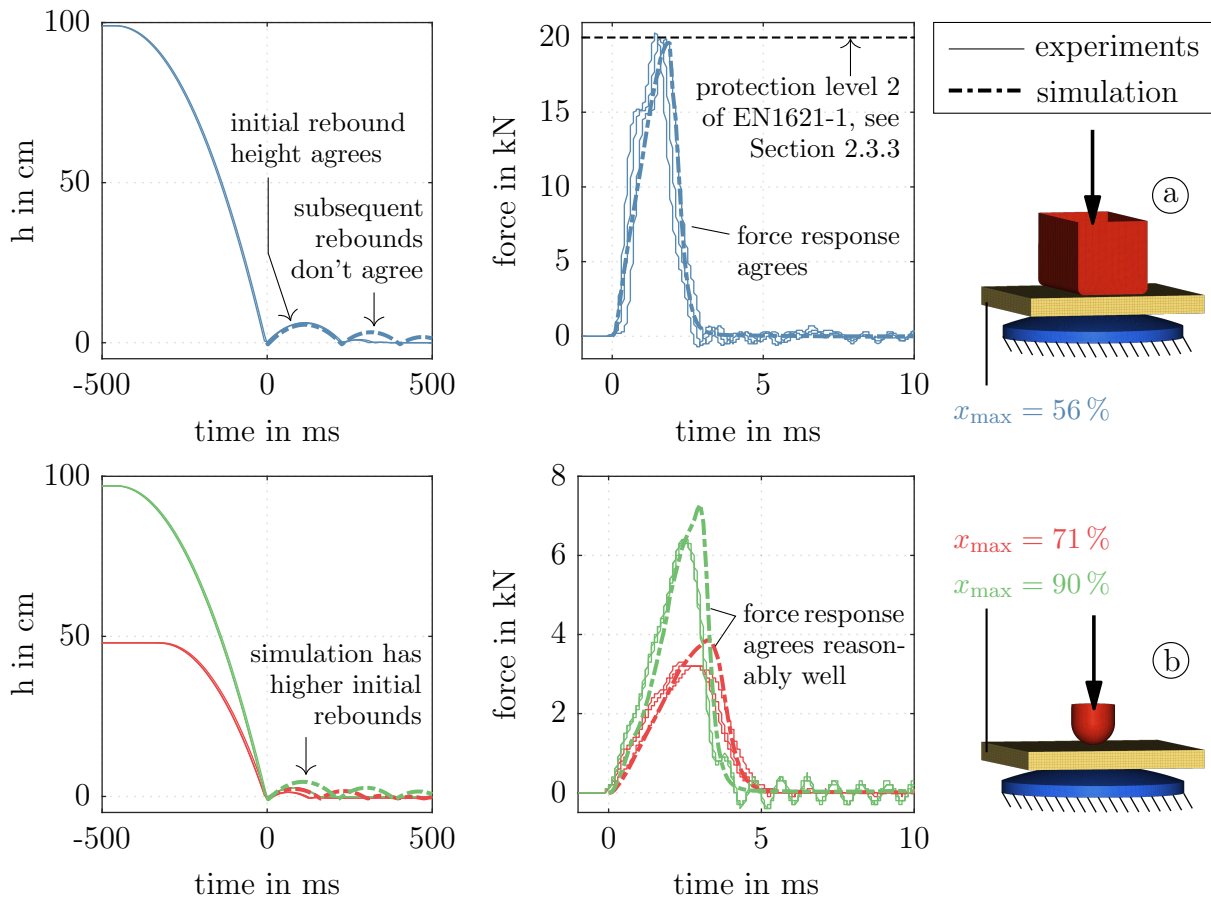
Figure 4.30: Simulated impactor height, anvil force, and maximal strain responses compared to drop tower impactor experiments for the 425 g/l foam.

4.4   Rider Surrogates

At best, multiple surrogates represent a diverse society biofidelic, i.e., they accurately predict the real biological system of a broad range of human individuals. In passive vehicle safety, primarily ATDs are used, as already briefly introduced in Section 2.4.2. However, they are only a relatively coarse discrete sampling of the population and, as mechanical systems, are limited in their biofidelity. Therefore, a whole range of digital-only HBMs, representing humans in low-dynamic driving operations to high-load in-crash accident scenarios, are getting increasingly integrated into the development of new vehicles, as we comprehensively overviewed in [FahseEtAl23].

Starting from the introduction to the different seating positions on a motorcycle given in Section 2.2, the definition of the Safe Motorcycle seating position is discussed on the modeling level. Suitable rider surrogate models are discussed and selected. First, these are computational models of ATDs, where the application on a two-wheeler combined with a rider restraint through seat belts imposes some compromise. Second, these are state-of-the-art FE HBMs, several of which, including sex variants, are used.

4.4.1 Riding Posture

The overall posture of a motorcyclist depends on its anthropometric dimension and the geometry of the motorcycle. As shown in Figure 4.31, in principle, the posture must fulfill four boundary conditions:

(i) The pelvis sits on the seat, while its absolute position can vary to a limited extent (surface contact).

(ii) The hands grip the handles of the handlebar (revolute joint).

(iii) The feet rest on the footrests (revolute joint).

(iv) The head complies with a visual condition, typically resulting in a slightly downward head orientation (orientational constraint).

This posture is unstable and must be maintained by static muscle power.

In ergonomic surveys, such target postures are determined experimentally with human subjects. Here, posture data from [Kolling97] is used. The study examines multiple subjects in tests conducted with different types of motorcycles in a wind tunnel at a frontal velocity of 120 km/h. Based on the classification of vehicle type and rider posture given in Section 2.2 the Safe Motorcycle corresponds to a typical posture of a motorcyclist on a sports bike. The corresponding angles according to the angle definitions in Figure 4.32 from [Kolling97] are given in Table 4.2.
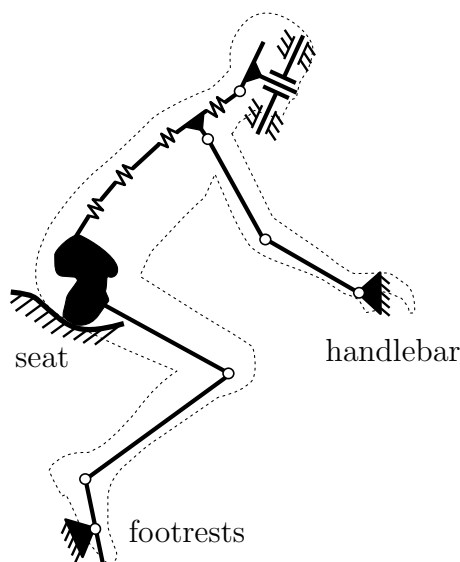
Figure 4.31: Principle framework to describe the posture of a rider on a motorcycle according to [Kolling97].
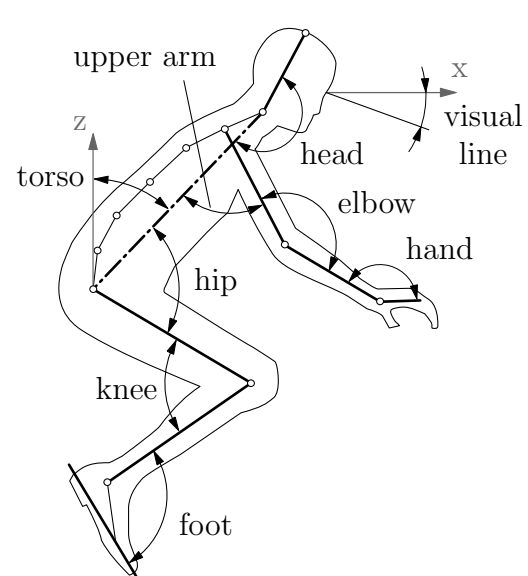
Figure 4.32: Angle definitions of a motorcycle rider's posture from [Kolling97].

Table 4.2: Posture angles of the seated rider on the Safe Motorcycle according to the convention from Figure 4.32.

visual line	head	torso	hip	upper arm	elbow	hand	knee	foot
10°	165°	70°	150°	150°	40°	75°	65°	115°

4.4.2 Standardized Anthropometric Test Devices

The standard ATD in vehicle safety to date is the Hybrid III 50th percentile, designed as the average male car occupant in an upright sitting position for a frontal impact. The Hybrid III adult family consists of the 5th percentile (small female), the 50th percentile (male), and the 95th percentile (large male) dummy variant with more child dummies representing different ages [MertzIrwin15]. Although rarely used, there are specific ATDs to represent motorcyclists.

- The standard ISO 13232 defines to use the Motorcyclist Anthropometric Test Device (MATD). This ATD is a modified Hybrid III 50th, designed to represent a motorcyclist, available only in a 50th percentile variant. These modifications include (i) a modified neck and head compatible with motorcycle helmets and for motorcyclist-specific head positioning, (ii) the sit/stand pelvis of the Hybrid III 50th pedestrian in standing configuration, (iii) hands that can be wrapped around handlebars and (iv) frangible components in the abdomen, upper and lower legs, and knees, as elaborated in [ZellnerEtAl96, Van AukenEtAl05].

- Just very recently the Powered Two-Wheeler Dummy, a modification of the Hybrid III pretty similar to the MATD, was introduced. It is the Hybrid III 50th pedestrian in standing configuration with a modified head and neck assembly and some modifications at multiple points of the spine, according to a work-in-progress status in [CarrollEtAl22].

Both of the above ATDs have the Hybrid III sit/stand pelvis. They are – apart from the fact that the Powered Two-Wheeler Dummy is introduced just now and thus too late anyway – not suitable for the application at hand. This pelvis type has significant clefts at the hip attachment points into which the belts would slip and is, therefore, not suitable for fastening thigh belts. Since a helmet is not worn, helmet compatibility is no requirement, and the Hybrid III 50th is also used in the simulation models of full-scale crash tests of Dekra (see Section 4.2.1), which in turn allows a direct comparison. Therefore it is decided to use the Hybrid III family instead. The Hybrid III model family has the advantage that sex variants and many virtual models for the used platforms are available. In this work, the MADYMO ellipsoid MB model and the small female and male variants of the LS-DYNA FE model, shown in Figure 4.33b and 4.33c, are used.

105 joints	221 joints	367 parts
93 rigid bodies	211 rigid bodies	279K nodes
		465K elements

(a) MADYMO MATD facet MB model[9]
(b) MADYMO Hybrid III 50th ellipsoid MB model[10]
(c) LS-DYNA Hybrid III 50th FE model[11]
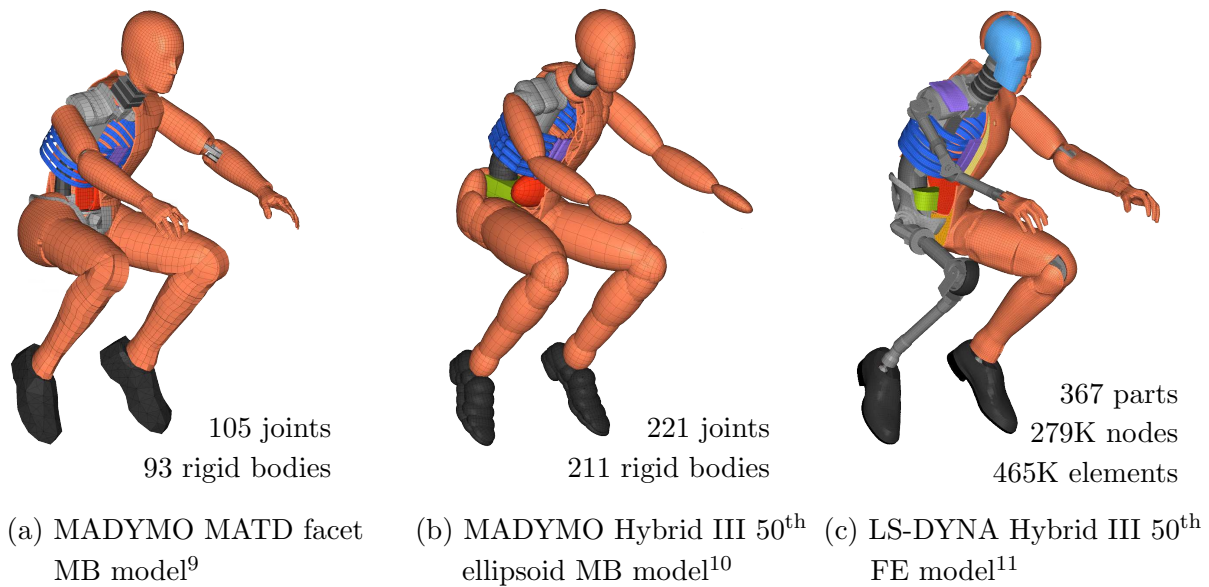
Figure 4.33: ATD models (partially blanked) in a motorcyclist's riding posture with model characteristics.

Positioning of Multibody and Finite Element Models of ATDs

The position and posture of an MB ATD are defined by the angles of the ideal joints. In principle, a posture manipulation of FE ATDs is based similarly on transforming node coordinates by constraints of the kinematic joints of the model. This procedure works well for arranging the upper and lower extremities, as it is intended for a Hybrid III and the nominal position of a car occupant. However, for greater variations in the posture, overlapping parts and elements can occur. Here, overlapping parts occur at the thighs-to-pelvis connections of the molded hip flexion angle, the knee bends, where the shanks touch the thighs, and the ATD wrists. To avoid overlapping, a transient simulation incorporates compliance between deformable parts. In the first step, an initial posture close to the desired posture is pre-processed by using the above-mentioned nodal displacements constrained by the kinematic joints. Subsequently, the joints are partially locked and constrained by elastic elements to prescribed motion nodes, as schematically shown in Figure 4.34a. Initially scaled and distorted geometries of the contact partners morph into the final motorcycle geometry. This rotates the wrists, spreads the legs, bends the knees, raises the head, and initializes contacts with the handles, footrests, seat, belts and cockpit surface to the final postures depicted in Figure 4.34b. To allow riders with different heights on the motorcycle, an adjustable handlebar and adjustable footrests are considered, which are available for motorcycles.

---

[9]MATD 50th percentile model, facet version 1.8, Siemens Industry Software and Services BV.

[10]Hybrid III 50th percentile model, ellipsoid version 2.0, Siemens Industry Software and Services BV.

[11]Detailed Hybrid III 50th percentile model, version 190217_BETA, Livermore Software Technology Corporation (LSTC).

(a) pre-positioned initial posture | (b) final seating postures with contact initialization
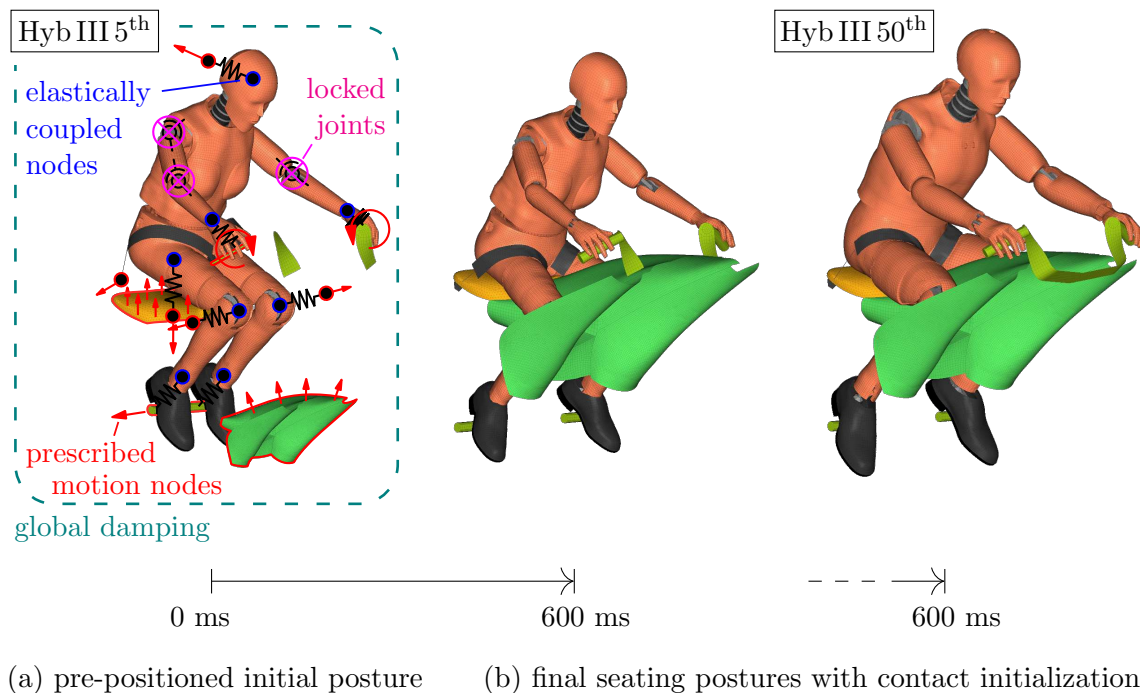
Figure 4.34: Seating and contact initialization procedure for FE ATDs.

4.4.3 Human Body Models

ATDs are designed and validated for specific – mostly only uni-axial – loading conditions, and are therefore not omnidirectional applicable. Their design targets rigidity for repeated tests which in turn sacrifices some degrees of freedom and therefore anatomical detail and associated biofidelic response. As listed above, there are ongoing efforts to enhance the biofidelity of ATDs for PTW applicability, but the choice of ATD here involves some compromise. Given the challenges of physical surrogates in this application, HBMs can compensate for these shortcomings and provide further insight. They model the human muscoskeletal system, the nervous system, and internal organs of the body as realistically as possible to capture the kinematics and injury mechanics human being. The geometry originates from whole-body MRI or CT scans of individual human subjects; the parameters for the materials and muscle activity from in-vivo and post-mortem animal and human subject tests. Ultimately, these models are designed for detailed injury assesment on bone and tissue level such as e.g., rib fracture risk based on element strain [FormanEtAl12] and brain damage based on element stress and strain [DeckWillinger08]. Facilitating morphing and scaling [HwangEtAl16, LarssonEtAl19], they aim to represent diverse humans.

There are many models available with an ever-increasing level of geometric detail, number of elements, and biofidelic features, see, e.g., [YangEtAl06]. In this work here, several passive HBMs are used that currently represent the state-of-the-art. Using passive HBMs means that currently muscle activity isn't considered in these high-load impacts. These models

are, the open-source academic female and male VIVA+, the open-acess THUMS, and the commercially available GHBMC, all in a mid-sized adult configuration, see Figure 4.35.

However, the very detailed and finely discretized modeling of HBMs also means that computation times can be many times higher than for models of ATDs, and they are more complex to position initially in or, as in this case, onto a vehicle. Compared to ATDs, which can be positioned by adjusting joint angles and applying nodal displacements based on these kinematic constraints, HBMs have complex joints and motion patterns with non-idealized degrees of freedom surrounded by deformable tissue. Positioning them can therefore be a laborious and time-consuming task. There are some efforts in the literature that describe the use of FE HBMs to represent PTW riders. In [KoflerEtAl20], a helmeted 50th percentile male THUMS is used to simulate the influence of the helmet design in primary and ground impacts of moped to car crashes. In [HuangEtAl18], a 50th percentile THUMS represents riders of an electric scooter and a bicycle in collisions with cars. In [CarmaiKoetniyomHossian19, CarmaiKoetniyomHossian20] the impact behavior of a 5th percentile THUMS as the rider of a small motorcycle and a six-year-old THUMS variant as a pillion passenger against a passenger car and a pickup truck is investigated. However, a systematic description of the rider position, a description of a positioning procedure, or a discussion of the resulting postures of the models are not presented in this work. Instead, the following procedure as part of [MaierEtAl22] is conceived.

♀	♂	♂	♂
50 years	50 years	26 years	39 years
162 cm	175 cm	176 cm	179 cm
62 kg	77 kg	76.8 kg	77.6 kg
866 parts	866 parts	1195 parts	1195 parts
739K nodes	739K nodes	1.9M nodes	1.9M nodes
490K elements	490K elements	1.36M elements	1.36M elements
(a) VIVA+ 50F[12]	(b) VIVA+ 50M[12]	(c) THUMS AM50[13]	(d) GHMBC M50[14]

Figure 4.35: Female and male LS-DYNA HBMs (partially blanked) in their default positions with human body metrics (top right) and model characteristics (bottom left).

---

[12]VIVA+ Human Body Models [SchubertEtAl21, JohnEtAl22], 50F and 50M seated versions 0.2.5 (retrieved from [OpenVT21]), VIRTUAL project.

[13]Total HUman Model for Safety (THUMS) [IwamotoNakahiraKimpara15], AM50 occupant version 4.1, Toyota Motor Corporation.

[14]GHBMC model [GayzikEtAl12], M50-O occupant version 5.0, Global Human Body Model Consortium (GHBMC).

Positioning of Human Body Models

The developed simulation based positioning workflow, illustrated in Figure 4.36, consists of three steps:

  (a) Posture pre-positioning: From its default position, each HBM is pre-positioned using the positioning and personalization capabilities of the pre-processing tool Piper[15]. It is an academically open-source software tool based on HBM-specific metadata. For positioning, it provides functions for interactive manipulation of FE structures within the software through lightweight and, therefore, fast physics models and the definition of simulations for transient manipulation. Here, Piper is used to defining a transient simulation by prescribing the motion of the skeletal structure via elastic elements. The target position determines the joint angles of the lower and upper extremity joints with fixed landmarks for the spine and head.

  (b) Seating and contact initialization: The rider-to-motorcycle contact surfaces, the seat, the handles, the footrests, and the other cockpit surfaces are initially scaled and distorted. Then, these geometries are morphed into the actual geometry of the motorcycle. This rotates the wrists and pushes the motorcycle against the human body. Prescribed spring elements are also used to push the head back, press the pelvis into the seat, and hold the feet to the footrests. Gravity is not applied yet.

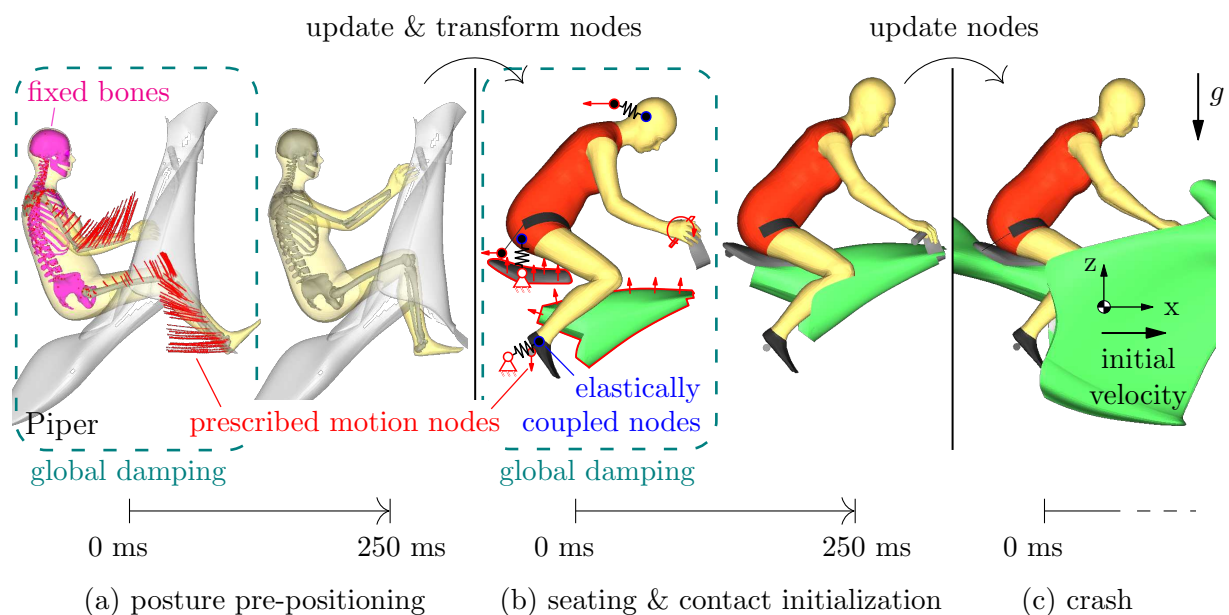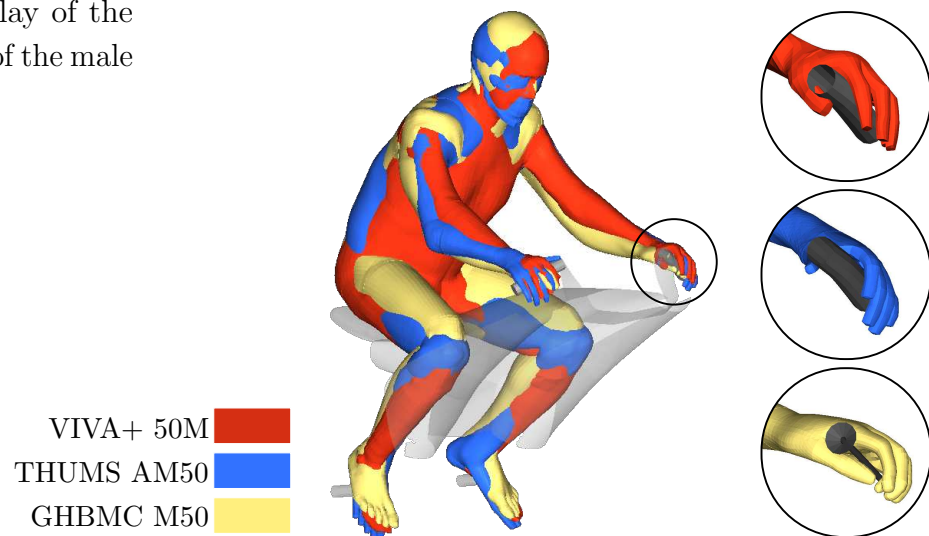 (c) Crash: The actual crash simulation starts immediately before the impact from an initial velocity.

Figure 4.36: Multi-step positioning procedure for HBMs.

_____

[15]PIPER software framework, version 1.0.1 [PIPER21], PIPER project, http://www.piper-project.org.

Figure 4.37: Overlay of the resulting postures of the male HBMs.

VIVA+ 50M

THUMS AM50

GHBMC M50

For quick positioning and achieving short simulation durations, global damping of the model is applied during steps (a) and (b), where a mass weighted nodal damping force f applies to each node with $f = -D(t)mv$. D is initially set to 0.02 to prevent evident oscillations in the soft tissue and then ramps down to 0 towards the very end of the simulation to allow for proper settling within the simulation runtime. Steps (a), (b), and (c) are separate simulations in between which the nodal coordinates of the FE mesh are exchanged via custom MATLAB procedures. All other information from the respective previous simulations is not considered in the crash simulation. This means that stresses and strains in the elements or geometry-dependent model parameters at the end of the simulation are not considered as initial conditions in the respective subsequent simulation steps. The effects of this restriction on the accident response have not yet been investigated.

The colored overlay in Figure 4.37 reveals some anthropometric differences of the male HBMs, although the resulting postures are similar overall. The elbow position and angles visibly differ significantly from each other. Another difference between the models is the result of the modeling of the hands. The VIVA+ and GHBMC hands are modeled as rigid parts, which means that the fingers pierce the handles (as with the VIVA+ hand), or thinner handles must be specially formed (as with the GHBMC hand). Only the THUMS allows for a realistic gripping of the handles with deformable modeling of the hands. For an overlay of the skeletal structure, see Figure 5.21.

4.5   Simulation Workflow and Model Overview

The chapter above summarizes the modeling of the many subcomponents involved. An overview of the overall modeling to conclude this extensive chapter may be in order.

On a simulation level, Figure 4.38 outlines the principle workflow, which is mainly controlled by MATLAB commands. These manipulate and manage the Maydmo and LS-DYNA input files (.xml/.key-files) and read and evaluate the respective simulation output data files (.h5/.binout-files). For visualisation of the animation output files (.kn3/.d3plot) Altair HyperView is used. The schematic does not show the entire workflow but draws the software chain and attempts to illustrate the main components and highlights some additional links between the layers that have not yet been covered. It explains that design iterations route through the stages I to III, where most of the design updates such as the design parameters are propagated automatically. Custom .xml-to-.key-file converters, e.g., for the airbag discretization, maintain an identical design in all the simulation stages automatically and fast.

On the model level, Table 4.3 gives an overview of the developed model variants. It shows the configurations in the three modeling stages with the required computing time. The last column shows the respective investigation, which also represents the structure of Chapter 5. Stage I features relatively few degrees of freedom and associated low numerical costs while capturing the essential physics of the impact. Stage II allows for an efficient way to use state-of-the-art FE HBMs as rider surrogates while reducing numerical costs by using prescribed vehicle motions from stage I. Stage III approximates the vehicle response with a high degree of detail to investigate the deformation characteristics of the motorcycle itself and the structural interaction with opposing vehicles. It is used to predict the performance of the finalized design accurately. The following chapter not only shows the performance results of the novel safety concept but also illustrates the merits of a simulation strategy that provides such diverse modeling variants.
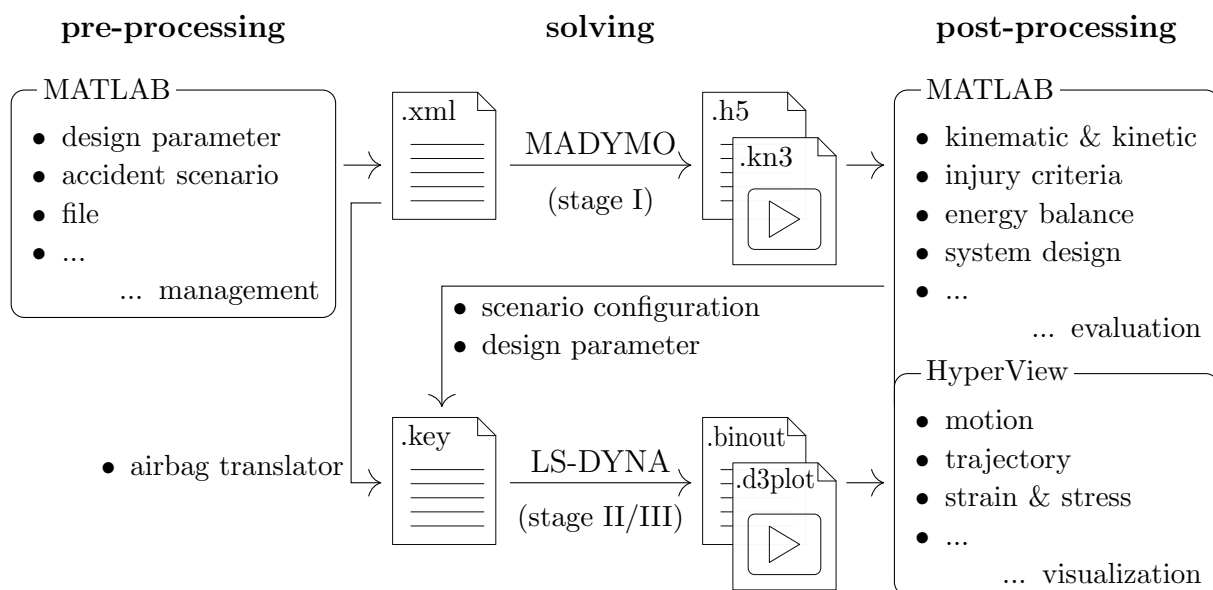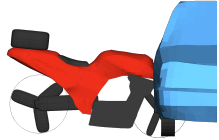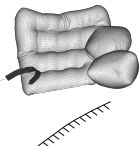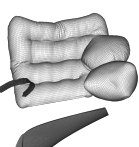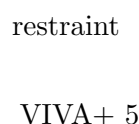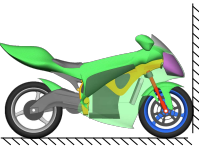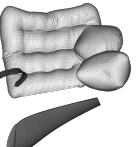
Figure 4.38: Principal simulation workflow.

Table 4.3: Model configuration overview with Chapter 5 outline.

model configurations with simulation run times*	investigation

MADYMO

stage I: combined MB/FE

conventional vehicle   Hyb III 50th

vehicle interaction   restraint   Hyb III 50th $\sim$36 min[a]

→ impact behavior (Sec. 5.1.1)

→ biomechanical loading (Sec. 5.1.2)

→ frontal impact kinematics and chronology (Sec. 5.1.3)

LS-DYNA

stage II: coupled FE/MB

restraint   Hyb III 5th & 50th $\sim$10 h[b]

   $\sim$23 h[b]

VIVA+ 50F/M, GHBMC, THUMBS

→ rider energy balance (Sec. 5.2.1)

→ ATD vs. HBM impact response (Sec. 5.2.2)

→ impact response of HBM variants (Sec. 5.2.3)

LS-DYNA

stage III: full FE

rigid wall interaction

vehicle interaction   restraint   Hyb III 50th $\sim$59 h[b]

→ motorcycle frontal deformation (Sec. 5.3.1)

→ structural interaction & vehicle intrusion (Sec. 5.3.2)

→ impact behavior & loading (Sec. 5.3.3)

*for a problem time of 300 ms with an AMD Ryzen 9 5950X 16-Core CPU@3.4GHz for the Hyb III 50th ATD and the VIVA+50M HBM

[a]16 CPUs/SMP (shared memory processing)

[b]16 CPUs/MPP (massively parallel processing)

Chapter 5

Simulation Results

After summarizing the fundamental aspects and current status of PTW rider safety and explaining the modeling and simulation strategy, the results are presented. This chapter determines the kinematic, kinetic, and energy-based relationships for a meaningful description of the functional principles of the safety concept. It exploits the individual advantages of the different simulation models and aims for a quantified performance evaluation for recommended representative accident scenarios, also in comparison to a conventional motorcycle accident.

The chapter is sectioned into the stages I-III, outlined in Figure 4.3. The investigations are limited to the primary impact phase, the immediate period after the first contact between the opposing vehicle (here 300 ms). The study summarises published assessment methods from the author's work from [MaierEtAl20] (stage I), [MaierEtAl21a] (stage II), [MaierFehr23a] (stage III), and from a workflow overview in [MaierFehr23b]. The simulation results are a continuous iteration of the developed workflow with coinciding system parameters. The stage III results for the Hybrid III 50th percentile have already been published in [MaierFehr23a].

5.1   Stage I – Combined Multibody and Finite Element Simulations

The standard ISO 13232 provides diverse impact scenarios (Section 2.2.2). In the following, the impact behavior of the motorcycle with rider restraint and a rider surrogate, a 50th percentile Hybrid III (average male) ATD, are shown in detail for five of the seven impact configurations. The two scenarios not shown are ⑤, which is redundant to ④, and ⑥ – a grazing collision – which has no significant loading in the primary accident phase. The corresponding quantitative overview of a comprehensive set of injury criteria relative to the respective biomechanical limits (see Table 2.5) for all configurations is given in Figure 5.1. For comparison with a conventional motorcycle accident, the results of scenario ⑦ are compared with the full-scale crash test SH01.01 of Section 4.2.1.

5.1.1 Impact Behavior in Representative Accident Scenarios

Impact Scenario ⑦

The motorcycle impacts at $13.4\,\mathrm{m/s}$ ($\approx 48\,\mathrm{km/h}$) at a right angle into the side of the stationary car at its center line, see Figure 5.1. The voluminous cockpit and overhanging nose result in a high impact point. It prevents the motorcycle from pitching around its transverse axis and rolling over, as observed in the full-scale crash tests of conventional motorcycles in Figure 4.6 vs. Figure 4.7. Pretensioning the belts around the thighs results in early force transmission. Restrained by the belts, the pelvis excursion (displacement in the forward direction) is continuously decelerated, resulting in an upper body rotation. This motion is decelerated by the front airbag, which is fully deployed to this point. It supports the head and the uppermost part of the chest. The rebound of the head is small.

The highest body loads are safety-concept-related the head, thorax, and pelvis accelerations, neck tensile forces, and forward neck moments, see Table 5.1. The biomechanical loads are mainly dependent on the implemented belt load limit, which is a trade-off between tolerable body loads and a feasible forward body excursion. More excursion enhances the risk of the rider's head hitting the car, and the elongated belts reduce the potential to restrain the rider in a subsequent secondary impact phase. The highest head acceleration loads (and hence also neck tensile forces) are due to the belt restraint at about $70\,\mathrm{ms}$, not the later airbag impact from about 80 to $130\,\mathrm{ms}$.

Figure 5.1: Accident response in the combined MB/FE simulations with a Hybrid III 50th ATD for scenario ⑦ in the primary impact phase. Trajectories for the head and pelvis (black) and the head linear acceleration (red) depict the resulting acceleration magnitude and direction. Note: The right airbags are not displayed.

Impact Scenario ③

The motorcycle impacts at 48 km/h at a right angle into the side of the moving car traveling at 6.7 m/s ($\approx$ 24 km/h), see Figure 5.2. The safety concept acts similarly to ⑦. The rider's forward motion is continuously decelerated, resulting in a rotating upper body motion, now decelerated by the smaller mirror airbag, preventing the head from hitting the car. In the current mode, the belt pay-out during belt force limitation is not reversible. It leads, as seen at 200 ms, to the restraint being very loose after the first impact.

The highest body loads are, again, the head, thorax, and pelvis accelerations and neck tensile forces and forward moments, as well as neck shear forces. Additionally, the BrIC, rating head rotation, is near the recommended biomechanical limit.

Impact Scenario ④

The motorcycle impacts the car traveling at 24 km/h at its center line at a speed of 48 km/h and a relative angle of 45 ° (Figure 5.3). The side airbag quickly deploys in between the rider and the car, acting as a reaction surface. It prevents the rider's head and torso from impacting the car side. For such scenarios, where the relative angle between the opposing vehicles is comparatively small, the motorcycle retains a large portion of the initial impact speed. This retained velocity extends the overall length of the accident, with the motorcycle eventually falling over to one side. Therefore, the side airbag must protect
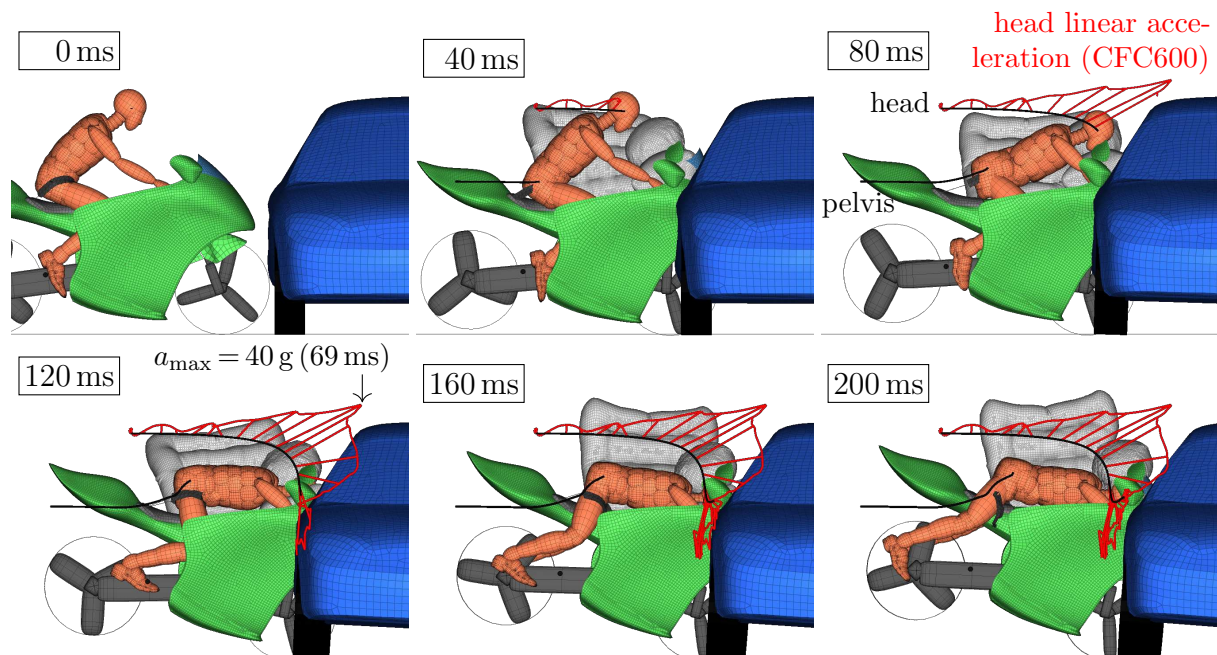

Figure 5.2: Accident trajectories in the combined MB/FE simulations with a Hybrid III 50th ATD for scenario ③ in the primary impact phase.

Figure 5.3: Accident trajectories in the combined MB/FE simulations with a Hybrid III 50$^{\text{th}}$ ATD for scenario ④ in the primary impact phase.

the rider in the following, presumably long, secondary accident phase. It motivates the airbag design without exhaust holes to keep it inflated for a potentially long accident.

The highest loads result from the impact into the relatively hard side airbag since it has no exhaust hole that would lead to a softer contact. The substantial loads are head, pelvis, and neck loading. The very high axial femoral forces are compression forces on the left leg when impacting the motorcycle body, as the intended leg protectors are not modeled in this stage.

Impact Scenario ①

The stationary motorcycle is hit laterally by the car traveling at $9.8\,\text{m/s}$ ($\approx 35\,\text{km/h}$) at a relative angle of $90°$ (Figure 5.4). The side airbag quickly deploys to the side of the rider, is pushed down by the rider's upper body lateral rotational motion, and is supported by the car's bonnet protecting the rider by cushioning the impact. As in ④, the belts support the pelvis and ensure that the rider stays within reach of the side airbag. The side fairing of the motorcycle body, aimed to protect them specifically in these accident scenarios, encloses the rider's lower extremities.

The highest body loads are the head translational (HIC) and rotational (BrIC) loads and neck tensile forces. The highest head acceleration occurs at about $110\,\text{ms}$ after the accident contact and results from the airbag deceleration. In this MB approach, the undeformed rigid car geometry pierces through the motorcycle geometry, resulting in high femur forces.

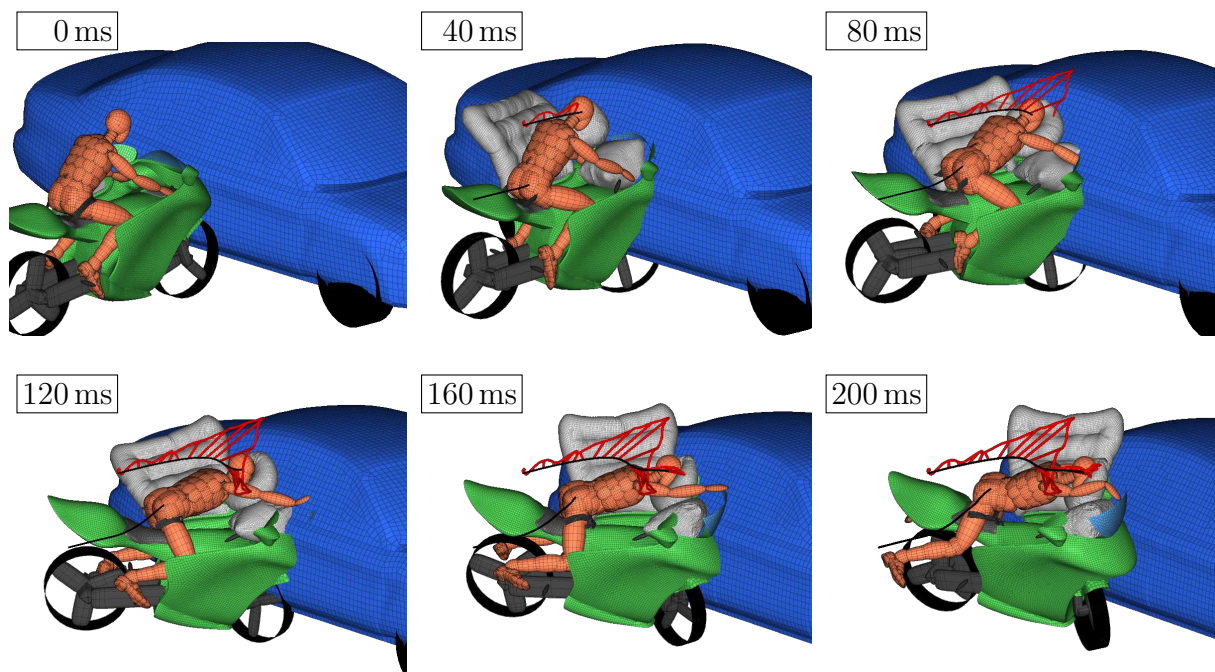$a_{\text{max}} = 37\,\text{g}\,(111\,\text{ms})$

Figure 5.4: Accident trajectories in the combined MB/FE simulations with a Hybrid III 50$^{\text{th}}$ ATD for scenario ① in the primary impact phase.

Impact Scenario ②

The motorcycle impacts at 48 km/h into the car front traveling at 24 km/h at a relative angle of 135° (Figure 5.4). Just like in ① the motorcycle rolls around its longitudinal axis, and the side airbag absorbs the rotational motion of the rider's upper body using the bonnet of the car as a reaction structure. The belts establish a pivot point for a guided upper-body trajectory, limiting the head's displacement within reach of the airbag. Additionally to ①, the motorcycle also yaws around its vertical axis, resulting in a multiaxial motion of the motorcycle with a partial counter-rotational motion of the rider. The multiaxial trajectory, the payed-out belt length due to the heavy first impact, and a potentially long secondary accident phase (the shallow impact angle results in a high retained motorcycle velocity) will cause significant challenges in guiding the motion of the rider in the secondary accident phase. At 200 ms, the ATD already slips out of the elongated belts.

Similar to ③, the highest criteria are the HIC, BrIC, and $M_{y,\text{fwd,max}}$-criterium as well as the thorax and resultant pelvis accelerations.

Impact Scenarios ⑤ and ⑥

Scenario ⑤ corresponds to ④, except that the motorcycle approaches the car at a relative angle of 135° opposing its traveling direction. In the MB/FE simulation, it leads to a similar trajectory as in ④ with similar ATD loads. Due to the shallow impact angle, a high proportion of the impact velocity is retained. In ⑥, the motorcycle grazes a stationary car at 48 km/h. It does not result in any significant ATD loading in the primary impact.
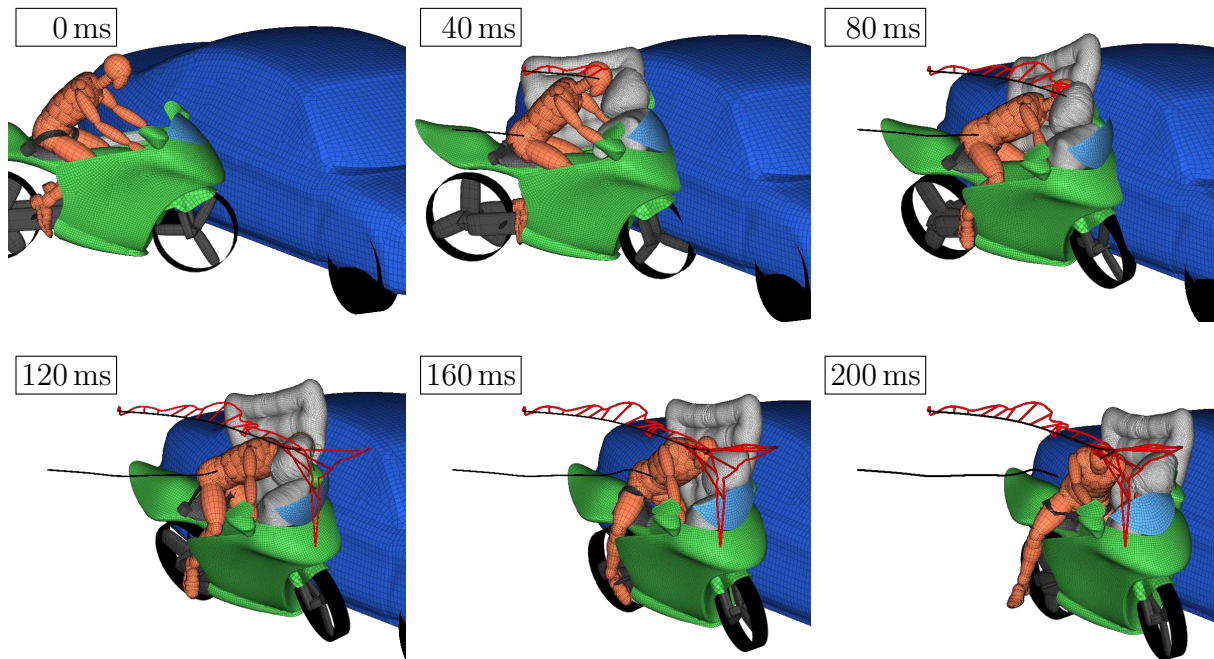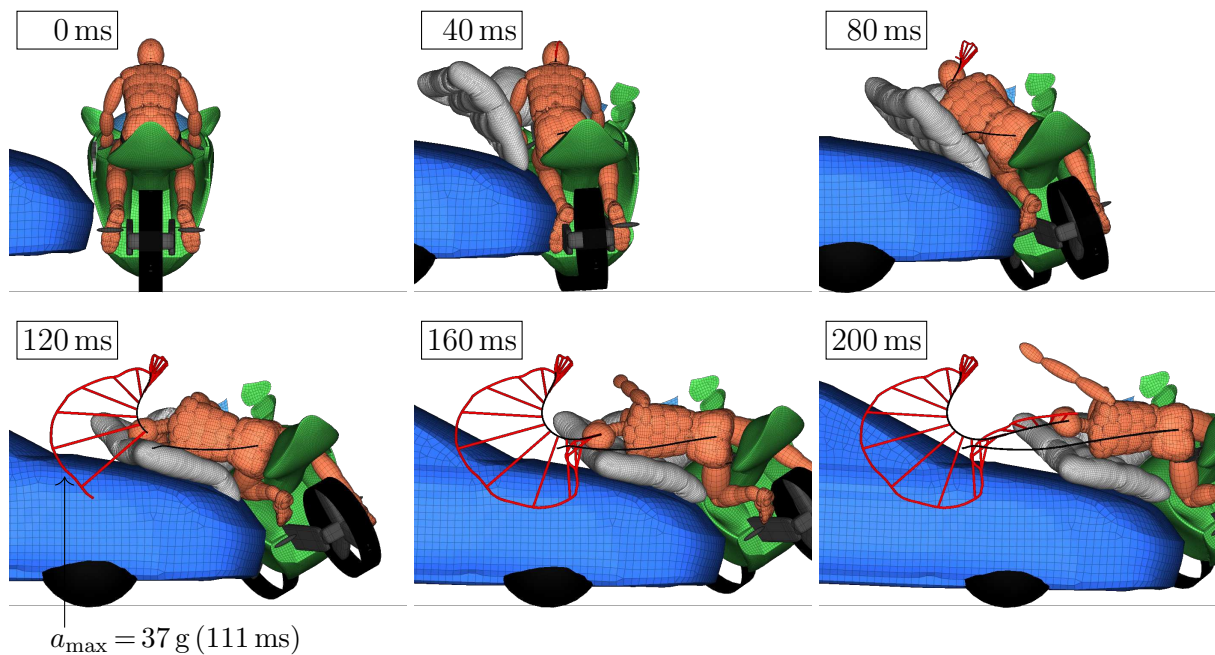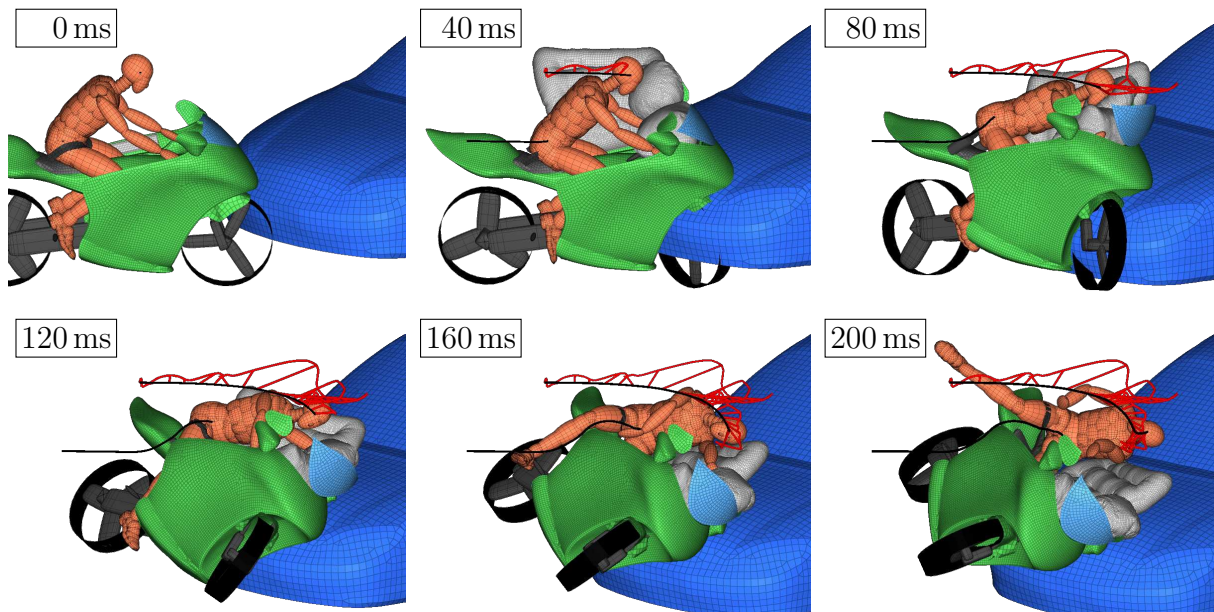
Figure 5.5: Accident trajectories in the combined MB/FE simulations with a Hybrid III 50th ATD for scenario ② in the primary impact phase.

The ISO 13232 scenario set ① – ⑦ does not include rear contact collisions at the motorcycle. As the behavior in ② indicates, the occupant may slip out of the belt when the load is applied in a rearward direction.

5.1.2   Biomechanical Impact Loading

The biomechanical limits of the chosen set of injury criteria are met for the primary impact phase except for femoral ($|F_z|_{max}$) and tibial (TI) loading. These high loadings are partially related to this MB approach because the leg protectors are not modeled and the undeformed rigid car geometry pierces through the motorcycle geometry, hitting the lower extremities. This will be further deducted in Section 5.3 with the full FE approach. The BrIC is right on its recommended limit in the lateral impact scenarios ① and ②. A value of 1 corresponds to a 50 % probability of AIS4+ brain injuries [SchmittEtAl19]. Similar to the GAMBIT, which has only low values here, it rates head rotations. While according to [SchmittEtAl19] the HIC and a_{3ms} are often used, the GAMBIT still lacks validation and is rarely used, and experience using the BrIC is still limited. A recent comparison of brain injury criteria [SahooEtAl20] found that BrIC mostly overpredicted the reconstructed and simulated real-world brain trauma injury cases.

Otherwise, the loading on the body regions is mostly low since, for all the examined accidents, a direct impact of the ATD on the opposing vehicle is avoided. Instead, the belt and airbag restraint results in a more evenly distributed loading over a more extended period. The highest loads are due to head, thorax, and pelvis accelerations as well as neck tensile forces, mainly dependent on the implemented belt load limit, a trade-off between tolerable resulting body loads, and feasible body displacements within reach of the airbags.

Table 5.1: Injury criteria normalized to their respective biomechanical limits for the primary impact phase up to 300 ms of the Hybrid III 50th ATD in the combined MB/FE simulations. The criteria are color-coded, indicating the severity of the body loads.

Hyb III 50th		scenario							limits
		①	②	③	④	⑤	⑥	⑦*	
head	a_{3ms}	0.46	0.49	0.51	0.49	0.34	0.1	0.48	80 g
	HIC(36)	0.24	0.12	0.24	0.27	0.12	0	0.17	1000
	GAMBIT	0.17	0.2	0.2	0.28	0.51	0.1	0.16	1
	BrIC(CSDM)	0.99	0.96	0.87	0.51	0.62	0.23	0.35	1
neck	$F_{z,tens,1ms}$	0.45	0.3	0.44	0.31	0.21	0.1	0.49	3.3 kN
	$F_{z,tens,45ms}$	0.45	0.33	0.18	0.21	0.39	0.03	0.64	1.1 kN
	$F_{z,compr,1ms}$	0.03	0.04	0.08	0.04	0.07	0.05	0.11	4 kN
	$F_{z,compr,45ms}$	0	0	0	0	0	0	0	1.1 kN
	$F_{xy,1ms}$	0.16	0.22	0.38	0.12	0.16	0.09	0.22	3.1 kN
	$F_{xy,45ms}$	0.16	0.31	0.53	0.19	0.19	0.2	0.37	1.1 kN
	$M_{y,fwd,max}$	0.17	0.28	0.13	0.18	0.17	0.14	0.18	190 Nm
	$M_{y,rwd,max}$	0.31	0.73	0.96	0.17	0.25	0.17	0.54	57 Nm
	Nij_{max}	0.34	0.43	0.3	0.31	0.26	0.19	0.41	1
thorax	a_{3ms}	0.31	0.55	0.51	0.31	0.25	0.12	0.56	60 g
	ThCC	0.04	0.14	0.17	0.11	0.12	0.05	0.16	50 mm
	VC_{max}	0	0.01	0.02	0.01	0.02	0	0.02	1 m/s
pelvis	a_{3ms}	0.5	0.57	0.45	0.54	0.53	0.18	0.58	60 g
femur	$|F_z|_{max}$	0.98	1.85	0.56	1.3	1.89	0.05	0.59	9.07 kN
tibia	TI_{max}	3.31	4.05	3.2	4.33	4.95	0.26	0.92	1.3

*see Appendix A.1 for exemplary determination of injury criteria for scenario ⑦

Scenario ① can be compared to a pedestrian frontal car impact where the pedestrian head impacts the bonnet. Examinations in standardised tests often lead to high head impact loads [AvalleBelingardiScattina13]. The best rating of the Euro NCAP test protocotol to rate head impact [EuroNCAP21] for an adult headform at a head impact speed of 40 km/h is a HIC(15)< 650. For an approximate comparison, in scenario ① the relative head impact speed is about 38 km/h and the resulting HIC(15) well below at 116.

Injury Risks

Injury risk curves correlate the biomechanical tolerance of the population to the associated criterion value. Here, the head and neck are among the most loaded body regions. Available

injury risk curves and their evaluation for the HIC(36) in Figure 5.6 and for the Nij_{max} in Figure 5.7 show the risks for all the simulated scenarios. Based on the injury risk curves for HIC(36) [NHTSA95], the risks of AIS3+ injuries are not higher than 4.3 %. According to the injury risk curves for Nij_{max} [EppingerEtAl99] the risks for AIS3+ and for AIS4+ are for all the scenarios below 10.2 %.
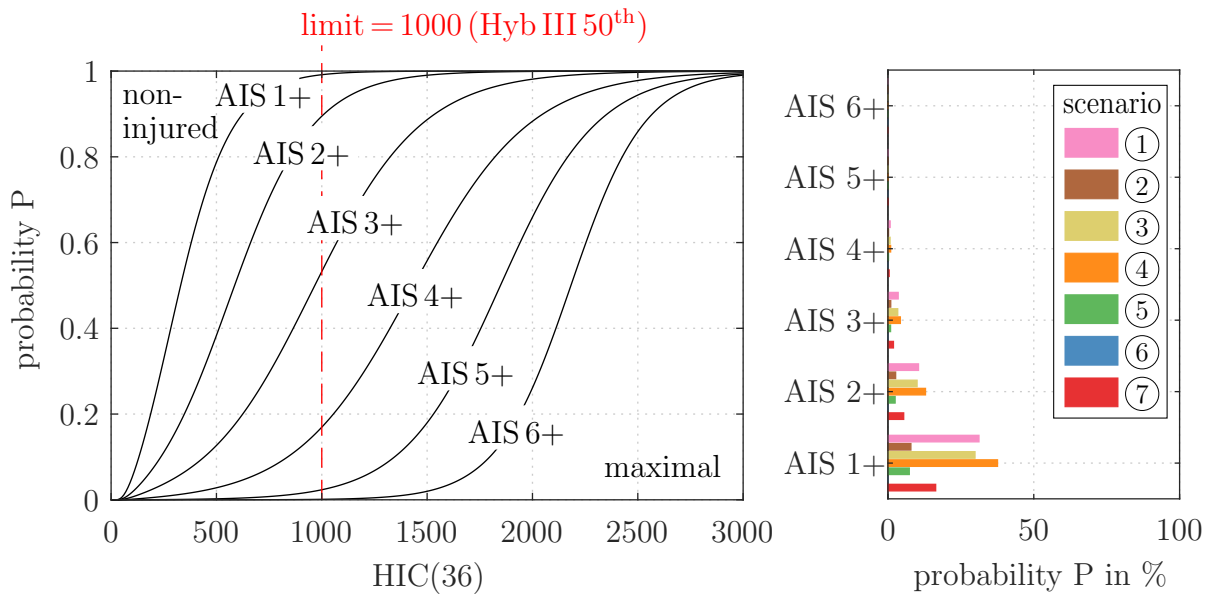
Figure 5.6: AIS injury risk curves for the head injury criterion from [NHTSA95] and the resulting AIS probabilities for scenarios ① to ⑦ from Tab. 5.1.
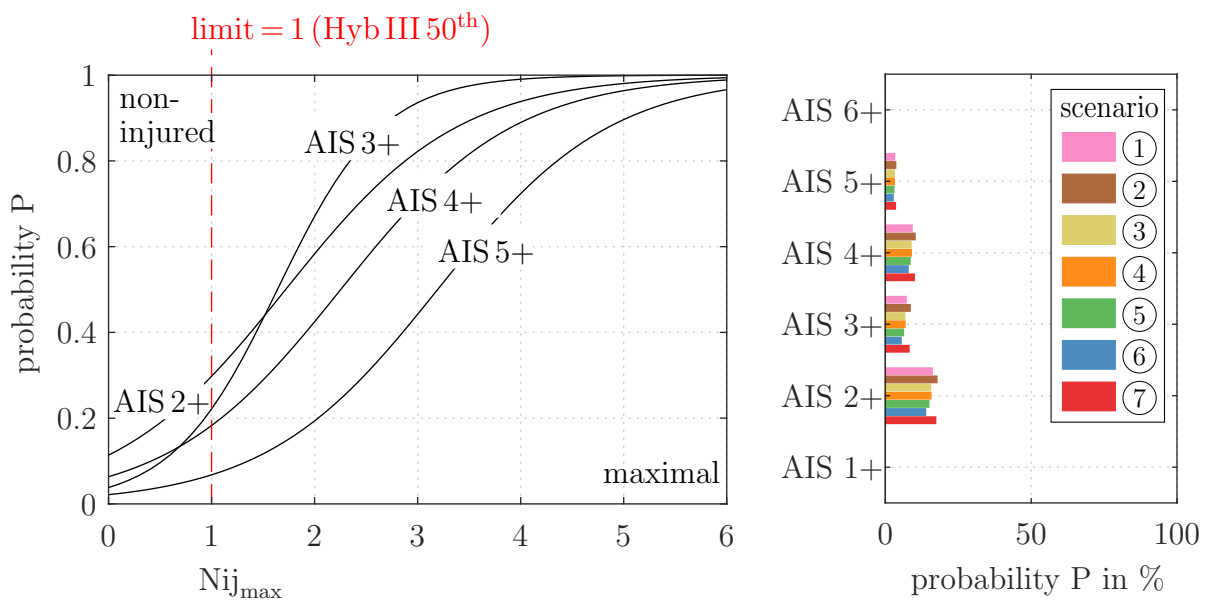
Figure 5.7: AIS injury risk curves for the neck injury criterion from [EppingerEtAl99] and the resulting AIS probabilities for scenarios ① to ⑦ from Tab. 5.1.

5.1.3   Frontal Impact Kinematics and Chronology

According to the evaluation of in-depth accident data in Section 2.2.1, an impact at the motorcycle front is a very frequent accident type. In the following, the results of the novel safety concept in the frontal impact scenario ⑦ are compared to the full-scale crash test SH01.01 [BergEtAl04] with a conventional motorcycle and a helmeted ATD, shown in Figure 4.6.

Conventional Motorcycle

In the conventional accident, the non-restrained rider's trajectory is not controlled, and short-duration impacts decelerate the rider rapidly, see Figure 5.8. The motorcycle decelerates continuously, resulting in a forward rotation, i.e., pitching about the transverse axis. The pelvis hits the motorcycle tank, and the helmeted head impacts the roof rail of the car. According to the collision type classification in Figure 2.7, this collision corresponds to a typical direct impact with a high energy transfer. An abstraction of the vehicle and main body part velocities to an accident chronology summarises the fundamental accident history; see Figure 5.9. Long dead times for the pelvis, torso, and head, followed by short and violent impacts, characterize the accident behavior.
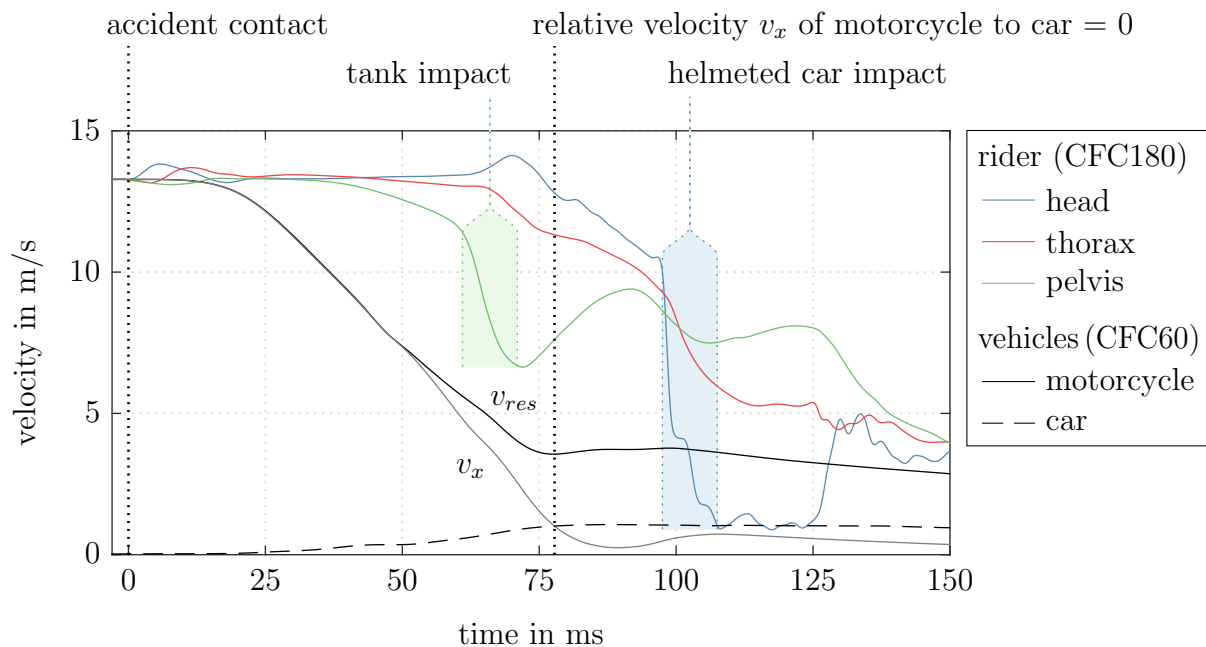
Figure 5.8: Velocities of the conventional motorcycle and the motorcyclist's main body parts in a frontal collision according to scenario ⑦ in the MB simulation with a helmeted Hybrid III 50$^{\text{th}}$ ATD, shown in Figure 4.6.
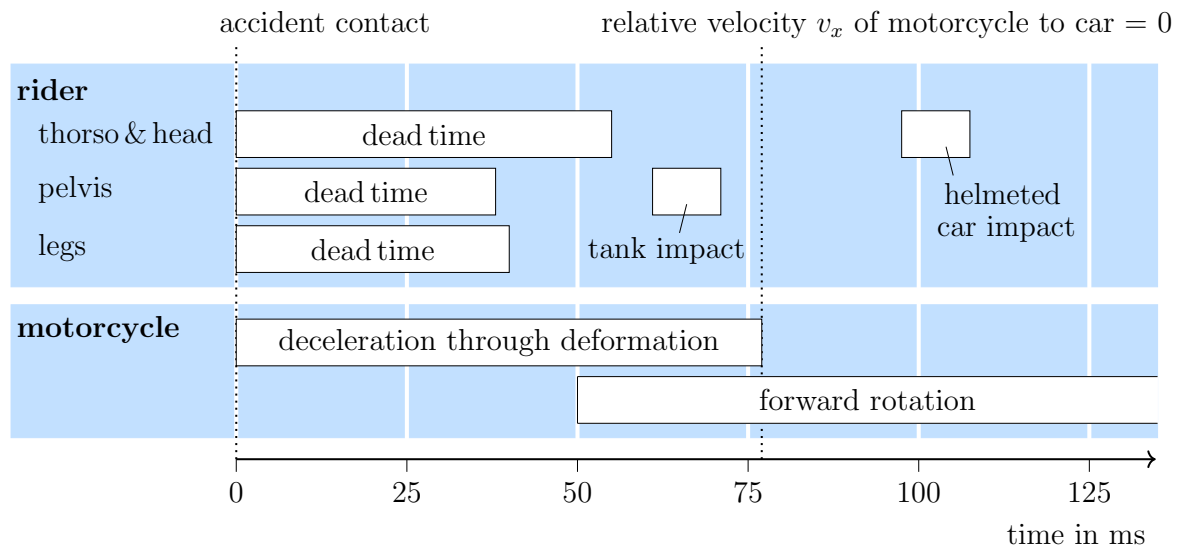
Figure 5.9: Schematic chronology of the conventional motorcycle and rider in Figure 5.8.

Motorcycle with Restraint Safety Concept

In comparison, the restrained rider's trajectory on the motorcycle with the novel restraint safety concept is guided and controlled. The rider is continuously decelerated over a more extended time period. Figures 5.10 and 5.11 illustrate the benefits of the restrained safety concept. The crash structure of the motorcycle reacts much stiffer – a forward rotation does not occur. The belts interact early, reducing the dead times of the rider's main body parts and leading to a uniform deceleration by restraining the pelvis. After 83 ms, the front airbag decelerates the upper body rotation. Overall the main body parts are decelerated more continuously over an increased period, compared to the short-term impacts of the conventional motorcycle. The detailed time history of the thigh belt force control and frontal airbag variables are already given in Figures 4.22 and 4.17. From these time histories, the subdivision of the seat belt and airbag functional regimes into several phases is derived.

The comparison of the ATD loads in the line-up against the conventional motorcycle impact in Figure 5.12 shows that overall the loads are reduced. It compares experimental sensor data of full-scale crash test SH01.01 with a non-restrained rider to simulation results from the combined MB/FE simulation of the restrained rider. Limits that exceed the recommended limits are obviated, and the values above 0.75 are reduced to just one. Safety-concept-related higher loads occur for neck axial tension criteria and thorax acceleration criterion; the pelvis acceleration criterion is not reduced. Criteria that cannot be calculated due to missing sensor data are marked as not applicable (n/a).
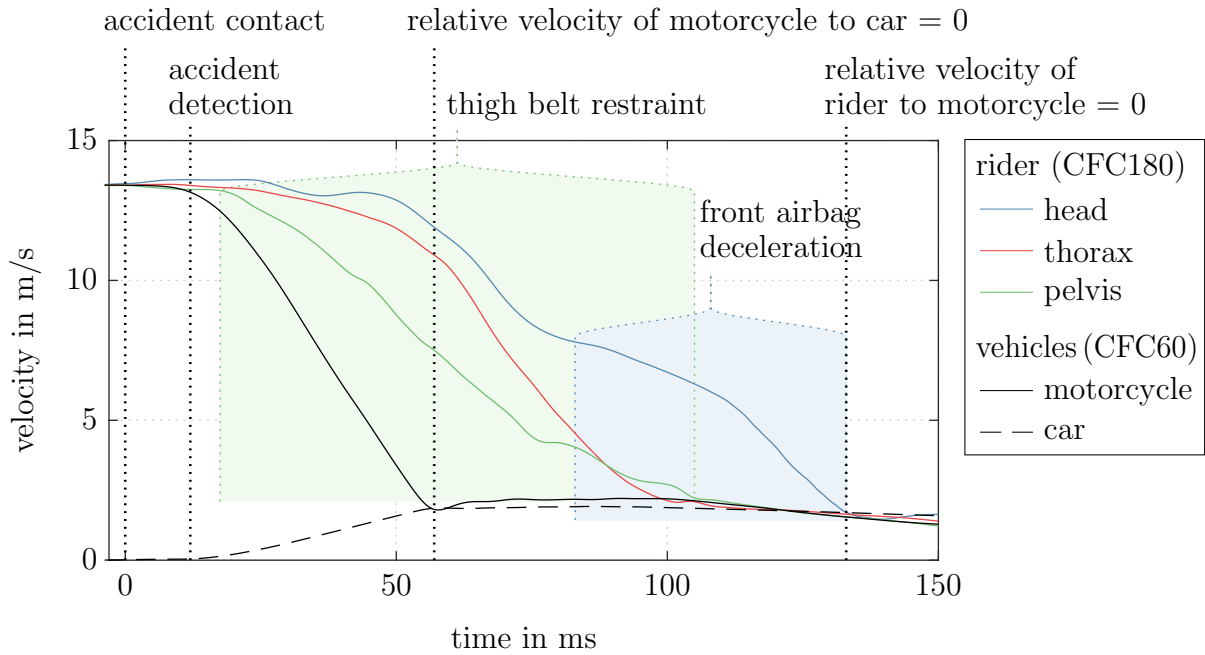
Figure 5.10: Velocities of the motorcycle with restraint safety systems and the motorcyclist's main body parts in a frontal collision according to scenario ⑦, shown in Figure 5.1.
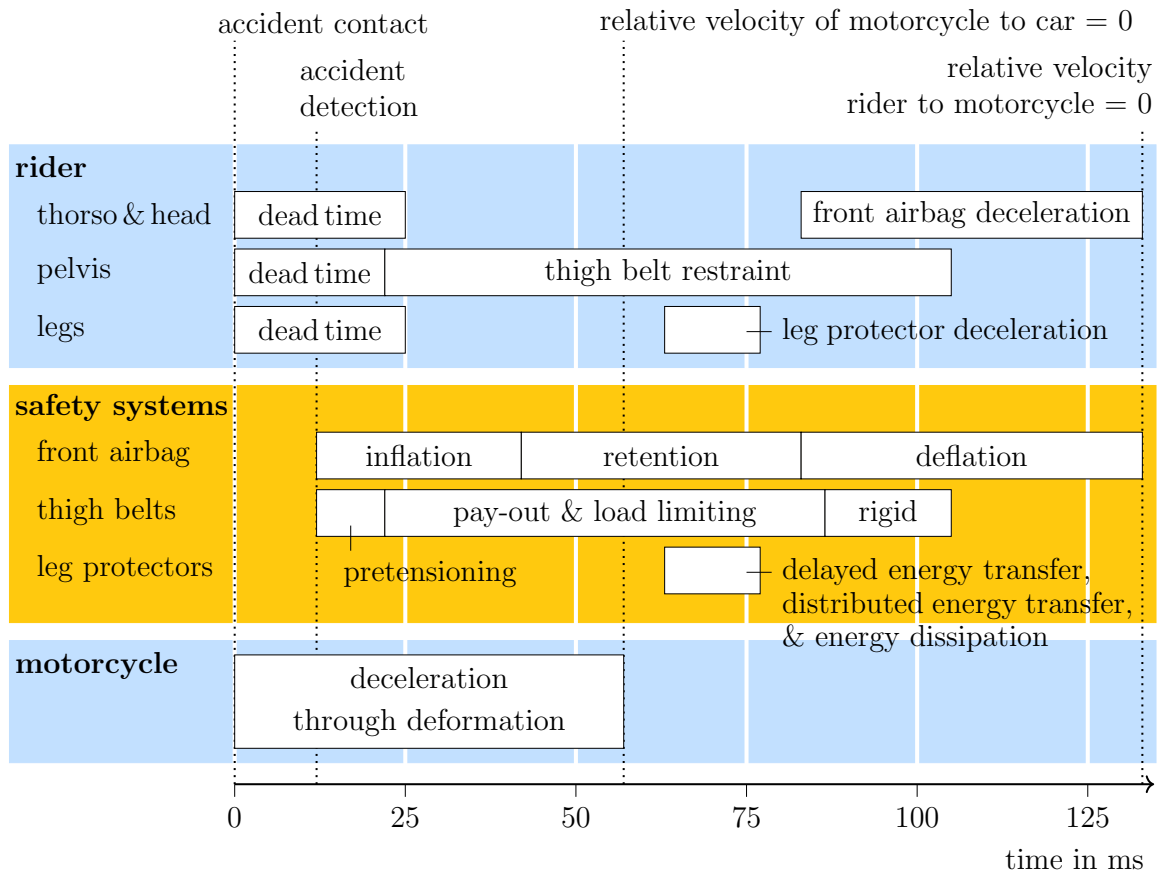
Figure 5.11: Schematic chronology of the motorcycle with restrained rider in Figure 5.10.

	head				neck									thorax			pelvis	femur	tibia
	$HIC(36)$	a_{3ms}	GAMBIT	BrIC(CSDM)	$F_{z,tens,1ms}$	$F_{z,tens,45ms}$	$F_{z,compr,1ms}$	$F_{z,compr,45ms}$	$F_{xy,1ms}$	$F_{xy,45ms}$	$M_{y,fwd,max}$	$M_{y,rwd,max}$	Nij_{max}	a_{3ms}	ThCC	VC	a_{3ms}	$|F_z|_{max}$	TI
SH 01.01	0.4	0.97	n/a	n/a	0.25	0.37	1.03	0.23	0.67	0.81	0.12	1.7	0.88	0.31	0.04	0	0.57	1.02	n/a
safe mot.	0.17	0.48	0.16	0.35	0.49	0.64	0.11	0	0.22	0.37	0.18	0.54	0.41	0.56	0.16	0.02	0.58	0.59	0.92
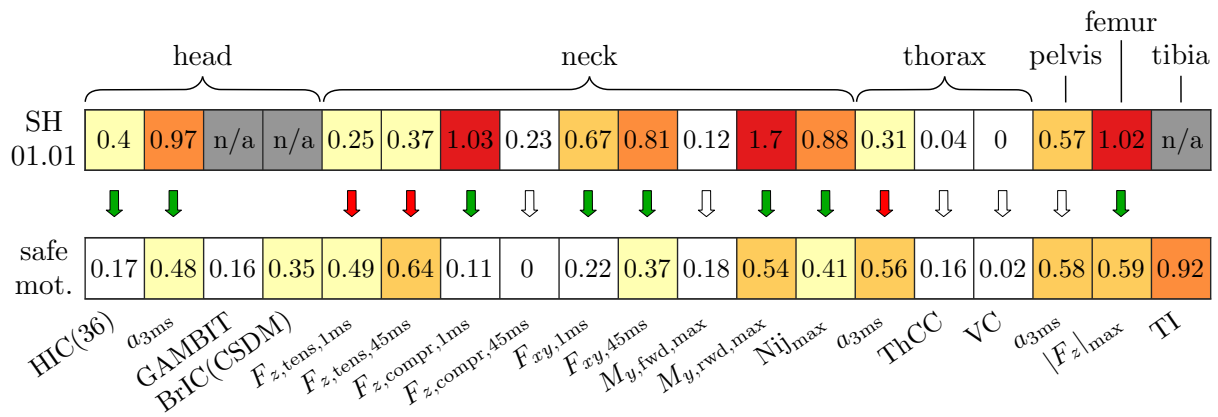
Figure 5.12: Injury criteria of the conventional motorcycle (top; experimental data of SH01.01) vs. the motorcycle with rider restraint (bottom; MB/FE simulation) in scenario ⑦. Change for the better or the worse is highlighted by green and red arrows.

5.2   Stage II – Coupled Finite Element and Multibody Simulations

To ensure the robustness of the study, the stage II approach investigates diverse rider surrogate models while focusing on the interaction behavior with the safety systems, using the accident trajectories from stage I as prescribed vehicle motions, see Figure 5.13. It isolates the vehicle trajectories from the response of different riders and reduces the computational effort. In the following, this is done for ATD variants and multiple HBM models, including sex variants. They are evaluated by energy-based balancing, motion analyses, and biomechanical injury criteria.

Hybrid III 5th   Hybrid III 50th

① 143-9.8/0

② 114-6.7/13.4

③ 413-6.7/13.4

④ 412-6.7/13.4

⑤ 414-6.7/13.4

⑥ 225-0/13.4

⑦ 413-0/13.4

motorcycle speed in m/s
car speed in m/s
geometry code (Figure 2.5)
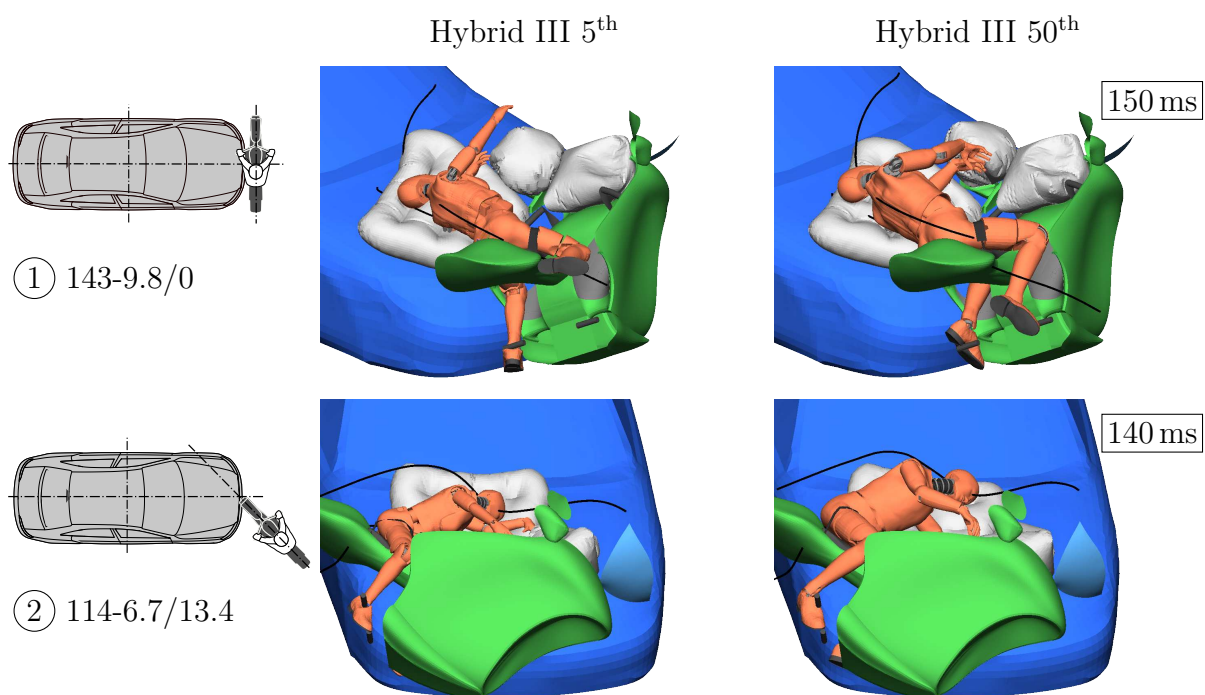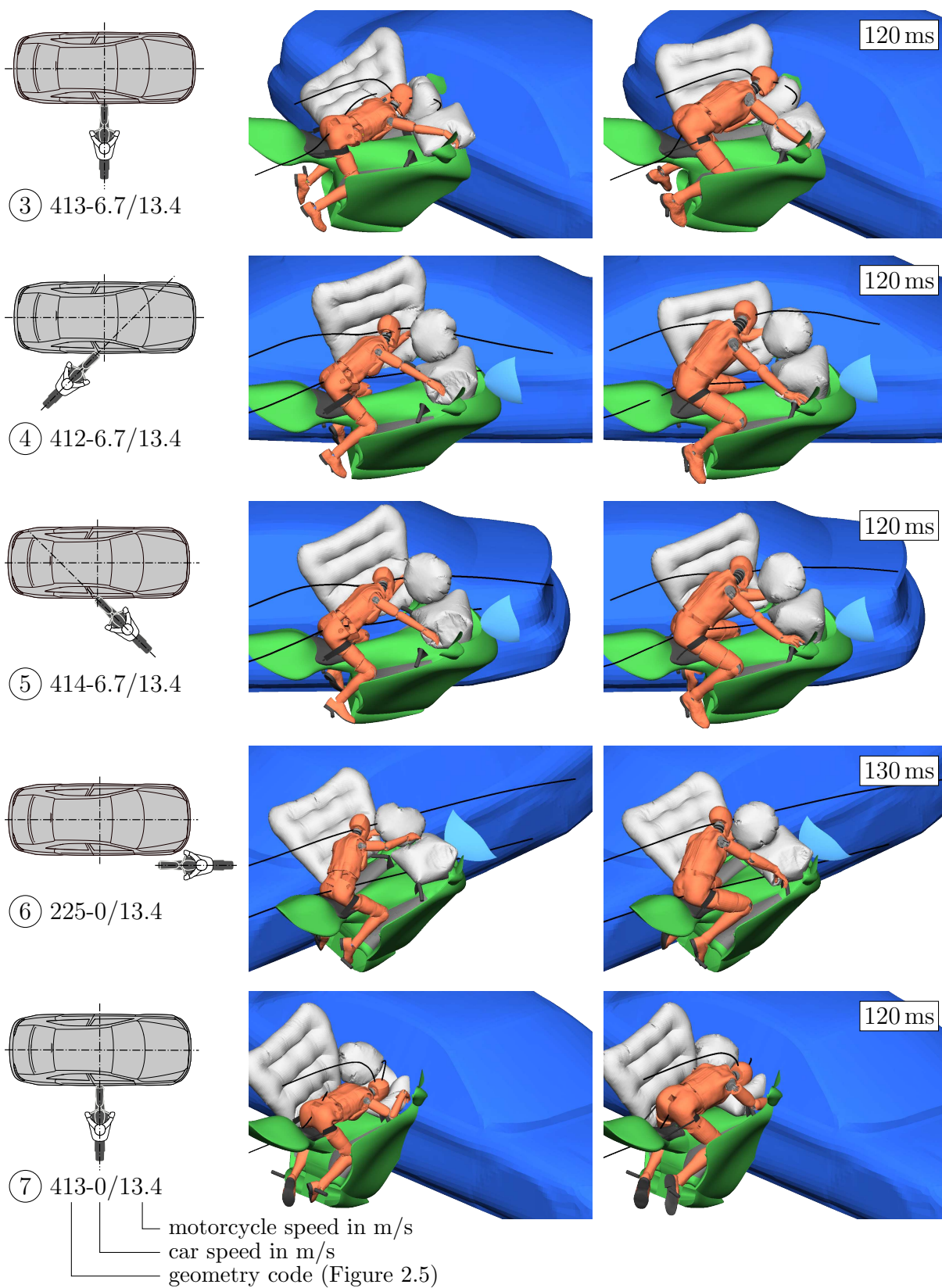
Figure 5.13: Impact response of the small female (left: Hybrid III 5th) and the average male (right: Hybrid III 50th) ATD in the coupled FE/MB simulations using vehicle trajectories from Section 5.1. Head and pelvis trajectories are in black.

5.2.1   Rider Energy Balance

To decelerate the motorcyclist, its kinetic energy must be dissipated through the application of forces. Anything that applies these forces, in this case, the airbags, the belts, the leg impact protectors, and the remaining cockpit surfaces, can be considered part of the restraint system. To evaluate the energy transfer of the individual restraint contribution, the energy balance of the rider is investigated. In LS-DYNA, the energy balance is

$$E_{\text{total,LS-DYNA}}(t) = E_{\text{kinetic}}(t) + E_{\text{internal}}(t) + E_{\text{potential}}(t)$$
$$+ E_{\text{contact}}(t) + E_{\text{sliding interface}}(t) + E_{\text{hourglass}}(t). \tag{5.1}$$

The kinetic, internal, and potential energies represent the current energy level of a system. The contact energy describes the energy transfer of the contacts with external contact partners outside of the system. The sliding interface energy is the stored energy of the internal contacts. The hourglass energy is a LS-DYNA-specific numerical quantity occurring in single integration point solids and should be comparably low.

Both the energy transfer time history and the final balance of energy levels at the end of the primary impact are meaningful. Exemplarily, the rider energy balances of the Hybrid III 50$^{\text{th}}$ ATD in scenarios ⑦ and ① are shown in Figures 5.14, where the energies are stacked on top of each other. In ⑦, the rider's initial velocity is represented as kinetic energy. In ①, the initial velocity, and therefore kinetic energy, is zero. The sign of the accumulated contact energies thus indicates whether energies are absorbed or emitted via the contacts of the rider. In ⑦, basically all the kinetic energy is transferred, either via external contact partners or dissipated as internal energy. In ①, the proportion of kinetic
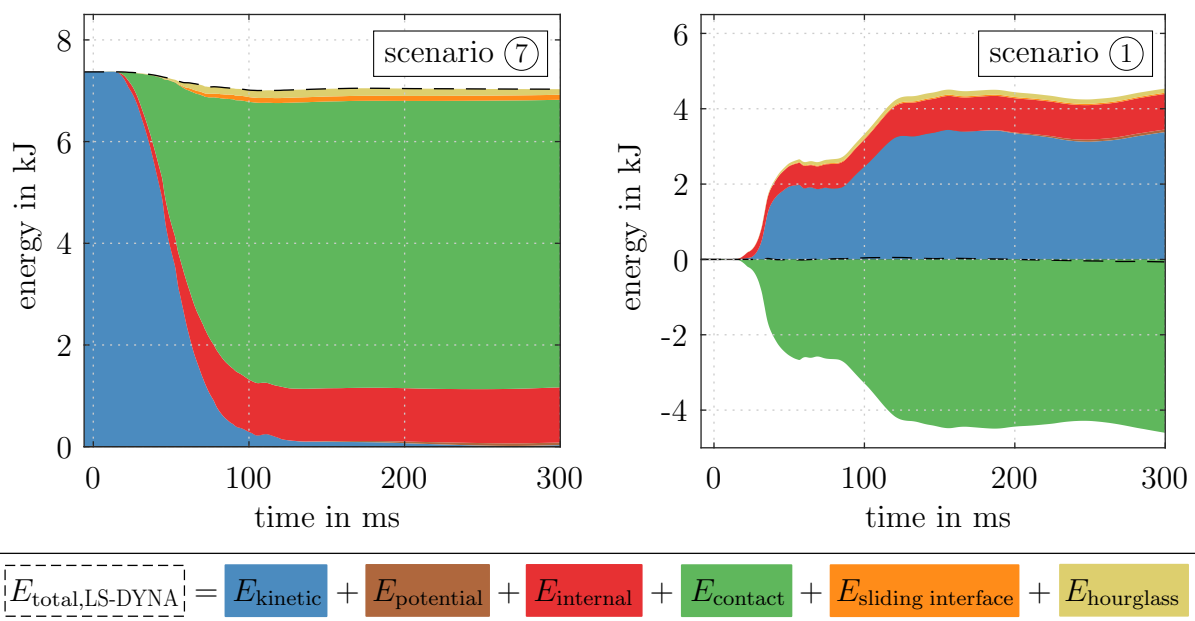
Figure 5.14: Rider energy balance of the Hybrid III 50$^{\text{th}}$ ATD in the coupled FE/MB simulations in scenario ⑦ (left) and scenario ① (right).

energy is still significant at the end of the primary impact at 300 ms. It indicates that this accident scenario will have a significant secondary accident phase.

The contact energies quantify the share of the individual system in restraining the rider. Figure 5.15 gives the remaining energy portions of the simulations' final state at 300 ms. The contact energy E_{contact} is split for its contributing contact partners. Examining the contributors to the contact energies for the Hybrid III 50th, the cumulative belt contact energy transfer in the final state has the largest share (52 - 83 %). Depending on the configuration, the airbags and leg protectors have varying shares. There are still some significant energy portions that got transferred into the seat and other motorcycle cockpit surfaces. In ⑦ and ③, the airbags decelerate the rider's significant upper-body rotation. In ④ and ⑤, with shallow impact angle and a more lateral motion of the rider, the airbags absorb less energy, but the leg protectors absorb more energy. The distribution in ⑥ shows that the final state of energy transfers through belt vs. cockpit surfaces and seat almost completely counteract each other, with very low resultant contact energy transfer. Confirming the robustness for rider variants, the results 50th and 5th percentile ATDs show qualitatively very similar results.
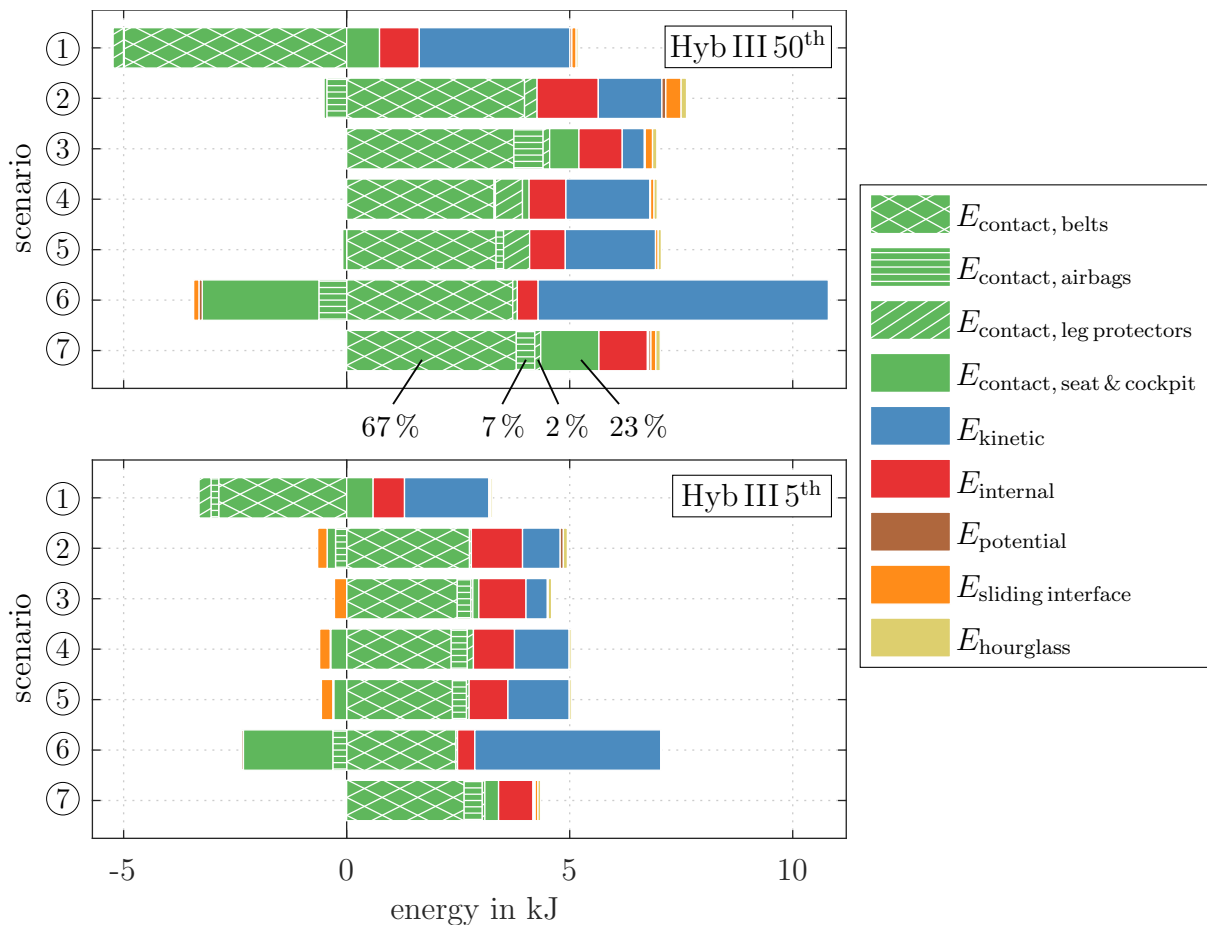
Figure 5.15: Rider energy balance in the simulations' final state at 300 ms of the Hybrid III 50th (top) and the 5th (bottom) ATD from Figure 5.13.

5.2.2 Anthropometric Test Devices vs. Human Body Models

ATDs are not applicable omnidirectional. Instead, they are specific for different loading conditions and postures and are most often designed to depict the occupants of automobiles. The current development of HBMs provide increasingly valuable tools for assessing accident response and injury mechanisms. Scenarios ⑦ and ① are particularly suitable for the isolated observation of frontal and lateral loading of the rider, with most of the movement occurring in the sagittal and the coronal plane, respectively. Figures 5.16 and 5.17 show
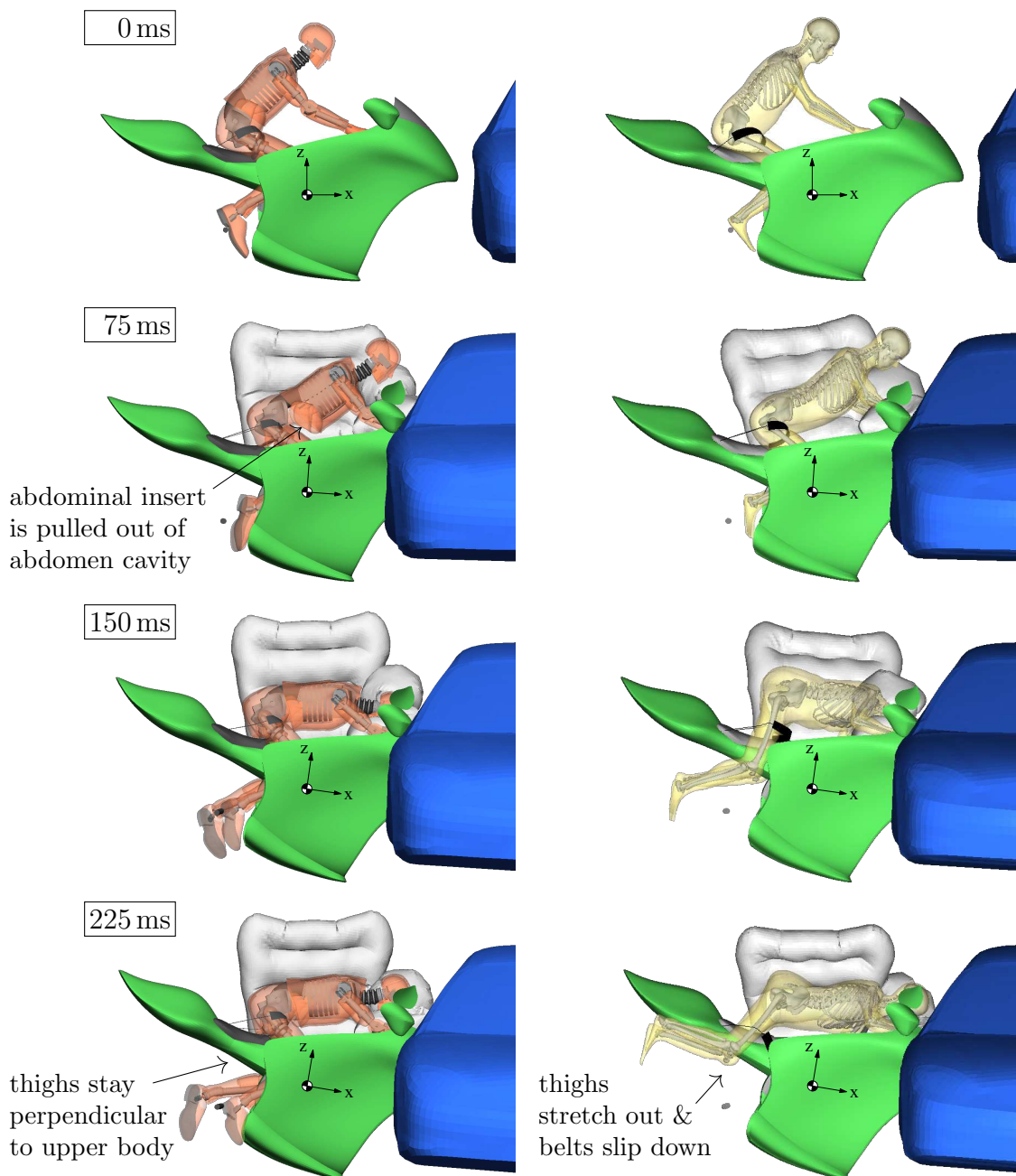
Figure 5.16: Comparison of an ATD (left: Hybrid III 50th) and a HBM (right: VIVA+ 50M) impact response in the coupled FE/MB simulations of scenario ⑦.

distinct differences in the kinematic impact responses. In ⑦, the upper-body motions are very similar, while the molded flesh in the pelvic region of the ATD keeps the thighs perpendicular to the upper body, unlike for the HBM. As a result, in the HBM simulation, the belt slips down after the impact, see snapshots at 150 and 225 ms. Contrary to its design, the abdominal foam insert of the ATD is pulled out of the abdomen cavity. The insert is actually designed to measure the depth and rate of a steering wheel penetration into the abdomen [MooneyCollins86]. In ①, the motion sequence of the upper bodies shows
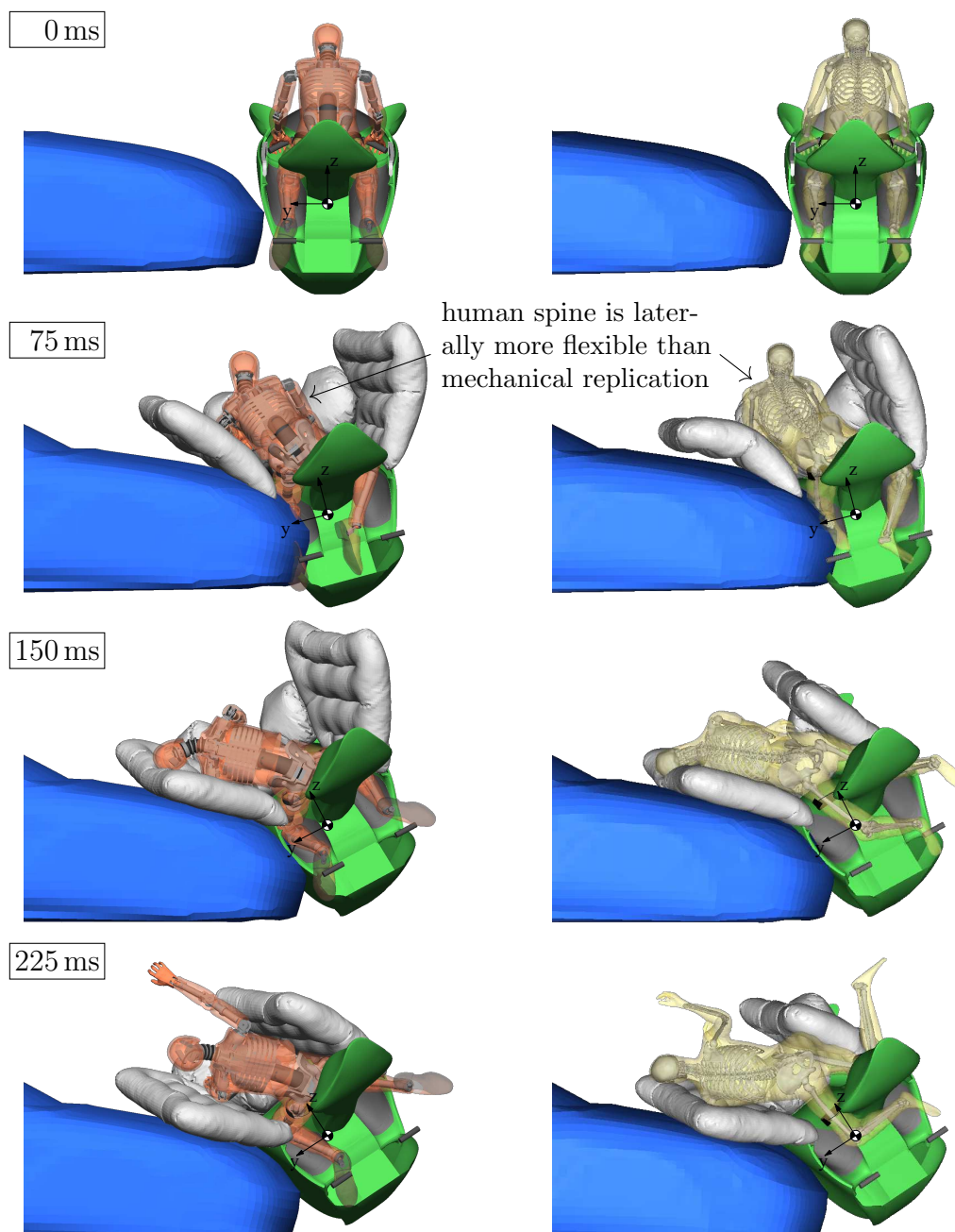
Figure 5.17: Comparison of an ATD (left: Hybrid III 50th) and a HBM (right: VIVA+ 50M) kinematic impact response in the coupled FE/MB simulations of scenario ①.

distinct differences. The spine of the HBM is laterally more flexible than the mechanical replication of the ATD. At 75 ms by a delayed motion of the head and at 150 ms by a more consistently deflected spine, including the neck.

Figures 5.18 and 5.19 show a comparison of the sex variants of the VIVA+ HBM, an average female and male. The skeletal structure of the head COG (red), the cervical (blue), thoracic (green), and lumbar spine (orange), as well as upper (brown) and lower (grey)

Figure 5.18: VIVA+ 50F (left) and 50M (right) impact response with skeletal trajectories relative to the motorcycle's center of gravity in the coupled FE/MB simulations of scenario ⑦. Note: For ⑦ only the right arm and leg skeletal trajectories are displayed.

extremities, are displayed on top of the FE result visualization. The trajectories detail the spatial and temporal sequence of the head COG, C7, T12, and L5, tracked relative to the motorcycle COG. Both in ⑦ and ①, the overall model kinematics are very similar. Only when rebounding from the front airbag in ⑦, the female variant receives more recoil as indicated by the L12, C7, and HC trajectories. It shows that the frontal airbag design, which is determined by the geometry of the airbag, the mass inflow parameters, and the exhaust area, is sensitive to the mass of the rider, which admittedly was to be expected.
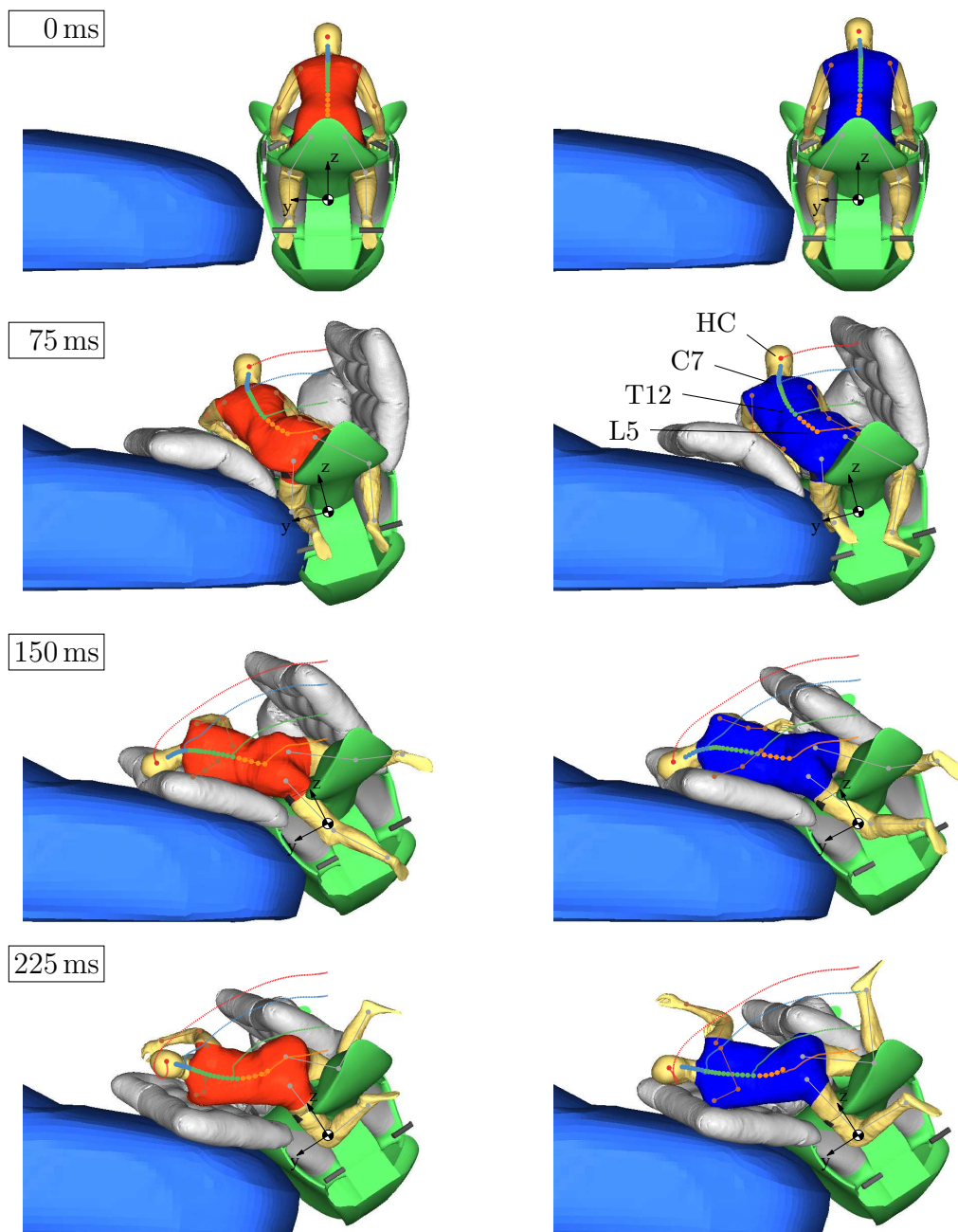
Figure 5.19: VIVA+ 50F (left) and 50M (right) impact response with skeletal trajectories relative to the motorcycle's center of gravity in the coupled FE/MB simulations of scenario ①.

ATD vs. HBM head loading and respective injury criteria show significant quantitative differences. The VIVA+ models provide a default output for head COG node history based on an interpolated node set constraint. Figure 5.20 gives the head COG linear accelerations head and injury criteria that are also based on angular velocity and acceleration for the rider surrogate simulations. The derived HIC(36) and $a_{3\mathrm{ms}}$ injury criteria in ⑦ are of the same magnitude. For ① they occur later ($\approx 0.150\,\mathrm{s}$ vs. $\approx 0.09\,\mathrm{s}$) and are considerably higher for the HBMs. The later response of the head, due to a less stiff spine and neck, results in significantly greater acceleration values. The upper body and neck of the HBM are laterally more flexible than the mechanical replication of the ATD and accelerate the head like a whip. The injury criteria that also rate head rotation, the GAMBIT and BrIC criterion, are for the HBMs also higher compared to those of the ATDs, even above the recommended limit.

injury criteria	HIC(36)/a_{3ms}			
scenario	⑦		①	
Hyb III 5th	0.29	0.65	0.14	0.39
Hyb III 50th	0.18	0.62	0.13	0.44
VIVA+ 50F	0.43	0.64	0.44	0.74
VIVA+ 50M	0.19	0.47	0.42	0.62

injury criteria	GAMBIT/BrIC(CSDM)			
scenario	⑦		①	
Hyb III 5th	0.31	0.58	0.25	0.84
Hyb III 50th	0.31	0.50	0.20	0.80
VIVA+ 50F	0.37	0.76	0.34	1.5
VIVA+ 50M	0.31	0.89	0.60	1.48

Figure 5.20: Resulting head COG linear accelerations and head injury criteria for the Hybrid III ATDs and VIVA+ HBMs in scenario ⑦ and ① (Figures 5.16-5.19).

5.2.3   Accident Response of Human Body Model Variants

The results from the different HBMs, including sex variants, exhibit some kinematic variations in accident response but do not fundamentally contradict each other. To analyse the kinematic response, Figure 5.21 shows the impact time history of the skeletal structure of the selected male HBMs. For each of the temporal snapshots, the main skeleton structure is overlayed, and the trajectories of head COG, C7, T12, and L5 are spatially traced. The positions of the skeletal markers are selected to be equivalent. The initial positions show minor variations in the skeletal structures, which is a result of the anthropometric differences discussed in Section 4.4.3 and also, to a minor extent, slight variances of the positions of the markers at the individual bones. Note that the THUMS simulation of configuration ⑦ aborted at 135 ms, because of failing brain elements. It was not possible to fix this, although the troubleshooting guidelines [Toyota21] were applied. The individual animations showing each of the individual simulations are provided in Appendix A.1.

Comparing multiple male HBM variants show some diverging results for frontal (scenario ⑦) and lateral (①) loading. In ⑦, the accident trajectory and the HC, C7, T12 and L5 trajectories after 135 ms initially agree quite well. When rebounding from the airbag, the two variants that terminated normally show different rebound heights for the head. In contrast to the VIVA+ variant, where the legs are stretched at the end of the impact, the legs of the GHMBC remain bent, as shown in the ATD model (Figure 5.16). In ① the initial response at 75 ms is very similar, at 150 ms they already diverged. In comparison, the VIVA+ slips furthest out of the thigh belts. The slipping does not cause it to leave the effective range of the side airbag and miss it, but it could be detrimental in the subsequent accident phase. The THUMS simulation features a phenomenon not yet observed. After the impact, the left arm pulls the side airbag slightly downwards, which causes the head to miss the airbag. The head missing the airbag results in a large lateral bending of the neck (from C1 to the head, visible in Figure A.16). Contrary to the VIVA+ results, both the THUMS and the GHBMC exhibit a rearward motion of the head after 150 ms with a rearward extended neck.

Figure 5.22 gives the resultant linear acceleration of the head COG and derived injury criteria. The VIVA+ 50M and GHBMC models provide default outputs for head COG based on interpolated node set constraints of the deformable brain. The THUMS does not provide such a default output. The linear accelerations show a similar qualitative course for the two HBMs, with the time histories of the HIC(36) and the $a_{3\mathrm{ms}}$ of the GHBMC quantitatively between VIVA+ 50M and 50th percentile Hybrid III ATD. The same applies to the angular accelerations and the BrIC criterion from angular velocities. Here the values of the GHBMC are lower than those of VIVA+. In summary: As expected, the HBMs exhibit some significant deviations from the ATD results and among themselves. The first is somewhat as expected since the Hybrid III ATD has been developed to be biofidelic only in particular load cases, here frontal loading of an upright occupant.

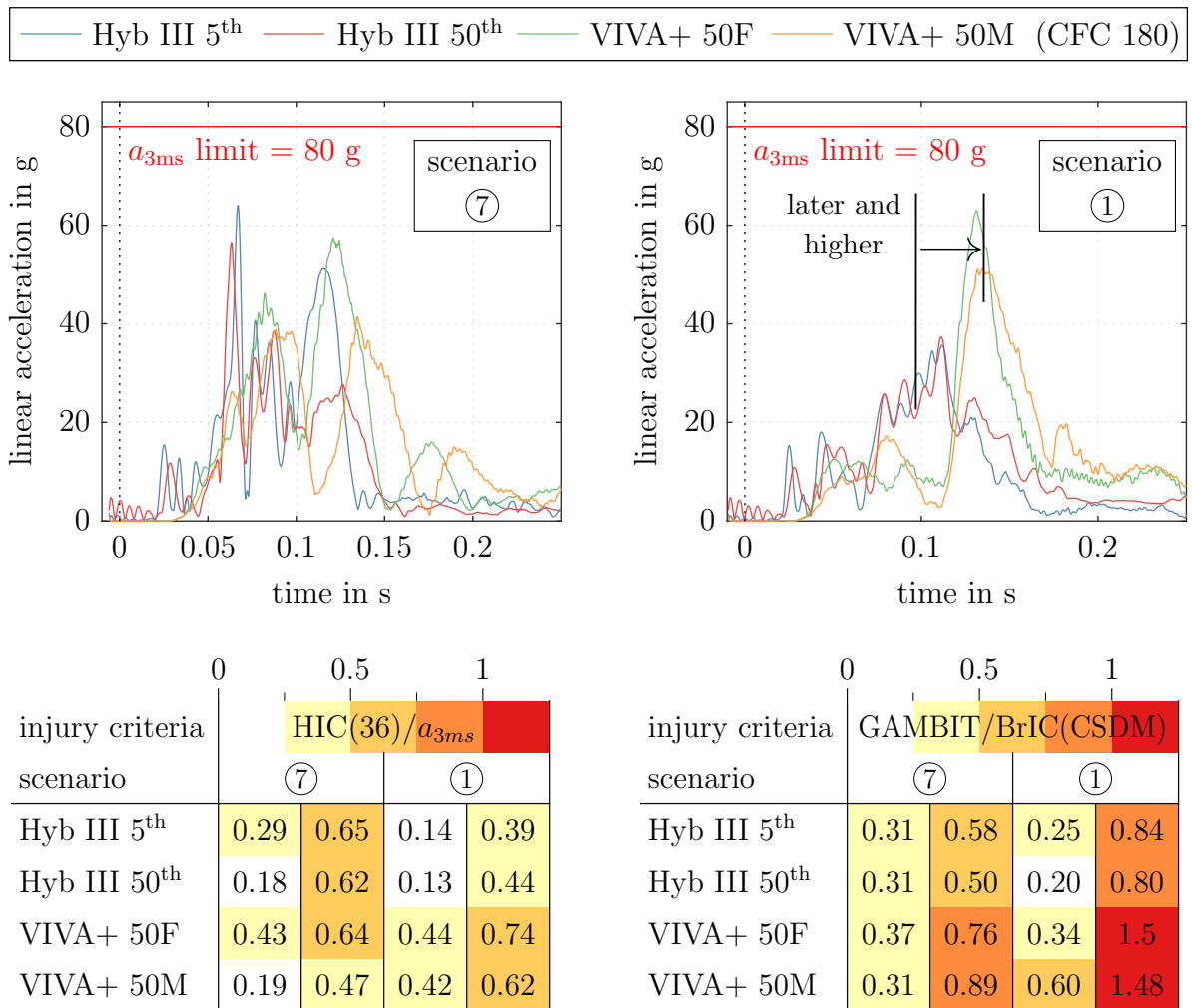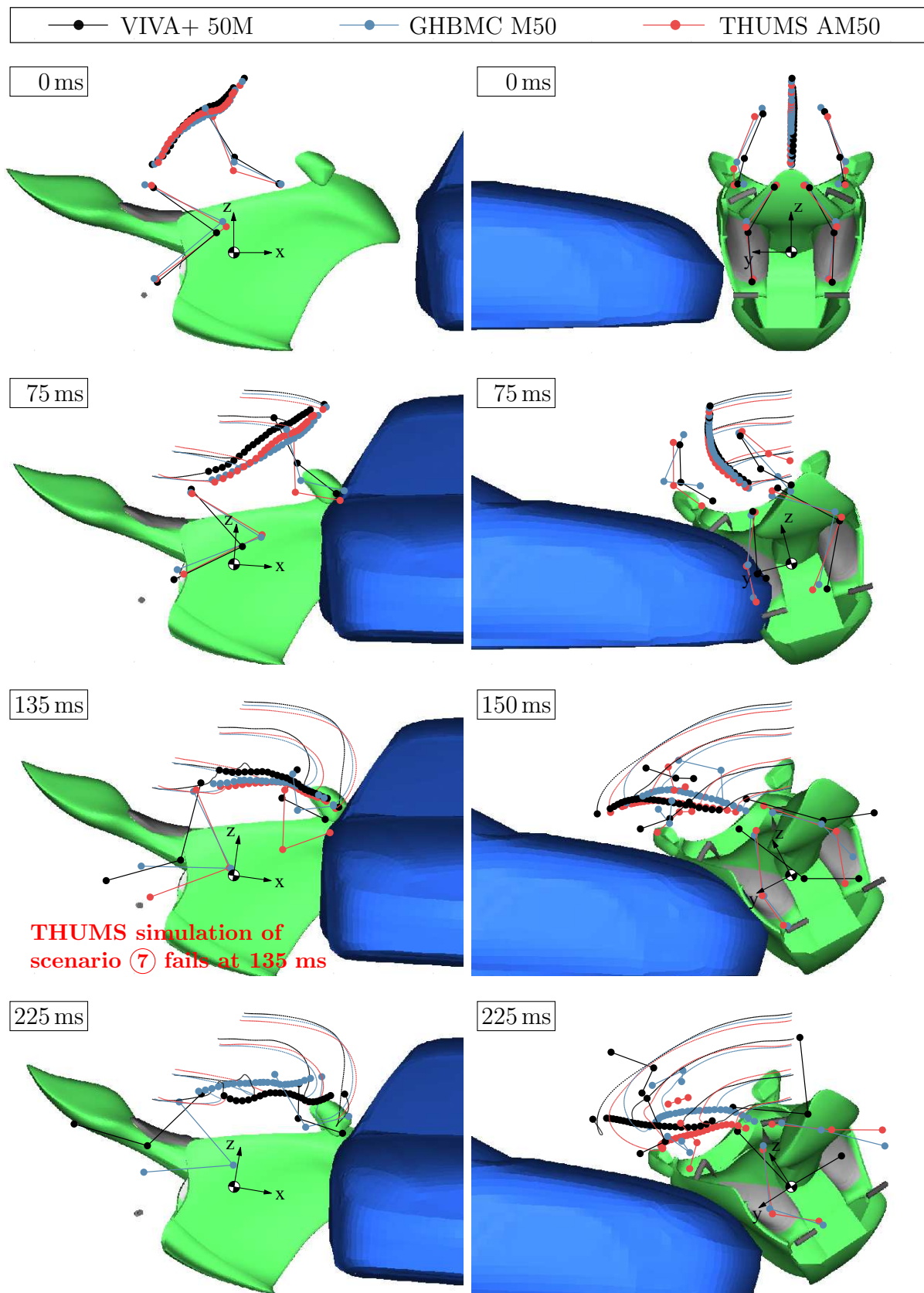Figure 5.21: Male HBM impact response in scenario ⑦ (left) and ① (right) with skeletal trajectories relative to the motorcycle's center of gravity in coupled FE/MB simulations.

| | Hyb III 50th | VIVA+ 50M | GHBMC M50 | (CFC 180) |
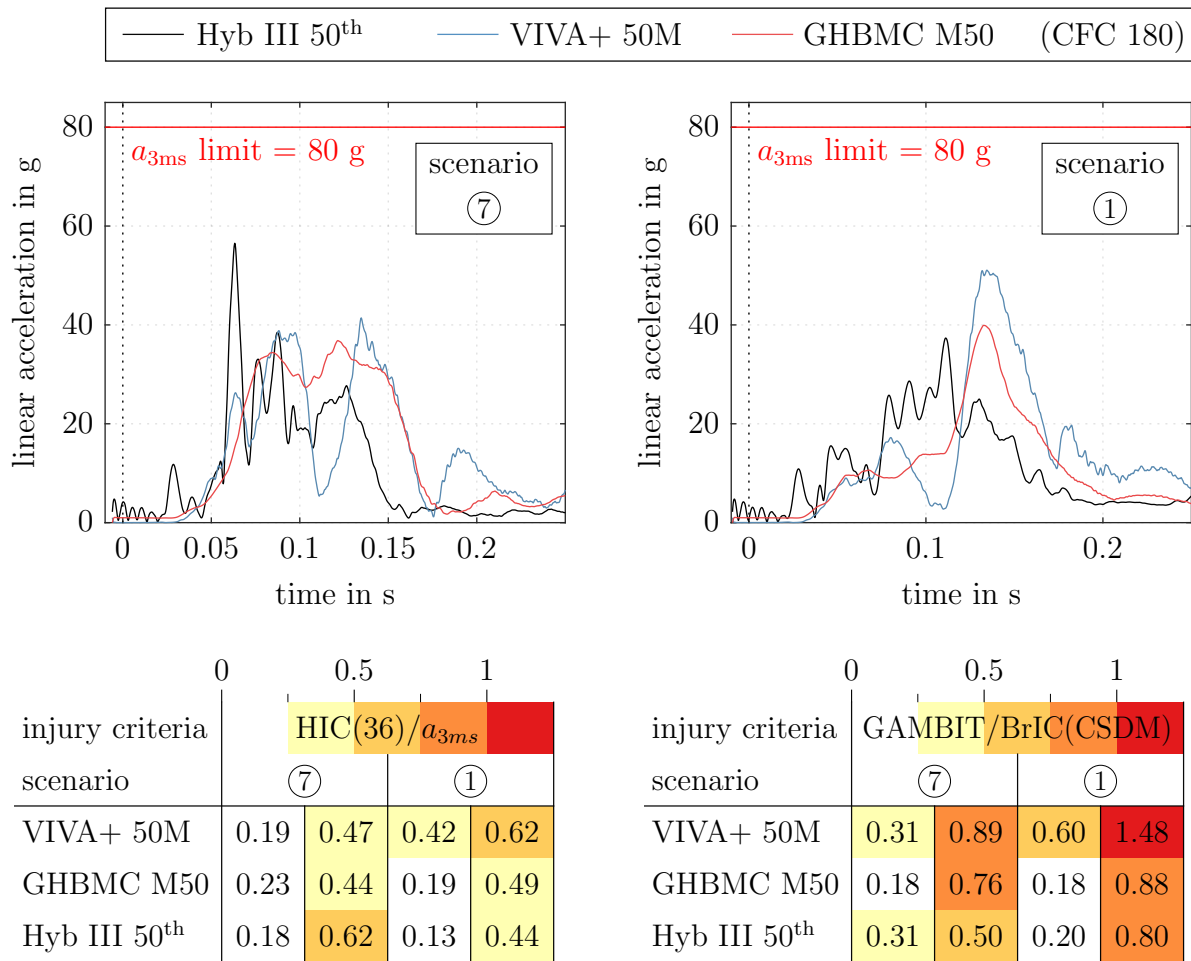
Figure 5.22: Resulting head COG linear accelerations and head injury criteria for the male ATD and HBM variants in scenario ⑦ and ①.

5.3 Stage III – Full Finite Element Simulations

The stage III full FE approach aims to replicate every impact-relevant structural component of the motorcycle and an opposing vehicle, a passenger car. The goal is to accurately predict the performance of the finalized design of the motorcycle and passive safety systems. In the following, the deformation behavior of the motorcycle is first examined independently from a specific impact opponent. Force and energy curves of a rigid wall collision interpret the deformation characteristics. The structural interaction and intrusion behavior of a passenger car impact are then investigated, and finally, simulations of all ISO 13232 scenarios are shown.

5.3.1   Motorcycle Frontal Deformation

In passenger car design, the structural vehicle components are designed and dimensioned to manage the impact energy from a collision. This transfer is a conversion of kinetic energy into deformation work. The passenger compartment structure is designed to be very stiff to create a survival space for the occupants and to provide seat and seat belt attachment points with sufficient strength. The structural components around the safety cell are designed to undergo large amounts of deformation, thereby dissipating impact energy as much as possible and reducing peak impact forces that would otherwise be transmitted to the safety cell and onto the occupants. The design objective for the safety concept of the motorcycle with the restraint system is similar.

The seat belt anchoring needs solid attachment points, and the rider's space on the motorcycle should be strong enough to remain geometrically intact so that the airbags can be deployed and supported by the motorcycle cockpit surfaces. In a frontal impact, the cockpit should allow for sufficient space for a forward excursion of the rider; in a lateral impact, the fairing with side impact structure should geometrically isolate the pelvis and lower extremities. The deformable energy-absorbing structures of the motorcycle, the front fork and tire, the main frame, the crash box, and the side fairing (the unique features of the proposed motorcycle structure), as well as the deformation of the accident opponent, determine the vehicle deceleration, which in turn significantly influences the design of the restraint safety systems. The deformation structures should distribute the force or acceleration over an increased period and reduce peak loads on the motorcycle main structure. This behavior is first determined for a frontal impact with a rigid wall impact without a rider, see Figure 5.23.

The evaluation of the rigid wall impact shows a characteristic deformation response and quantifies the contribution of specific motorcycle components. The impact has an initial velocity of $v_{\text{Moto}} =13.4\,\text{m/s}$ ($\approx 48.4\,\text{km/h}$). The structure deforms so that the vehicle length in front of the COG reduces by about 30 cm with a peak force of 200 kN and a maximal deformation of 30 cm. The plot of the COG displacement distance d against the resulting rigid wall force shows several phases of impact deformation. It is initially a progressive force response that can be divided into the compression of the front tire, followed by the collapse of the front wheel rim, and then the collapse of the front fork. Afterward, the force decreases and then increases again to the overall peak force. The area within the graph corresponds to the dissipated energy. Below, the stacked bar graph evaluates the internal energy absorption of the involved main structural components (see colored motorcycle parts). It shows that after the second increase in the force level, the energy is mainly absorbed by the crash box (purple), the main frame (yellow), and the fairing (green). Since these parts all act at a high contact point, it counteracts pitching of the motorcycle. As the results show, the frontal impact response can certainly be further
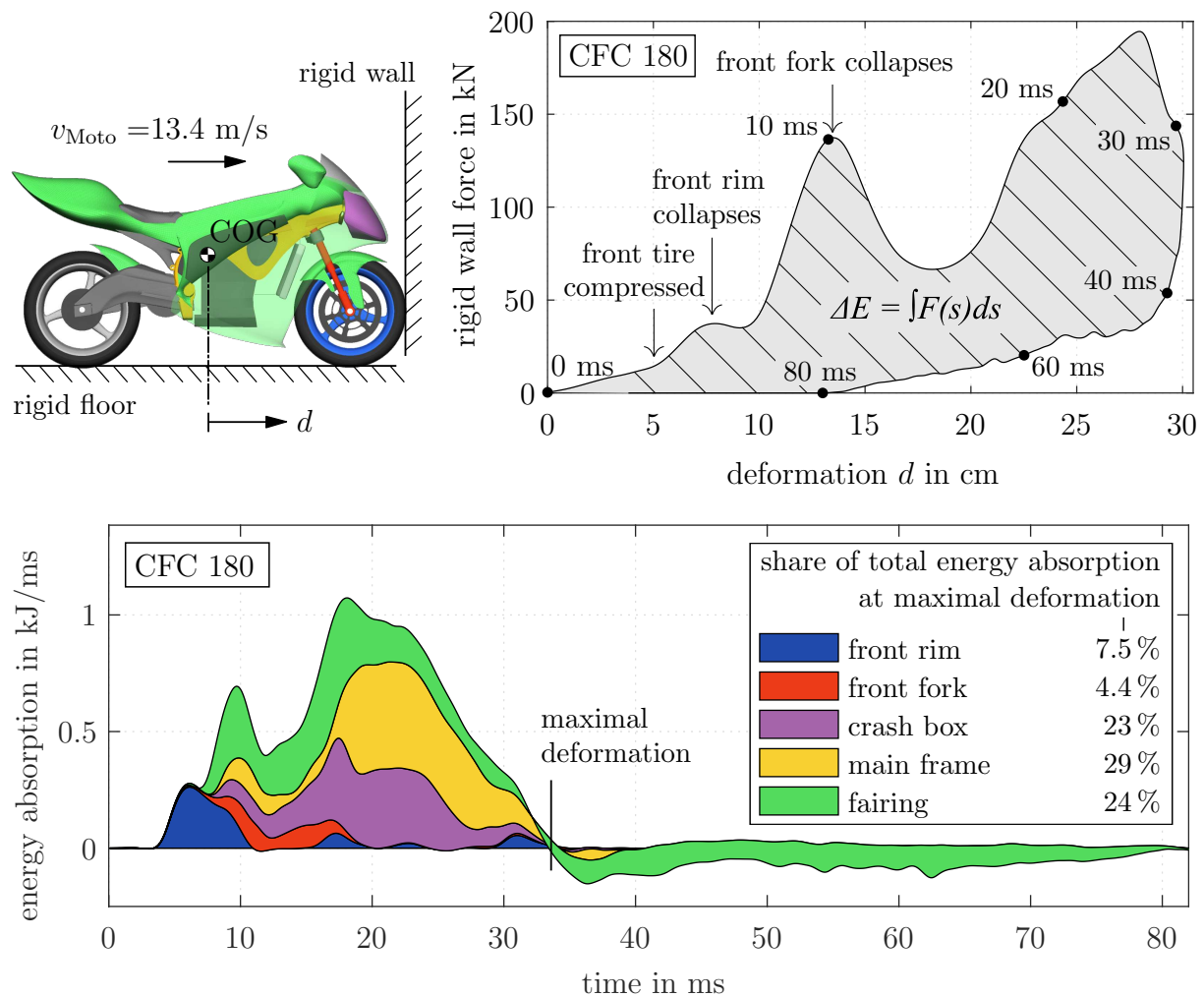
Figure 5.23: Frontal deformation characteristics of the full FE motorcycle model in a rigid wall impact. Force and deformation response (top) and stacked internal energy absorption of the main structural motorcycle components (bottom).

optimized. It would be better if the force level increases progressively throughout on a high force level, as [FranzEtAl13] outlined it for passenger car frontal deformation structures. Of course, such a small vehicle is limited in its overall capacity to absorb deformation work.

5.3.2 Structural Interaction and Vehicle Intrusion

The structural interaction and intrusion behavior between the motorcycle and an opposing vehicle shows that deceleration occurs without excessive pitching. It is illustrated by a section cut through the opposing car, shown in Figure 5.24. The motorcycle impacts into the passenger side of the car according to ISO 13232 ⑦ with 13.4 m/s ($\approx$ 48.4 km/h). The motorcycle front wheel collides with the robust front door sill. The motorcycle cockpit

Figure 5.24: Structural vehicle interaction and intrusion behavior in the full FE simulations in scenario ⑦.
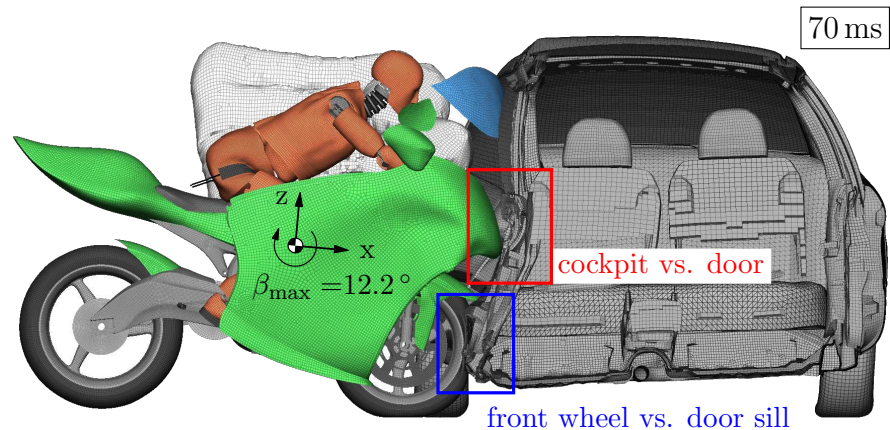
with the crash box in the nose deforms the car door inwards, while the motorcycle cockpit itself is little deformed. The motorcycle main frame and powertrain assembly ensure that the rider area remains intact. The deformation of the car door provides sufficient room for the rider's forward excursion, induced by the belt load-limiter-dependent belt pay-out. This analysis shows that the very firm door sill structure promotes motorcycle pitching. Nevertheless, the proposed motorcycle does not roll over about its transverse axis during a frontal impact. The maximum pitching angle in this simulation is $\beta_{max} = 12.2\,°$.

The experience from the results shown here is used to refine the definition of the vehicle interaction in the stage I MB approach. This means that the initially stiffer assumed vehicle contact interaction and front fork deformation (published in [MaierEtAl20]) is now scaled for a softer interaction with, i.a., greater contact penetration. The MB vehicle interaction, i.e., the magnitude of deceleration and penetration depth, is now similar to the FE vehicle interaction of scenario ⑦ shown here. The MB motorcycle still rotates slightly more (compare Figure 5.1). An automated procedure that correlates the MB vehicle interaction to the results of (all) the full FE simulation results would certainly be very useful but is currently not realized.

5.3.3 Impact Behavior and Biomechanical Loading in Representative Accident Scenarios

At last, the modeling efforts are merged into one aggregated model and simulated for the ISO 13232 impact configurations. At this point, modifications or further iterations of the design or on the set of parameters of the passive safety systems are minimal (with the exception of the stowage of the airbags – these are now behind hinged lids and inside flexible enclosures), and one can concentrate on the numerical robustness of the simulations. Due to the many involved subsystems and sheer model size – about 1.56 million nodes and 1.85 million elements when surrogating the rider with a model of an ATD – with now very long simulation times – about 100 h for a problem time of 500 ms – this task is

challenging enough. All seven ISO 13232 scenarios are simulated for the primary impact; see the visualization of the accident behavior up to 500 ms in Figure 5.25 for the 50$^{\text{th}}$ percentile Hybrid III ATD. The visualization for the 5$^{\text{th}}$ percentile Hybrid III ATD is given in Figure A.17 of Appendix A.4. The respective injury criteria resulting from biomechanical loading of both ATD variants are summarized and color-coded for injury severity in Table 5.2.

The accident kinematics of the vehicles and the ATD confirm the previous results. The rider is effectively restrained to the motorcycle in all cases as a contact of the rider against the opposing vehicle is mitigated. Some differences can be observed in the visual comparison with the motorcycle accident trajectories in the MB simulations. In ④ and ⑤, instead of sliding along the car and retaining a large portion of the initial velocity while bouncing off in a shallow angle, the FE motorcycle gets caught in the car side and is decelerated much more fiercely. As a result, in ④ the ATD head does not hit the side airbag but the mirror airbag. In ⑤, the motorcycle intrudes into the rear door and collides with the inner sill of the rear wheel arch and is decelerated so rapidly (similar to ⑦) that the ATD torso and head are pushed into the frontal airbag. The accident trajectories of the other scenarios are largely consistent with the stage I results. Assessing the biomechanical loads shows:

- The values of the biomechanical injury criteria for the vital body parts are almost all below their respective biomechanical limit. Exceptions are the BRIC(CSDM) for both ATD variants and the thorax acceleration in ③ for the 50$^{\text{th}}$ percentile Hybrid III.

- Many of the criteria that show high values in the stage I results (Table 5.1) are even higher in the stage III results. These are the values of head acceleration ($a_{3\text{ms}}$ and HIC), neck tension ($F_{z,\text{tens,1ms}}$ and $F_{z,\text{tens,45ms}}$), and thorax and pelvis accelerations ($a_{3\text{ms}}$). An exemplary comparison of the linear head acceleration of scenario ⑦ in Figure 5.26 shows that the FE ATD predicts a higher head acceleration. In stage II, using identical MB vehicle trajectories as in stage I, the FE ATD results show higher head accelerations.

- This model eliminates the shortcomings of the previous modeling approaches. While in stage I and II, the rigid car pierces through the motorcycle geometry, vehicle interaction and side protection are now fully considered. This significantly lowered femoral and tibial loading. Compared to the recommended biomechanical limits, the femoral loading is well within the limits; the tibial load is except for ② for the 50$^{\text{th}}$ percentile Hybrid III below the recommended limits.

- The neck tensile forces result from the deceleration of the head. The fact that no safety helmet is worn has a positive effect on this loading since a helmet would increase the mass pulling on the neck. An increase in neck forces when wearing a helmet with a certain weight has yet to be investigated.
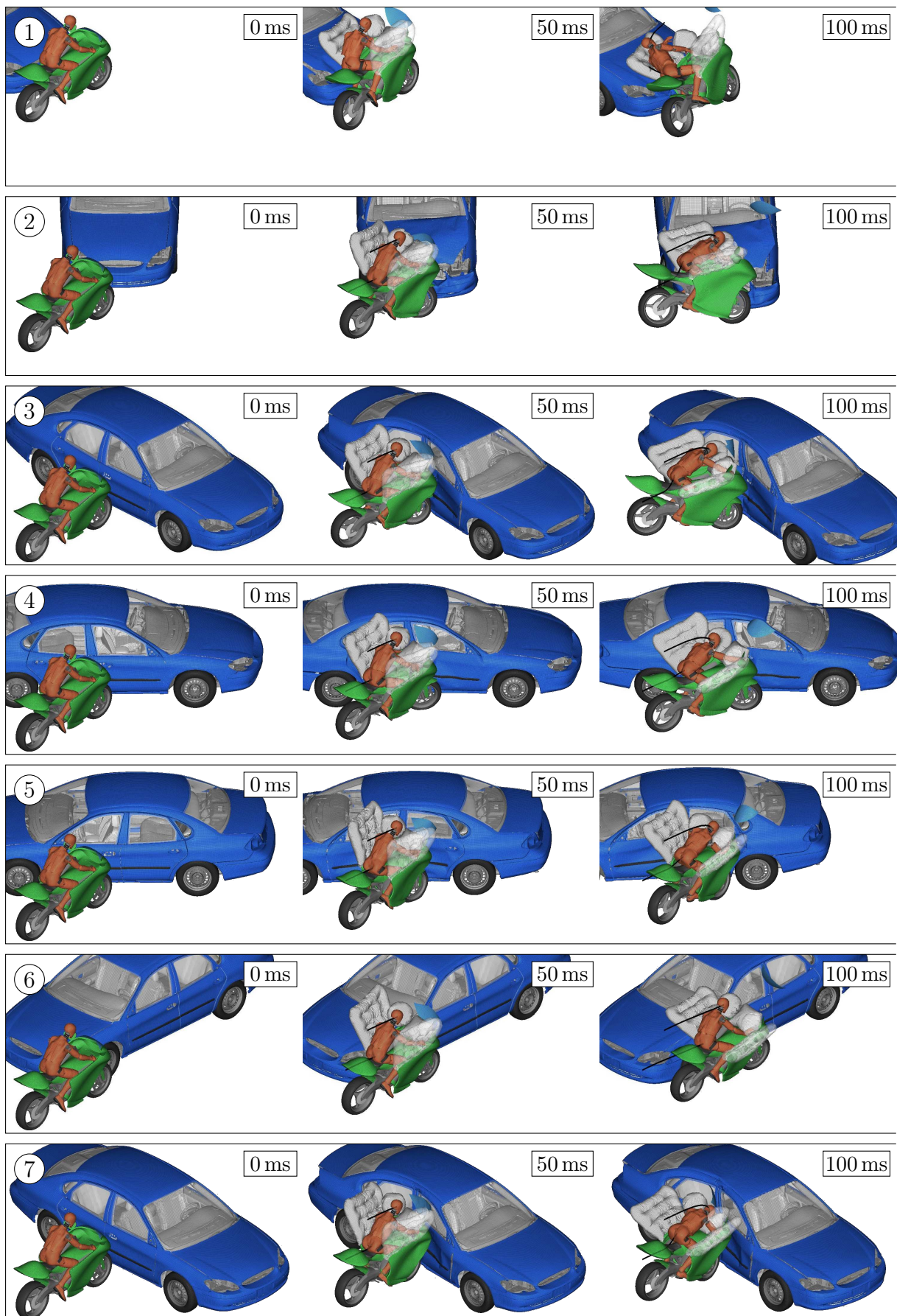
Figure 5.25: Full FE simulations of Hyb III 50th with head and pelvis trajectories (black).
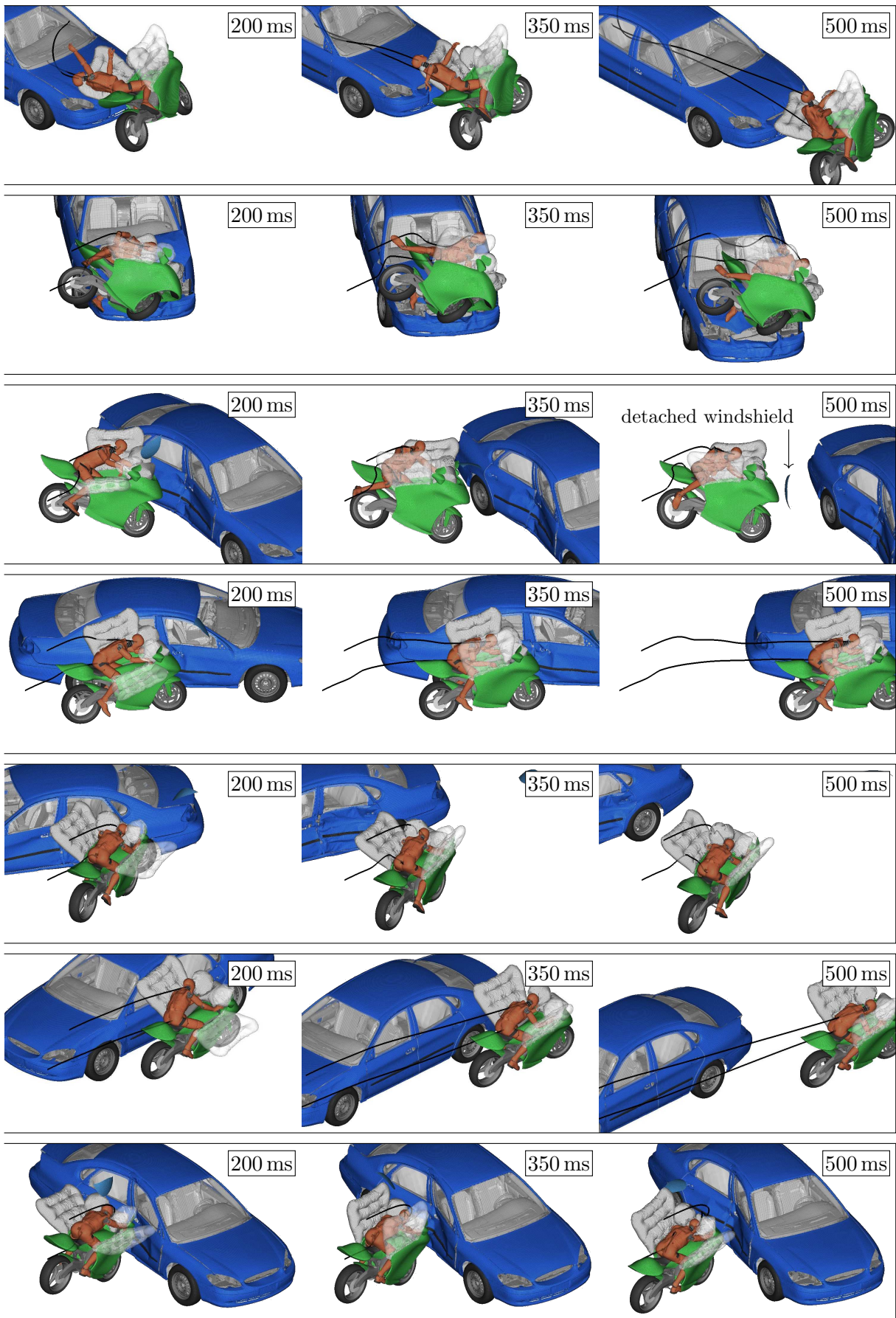
detached windshield

Table 5.2: Injury criteria normalized to their respective biomechanical limit for the primary impact up to 500 ms in the full FE simulations with the Hybrid III 50th and 5th ATDs.

Hyb III 50th / Hyb III 5th	criterion	ATD	①	②	③	④	⑤	⑥	⑦	limits
head	a_{3ms}	50th	0.59	0.49	0.73	0.39	0.52	0.13	0.69	80 g
		5th	0.7	0.36	0.46	0.19	0.55	0.08	0.43	80 g
	HIC(36) / HIC(15)	50th	0.38	0.21	0.26	0.13	0.12	0	0.33	1000
		5th	0.66	0.15	0.25	0.03	0.44	0.01	0.26	700
	GAMBIT	50th	0.21	0.23	0.43	0.19	0.26	0.08	0.28	1
		5th	0.38	0.26	0.26	0.16	0.31	0.11	0.28	1
	BrIC(CSDM)	50th	1.06	1.08	1.14	0.66	0.64	0.21	0.87	1
		5th	1.24	1.08	0.49	0.53	0.92	0.25	0.57	1
neck	$F_{z,\text{tens},1ms}$	50th	0.63	0.45	0.43	0.25	0.57	0.14	0.65	3.3 kN
		5th	0.67	0.54	0.4	0.2	0.38	0.18	0.48	2.9 kN
	$F_{z,\text{tens},45ms}$	50th	0.97	0.35	0.06	0.24	0.23	0.01	0.54	1.1 kN
		5th	0.55	0.07	0.1	0.24	0.39	0.04	0.4	1.1 kN
	$F_{z,\text{compr},1ms}$	50th	0.06	0.03	0.06	0.06	0.06	0.03	0.02	4 kN
		5th	0.08	0.09	0.2	0.06	0.07	0.06	0.03	4 kN
	$F_{z,\text{compr},45ms}$	50th	0	0	0.02	0.02	0.04	0.01	0	1.1 kN
		5th	0	0	0	0	0.03	0	0	1.1 kN
	$F_{xy,1ms}$	50th	0.15	0.15	0.33	0.12	0.23	0.08	0.3	3.1 kN
		5th	0.26	0.17	0.13	0.07	0.13	0.05	0.15	2.7 kN
	$F_{xy,45ms}$	50th	0.24	0.17	0.12	0.13	0.08	0.14	0.09	1.1 kN
		5th	0.24	0.13	0.1	0.11	0.06	0.07	0.04	1.1 kN
	$M_{y,\text{fwd},max}$	50th	0	0.02	0.03	0.04	0.01	0	0	190 Nm
		5th	0.06	0.1	0.03	0.04	0.01	0.01	0.01	190 Nm
	$M_{y,\text{rwd},max}$	50th	0	0.4	0.12	0.19	0.06	0.11	0	57 Nm
		5th	0.47	0.3	0.09	0.09	0.17	0.01	0	57 Nm
	Nij_{max}	50th	0.32	0.24	0.24	0.13	0.31	0.08	0.37	1
		5th	0.49	0.43	0.31	0.16	0.29	0.15	0.35	1
thorax	a_{3ms}	50th	0.36	0.74	1.24	0.44	0.74	0.12	0.72	60 g
		5th	0.46	0.61	0.52	0.3	0.5	0.17	0.54	60 g
	ThCC	50th	0.07	0.39	0.5	0.19	0.29	0.06	0.34	50 mm
		5th	0.04	0.22	0.1	0.07	0.08	0.03	0.11	34 mm
	VC_{max}	50th	0.01	0.14	0.35	0.04	0.11	0.01	0.09	1 m/s
		5th	0.01	0.04	0.01	0	0.19	0	0.16	1 m/s
pelvis	a_{3ms}	50th	0.49	0.93	0.7	0.36	0.43	0.29	0.62	60 g
		5th	0.43	0.71	0.4	0.41	0.46	0.4	0.55	60 g
femur	$|F_z|_{max}$	50th	0.24	0.23	0.25	0.16	0.19	0.13	0.23	9.07 kN
		5th	0.11	0.31	0.23	0.17	0.23	0.12	0.24	6.085 kN
tibia	TI_{max}	50th	0.69	1.02	0.79	0.68	0.47	0.53	0.49	1.3
		5th	0.34	0.87	0.72	0.52	0.7	0.43	0.65	1.3

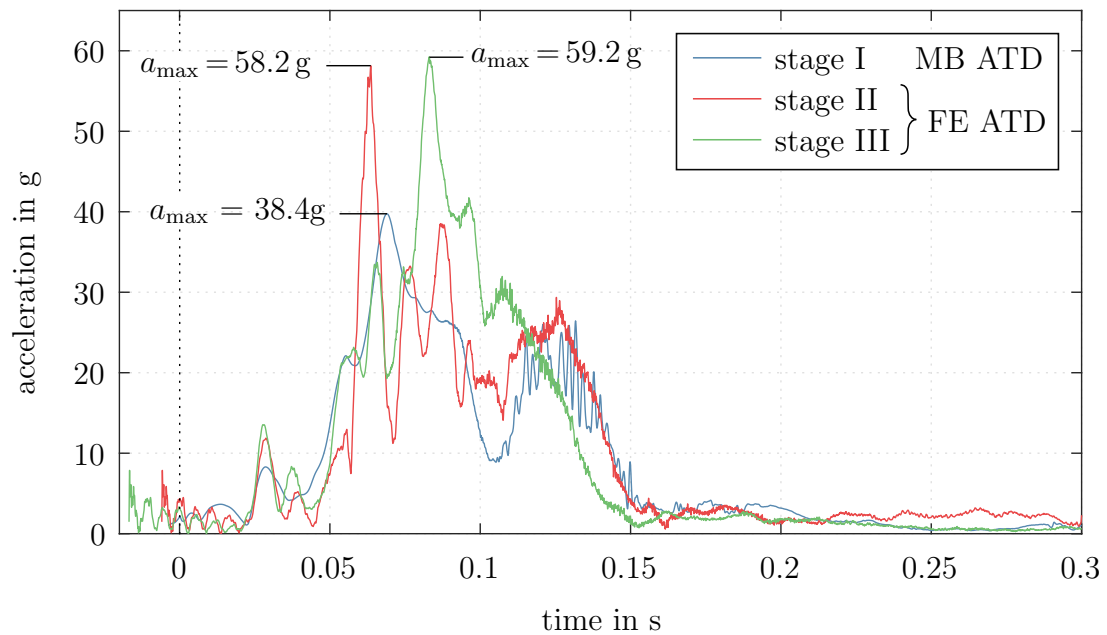Scale legend (limits): 0   0.5   1

Figure 5.26: Head linear acceleration of the Hybrid III 50th for scenario ⑦ in stages I–III.

Chapter 6

Discussion

This chapter revisits the incipiently set objectives (O1-O4). They are discussed individually in terms of their degree of fulfillment and regarding the limitations of this study.

(O1) Simulation Strategy and Modeling Approach

With suitable computational models, a passive safety solution can be investigated with very little time and financial effort. Target-oriented variations of design variables allow a structure or system to be analyzed and improved relatively quickly. Based on a review and the selection of suitable methods and models to investigate the accident behavior of the safety concept, models with varying levels of detail and complexity have been developed: an MB model (stage I), an FE model (stage III), and a hybrid model approach in between (stage II). The models have modular input decks for restraint systems, rider surrogate models, and opposing vehicle structures. Pre- and post-processing routines and custom translators are used for automized exchange between the software environments, which transfer, e.g., scenario configuration parameters and FE meshes from design iterations. Each simulation environment has different simulation runtimes and model fidelity, qualifying them for specific investigations, suitable for systematically assessing and optimizing various aspects of accident behavior.

The first stage MB approach features low complexity and low numerical costs while capturing the essential physics of the collision. It is particularly suitable for obtaining initial results at an early stage. If it also computes quickly, all the better. This computational method represents a numerically efficient way to tinker with the safety systems and tune and improve them, i.e., adapting their geometry, location, and system parameters. The third stage full FE approach aims to fully represent the interaction of the collision to accurately predict the performance of the finalized design by replicating every significant structural component of the vehicles in great detail. However, the higher fidelity is bought by a challenging model generation and significantly increased computational costs. The
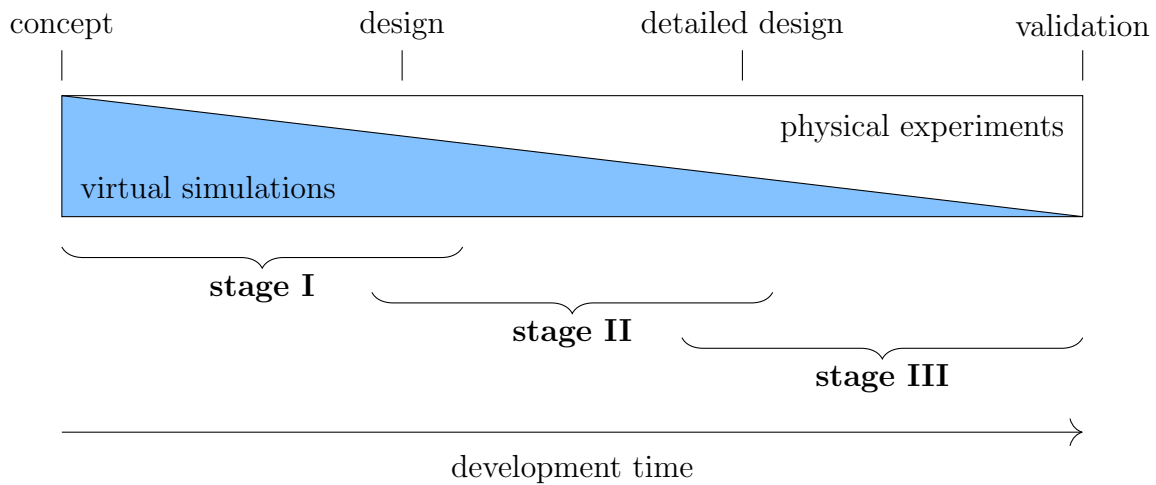
Figure 6.1: Use of the presented stages in the development process.

advantages of the stage II partial FE approach using MB vehicle interaction are the successive and methodological model generation with a gradually increased level of detail and expected fidelity from stage I while significantly reducing computation time compared to a full FE model representation. The hybrid model is comparable to already realized approaches for occupants in cars, see e.g. [ReichertEtAl14]. It offers the possibility to consider a larger variance of accident scenarios or occupant diversity or to enable very complex and numerically expensive investigations with state-of-the-art HBMs at reduced computational effort. Revisiting the use of the tools in the development process of passive safety from Section 1.3, the stages are particularly suitable as a sequential progression, as shown in Figure 6.1.

(O2) Reproduction of Accident Behavior

Crash simulations represent highly complex physical processes with many degrees of freedom. Although realistic visualizations of detailed simulations suggest an exact reproduction of an accident, one should be aware that approximations are made. Therefore, even though the numerical results are checked carefully by consistency and plausibility, i.a., by energy balances, such computational models require a high level of physical validation to assure accurate results. After all, actual human inviolacy depends on the technical design. Therefore, sufficient final verification of the results for proof of functionality in a standardized and legislative framework should take place in full-scale laboratory tests of the entire system.

The study's simulation strategy stems from the necessity to build models of the given complex problem piece by piece. This stepwise modeling approach coincides with Rouchon's testing pyramid (Figure 1.9), allowing for a structured model verification at multiple levels in increasingly more elaborate experiments. At coupon and element level, a model verifi-

cation has been done for the foam leg protectors within the scope of this work; for generic materials and components from occupant safety such as belts and airbags, existing knowledge and experience in modeling has been used. Driven by automotive vehicle safety development, the modeling of occupant interaction with passive safety systems such as belts and airbags is well advanced. On the full system level of a conventional motorcycle, a comparison of the simulated vehicle interaction with full-scale crash tests shows that the MB approach can reproduce the main accident kinematics of a conventional two-wheeler, an opposing vehicle, and a rider surrogate. What has not yet been done is a verification of the simulation results at the level of the subsystems and the full-scale level of the entire system of the safety concept. The hybrid approach is well suited for the subsystem level in an intermediate step. Decoupled from a real-world vehicle interaction, physical sled tests can reproduce the rider interaction with the airbags, belts, protectors, and other motorcycle components with rider interaction. For this purpose, a uniaxial impulse could be approximated in a linear sled crash test and compared to a corresponding stage II simulation. Ultimately, only a full-scale test of the entire system with an ATD and an accident opponent can verify the capability of a realistic and reliable prediction of the accident outcome. This step requires a high level of detail in the development and large financial resources to build a suitable prototype and conduct crash experiments. The developed modeling and simulation strategy provides a suitable framework that already accounts for such a testing strategy.

Physical crash tests can lack biofidelity because they are typically limited to using mechanical surrogates for the rider, and they only cover a few load cases due to financial limitations. Therefore, it is currently pursued to intensify the use of complementary virtual tests for passive safety [EuroNCAP17, EuroNCAP22], which already started with consumer rating assessment of active pedestrian protection systems [KlugEtAl19, KlugEllway21]. It concerns the use of HBMs in additional load cases where the biofidelity of ATDs is considered insufficient and aims to increase robustness through greater variance in scenarios and human diversity. Despite many challenges, such as ensuring integrity and authenticity and concerns about the protection of intellectual property when exchanging sensitive simulation data [GalijatovicEtAl22], it can be expected that this approach will extend to certification and regulatory approval of future vehicles. The developed computational approach in this thesis, incorporating further improving and increasingly valid virtual HBMs, should be well suited to holistically investigate the safety concept realistically.

(O3) Safety Principle

The thesis aims to model and investigate a novel safety concept of a motorcycle. To understand whether the new idea operates and performs well, the state-of-the-art and existing solutions and how these operate and perform are examined. A detailed summary shows that the accident behavior of motorcycles and motorcyclists is intrinsically unpredictable:

PTW crash configurations and the resulting accident behavior are manifold; the rider's accident kinematics are not guided and are rather chaotic when the rider dismounts from the PTW; and, therefore, the protection principle is decisively based on coincidence. The consequences are injuries to all body parts. There is considerable and fundamental potential for improvement that goes beyond the improved protection of single-body regions, but that considers a whole-body protection strategy. As summarized, attempts have been made in the past to improve the passive safety of PTW riders, and solutions have been developed that go beyond the existing protective effect of personally worn protective equipment. However, these have not caught on or are still niche products.

The restraint safety concept is investigated by the kinematic, kinetic, and energy-based relationships. Restraining a single, non-helmeted rider with belts and leg impact protectors and decelerating the resulting upper body motion relative to the motorcycle with multiple surrounding airbags leads to a guided and controlled rider trajectory for the primary accident phase. The cockpit, the lateral impact structures, and the side airbags create a protective shell around the rider, mitigating hard surface contacts. The combination of multiple passive safety systems – the novelty of the safety concept – crucially minimizes the intrinsic incalculability of a motorcycle rider's motion when dismounting uncontrolled during an accident. For a controlled and guided trajectory, the safety systems are designed and dimensioned to distribute the loads on the human body spatially and temporally. This involves load-limiting of the belt restraints, airbag chamber pressure regulation, and material characteristics of the energy-absorbing foam of the leg impact protectors. Interestingly, the proposed novel safety concept is a combination of the already individually conceived safety considerations for PTWs. It consists of airbags (like the Honda Goldwing touring motorcycle), a seat belt system and frontal crumple structure (like the BMW C1 scooter), and leg impact protectors for leg restraint (like the UKDS motorcycle leg protector device), all discussed in detail in Section 2.3.2. Their cooperation shows a promising effect.

The impact velocities and schematic chronology of a frontal impact with the restraint safety concept illustrates the advantages for a primary impact compared to the same impact with a conventional motorcycle. The schematic chronology methodically detail multiple regimes of the operation of the safety systems and their effect on the deceleration behavior of the rider's body parts. It provides a meaningful description of the operation, delineating the safety principle. Figure 6.2 summarises the functional approach further and arranges it hierarchically. On a macro-functional level, the safety principle can be divided into guiding and controlling the rider's motion to reduce body loads during deceleration and providing a sufficient survival space to prevent injuries from crushing. Individual functions of the passive safety systems can be assigned to these two main functions at a further meso-functional level. These, in turn, can then be broken down into further subfunctions at a micro-functional level. These here-called micro functions are the elements of the schematic chronology that describe the functional regime of the passive systems.

The secondary accident phases of the investigated accident scenarios are not part of the evaluations in this thesis. Rear-end collisions and solo accidents or scenarios where a rollover of the PTW is inevitable are not part of the seven recommended ISO 13232 accident scenarios and are also not considered. In the current design, the belt is elongated due to belt pay-out from load-limiting in scenarios where the belt system transfers significant contact energy. After primary impact loading, the belt is no longer tight but restrains the legs very loosely. Suppose the rider or the vehicle still has a lot of kinetic energy. In that case, inadequate belt restraint can have serious negative consequences in the subsequent accident phases, especially for a safety concept for which personal protective equipment is abandoned. The same applies to rear-end impacts where the rider is prone to slipping out of the thigh belts, and any resulting rearward upper body displacement and/or rotation will not be supported. Here, further ideas for a rider restraint have to be developed, e.g., by extending the belt pay-out regime by recollecting belt material or changing the belt attachment points and layout or harness variants. A rear airbag or another support structure may be able to provide rearward support and survival space. Furthermore, it must be clarified what the consequences of a topside collision load are, e.g., as a result of a rollover or a collision with roadside objects. Can the airbags provide a survival space, or will the rider be crushed? How does the safety concept perform in these situations compared to a non-restrained motorcyclist?
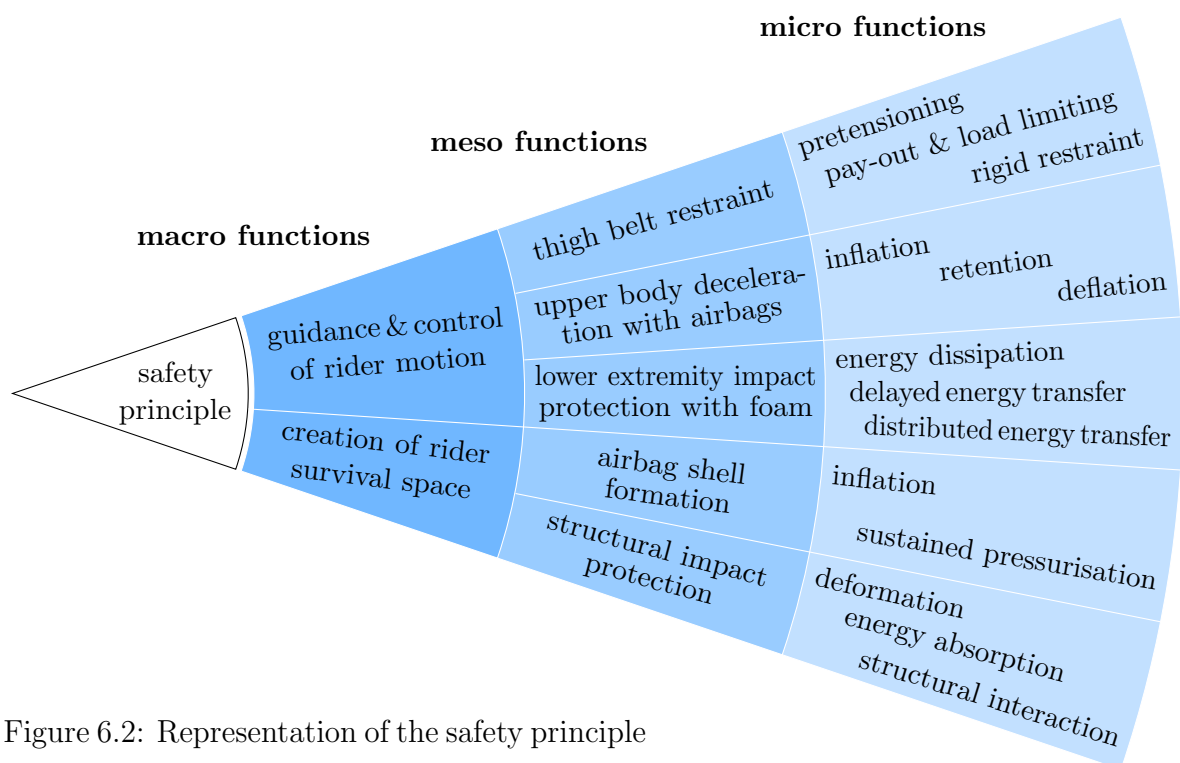

Figure 6.2: Representation of the safety principle as superimposed functional levels.

(O4) Performance Evaluation

The academic work presented here is in no way intended to attest or prove a guaranteed safety effect. It cannot fulfill this. A convincing holistic verification is already refuted by the discussion in the immediately preceding paragraph. Instead, the focus is primarily on the systematic description of the safety principle. A quantified performance evaluation predicts and evaluates the safety effect and injury risks on the basis of a comprehensive set of injury criteria and corresponding biomechanical limits concerning all body parts. For the evaluation, a suitable and widely-used set of representative impact scenarios is selected. Within this work, the evaluation is limited to the primary accident phase.

The evaluation of the accident performance in a frontal impact (scenario ⑦) shows a promising effect. In simulations of the restraint safety concept with ATD surrogates in this load case, all injury criteria are below their recommended biomechanical limits. The direct comparison to a laboratory test with a conventional motorcycle with a non-restrained rider shows that although individual body parts and evaluated criteria are increased safety-concept-related, high loadings near the limit value are overall, often dramatically, reduced. The evaluation of all the recommended representative ISO 13232 scenarios shows that, with the exception of the BrIC, the vital body regions are below the recommended biomechanical limits. However, the BrIC is associated with overpredicting brain injury risk [SahooEtAl20]. These results from the ATDs must be treated with caution. The Hybrid III design is not intended for this use case and loading condition, evidenced, i.a. by the abdominal insert slipping out of the abdomen cavity. Therefore, HBMs are used as an interesting addition and omnidirectional tool.

The multiple HBMs exhibit specific differences in predicting the impact response of real-world human behavior that could not be observed with ATDs. These differences result in increased head injury criteria that rate head rotation in the frontal scenario ⑦ and overall higher head loading in the lateral scenario ①. Although the HBMs are anthropometrically very similar, they also show differences in accident kinematics and loading. In ⑦ and ①, the belts slip from the VIVA+ thighs; in ①, the THUMS head misses the side airbag. To better understand and evaluate the consequences of the impacts on the whole body, many more available injury criteria (recently summarized [GermanettiEtAl22]) must be considered, such as injury mechanisms that are strain or stress-based. Additional scenario-specific validations of HBMs are needed to solidify the biofidelity of the HBMs, i.e., their lateral spine flexibility, in this type of impact loading. Validations of HBMs, currently based mainly on standard lateral car crashes with a 3-point seat-belt, should be extended because the motorcycle rider shows larger head, torso, and thus spine displacements in ① due to a less restrained posture.

Using simulations, the evaluation is not limited to physically reproducible sensors; instead, the observer can extract practically omnisciently any system variables. The energy

absorption describes the deformation characteristic of the motorcycle. The energy balances of the rider quantify the contribution of the involved safety components, identifying the belts as the main restraint. The energy balances simulations' final states also show that there are scenarios based on the chosen set of representative accident configurations, for which consideration of a subsequent secondary accident phase will be necessary. Combined with the potentially very complex nature of motorcycle accidents, especially after the first impact, and the variety of possible accident opponents, the potentially complex accident behavior presents major challenges for future studies to verify a sufficient performance of the protective measures in the subsequent accident phases. The safety concept proposes not to wear a safety helmet. The legal helmet requirement in many European countries was waived before for the BMW C1 scooter. However, this makes it all the more difficult to prevent adverse effects in beyond-design-basis scenarios of the proposed safety idea. Wearing a helmet, on the other hand, could increase the tensile forces in the neck too much, which would also be harmful.

Chapter 7

Conclusions and Outlook

PTWs have already a significant share in global mobility. Considering societal, economic, and environmental aspects, they have a promising future. However, their passive safety is far from the level of protection of passenger cars. Although an indispensable tool for designing and optimizing safety systems, virtual investigation methods of PTW passive safety are likewise not on par with those used for occupant protection. This study aims for a "proof of concept" through a virtual realization of the novel idea of PTW passive safety and predicting its performance to demonstrate if the idea has practical potential.

(RQ1) Is it safer to be restrained to a motorcycle?

The safety principle positively influences the intrinsic chaotic behavior of a motorcyclist in an accident impact, thereby drastically reducing impact loading. Compared to a chaotic and uncontrolled dismount, where the rider is exposed to the unpredictability of a motorcycle accident, in recommended representative accident configurations the rider shows predictable behavior and overall less critical biomechanical loads. It is an innovative passive safety idea for motorcycles in very different load cases without compromising a motorcycle's specific advantages as a compact means of transport, such as the great all-around visibility, and without losing its unique driving behavior. Similar to passive safety systems for automobile occupants, several safety systems effectively control and guide the motorcyclist's accident trajectory. Building on a robust accident response, the vehicle and rider behavior in other accident configurations can be continuously improved by refining system parameters, trying new system layouts and variants, or incorporating additional other safety systems.

So far, investigations of the restraint safety principle are limited to primary impacts in collisions with a passenger car according to a recognized standard. Thus, the performance is not designed and investigated in secondary impacts, rear-end scenarios, and solo accidents. Maintaining sufficient belt restraint and granting a protective cover for all possible load

directions will be challenging. In particular, the investigation with HBMs show that much needs to be examined in detail. Not wearing a helmet is an additional hurdle for an appropriate strategy and sufficient evidence to exclude detrimental effects in off-design scenarios holistically. However, wearing a helmet could increase neck tensile forces, which also needs to be investigated first.

(RQ2) What virtual models and numerical methods allow us to answer this?

This study presents computational models and methods to design a robust safety concept for a motorcycle in a systematic simulation workflow. The numerical research strategy is a multi-stage development process featuring models of successively increasing levels of model complexity and computational effort. The modeling features:

- An efficient multi-model approach that couples the full vehicle interaction of a PTW and an accident opponent from MB simulations with a detailed FE model of rider interaction surfaces of the PTW.

- An effective characterization of a computational material model of a foam material through a polynomial representation of experimental test data incorporating material card requirements and knowledge of material properties.

- A simulation-based method for positioning complex FE HBMs, including sex variants, in the characteristic posture of a motorcyclist.

It allows for a detailed representation of diverse motorcyclists and their interaction with a motorcycle and its passive safety systems. The strategy enables the virtual design and dimensioning of the novel restrain safety concept with minimal time and resources. With this variety of models, a large number of variants was covered by efficient low-fidelity models, thus enabling a fast and robust design of the safety systems. Equivalent high-fidelity models represent complex vehicle interactions, and up-to-date rider surrogate models allowed for investigating questions of great detail.

This methodology demonstrates a meaningful combination of current state-of-the-art MB and FE simulation software environments to model the same problem with method-specific advantages and disadvantages, outlining a novel procedure in virtual motorcycle accident research and passive safety equipment development. Although the procedure was applied for a motorcycle with a novel restraint safety concept, applying similar procedures in virtual research for conventional (powered) two-wheelers is highly desirable.

Outlook

In addition to investigating more accident scenarios, laboratory tests of the entire system will ultimately be necessary for the approval of the safety concept. With these experiments,

the modeling of the motorcycle and the passive safety system must be further verified. In addition, there will be many detailed questions on packaging and ergonomics that need to be investigated. Reviewing ergonomics and usability while being stationary and during driving is important since for example the concept does not allow the motorcyclist to "hang off" when cornering due to the body fairing with side impact structure.

The development and application of HBMs is an interesting field of research that is making great progress. This work shows in their special application as riders of PTWs that processes such as the positioning need to be further systematized, automated, and improved, e.g., through stress initialization. In the future, active HBMs may enable modeling a rider that holds on to the vehicle, whether while driving in the pre-crash phase or in low-dynamic accident phases, which could be a significant factor in an accident outcome. Scalable HBMs can model a diverse society.

The given simulation workflow and models offer many possibilities for additional links. An online-coupling between MB vehicle interaction in MADYMO and the detailed FE rider interaction modeling in Ls-Dyna may be useful. The vehicle interaction could also be extracted from the full FE simulations. These could then be used in an offline-coupling for the stage II simulations or be used as starting conditions for the stage I simulation, which after a prescribed primary impact, computationally efficiently predicts a long subsequent accident phase followed by a ground impact. To exploit the full range of modeling categories presented in Section 3.1.2, mathematical surrogate models can be developed. These could represent essential relationships for optimizations with significantly less computational effort.

Appendix

A.1 Exemplary Determination of Injury Criteria

Time History Data and Injury Criteria for Scenario ⑦ in Table 5.1
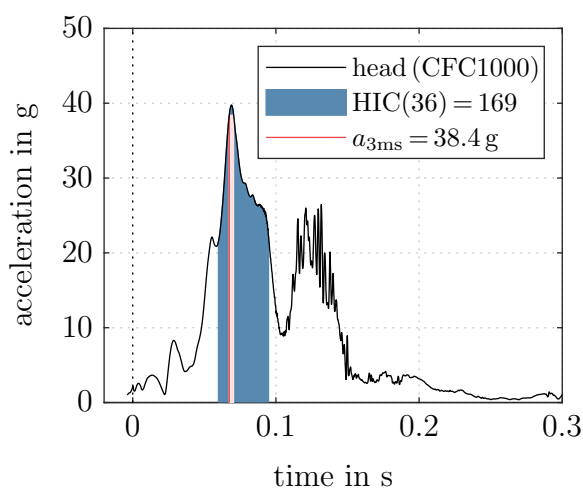
Figure A.1: Head linear acceleration.
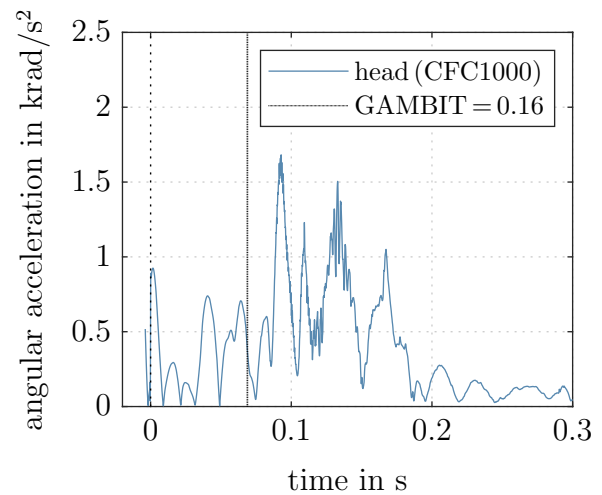
Figure A.2: Head angular acceleration.
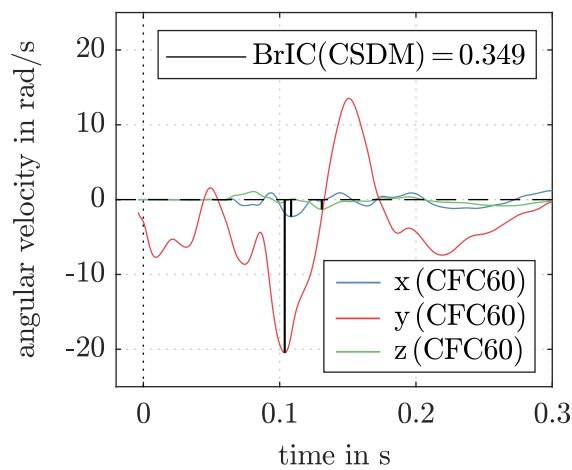
Figure A.3: Head angular velocity.
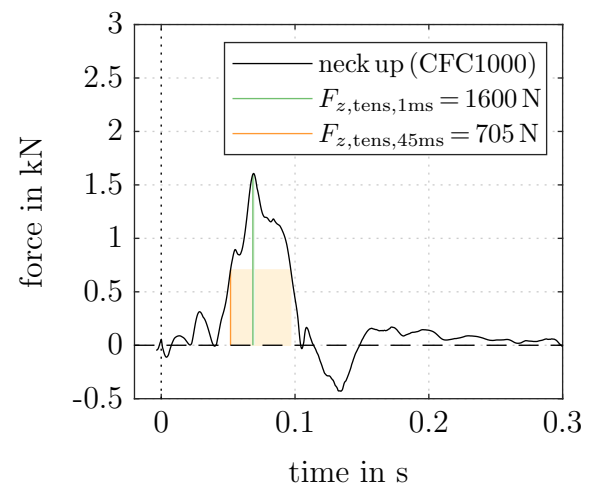
Figure A.4: Neck tensile force.
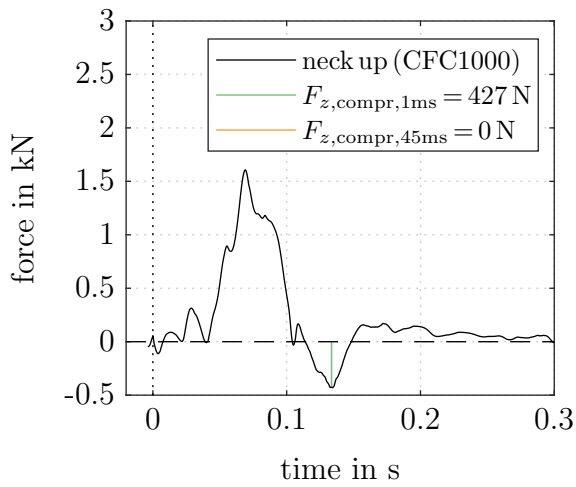
Figure A.5: Neck compression force.
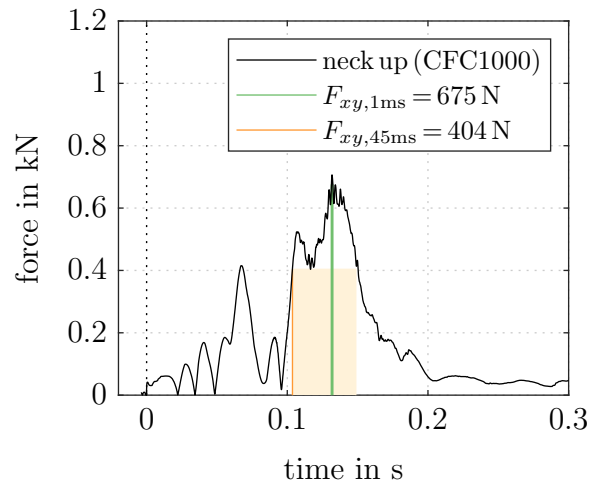
Figure A.6: Neck shear force.
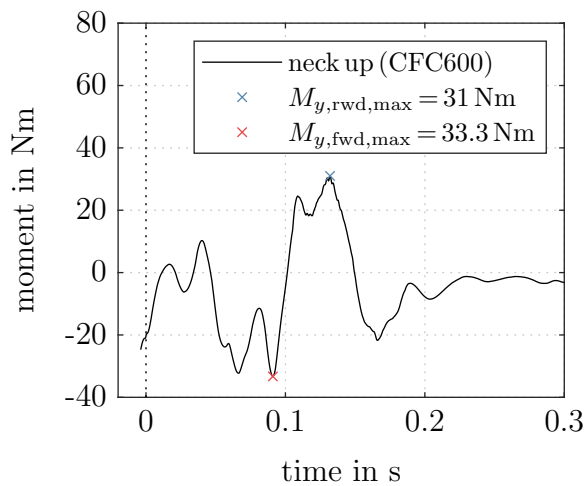
Figure A.7: Neck flexion and extension.
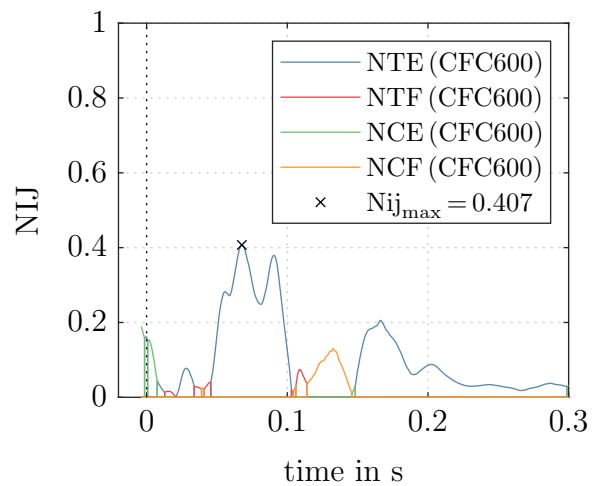
Figure A.8: Neck injury criterion.
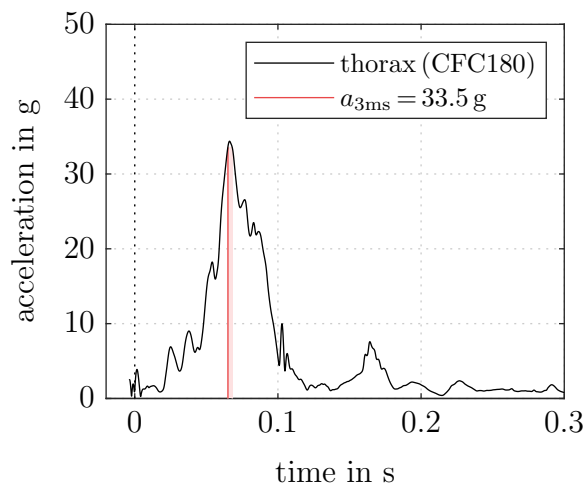
Figure A.9: Thorax linear acceleration.
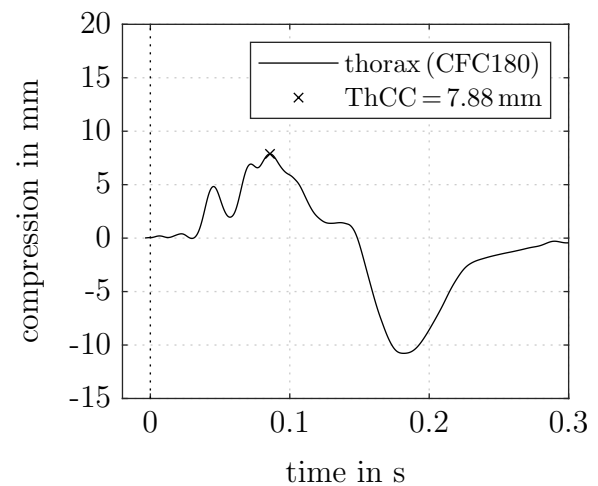
Figure A.10: Thorax compression.
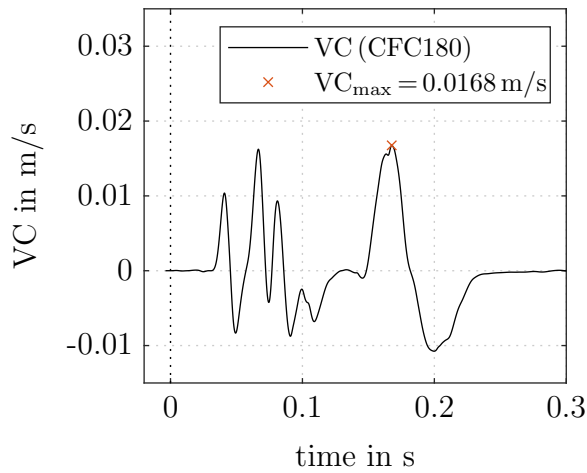
Figure A.11: Viscous criterion.
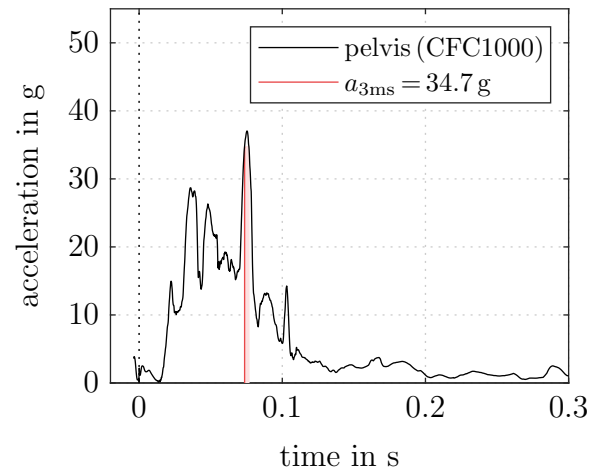
Figure A.12: Pelvis linear acceleration.
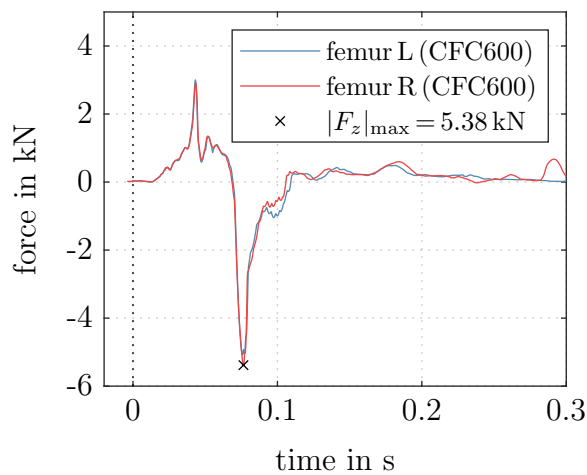
Figure A.13: Femur axial force.

Figure A.14: Tibia index.

A.2 Causes of Deaths

Leading Causes of Worldwide Deaths by Age Group, Compiled from the Data Set and Classification According to [WHO20] for 2019.

Ranking of the 116 different causes of death. The widths of the profiles at the tick marks represent the number of deaths.

0-28 days	1-59 months	5-14 years	15-29 years

preterm birth complications
birth asphyxia and birth trauma
neonatal sepsis and infections
lower respiratory infections
other congenital anomalies
other neonatal conditions
congenital heart anomalies
neural tube defects
childhood-cluster diseases
meningitis
stds excluding hiv
diarrhoeal diseases
other unintentional injuries
other chromosomal anomalies
down syndrome
exposure to mechanical forces
collective violence and legal intervention
encephalitis
other infectious diseases
falls
cleft lip and cleft palate
road injury
poisonings
fire, heat and hot substances
drowning
paralytic ileus and intestinal obstruction
other endocrine, blood and immune disorders
hiv/aids
stroke
other circulatory diseases
cardiomyopathy, myocarditis, endocarditis
other digestive diseases
thalassaemias
other malignant neoplasms
other urinary diseases
parasitic and vector diseases
leukaemia
brain and nervous system cancers
sickle cell disorders and trait
liver cancer
upper respiratory infections
otitis media
natural disasters
kidney cancer
other haemoglobinopathies and haemolytic anaemias
other neurological conditions
testicular cancer
interpersonal violence
self-harm
other musculoskeletal disorders
back and neck pain
gout
osteoarthritis
rheumatoid arthritis
gynecological diseases
infertility
urolithiasis
benign prostatic hyperplasia
kidney diseases
pancreatitis
gallbladder and biliary diseases
inflammatory bowel disease
gastritis and duodenitis
appendicitis
cirrhosis of the liver
peptic ulcer disease
other respiratory diseases
asthma
chronic obstructive pulmonary disease
ischaemic heart disease
hypertensive heart disease
rheumatic heart disease
non-migraine headache
migraine
multiple sclerosis
epilepsy
parkinson disease
alzheimer disease and other dementias
other mental and behavioural disorders
idiopathic intellectual disability
childhood behavioural disorders
autism and asperger syndrome
eating disorders
anxiety disorders
drug use disorders
alcohol use disorders
schizophrenia
bipolar disorder
depressive disorders
lymphomas, multiple myeloma
mesothelioma
thyroid cancer
larynx cancer
gallbladder and biliary tract cancer
bladder cancer
prostate cancer
ovary cancer
corpus uteri cancer
cervix uteri cancer
breast cancer
melanoma and other skin cancers
trachea, bronchus, lung cancers
pancreas cancer
colon and rectum cancers
stomach cancer
oesophagus cancer
mouth and oropharynx cancers
other nutritional deficiencies
iron-deficiency anaemia
vitamin a deficiency
iodine deficiency
protein-energy malnutrition
leprosy
intestinal nematode infections
hepatitis
tuberculosis

30-49 years	50-59 years	60-69 years	70+ years

ischaemic heart disease
stroke
chronic obstructive pulmonary disease
alzheimer disease and other dementias
lower respiratory infections
trachea, bronchus, lung cancers
hypertensive heart disease
kidney diseases
other circulatory diseases
diarrhoeal diseases
colon and rectum cancers
falls
stomach cancer
cirrhosis of the liver
other respiratory diseases
prostate cancer
parkinson disease
other digestive diseases
pancreas cancer
asthma
liver cancer
breast cancer
oesophagus cancer
other malignant neoplasms
other unintentional injuries
other urinary diseases
lymphomas, multiple myeloma
other infectious diseases
cardiomyopathy, myocarditis, endocarditis
road injury
bladder cancer
tuberculosis
rheumatic heart disease
leukaemia
mouth and oropharynx cancers
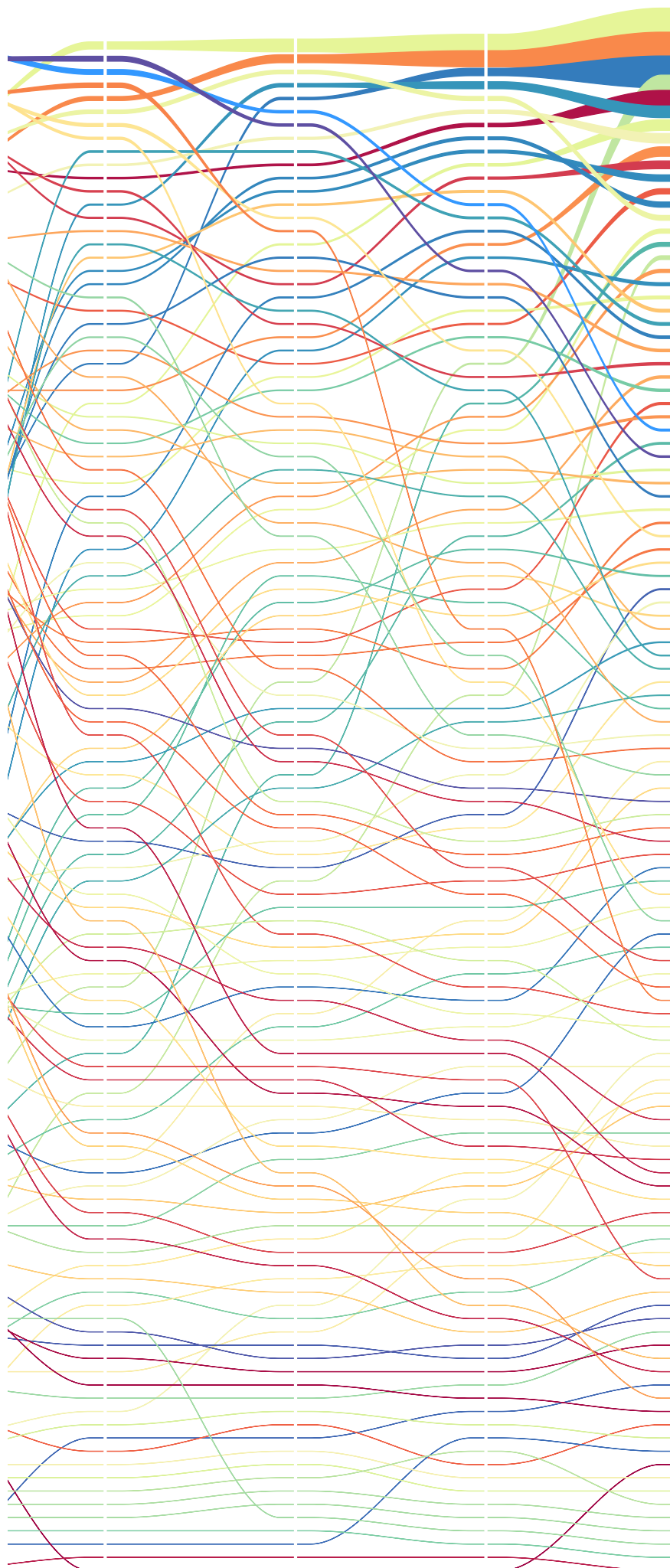peptic ulcer disease
other endocrine, blood and immune disorders
self-harm
paralytic ileus and intestinal obstruction
other neurological conditions
gallbladder and biliary tract cancer
protein-energy malnutrition
gallbladder and biliary diseases
kidney cancer
brain and nervous system cancers
melanoma and other skin cancers
cervix uteri cancer
ovary cancer
other musculoskeletal disorders
corpus uteri cancer
larynx cancer
parasitic and vector diseases
pancreatitis
drowning
rheumatoid arthritis
drug use disorders
other haemoglobinopathies and haemolytic anaemias
hepatitis
epilepsy
fire, heat and hot substances
meningitis
encephalitis
other nutritional deficiencies
thyroid cancer
interpersonal violence
gastritis and duodenitis
alcohol use disorders
iron-deficiency anaemia
mesothelioma
exposure to mechanical forces
inflammatory bowel disease
poisonings
hiv/aids
collective violence and legal intervention
appendicitis
multiple sclerosis
benign prostatic hyperplasia
urolithiasis
osteoarthritis
back and neck pain
upper respiratory infections
childhood-cluster diseases
schizophrenia
gynecological diseases
stds excluding hiv
congenital heart anomalies
other congenital anomalies
testicular cancer
other chromosomal anomalies
idiopathic intellectual disability
bipolar disorder
gout
natural disasters
down syndrome
otitis media
leprosy
intestinal nematode infections
anxiety disorders
neonatal sepsis and infections
sickle cell disorders and trait
neural tube defects
iodine deficiency
thalassaemias
birth asphyxia and birth trauma
cleft lip and cleft palate
migraine
vitamin a deficiency
preterm birth complications
infertility
non-migraine headache
other mental and behavioural disorders
childhood behavioural disorders
autism and asperger syndrome
eating disorders
depressive disorders
other neonatal conditions

A.3 Human Body Model Accident Response

Impact Response of Male HBM variants in Figur 5.21
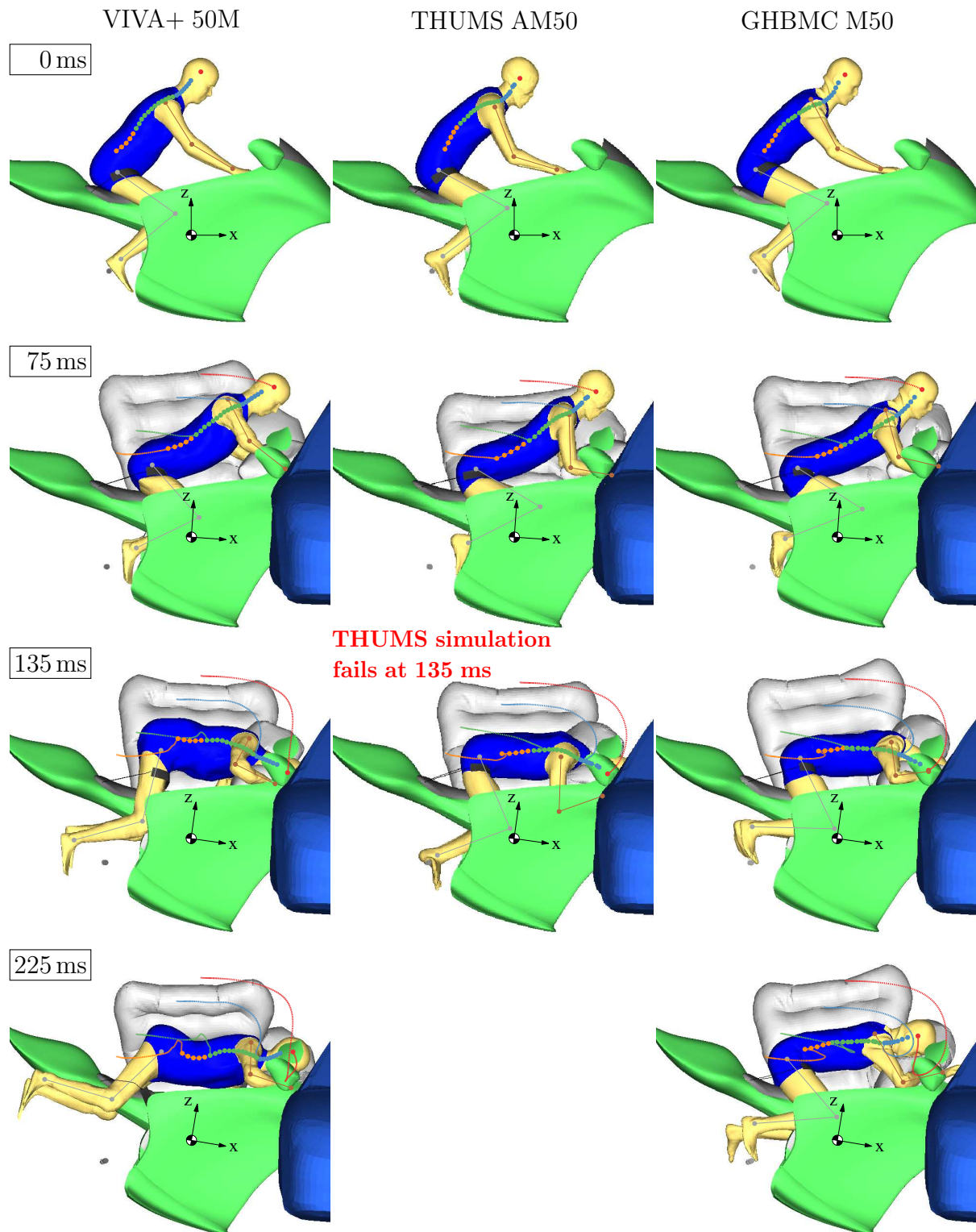
Figure A.15: Impact response in scenario ⑦.

VIVA+ 50M   THUMS AM50   GHBMC M50
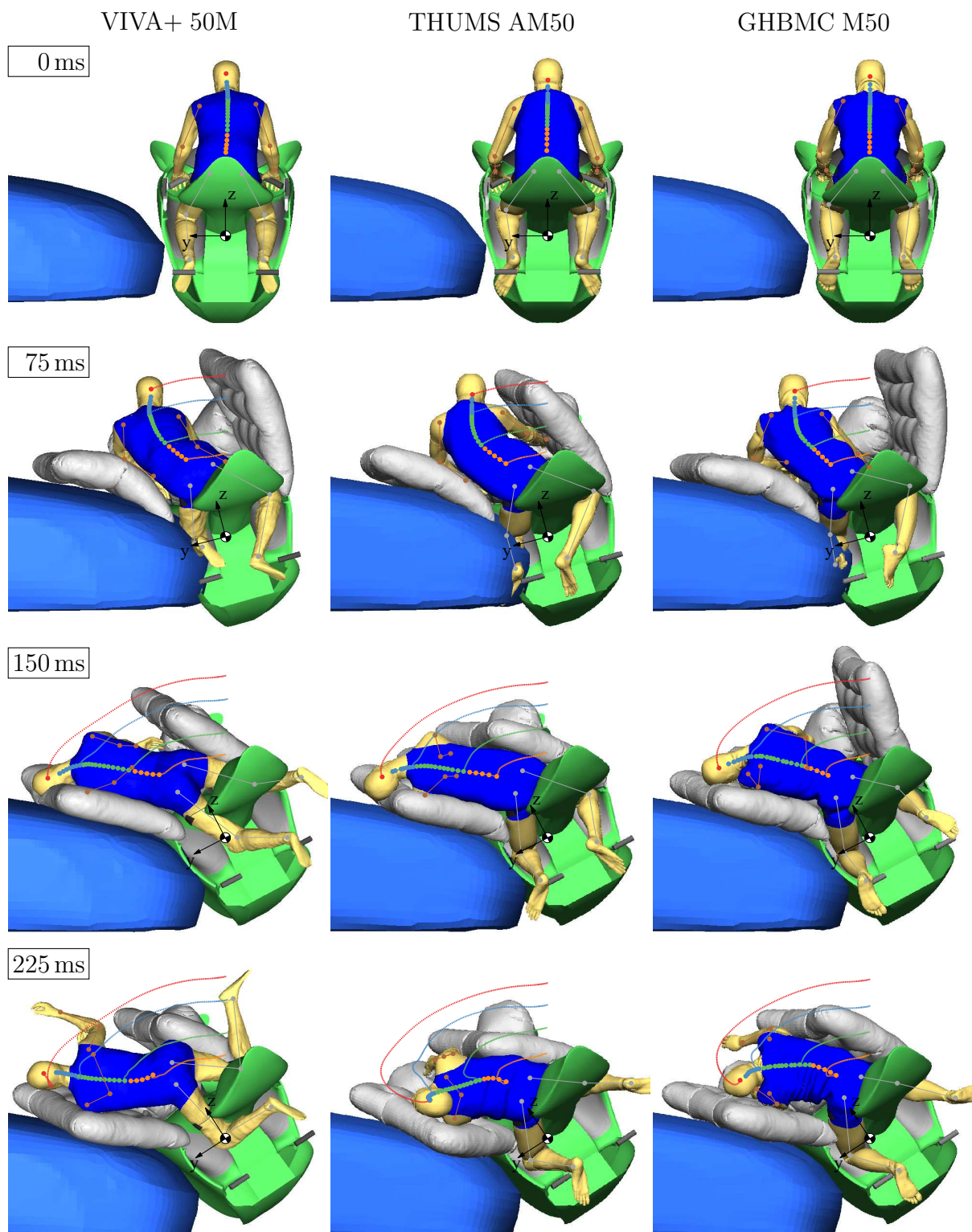
0 ms

75 ms

150 ms

225 ms

Figure A.16: Impact response in scenario ①.

A.4   Full FE Response of a Small Female ATD

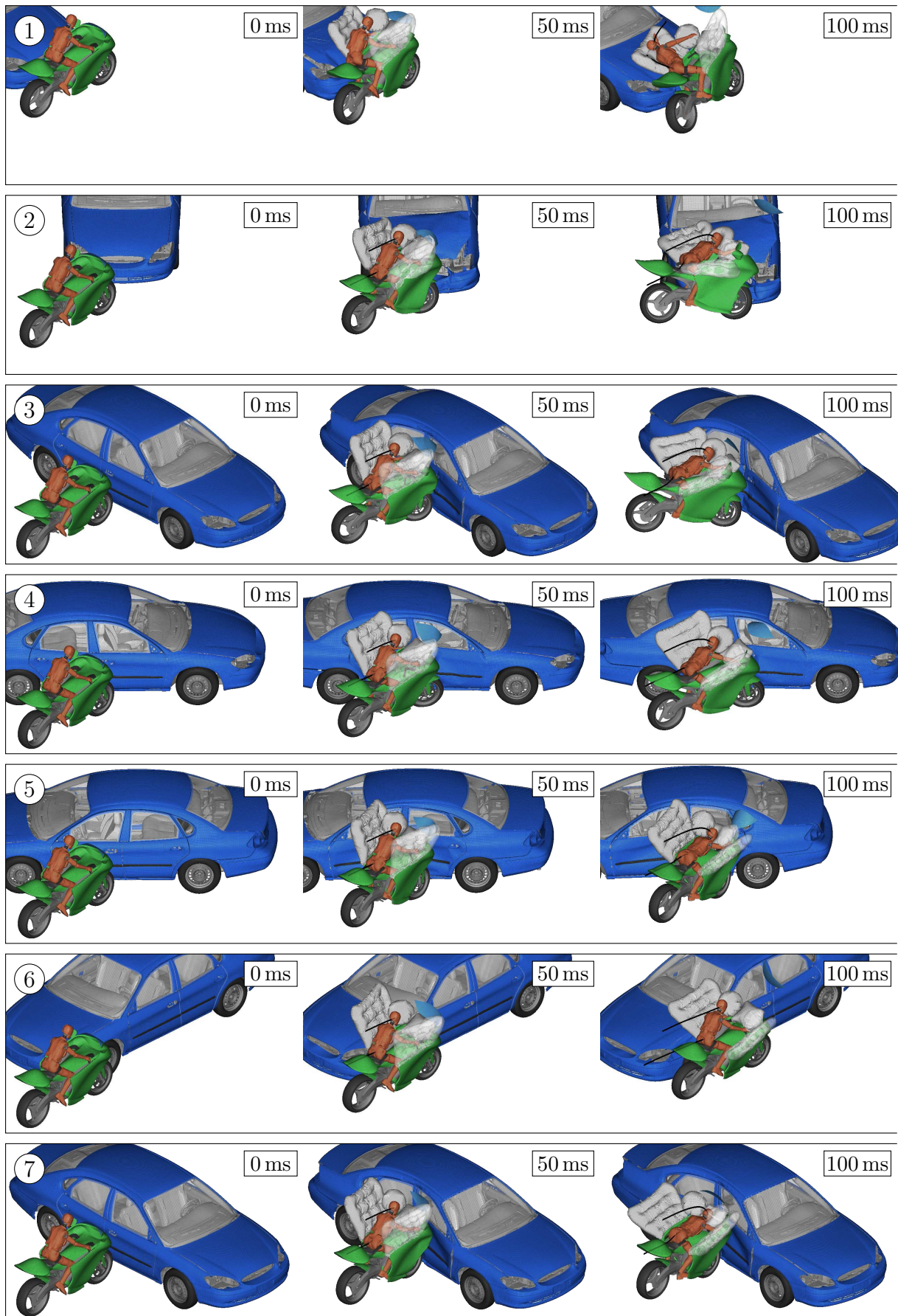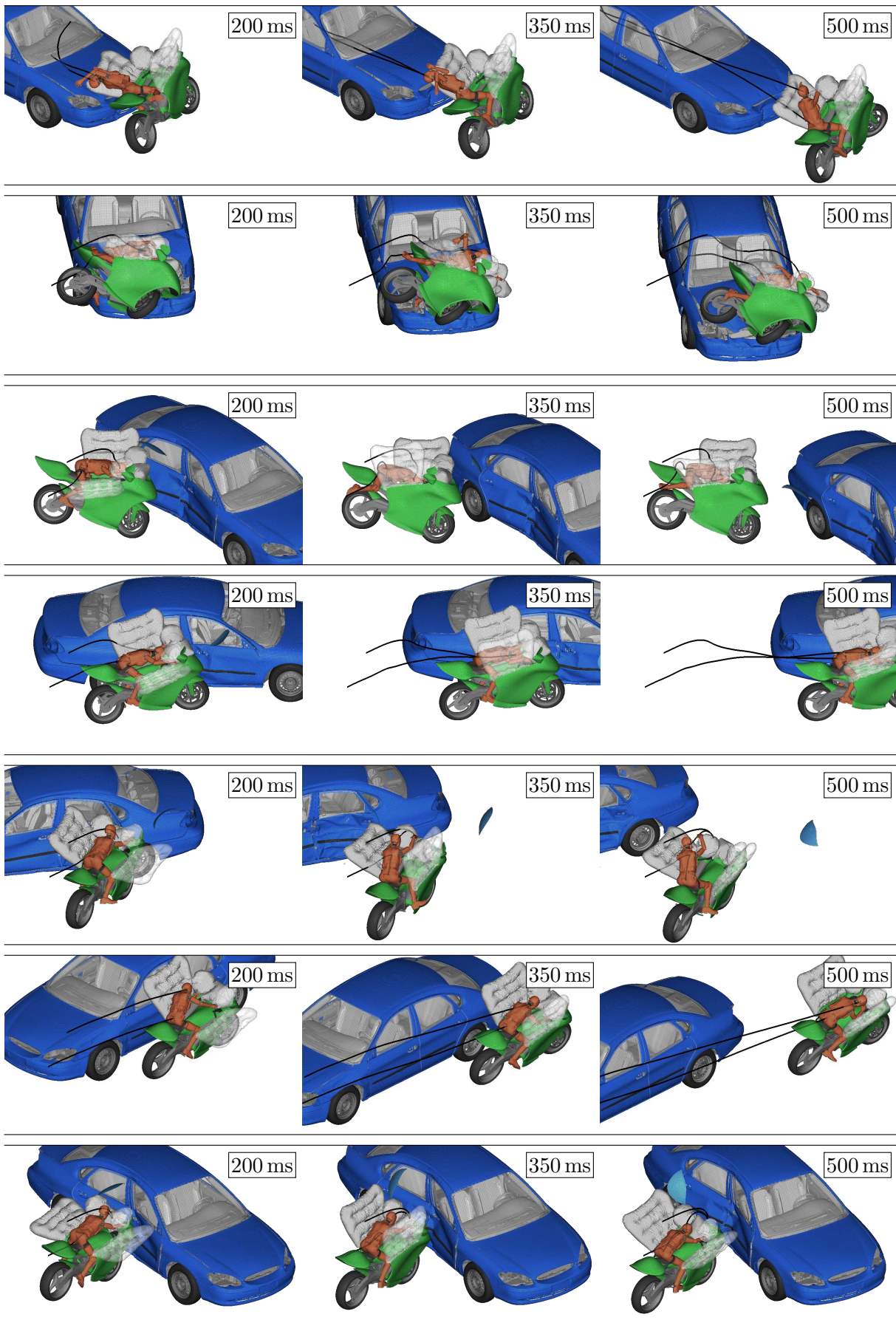**Full FE Simulations of the ISO 13232 Scenarios with the Hybrid III 5th**

Figure A.17: Full FE simulations of Hyb III 5$^{\text{th}}$ with head and pelvis trajectories (black).

Bibliography

[AbayazidEtAl21] Abayazid, F.; Ding, K.; Zimmerman, K.; Stigson, H.; Ghajari, M.: A New Assessment of Bicycle Helmets: The Brain Injury Mitigation Effects of New Technologies in Oblique Impacts. Annals of Biomedical Engineering, Vol. 49, No. 10, pp. 2716–2733, 2021.

[ACEM03] ACEM: MAIDS – In-depth Investigations of Accidents Involving Powered Two Wheelers, Report on the Project Methodology and Process. European Association of Motorcycle Manufacturers (ACEM), Brussels, Belgium, 2003.

[ACEM09a] ACEM: MAIDS – In-depth Investigations of Accidents Involving Powered Two Wheelers, Final Report 2.0. European Association of Motorcycle Manufacturers (ACEM), Brussels, Belgium, 2009.

[ACEM09b] ACEM: MAIDS – In-depth Investigations of Accidents Involving Powered Two Wheelers, Presentation of the MAIDS Report with L1-L3 Comparison. European Association of Motorcycle Manufacturers (ACEM), Brussels, Belgium, 2009.

[AikyoEtAl15] Aikyo, Y.; Kobayashi, Y.; Akashi, T.; Ishiwatari, M.: Feasibility Study of Airbag Concept Applicable to Motorcycles Without Sufficient Reaction Structure. Traffic Injury Prevention, Vol. 16, Supplement 1, pp. 148–152, 2015.

[AlbaneseEtAl17] Albanese, B.; Gibson, T.; Whyte, T.; Meredith, L.; Savino, G.; de Rome, L.; Baldock, M.; Fitzharris, M.; Brown, J.: Energy Attenuation Performance of Impact Protection Worn by Motorcyclists in Real-world Crashes. Traffic Injury Prevention, Vol. 18, Supplement 1, pp. 116–121, 2017.

[AppelOtteWüstemann86] Appel, H.; Otte, D.; Wüstemann, J.: Epidemiologie von Unfällen motorisierter Zweiradfahrer in der Bundesrepublik Deutschland - Sicherheitsaspekte (in German). In Koch, H. (Ed.): Der Motorradunfall: Beschreibung, Analyse, Prävention, Forschungshefte Zweiradsicherheit, pp. 47–92, Bremerhaven: Wirtschaftsverlag NW, 1986.

[ArunachalamEtAl19] Arunachalam, M.; Mondal, C.; Singh, G.; Karmakar, S.: Motorcycle Riding Posture: A Review. Measurement, Vol. 134, pp. 390–399, 2019.

[Autoliv22] Autoliv: Annual and Sustainability Report 2021. Autoliv Inc., Stockholm, Sweden, 2022.

[AvalleBelingardiScattina13] Avalle, M.; Belingardi, G.; Scattina, A.: Numerical and Experimental Investigation of a Lightweight Bonnet for Pedestrian Safety. International Journal of Crashworthiness, Vol. 18, No. 1, pp. 29–39, 2013.

[BarbaniBaldanziniPierini14] Barbani, D.; Baldanzini, N.; Pierini, M.: Development and Validation of an FE Model for Motorcycle–Car Crash Test Simulations. International Journal of Crashworthiness, Vol. 19, No. 3, pp. 244–263, 2014.

[BASt23] BASt: Verkehrs- und Unfalldaten, Kurzzusammenstellung der Entwicklung in Deutschland (in German), Bundesanstalt für Straßenwesen (BASt), Bergisch Gladbach, Germany, 2023.
https://www.bast.de/DE/Publikationen/Medien/VU-Daten/VU.html, accessed March 29, 2023.

[Bathe96] Bathe, K.J.: Finite Element Procedures. Upper Saddle River: Prentice-Hall, 1996.

[Beckmann20] Beckmann, D.: Entwicklung eines Finite-Elemente Modells eines Motorrads in LS-DYNA (in German). Studienarbeit STUD-496, Institut für Technische und Numerische Mechanik, Universität Stuttgart, 2020.

[Belytschko92] Belytschko, T.: On Computational Methods for Crashworthiness. Computers & Structures, Vol. 42, No. 2, pp. 271–279, 1992.

[BelytschkoLiuMoran00] Belytschko, T.; Liu, W.K.; Moran, B.: Nonlinear Finite Elements for Continua and Structures. Chichester: John Wiley & Sons, 2000.

[BergBürkleSchmidts98] Berg, F.A.; Bürkle, H.; Schmidts, F.: Analysis of the Passive Safety of Motorcycles Using Accident Investigations and Crash Tests. In Proceedings of the 16th International Technical Conference on the Enhanced Safety of Vehicles (ESV), 98-S10-O-11, pp. 2221–2236, Winsor Ontario, Canada, 1998.

[BergEtAl04] Berg, F.A.; Rücker, P.; Bürkle, H.; Mattern, R.; Kallieris, D.: Prüfverfahren für die passive Sicherheit motorisierter Zweiräder: Bericht zum Forschungsprojekt FE 82.121/1997 (in German). Berichte der Bundesanstalt für Straßenwesen. F, Fahrzeugtechnik; 49. Bremerhaven: Wirtschaftsverlag NW, Verlag für neue Wissenschaft, 2004.

[Bhosale13] Bhosale, P.V.: Exploratory Study on the Suitability of an Airbag for an Indian Motorcycle Using Finite Element Computer Simulations of Rigid Wall Barrier Test. In Proceedings of the 23rd International Technical Conference on the Enhanced Safety of Vehicles (ESV), 13-0195, Seoul, Korea, 2013.

[BońkowskiHynčíkLv20] Bońkowski, T.; Hynčík, L.; Lv, W.: PTW Passive Safety: Numerical Study of Standard Impact Scenarios with Rider Injury Risk Assessment. SAE Technical Paper 2020-01-0930, pp. 1–27, 2020.

[BothwellKnightPeterson73] Bothwell, P.W.; Knight, R.E.; Peterson, H.C.: Motorcycle Crash Safety Research. In Proceedings of the Vehicle Safety Research Symposium, pp. 217–241, Washington, DC: U.S. Department of Transportation, National Highway Traffic Safety Administration, 1973.

[BrunnerEtAl18] Brunner, H.; Hirz, M.; Hirschberg, W.; Fallast, K.: Evaluation of Various Means of Transport for Urban Areas. Energy, Sustainability and Society, Vol. 8, pp. 117–121, 2018.

[BTS21] BTS: National Transportation Statistics 2021, 50$^{\text{th}}$ Anniversary Edition. U.S. Department of Transportatio, Bureau of Transportation Statistics (BTS), Washington, DC, 2021.

[BürkleBerg01] Bürkle, H.; Berg, F.A.: Anprallversuche mit Motorrädern an passiven Schutzeinrichtungen: Bericht zum Forschungsprojekt 03.318/1998/FRB des Bundesministeriums für Verkehr, Bau- und Wohnungswesen (in German). Berichte der Bundesanstalt für Straßenwesen. V, Verkehrstechnik; 90. Bremerhaven: Wirtschaftsverlag NW, Verlag für neue Wissenschaft, 2001.

[CanapleEtAl02] Canaple, B.; Rungen, G.P.; Markiewicz, E.; Drazetic, P.; Happian-Smith, J.; Chinn, B.P.; Cesari, D.: Impact Model Development for the Reconstruction of Current Motorcycle Accidents. International Journal of Crashworthiness, Vol. 7, No. 3, pp. 307–320, 2002.

[CarmaiKoetniyomHossian19] Carmai, J.; Koetniyom, S.; Hossian, W.: Analysis of Rider and Child Pillion Passenger Kinematics Along with Injury Mechanisms During Motorcycle Crash. Traffic Injury Prevention, Vol. 20, Supplement 1, pp. 13–20, 2019.

[CarmaiKoetniyomHossian20] Carmai, J.; Koetniyom, S.; Hossian, W.: Study of Motorcyclist's Injury Patterns in Motorcycle-Pickup Truck Collision Using Finite Element Simulations. In Proceedings of the IRCOBI Conference Asia, IRC-A-20-26, pp. 68–71, Beijing, China, 2020.

[CarrollEtAl22] Carroll, J.; Been, B.; Sundmark, H.; Burleigh, M.; Li, B.: A Powered Two-Wheeler Crash Test Dummy. In Proceedings of the IRCOBI Conference, IRC-22-26, pp. 114–115, Porto, Portugal, 2022.

[ChawlaBhosaleMukherjee05] Chawla, A.; Bhosale, P.V.; Mukherjee, S.: Modeling of Folding of Passenger Side Airbag Mesh. SAE Paper No. 2005-26-059, pp. 687–693, 2005.

[ChawlaEtAl05] Chawla, A.; Mukherjee, S.; Mohan, D.; Bose, D.; Rawat, P.; Nakatani, T.; Sakurai, M.: FE Simulations of Motorcycle – Car Frontal Crashes, Validations and Observations. International Journal of Crashworthiness, Vol. 10, No. 4, pp. 319–326, 2005.

[ChawlaMukherjee07] Chawla, A.; Mukherjee, S.: Motorcycle Safety Device Investigation: A Case Study on Airbags. Sadhana, Vol. 32, pp. 427–443, 2007.

[ChinnEtAl96] Chinn, B.P.; Okello, J.A.; McDonough; P J, G. Grose: Development and Testing of a Purpose Built Motorcycle Airbag Restraint System. In Proceedings of the 15th International Technical Conference on the Enhanced Safety of Vehicles (ESV), 96-S7-O-13, pp. 1167–1188, Melbourne, Australia, 1996.

[ChristBüttner12] Christ, A.; Büttner, J.: Detailed Passenger Airbag Modelling for Early Stage Events. In Proceedings of the 11th German LS-DYNA Forum, Ulm, Germany, 2012.

[CroopLobo09] Croop, B.; Lobo, H.: Selecting Material Models for the Simulation of Foams in LS-DYNA. In Proceedings of the 7th European LS-DYNA Conference, Salzburg, Austria, 2009.

[DanielloCristinoGabler13] Daniello, A.; Cristino, D.; Gabler, H.C.: Relationship between Rider Trajectory and Injury Outcome in Motorcycle-to-Barrier Crashes. Transportation Research Record, Vol. 2388, No. 1, pp. 47–53, 2013.

[Daub21] Daub, S.: Untersuchung von Sensorkonzepten zur Unfallerkennung von Motorrädern (in German). Bachelorarbeit BSC-137, Institut für Technische und Numerische Mechanik, Universität Stuttgart, 2021.

[de RomeEtAl11] de Rome, L.; Ivers, R.; Fitzharris, M.; Du, W.; Haworth, N.; Heritier, S.; Richardson, D.: Motorcycle Protective Clothing: Protection from Injury or Just the Weather? Accident Analysis & Prevention, Vol. 43, No. 6, pp. 1893–1900, 2011.

[DeanEtAl21] Dean, M.; Haus, S.H.; Sherony, R.; Gabler, H.C.: Potential Crash Benefits of Motorcycle-Detecting Automatic Emergency Braking Systems. In Proceedings of the IRCOBI Conference, IRC-21-15, pp. 39–50, Munich, Germany, 2021.

[DeckWillinger08] Deck, C.; Willinger, R.: Improved Head Injury Criteria Based on Head FE Model. International Journal of Crashworthiness, Vol. 13, pp. 667–678, 2008.

[Destatis21a] Destatis: Kraftrad- und Fahrradunfälle im Straßenverkehr 2020 (in German). Statistisches Bundesamt (Destatis), 2021.

[Destatis21b] Destatis: Verkehrsunfälle 2020, Verkehr, Fachserie 8, Reihe 7 (in German). Statistisches Bundesamt (Destatis), 2021.

[DorockiWantuch-Matla21] Dorocki, S.; Wantuch-Matla, D.: Power Two-Wheelers as an Element of Sustainable Urban Mobility in Europe. Land, Vol. 10, No. 6, 2021.

[Du BoisEtAl04] Du Bois, P.; Chou, C.C.; Fileta, B.B.; Khalil, T.B.; King, A.I.; Mahmood, H.F.; Mertz, H.J.; Wismans, J.: Vehicle Crashworthiness and Occupant Protection. Southfield, MI: American Iron and Steel Institute, 2004.

[DuddeckWehrle15] Duddeck, F.; Wehrle, E.: Recent Advances on Surrogate Modeling for Robustness Assessment of Structures with Respect to Crashworthiness Requirements. In Proceedings of the 10th European LS-DYNA Users Conference, Würzburg, Germany, 2015.

[EberhardSchiehlen06] Eberhard, P.; Schiehlen, W.: Computational Dynamics of Multibody Systems: History, Formalisms, and Applications. Journal of Computational and Nonlinear Dynamics, Vol. 1, No. 1, pp. 3–12, 2006.

[EkmejianEtAl16] Ekmejian, R.; Sarrami, P.; Naylor, J.M.; Harris, I.A.: A Systematic Review on the Effectiveness of Back Protectors for Motorcyclists. Scandinavian Journal of Trauma, Resuscitation and Emergency Medicine, Vol. 24, No. 115, 2016.

[EN1621-1:2012] EN 1621-1:2012: Motorcyclists' Protective Clothing Against Mechanical Impact – Part 1: Motorcyclists' Limb Joint Impact Protectors - Requirements and Test Methods. European Committee for Standardization, Brussels, Belgium, 2012.

[EN1621-2:2014] EN 1621-2:2014: Motorcyclists' Protective Clothing Against Mechanical Impact – Part 2: Motorcyclists' Back Protectors - Requirements and Test Methods. European Committee for Standardization, Brussels, Belgium, 2014.

[Engel92] Engel, A.: Airbag für motorisierte Zweiräder: Bericht zum Projekt 1.8903 der fahrzeugtechnischen Forschung des Bundesministers für Verkehr (in German). Forschungsberichte des Bundesministers für Verkehr, Bereich Fahrzeugtechnik; 8. Bergisch Gladbach: Bundesanstalt für Straßenwesen, 1992.

[EppingerEtAl99] Eppinger, R.; Sun, E.; Bandak, F.; Haffner, M.; Khaewpong, N.; Maltese, M.; Kuppa, S.; Nguyen, T.; Takhounts, E.; Tannous, R.; Zhang, A.; Saul, R.: Development of Improved Injury Criteria for the Assessment of Advanced Automotive Restraint Systems – II, NHTSA Docket No. 99-6407-5. National Highway Transport Safety Association (NHTSA), Washington, DC, 1999.

[EuroNCAP17] Euro NCAP: Euro NCAP Road Map 2025 – In Pursuit of Vision Zero. European New Car Assessment Programme (Euro NCAP), Leuven, Belgium, 2017.

[EuroNCAP21] Euro NCAP: Vulnerable Road User Testing Protocol, Version 9.0. European New Car Assessment Programme (Euro NCAP), Brussels, Belgium, 2021.

[EuroNCAP22] Euro NCAP: Euro NCAP Vision 2030 – A Safer Future for Mobility. European New Car Assessment Programme (Euro NCAP), Leuven, Belgium, 2022.

[EuropeanParliamentandCouncil13] European Parliament and Council: Regulation (EU) No 168/2013 of the European Parliament and of the Council of 15 January 2013 on the Approval and Market Surveillance of Two- or Three-Wheel Vehicles and Quadricycles, 2013.

[FahseEtAl23] Fahse, N.; Millard, M.; Kempter, F.; Maier, S.; Roller, M.; Fehr, J.: Dynamic Human Body Models in Vehicle Safety: An Overview. GAMM Mitteilungen, 2023.

[Fehr11] Fehr, J.: Automated and Error-Controlled Model Reduction in Elastic Multibody Systems (in German). Dissertation, Schriften aus dem Institut für Technische und Numerische Mechanik der Universität Stuttgart, Vol. 21. Aachen: Shaker Verlag, 2011.

[FehrEberhard11] Fehr, J.; Eberhard, P.: Simulation Process of Flexible Multibody Systems with Non-modal Model Order Reduction Techniques. Multibody System Dynamics, Vol. 25, No. 3, pp. 313–334, 2011.

[FehrEtAl18] Fehr, J.; Grunert, D.; Holzwarth, P.; Fröhlich, B.; Walker, N.; Eberhard, P.: Morembs—A Model Order Reduction Package for Elastic Multibody Systems and Beyond. In Keiper, W.; Milde, A.; Volkwein, S. (Eds.): Reduced-Order Modeling (ROM) for Simulation and Optimization: Powerful Algorithms as Key Enablers for Scientific Computing, pp. 141–166. Cham: Springer International Publishing, 2018.

[FernandesAlves de Sousa13] Fernandes, F.; Alves de Sousa, R.: Motorcycle Helmets – A State of the Art Review. Accident Analysis & Prevention, Vol. 56, pp. 1–21, 2013.

[FiorelloEtAl16] Fiorello, D.; Martino, A.; Zani, L.; Christidis, P.; Navajas-Cawood, E.: Mobility Data Across the EU 28 Member States: Results from an Extensive CAWI Survey. Transportation Research Procedia, Vol. 14, pp. 1104–1113, 2016.

[FloresLankarani16] Flores, P.; Lankarani, H.M.: Contact Force Models for Multibody Dynamics, Vol. 226 of Solid Mechanics and Its Applications. Cham, Switzerland: Springer, 2016.

[FokinLokhandeFredriksson03] Fokin, D.; Lokhande, N.; Fredriksson, L.: On Airbag Simulation in LS-DYNA With the Use of the Arbitrary Lagrangian-Eulerian Method. In Proceedings of the 4th European LS-DYNA Users Conference, pp. 11–22, Ulm, Germany, 2003.

[FormanEtAl12] Forman, J.L.; Kent, R.W.; Mroz, K.; Pipkorn, B.; Bostrom, O.; Segui-Gomez, M.: Predicting Rib Fracture Risk With Whole-Body Finite Element Models:

Development and Preliminary Evaluation of a Probabilistic Analytical Framework. In Annals of Advances in Automotive Medicine/Annual Scientific Conference, Vol. 56, pp. 109–124, Seattle, WA: Association for the Advancement of Automotive Medicine, 2012.

[FranzEtAl13] Franz, U.; Lorenz, B.; Remfrey, J.; Schöneburg, R.: Integrale Sicherheit von Kraftfahrzeugen: Biomechanik - Simulation - Sicherheit im Entwicklungsprozess (in German). Wiesbaden: Springer Vieweg, 4th Edn., 2013.

[GalijatovicEtAl22] Galijatovic, E.; Eichlseder, M.; Heindl, S.F.; Klug, C.: Integrity of Virtual Testing for Crash Protection. Frontiers in Future Transportation, Vol. 3, pp. 1–12, 2022.

[GärtnerRückerBerg06] Gärtner, M.; Rücker, P.; Berg, F.A.: Entwicklung und Prüfung der Anforderungen an Schutzeinrichtungen zur Verbesserung der Sicherheit von Motorradfahrern: Bericht zum Forschungs- und Entwicklungsvorhaben 03.345/2001/FRB des Bundesministeriums für Verkehr, Bau und Stadtentwicklung (in German). Forschung Straßenbau und Straßenverkehrstechnik; 940. Bremerhaven: Wirtschaftsverlag NW, Verlag für neue Wissenschaft, 2006.

[GayzikEtAl12] Gayzik, F.S.; Moreno, D.P.; Vavalle, N.A.; Rhyne, A.C.; Stitzel, J.D.: Development of a Full Human Body Finite Element Model for Blunt Injury Prediction Utilizing a Multi-Modality Medical Imaging Protocol. In Proceedings of the 12th International LS-DYNA Users Conference, pp. 1–14, Dearborn, MI, USA, 2012.

[GehreGadesWernicke09] Gehre, C.; Gades, H.; Wernicke, P.: Objective Rating of Signals Using Test and Simulation Responses. In Proceedings of the 21st International Technical Conference on the Enhanced Safety of Vehicles (ESV), 09-0407, Stuttgart, Germany, 2009.

[Gennarelli08] Gennarelli, T.A.; Wodzin, E. (Eds.): Abbreviated Injury Scale 2005 - Update 2008. Association for the Advancement of Automotive Medicine (AAAM), Barrington, IL, 2008.

[GennarelliWodzin06] Gennarelli, T.A.; Wodzin, E.: AIS 2005: A Contemporary Injury Scale. Injury, Vol. 37, No. 12, pp. 1083–1091, 2006. Special Issue: Trauma Outcomes.

[GermanettiEtAl22] Germanetti, F.; Fiumarella, D.; Belingardi, G.; Scattina, A.: Injury Criteria for Vehicle Safety Assessment: A Review with a Focus Using Human Body Models. Vehicles, Vol. 4, No. 4, pp. 1080–1095, 2022.

[GrandelSchapter87] Grandel, J.; Schapter, D.: Investigation Into Motorcycle, Driver and Passenger Safety in Motorcycle Accidents with Two Motorcycle Riders. In Proceedings of the 11th International Technical Conference on the Experimental Safety of Vehicles (ESV), pp. 888–900, Washington, DC, 1987.

[GrassiEtAl18a] Grassi, A.; Baldanzini, N.; Barbani, D.; Pierini, M.: A Comparative Analysis of MAIDS and ISO13232 Databases for the Identification of the Most Representative Impact Scenarios for Powered 2-Wheelers in Europe. Traffic Injury Prevention, Vol. 19, No. 7, pp. 766–772, 2018.

[GrassiEtAl18b] Grassi, A.; Barbani, D.; Baldanzini, N.; Barbieri, R.; Pierini, M.: Belted Safety Jacket: A New Concept in Powered Two-Wheeler Passive Safety. Procedia Structural Integrity, Vol. 8, pp. 573–593, 2018.

[GrunertFehr16] Grunert, D.; Fehr, J.: Identification of Nonlinear Behavior with Clustering Techniques in Car Crash Simulations for Better Model Reduction. Advanced Modeling and Simulation in Engineering Sciences, Vol. 3, No. 1, pp. 1–19, 2016.

[Gu22] Gu, L.: Inflation, Weak Growth and Uncertainties Cloud Global Auto Sales Outlook. Scotiabank Economics, 2022.
https://www.scotiabank.com/ca/en/about/economics/economics-publications/post.other-publications.autos.global-auto-report.september-22--2022.html, accessed January 10, 2023.

[Hallquist06] Hallquist, J.O.: LS-DYNA Theory Manual. Livermore Software Technology Corporation (LSTC), Livermore, CA, 2006.

[HallquistEtAl06] Hallquist, J.O.; et al.: LS-DYNA Theory Manual. Livermore software Technology corporation, Vol. 3, pp. 25–31, 2006.

[Happian-SmithMacaulayChinn87] Happian-Smith, J.; Macaulay, M.; Chinn, B.: Motorcycle Impact Simulation and Practical Verification. In Proceedings of the 11th International Technical Conference on the Experimental Safety of Vehicles (ESV), pp. 858–865, Washington, DC, 1987.

[Haworth03] Haworth, N.: How Valid are Motorcycle Safety Data? In Proceedings of the Australasian Road Safety Research, Policing and Education Conference, Vol. 7, pp. 143–149, Monash University, 2003.

[Haworth12] Haworth, N.: Powered Two Wheelers in a Changing World—Challenges and Opportunities. Accident Analysis & Prevention, Vol. 44, No. 1, pp. 12–18, 2012.

[Hay22] Hay, J.: A Surrogate Model-enhanced Simulation Framework for Safety Performance Assessment of Integrated Vehicle Safety Systems. Dissertation, Schriften aus dem Institut für Technische und Numerische Mechanik der Universität Stuttgart, Vol. 75. Aachen: Shaker Verlag, 2022.

[HayFehrSchories20] Hay, J.; Fehr, J.; Schories, L.: Crash Pulse Prediction for Scenario-based Vehicle Crash FE-Simulations. In Proceedings of the IRCOBI Conference, IRC-20-22, pp. 199–200, Munich, Germany, 2020.

[Hiemer05] Hiemer, M.: Model Based Detection and Reconstruction of Road Traffic Accidents. Karlsruhe: Universitätsverlag Karlsruhe, 2005.

[HirthHaufeOlovsson07] Hirth, A.; Haufe, A.; Olovsson, L.: Airbag Simulation with LS-DYNA Past – Present – Future. In Proceedings of the 6th German LS-DYNA Forum, pp. 57–74, Frankenthal, Germany, 2007.

[Håland06] Håland, Y.: The Evolution of the Three Point Seat Belt from Yesterday to Tomorrow. In Proceedings of the IRCOBI Conference, pp. 3–15, Madrid, Spain, 2006.

[HuangEtAl18] Huang, Y.; Zhou, Q.; Tang, J.; Nie1, B.: A Preliminary Comparative Study on Rider Kinematics and Injury Mechanism in Car-to-Two-Wheelers Collisions. In Proceedings of the IRCOBI Conference, IRC-18-28, pp. 184–186, Athens, Greece, 2018.

[HwangEtAl16] Hwang, J.; Knapik, G.G.; Dufour, J.S.; Marras, W.S.: Curved Muscles in Biomechanical Models of the Spine: a Systematic Literature Review. Ergonomics, pp. 1–12, 2016.

[IbitoyeEtAl09] Ibitoye, A.B.; Hamouda, A.M.S.; Wong, S.V.; Umar, R.S.R.: Simulation of Motorcycle Crashes with W-beam Guardrail: Injury Patterns and Analysis. Proceedings of the Institution of Mechanical Engineers, Part H: Journal of Engineering in Medicine, Vol. 223, No. 8, pp. 1033–1040, 2009.

[ISO13232:2005] ISO 13232:2005: Motorcycles – Test and Analysis Procedures for Research Evaluation of Rider Crash Protective Devices Fitted to Motorcycles. International Organization for Standardization, Geneva, Switzerland, 2005.

[ISO/TS18571:2014] ISO/TS 18571:2014: Road Vehicles – Objective Rating Metric for Non-Ambiguous Signals. International Organization for Standardization, Geneva, Switzerland, 2014.

[IwamotoNakahiraKimpara15] Iwamoto, M.; Nakahira, Y.; Kimpara, H.: Development and Validation of the Total HUman Model for Safety (THUMS) Toward Further Understanding of Occupant Injury Mechanisms in Precrash and During Crash. Traffic Injury Prevention, Vol. 16, pp. 36–48, 2015.

[JohnEtAl22] John, J.D.; Klug, C.; Kranjec, M.; Svenning, E.; Iraeus, J.: Hello, world! VIVA+: A Human Body Model Lineup to Evaluate Sex-Differences in Crash Protection. Frontiers in Bioengineering and Biotechnology, Vol. 10, 2022.

[KalliskeAlbus98] Kalliske, I.; Albus, C.: Safety Potential of Future Two-Wheel Concepts – A Challenge. In Proceedings of the 16th International Technical Conference on

the Enhanced Safety of Vehicles (ESV), 98-S10-O-15, pp. 2279–92, Winsor Ontario, Canada, 1998.

[KalliskeAlbusFaerber98] Kalliske, I.; Albus, C.; Faerber, E.: Beurteilung der Sicherheitsaspekte eines neuartigen Zweiradkonzeptes: Bericht zum Forschungsprojekt 96526 (in German). Berichte der Bundesanstalt für Straßenwesen. F, Fahrzeugtechnik; 24. Bremerhaven: Wirtschaftsverlag NW, Verlag für neue Wissenschaft, 1998.

[Kamal70] Kamal, M.M.: Analysis and Simulation of Vehicle to Barrier Impact. SAE Transactions, Vol. 79, pp. 1498–1503, 1970.

[KanbeDeguchiHannya07] Kanbe, S.; Deguchi, M.; Hannya, Y.: Basic Research for a New Airbag System for Motorcycle. In Proceedings of the 20th International Technical Conference on the Enhanced Safety of Vehicles (ESV), 07-0095, Lyon, France, 2007.

[KentForman14] Kent, R.W.; Forman, J.: Restraint System Biomechanics. In Yoganandan, N.; Nahum, A.M.; Melvin, J.W.; The Medical College of Wisconsin Inc on behalf of Narayan Yoganandan (Eds.): Accidental Injury: Biomechanics and Prevention, pp. 113–141, New York, NY: Springer New York, 2014.

[KhalilDu Bois04] Khalil, T.B.; Du Bois, P.: Finite Element Analytical Techniques and Applications to Structural Design. In Vehicle Crashworthiness and Occupant Protection, pp. 111–158. Southfield, MI: American Iron and Steel Institute, 2004.

[KleinbergerEtAl98] Kleinberger, M.; Sun, E.; Eppinger, R.; Kuppa, S.; Saul, R.: Development of Improved Injury Criteria for the Assessment of Advanced Automotive Restraint Systems, NHTSA Docket No. 98-4405-9. National Highway Transport Safety Association (NHTSA), Washington, DC, 1998.

[KlugEllway21] Klug, C.; Ellway, J.: Technical Bulletin 024 – Pedestrian Human Model Certification, Version 3.0.1. European New Car Assessment Programme (Euro NCAP), Leuven, Belgium, 2021.

[KlugEtAl19] Klug, C.; Feist, F.; Schneider, B.; Sinz, W.; Ellway, J.; van Ratingen, M.: Development Of a Certification Procedure For Numerical Pedestrian Models. In Proceedings of the 26th ESV Conference, 19-0310, pp. 1–24, Eindhoven, Netherlands, 2019.

[KneiflGrunertFehr21] Kneifl, J.; Grunert, D.; Fehr, J.: A Non-intrusive Nonlinear Model Reduction Method for Structural Dynamical Problems Based on Machine Learning. International Journal for Numerical Methods in Engineering, 2021.

[KneiflHayFehr22] Kneifl, J.; Hay, J.; Fehr, J.: Real-time Human Response Prediction Using a Non-intrusive Data-driven Model Reduction Scheme. IFAC-PapersOnLine, Vol. 55, No. 20, pp. 283–288, 2022.

[KobayashiMakabe13] Kobayashi, Y.; Makabe, T.: Crash Detection Method for Motor-cycle Airbag System with Sensors on the Front Fork. In Proceedings of the 23rd International Technical Conference on the Enhanced Safety of Vehicles (ESV), 13-0344, Seoul, Korea, 2013.

[KoflerEtAl20] Kofler, D.; Tomasch, E.; Spitzer, P.; Klug, C.: Analysis of the Effect of Different Helmet Types and Conditions in Two Real-world Accident Scenarios with a Human Body Model. In Proceedings of the IRCOBI Conference, IRC-20-10, pp. 1–26, Munich, Germany, 2020.

[Kolling97] Kolling, J.: Validierung und Weiterentwicklung eines CAD-Menschmodells für die Fahrzeuggestaltung (in German). Dissertation. Technische Universität München, 1997.

[Kramer90] Kramer, F.: Schutzkriterien für den Fahrzeug-Insassen im Falle sagittaler Belastung (in German), Fortschritt-Berichte, VDI Reihe 12: Verkehrtechnis/-Fahrzeugtechnik, Nr. 137. Düsseldorf: VDI-Verlag, 1990.

[Kronwitter21] Kronwitter, S.: Simulation von Motorradunfallszenarien mit Menschmod-ellen (in German). Studienarbeit STUD-506, Institut für Technische und Numerische Mechanik, Universität Stuttgart, 2021.

[KuroeNamikiIijima05] Kuroe, T.; Namiki, H.; Iijima, S.: Exploratory Study of an Airbag Concept for a Large Touring Motorcycle: Further Research Second Report. In Proceedings of the 19th International Technical Conference on the Enhanced Safety of Vehicles (ESV), 05-0316, Washington, DC, 2005.

[LangwiederSpornerPolauke87] Langwieder, K.; Sporner, A.; Polauke, J.: Stand der pas-siven Sicherheit für den Motorradfahrer und mögliche Entwicklungstendenzen (in German). In Gesellschaft Fahrzeugtechnik (Ed.): Aktive und passive Sicherheit von Krafträdern: Tagung, Berlin, 8. u. 9. Oktober 1987, VDI-Berichte 657, pp. 29–52, Düsseldorf: VDI-Verlag, 1987.

[LarssonEtAl19] Larsson, K.J.; Pipkorn, B.; Iraeus, J.; Bolte IV, J.H.; Agnew, A.M.; Hu, J.; Reed, M.P.; Sunnevång, C.: Evaluation of the Benefits of Parametric Human Body Model Morphing for Prediction of Injury to Elderly Occupants in Side Impact. In Proceedings of the IRCOBI Conference, IRC-19-33, pp. 150–174, Florence, Italy, 2019.

[LauViano86] Lau, I.V.; Viano, D.C.: The Viscous Criterion – Bases and Applications of an Injury Severity Index for Soft Tissues. SAE Transactions, Vol. 95, pp. 672–691, 1986.

[Lawrence55] Lawrence, T.E.: The Mint: A Day-Book of the R.A.F. Depot Between August and December 1922 with Later Notes by 352087 A/C Ross. London: Jonathan Cape, 1955.

[Lechner86] Lechner, M.: Der Zweirad-Alleinunfall: Relation zwischen realem Unfall, Versuch u. mathematischer Simulation (in German). Dissertation. Technische Universität München, 1986.

[Leek12] Leek, J.: BMW: Motorräder seit 1945. Stuttgart: Motorbuch Verlag, 1st Edn., 2012.

[Leschke20] Leschke, A.: Algorithm Concept for Crash Detection in Passenger Cars. Wiesbaden, Germany: Springer Vieweg, 2020.

[LinCheng18] Lin, C.H.; Cheng, Y.P.: Evaluation of LS-DYNA Corpuscular Particle Method – Passenger Airbag Applications. In Proceedings of the 15th International LS-DYNA Users Conference, Detroit, MI, 2018.

[LindenmannGrandelBerg86] Lindenmann, M.; Grandel, J.; Berg, F.: Collision Dynamics in Experimental Simulations of 90° Motorcycle Collisions Against the Side of Moving Passenger Cars. In Proceedings of the IRCOBI Conference, pp. 289–302, Zurich, Switzerland, 1986.

[Liu20] Liu, H.: Weiterentwicklung eines Finite-Elemente Modells eines Motorrads in LS-DYNA (in German). Studienarbeit STUD-504, Institut für Technische und Numerische Mechanik, Universität Stuttgart, 2020.

[LiuEtAl08] Liu, B.C.; Ivers, R.; Norton, R.; Boufous, S.; Blows, S.; Lo, S.K.: Helmets for Preventing Injury in Motorcycle Riders. Cochrane Database of Systematic Reviews, Vol. 1, CD004333, 2008.

[LoftisPriceGillich18] Loftis, K.L.; Price, J.P.; Gillich, P.J.: Evolution of the Abbreviated Injury Scale: 1990–2015. Traffic Injury Prevention, Vol. 19, Supplement 2, pp. 109–113, 2018.

[LSTC18] LSTC: LS-DYNA Keyword User's Manual Volume II Material Models, LS-DYNA R11. Livermore Software Technology Corporation (LSTC), Livermore, CA, 2018.

[LvHynčíkBońkowski19] Lv, W.; Hynčík, L.; Bońkowski, T.: Rider Stature Influence to Injury Risk in Motorcycle Rear Impact to Car. SAE Technical Paper 2019-01-1436, pp. 1–7, 2019.

[Maier20] Maier, S.: Sicheres Motorrad – Ein Projekt des Technologietransferprogramms (in German). YouTube Kanal der e-mobil BW GmbH, Landesagentur für neue

Mobilitätslösungen und Automotive Baden-Württemberg, 2020.
https://www.youtube.com/watch?v=4NAfxNl9fE4, accessed February 16, 2023.

[Maier23] Maier, S.: Registered Cars and Motorized Two- and Three-wheelers in World-wide Countries, DaRUS, version V1, 2023.
https://doi.org/10.18419/darus-3378, accessed March 20, 2023.

[MaierEtAl20] Maier, S.; Doléac, L.; Hertneck, H.; Stahlschmidt, S.; Fehr, J.: Evaluation of a Novel Passive Safety Concept for Motorcycles with Combined Multi-Body and Finite Element Simulations. In Proceedings of the IRCOBI Conference, IRC-20-38, pp. 250–265, Munich, Germany, 2020.

[MaierEtAl21a] Maier, S.; Doléac, L.; Hertneck, H.; Stahlschmidt, S.; Fehr, J.: Finite Element Simulations of Motorcyclist Interaction with a Novel Passive Safety Concept for Motorcycles. In Proceedings of the IRCOBI Conference, IRC-21-17, pp. 60–78, Munich, Germany, 2021.

[MaierEtAl21b] Maier, S.; Helbig, M.; Hertneck, H.; Fehr, J.: Characterisation of an Energy Absorbing Foam for Motorcycle Rider Protection in LS-DYNA. In Proceedings of the 13th European LS-DYNA Users Conference, pp. 1–10, Ulm, Germany, 2021.

[MaierEtAl22] Maier, S.; Kempter, F.; Kronwitter, S.; Fehr, J.: Positioning and Simulation of Human Body Models on a Motorcycle with a Novel Restraint System. In Proceedings of the IRCOBI Conference, IRC-22-22, pp. 82–96, Porto, Portugal, 2022.

[MaierFehr21] Maier, S.; Fehr, J.: Multi-stage MBS and FE Simulation Strategy to Design a Safe Motorcycle (Extended Abstract). In Proceedings of the 10th ECCOMAS Thematic Conference on Multibody Dynamics, Book of Abstracts, 2021.

[MaierFehr23a] Maier, S.; Fehr, J.: Accident Simulations of a Novel Restraint Safety Concept for Motorcyclists. In Proceedings of the 27th International Technical Conference on the Enhanced Safety of Vehicles (ESV), 23-0189, Yokohama, Japan, 2023.

[MaierFehr23b] Maier, S.; Fehr, J.: Efficient Simulation Strategy to Design a Safer Motorcycle. Multibody System Dynamics, 2023.

[MarzouguiEtAl12] Marzougui, D.; Samaha, R.R.; Cui, C.; Kan, C.D.S.: Extended Validation of the Finite Element Model for the 2001 Ford Taurus Passenger Sedan. Tech. Rep. NCAC 2012-W-004, The National Crash Analysis Center (NCAC), The George Washington University, Ashburn, VI, 2012.

[Melvin85] Melvin, J.W.: The Engineering Design, Development, Testing, and Evaluation Of an Advanced Anthropomorphic Test Device, Phase 1: Concept Definition,

Report to Contract No. DTNH22-83-C-07005. National Highway Transport Safety Association (NHTSA), Washington, DC, 1985.

[Mertz93] Mertz, H.J.: Anthropometric Test Devices. In Nahum, A.M.; Melvin, J.W. (Eds.): Accidental Injury: Biomechanics and Prevention, pp. 66–84, New York, NY: Springer New York, 1993.

[MertzIrwin15] Mertz, H.J.; Irwin, A.L.: Anthropomorphic Test Devices and Injury Risk Assessments. In Yoganandan, N.; Nahum, A.M.; Melvin, J.W. (Eds.): Accidental Injury: Biomechanics and Prevention, pp. 83–112. New York, NY: Springer New York, 2015.

[MertzPatrick71] Mertz, H.J.; Patrick, L.M.: Strength and Response of the Human Neck. SAE Transactions, Vol. 80, pp. 2903–2908, 1971.

[MohaymanyEghbalian07] Mohaymany, A.S.; Eghbalian, A.: Investigating the Impact of Using Motorcycle Leg Protectors on Reducing Accident Injuries. In Proceedings of the 20th International Technical Conference on the Enhanced Safety of Vehicles (ESV), 07-0018, Lyon, France, 2007.

[MongiardiniEtAl17] Mongiardini, M.; Walton, B.; Grzebieta, R.H.; McKay, M.; Menictas, C.; Berg, A.; Rücker, P.: Development of a Motorcycle FE Model for Simulating Impacts into Roadside Safety Barriers. In Proceedings of the First International Roadside Safety Conference, E-C220, pp. 657–673, San Francisco, CA, 2017.

[MooneyCollins86] Mooney, M.T.; Collins, J.A.: Abdominal Penetration Measurement Insert for the Hybrid III Dummy. SAE Technical Paper 860653, pp. 285–289, 1986.

[MoradiLankarani11] Moradi, R.; Lankarani, H.M.: In A Multi-Body Modeling and Design of Experiment Investigation of a Motorcyclist Impact on Roadside Barriers at Upright and Sliding Configurations. Vol. 7 of ASME International Mechanical Engineering Congress and Exposition, pp. 697–705, 2011.

[Murri07] Murri, R.: Sicherheitsgurt für Motorräder – Lösungsansätze, Schutzpotenzial und Crashergebnisse (in German). Verkehrsunfall und Fahrzeugtechnik, Vol. 45, No. 12, pp. 341–344, 2007.

[NamikiNakamuraIijima05] Namiki, H.; Nakamura, T.; Iijima, S.: A Computer Simulation for Motorcycle Rider Injury Evaluation in Collision. In Proceedings of the 19th International Technical Conference on the Enhanced Safety of Vehicles (ESV), 05-0309, Washington, DC, 2005.

[NatarajanRajan22] Natarajan, G.; Rajan, T.P.: Review on the Performance Characteristics and Quality Standards of Motorcycle Protective Clothing. Journal of Industrial Textiles, Vol. 51, No. 5S, pp. 7409S–7427S, 2022.

[NayakEtAl13] Nayak, R.; Padhye, R.; Sinnappoo, K.; Arnold, L.; Behera, B.K.: Airbags. Textile Progress, Vol. 45, No. 4, pp. 209–301, 2013.

[Newman86] Newman, J.A.: A Generalized Acceleration Model for Brain Injury Threshold (GAMBIT). In Proceedings of the IRCOBI Conference, pp. 121–131, Zurich, Switzerland, 1986.

[NHTSA95] NHTSA: Injury Risk Curves and Protection Reference Values, National Highway Transport Safety Association (NHTSA), Washington, DC, 1995. https://one.nhtsa.gov/cars/rules/rulings/80g/80GII.html, accessed July 10, 2021.

[NHTSA11] NHTSA: 49 CFR, Section 571.208 – Standard No. 208; Occupant Crash Protection. National Highway Transport Safety Association (NHTSA), Washington, DC, 2011.

[NHTSA12] NHTSA: Ford Taurus (2001) LS-Dyna FE, Crash Simulation Vehicle Models, National Highway Transport Safety Association (NHTSA), Washington, DC, 2012. https://www.nhtsa.gov/crash-simulation-vehicle-models, accessed June 27, 2022.

[NHTSA20] NHTSA: 49 CFR, Section 571.218 – Standard No. 218; Motorcycle Helmets. National Highway Transport Safety Association (NHTSA), Washington, DC, 2020.

[NHTSA21] NHTSA: Motorcycles, Traffic Safety Facts, Report No. DOT HS 813 112. National Highway Transport Safety Association (NHTSA), Washington, DC, 2021.

[NoorsumarEtAl21] Noorsumar, G.; Rogovchenko, S.; Robbersmyr, K.G.; Vysochinskiy, D.: Mathematical Models for Assessment of Vehicle Crashworthiness: a Review. International Journal of Crashworthiness, pp. 1–15, 2021.

[OPEC20] OPEC: World Oil Outlook 2045. Organization of the Petroleum Exporting Countries (OPEC), Vienna, Austria, 2020.

[OpenVT21] OpenVT: 50F and 50M Seated, version 0.2.5, VIVA+ Open Human Body Models, VIRTUAL OpenVT Gitlab Platform Repository, 2021. https://openvt.eu/fem/viva/vivaplus, accessed September 9, 2021.

[OpenVT22] OpenVT: 50M Standing, version 0.3.2, VIVA+ Open Human Body Models, VIRTUAL OpenVT Gitlab Platform Repository, 2022. https://openvt.eu/fem/viva/vivaplus, accessed August 4, 2022.

[OsendorferRauscher01] Osendorfer, H.; Rauscher, S.: The Development of a New Class of Two-wheeler Vehicles. In Proceedings of the 17th International Technical Conference on the Enhanced Safety of Vehicles (ESV), 01-S8-O-475, Amsterdam, Netherlands, 2001.

[Oxford89] Ow - poisant, Vol. 11 of The Oxford English dictionary; 11. Oxford: Clarendon Pr., 2nd Edn., 1989.

[PallacciEtAl19] Pallacci, T.; Baldanzini, N.; Barbani, D.; Pierini, M.: Preliminary Effectiveness Assessment of an Airbag-based Device for Riders' Leg Protection in Side Impacts. Procedia Structural Integrity, Vol. 24, pp. 240–250, 2019.

[Peldschus09] Peldschus, S.: Entwicklung einer Simulationsmethode zur biomechanischen Untersuchung des Anpralls von Zweirad-Aufsassen an passive Straßenschutzeinrichtungen (in German). Dissertation. Ludwig-Maximilians-Universität München, 2009.

[Perlot21] Perlot, A.: PTW in Different Regions in the World - Europe, Motorcyclists Safety Workshop: Riding in a Safe System, European Association of Motorcycle Manufacturers (ACEM), Brussels, Belgium, 2021.
https://www.itf-oecd.org/sites/default/files/docs/ptw-in-different-regions-world-europe-acem.pdf, accessed September 18, 2022.

[PetitEtAl20] Petit, L.; Zaki, T.; Hsiang, W.; Leslie, M.; Wiznia, D.: A Review of Common Motorcycle Collision Mechanisms of Injury. EFORT Open Reviews, Vol. 5, pp. 544–548, 2020.

[PIPER21] PIPER: PIPER Project Software Framework, version 1.0.1, 2021.
http://doc.piper-project.org/framework/1.0.1/html/index.html, accessed March 18, 2021.

[PortalDias06] Portal, R.J.F.; Dias, J.M.P.: Multibody Models for Vehicle Accident Reconstruction. In III European Conference on Computational Mechanics, Lisbon, Portugal: Springer Netherlands, 2006.

[PtakEtAl19] Ptak, M.; Wilhelm, J.; Klimas, O.; Reclik, G.; Garbaciak, L.: Numerical Simulation of a Motorcycle to Road Barrier Impact. In Proceedings of the 14th International Scientific Conference: Computer Aided Engineering, pp. 565–573, Springer International Publishing, 2019.

[PuthanEtAl21] Puthan, P.; Lubbe, N.; Shaikh, J.; Sui, B.; Davidsson, J.: Defining Crash Configurations for Powered Two-Wheelers: Comparing ISO 13232 to Recent In-Depth Crash Data From Germany, India and China. Accident Analysis & Prevention, Vol. 151, 105957, 2021.

[RametEtAl94] Ramet, M.; Bouquet, R.; Bouallegue, M.; Bermond, F.; Césari, D.: The Effect of Air Bag Inflation on the Cinematic and the Lesions of a Motorcyclist. In Proceedings of the 14th International Technical Conference on the Enhanced Safety of Vehicles (ESV), 94-S7-O-11, pp. 1241–1246, Munich, Germany, 1994.

[ReichertEtAl14] Reichert, R.; Kan, C.D.; Marzougui, D.; Mahadevaiah, U.; Morgan, R.G.; Park, C.K.; Tahan, F.: Methodologies and Examples for Efficient Short and Long Duration Integrated Occupant-Vehicle Crash Simulation. In Proceedings of the 13th International LS-DYNA Users Conference, Detroit, MI, 2014.

[Riedel00] Riedel, J.: BMW C1. KRADblatt, 2000. https://kradblatt.de/c1/, accessed January 26, 2023.

[Rodegast22] Rodegast, P.: Collision Detection of a Motorcycle in Accident Scenarios using Machine Learning Algorithms. Master Thesis MSC-326, Institute for Engineering and Computational Mechanics, University of Stuttgart, 2022.

[RogersZellner98] Rogers, N.M.; Zellner, J.W.: An Overall Evaluation of UKDS Motorcyclist Leg Protectors Based on IS0 13232. In Proceedings of the 16th International Technical Conference on the Enhanced Safety of Vehicles (ESV), 98-S10-O-13, pp. 2247–2259, Winsor Ontario, Canada, 1998.

[Rouchon90] Rouchon, J.: Certification of Large Airplane Composite Structures, Recent Progress and New Trends in Compliance Philosophy. In Proceedings of the 17th Congress of the International Council of the Aeronautical Sciences, Volume 2, ICAS-90-1.8.18, pp. 1439–1447, Stockholm, Sweden, 1990.

[RuffJostEichberger07] Ruff, C.; Jost, T.; Eichberger, A.: Simulation of an Airbag Deployment in Out-of-position Situations. Vehicle System Dynamics, Vol. 45, No. 10, pp. 953–967, 2007.

[SAEJ211-1:1995] SAEJ211-1:1995: Instrumentation for Impact Test – Part 1 – Electronic Instrumentation. Warrendale, PA, 1995.

[SahooEtAl20] Sahoo, D.; Coulongeat, F.; Fuerst, F.; Marini, G.: Comparison of Head Injury Criteria Based on Real-World Accident Simulations under Visual Performance Solution (VPS). In Proceedings of the IRCOBI Conference, IRC-20-63, pp. 529–542, Munich, Germany, 2020.

[Sakamoto90] Sakamoto, S.: Research History of Motorcycle Leg Protection. SAE Transactions, Vol. 90, pp. 1032–1063, 1990.

[SavinoEtAl20] Savino, G.; Lot, R.; Massaro, M.; Rizzi, M.; Symeonidis, I.; Will, S.; Brown, J.: Active Safety Systems for Powered Two-wheelers: A Systematic Review. Traffic Injury Prevention, Vol. 21, No. 1, pp. 78–86, 2020.

[SavinoPieriniFitzharris19] Savino, G.; Pierini, M.; Fitzharris, M.: Motorcycle Active Safety Systems: Assessment of the Function and Applicability Using a Population-Based Crash Data Set. Traffic Injury Prevention, Vol. 20, No. 4, pp. 406–412, 2019.

[SchiehlenEberhard14] Schiehlen, W.; Eberhard, P.: Applied Dynamics. Heidelberg: Springer, 1st Edn., 2014.

[Schmidt03] Schmidt, B.: Bye-bye, BMW C1 (in German). Frankfurter Allgemeine Zeitung, 2003.
https://www.faz.net/aktuell/technik-motor/motor/kommentar-bye-bye-bmw-c1-1118104.html, accessed January 26, 2023.

[SchmittEtAl19] Schmitt, K.U.; Niederer, P.F.; Cronin, D.S.; Morrison III, B.; Muser, M.H.; Walz, F.: Trauma Biomechanics: An Introduction to Injury Biomechanics. Cham, Switzerland: Springer, 5th Edn., 2019.

[SchubertEtAl21] Schubert, A.; Erlinger, N.; Leo, C.; Iraeus, J.; John, J.; Klug, C.: Development of a 50th Percentile Female Femur Model. In Proceedings of the IRCOBI Conference, IRC-21-38, pp. 308–332, Munich, Germany, 2021.

[SchulzDobrovolnyHurlebaus16] Schulz, N.; Dobrovolny, C.S.; Hurlebaus, S.: Development of a Finite Element Model of a Motorcycle. In Proceedings of the 14th International LS-DYNA Users Conference, Detroit, MI, 2016.

[SchwarzeHurschlerWelke19] Schwarze, M.; Hurschler, C.; Welke, B.: Force, Impulse and Energy During Falling with and without Knee Protection: An In-vitro Study. Scientific Reports, Vol. 7, No. 1:10336, 2019.

[SerreEtAl19] Serre, T.; Masson, C.; Llari, M.; Canu, B.; Py, M.; Perrin, C.: Airbag Jacket for Motorcyclists: Evaluation of Real Effectiveness. In Proceedings of the IRCOBI Conference, IRC-19-76, pp. 533–547, Florence, Italy, 2019.

[Shabana97] Shabana, A.A.: Flexible Multibody Dynamics: Review of Past and Recent Developments. Multibody System Dynamics, Vol. 1, No. 2, pp. 189–222, 1997.

[SISS20a] SISS: Simcenter Madymo Human Body Models Manual Release 2020.1. Siemens Industry Software and Services BV (SISS), Rijswijk, Netherlands, 2020.

[SISS20b] SISS: Simcenter Madymo Theory Manual, Version 2020.1. Siemens Industry Software and Services BV (SISS), Rijswijk, Netherlands, 2020.

[SousaEtAl08] Sousa, L.; Veríssimo, P.; Ambrósio, J.: Development of Generic Multibody Road Vehicle Models for Crashworthiness. Multibody System Dynamics, Vol. 19, pp. 133–158, 2008.

[Sporner82] Sporner, A.: Experimentelle und mathematische Simulation von Motorradkollisionen im Vergleich zum realen Unfallgeschehen (in German). Dissertation. Technische Universität München, 1982.

[SpornerLangwiederPolauke87] Sporner, A.; Langwieder, K.; Polauke, J.: Development of a Safety Concept for Motorcycles – Results From Accident Analysis and Crash Tests. In Proceedings of the 11th International Technical Conference on the Experimental Safety of Vehicles (ESV), pp. 835–842, Washington, DC, 1987.

[Statista23] Statista: Motorcycles. Statista, 2023. https://www.statista.com/outlook/mmo/motorcycles/worldwide, accessed January 10, 2023.

[StigsonEtAl17] Stigson, H.; Rizzi, M.; Ydenius, A.; Engström, E.; Kullgren, A.: Consumer Testing of Bicycle Helmets. In Proceedings of the IRCOBI Conference, IRC-17-30, pp. 173–181, Antwerp, Belgium, 2017.

[SudyoddeeEtAl19] Sudyoddee, H.; Behr, M.; Llari, M.; Koetniyom, S.; Carmai, J.: Investigation of Motorcyclist and Pillion Passenger Injuries Using Numerical Simulations. IOP Conference Series: Materials Science and Engineering, Vol. 501, 012009, 2019.

[SzymezakRybiczka08] Szymezak, P.; Rybiczka, D.M.: Honda Gold Wing – Geschichte eines Kultmotorrads. Königswinter: Heel Verlag, 2008.

[TabaryEtAl21] Tabary, M.; Ahmadi, S.; Amirzade-Iranaq, M.H.; Shojaei, M.; Sohrabi Asl, M.; Ghodsi, Z.; Azarhomayoun, A.; Ansari-Moghaddam, A.; Atlasi, R.; Araghi, F.; Shafieian, M.; Heydari, S.T.; Sharif-Alhoseini, M.; O'Reilly, G.; Rahimi-Movaghar, V.: The Effectiveness of Different Types of Motorcycle Helmets – A Scoping Review. Accident Analysis & Prevention, Vol. 154, 20200786, 2021.

[TakhountsEtAl13] Takhounts, E.; Craig, M.; Moorhouse, K.; McFadden, J.; Hasija, V.: Development of Brain Injury Criteria (BrIC). Stapp Car Crash Journal, Vol. 57, pp. 243–266, 2013.

[TanavdeEtAl95] Tanavde, A.S.; Khandelwal, H.; Lasry, D.; Ni, X.; Haug, E.; Schlosser, J.; Balakrishnan, P.: Airbag Modeling Using Initial Metric Methodology. SAE Technical Paper 950875, pp. 1–14, 1995.

[Thunert17] Thunert, C.: CORAplus Release 4.0.4 User's Manual. Gesellschaft für Numerische Simulation mbH, on behalf of pdb – Partnership for Dummy Technology and Biomechanics, Braunschweig, Germany, 2017.

[Toyota21] Toyota: Documentation Total Human for Safety (THUMS) AM50 Occupant Model Version 4.1. Toyota Motor Corporation and Toyota Central R&D Labs., Inc., 2021.

[UN19] UN: World Urbanization Prospects, The 2018 Revision. United Nations (UN), New York, NY, 2019.

[UNECE12] UNECE: Regulation No 94 of the Economic Commission for Europe of the United Nations (UN/ECE) – Uniform Provisions Concerning the Approval of Vehicles with Regard to the Protection of the Occupants in the Event of a Frontal Collision. United Nations Economic Commission for Europe (UNECE), Geneva, Switzerland, 2012.

[UNECE17] UNECE: Consolidated Resolution on the Construction of Vehicles (R.E.3). United Nations Economic Commission for Europe (UNECE), Geneva, Switzerland, 2017.

[UNECE21] UNECE: United Nations Regulation No. 22 Revision 5 – Uniform Provisions Concerning The Approval Of Protective Helmets And Their Visors For Drivers And Passengers Of Motor Cycles And Mopeds. United Nations Economic Commission for Europe (UNECE), Geneva, Switzerland, 2021.

[Van AukenEtAl05] Van Auken, R.M.; Zellner, J.W.; Smith, T.A.; Rogers, N.: Development of an Improved Neck Injury Assessment Criteria for the ISO 13232 Motorcyclist Anthropometric Test Dummy. In Proceedings of the 19th International Technical Conference on the Enhanced Safety of Vehicles (ESV), 05-0227, Washington, DC, 2005.

[Van Driessche94] Van Driessche, H.: Development of an ISO Standard for Motorcycle Research Impact Test Procedures. In Proceedings of the 14th International Technical Conference on the Enhanced Safety of Vehicles (ESV), 94-S7-O-05, pp. 1162–1176, Munich, Germany, 1994.

[Van ElslandeEtAl16] Van Elslande, P.; Feypell-de la Beaumelle, V.; Holgate, J.; Redant, K.; de Solère, H.; Margaritis, D.; Yannis, G.; Papadimitriou, E.; de Craen, S.; Inge Haslie, L.; Muguiro, J.; Grummas Granström, P.O.: Mobility and Safety of Powered Two-Wheelers in OECD Countries. In Traffic Safety, pp. 101–117. John Wiley & Sons, Ltd, 2016.

[Velten09] Velten, K.: Mathematical Modeling and Simulation: Introduction for Scientists and Engineers. Weinheim, Germany: Wiley-VCH, 2009.

[WangNefske88] Wang, J.T.; Nefske, D.J.: A New CAL3D Airbag Inflation Model. SAE Transactions, Vol. 97, pp. 697–706, 1988.

[WHO18] WHO: WHO Global Status Report on Road Safety 2018. World Health Organization (WHO), Geneva, Switzerland, 2018.

[WHO20] WHO: Global Health Estimates: Leading Causes of Death. World Health Organization (WHO), Geneva, Switzerland, 2020.
https://www.who.int/data/gho/data/themes/mortality-and-global-health-estimates/ghe-leading-causes-of-death, accessed August 9, 2021.

[WuEtAl19] Wu, D.; Hours, M.; Ndiaye, A.; Coquillat, A.; Martin, J.L.: Effectiveness of Protective Clothing for Motorized 2-wheeler Riders. Traffic Injury Prevention, Vol. 20, No. 2, pp. 196–203, 2019.

[YangEtAl06] Yang, K.; Hu, J.; White, N.; King, A.; Chou, C.; Prasad, P.: Development of Numerical Models for Injury Biomechanics Research: A Review of 50 Years of Publications in the Stapp Car Crash Conference. Stapp Car Crash Journal, Vol. 50, pp. 429–490, 2006.

[YoganandanNahumMelvin14] Yoganandan, N.; Nahum, A.M.; Melvin, J.W.; The Medical College of Wisconsin Inc on behalf of Narayan Yoganandan (Eds.): Accidental Injury: Biomechanics and Prevention. New York, NY: Springer New York, 3rd Edn., 2014.

[Yperman11] Yperman, I.: Commuting by Motorcycle: Impact Analysis, Report No. 10.69. Transport & Mobility Leuven, Leuven, Belgium, 2011.

[ZellnerEtAl96] Zellner, J.W.; Wiley, K.D.; Broen, N.L.; Newman, J.A.: A Standardized Motorcyclist Impact Dummy for Protective Device Research. In Proceedings of the 15th International Technical Conference on the Enhanced Safety of Vehicles (ESV), 96-S10-W-21, pp. 1756–1781, Melbourne, Australia, 1996.

[ZuardyHerrmann11] Zuardy, M.; Herrmann, A.: An Advanced Centre Box of a Vertical Tail Plane with a Side Panel from CFRP Foam-core Sandwich Structure. CEAS Aeronautical Journal, Vol. 2, pp. 253–269, 2011.